

The effect of LOXL2 enzyme inhibition on liver fibrosis

A thesis submitted to the University of Birmingham for the degree of:

DOCTOR OF MEDICINE

Sarah Ann Townsend[1]

Supervisors:

Dr. Christopher Weston, Professor Philip Newsome

[1] Institute of Immunology and Immunotherapy
College of Medical and Dental Sciences
University of Birmingham;
B15 2TT

UNIVERSITY OF
BIRMINGHAM

University of Birmingham Research Archive

e-theses repository

This unpublished thesis/dissertation is copyright of the author and/or third parties. The intellectual property rights of the author or third parties in respect of this work are as defined by The Copyright Designs and Patents Act 1988 or as modified by any successor legislation.

Any use made of information contained in this thesis/dissertation must be in accordance with that legislation and must be properly acknowledged. Further distribution or reproduction in any format is prohibited without the permission of the copyright holder.

Abstract

Fibrosis is the final common pathway of all chronic liver injury, and its pathological endpoint, cirrhosis, carries a growing and substantial health burden, accounting for over 2.5% of deaths worldwide. Lysyl oxidase-like protein 2 (LOXL2) is one of a family of five (LOX, LOXL1-4) amine oxidases expressed by fibrogenic cells. This enzyme oxidises lysine residues in collagens and elastin leading to covalent crosslinking and stabilisation of structural components within the extracellular matrix, conferring the tensile strength of collagen and elastic fibers. In the liver, LOXL2 is believed to contribute significantly to fibrogenesis, and inhibition of its enzymatic activity may have therapeutic benefit.

The aim of this study was to investigate the effect of LOXL2 enzyme inhibition *in vivo* using murine models of liver fibrosis and on fibroblast activity *in vitro*.

Preliminary data was gained by examining tissue from mice and rats receiving developmental compounds developed to inhibit LOXL2 in thioacetamide and carbon tetrachloride induced fibrosis. A selected pre-clinical compound was then tested in our own model of TAA induced fibrosis and fibrosis resolution, the *Mdr2-/-* model of biliary fibrosis, and during *in vitro* studies.

The results show that inhibition of LOXL2 with PXS5303 and PXS5338K did not significantly reduce fibrosis in murine models of liver injury and that PXS5338K did

not alter fibroblast activity at concentrations expected to inhibit LOXL2. The compound PXS5338K demonstrated some efficacy in reducing CCl_4-induced liver fibrosis in rats.

In conclusion, enzyme inhibition of LOXL2 has not demonstrated significant efficacy in reducing liver fibrosis during *in vitro* or *in vivo* testing in mice.

Dedication

This thesis is dedicated to my family and to David Mak, who have provided much appreciated support and diversion, in equal measure.

Acknowledgements

I would like to acknowledge the help, support and direction of my supervisors, Dr. Chris Weston and Professor Philip Newsome, and the assistance offered by Dr. Emma Shepherd, and Ms. Clare Thomas. A huge amount of time and support was generously given by Dr. Ditte Hedegaard, Dr. Danial Patten, and Dr. Debashis Haldar, who has also shared crucial data.

Funding from the National Institute of Health (NIHR) Birmingham Liver Biomedical Research Unit, and from our collaborators at Pharmaxis Ltd., is gratefully acknowledged.

Finally, I thank everyone at the Birmingham Centre for Liver and Gastrointestinal Research for their excellent advice, their time, and good humor offered during these last three years, which has made this work a pleasure.

Contents

	List of abbreviations	22
1	**Introduction**	28
1.1	**The burden of liver disease**	28
1.2	**Liver injury and fibrosis**	29
1.2.1	Cellular mechanisms of liver fibrosis	29
1.2.2	Extracellular matrix in fibrosis	31
1.2.3	Biliary fibrosis	32
1.2.4	Hepatocyte regeneration during liver injury	32
1.2.5	The immune system in liver disease	35
1.2.5.1	Adaptive immune cells	37
1.2.6	The role of lysyl oxidases and transglutaminases in liver fibrosis	41
1.2.7	Fibrosis resolution and regeneration	43
1.2.8	Persistent liver fibrosis	47
1.3	**Drug development targeting fibrosis**	48
1.3.1	Targeting early myofibroblast activation	48
1.3.2	Targeting hepatic myofibroblast properties	49
1.3.3	Increasing ECM degradation	50
1.3.4	Cell therapy	51
1.3.5	Altering the balance of MMPs and TIMPs	52
1.4	**Lysyl Oxidases: role and function**	53
1.4.1	The role of LOX	55
1.4.1.1	Active LOX	55
1.4.1.2	Lysyl oxidase propeptide (LOX-PP)	57
1.4.2	LOXL1	58
1.4.3	LOXL2	59
1.4.4	LOXL3	60

1.4.5	LOXL4	61
1.5	**A focus on the functions of LOXL2**	62
1.5.1	The role of LOXL2 in cancers	63
1.5.2	The role of LOXL2 in cartilage development	65
1.5.3	Fibrosis	66
1.5.3.1	Cardiac fibrosis	67
1.5.3.2	Pulmonary fibrosis	68
1.5.3.3	Liver fibrosis	69
1.5.3.3.1	LOXL2 in liver fibrosis: findings from preclinical studies	69
1.5.3.3.2	Targeting LOXL2 in human liver fibrosis	74
1.6	**Murine models of liver fibrosis**	82
1.6.1	Pan-lobular fibrosis	82
1.6.2	Biliary Fibrosis	83
1.6.3	Diet–induced fibrosis	85
1.7	**Hypothesis**	85
1.8	**Aims and objections**	86
2	**Materials and Methods**	88
2.1.	**Murine models for preliminary analysis, developed by Pharmalegacy (Shanghai, China): the use of thioacetamide and carbon tetrachloride to induce liver fibrosis**	88
2.1.1	Thioacetamide (TAA) induced liver fibrosis in mice	88
2.1.2	Carbon tetrachloride (CCl_4) induced liver fibrosis in rats	89
2.2	**Development of murine liver injury models for use in testing the efficacy of LOXL2 inhibitors**	90
2.2.1	Animal Husbandry	90
2.2.2	A study of PXS5338K in *Mdr2* knock out mice	91
2.2.3	PXS5338K in TAA induced liver fibrosis	93

2.2.3.1	Method 1: Model of chronic hepatic injury induced by 16 weeks of ad libitum TAA in drinking water and administration of PXS5338K from week 10	93
2.2.3.2	Method 2 (fibrosis resolution): Chronic hepatic injury was induced following 16 weeks of ad libitum TAA in drinking water, after which TAA was withdrawn and PXS5338K was administered for 2 weeks	94
2.2.4	Power calculations	95
2.2.5	Mouse sacrifice and collection of tissue for analysis	95
2.2.5.1	Extraction of leukocytes from mouse liver and flow cytometry	97
2.2.5.1.1	Isolation of murine hepatic leukocytes using Optiprep	97
2.2.5.1.2	Preparation of compensation beads for single colour staining for both lymphoid and myeloid panels	99
2.3	**Assessment of liver fibrosis and inflammation**	101
2.3.1	Haematoxylin and Eosin Staining	101
2.3.2	Immunohistochemistry	101
2.3.2.1	Staining for α-SMA	105
2.3.3	Staining for collagens with picrosirius red (PSR)	106
2.3.4	Morphometric analysis of PSR and IHC stained liver tissue sections	107
2.3.5.	Real time quantitative polymerase chain reaction (qPCR)	108
2.3.5.1	RNA extraction	108
2.3.5.2	cDNA synthesis	109
2.3.5.3	Real time quantitative polymerase chain reaction (qPCR)	110
2.4	**In vitro assessment of the effect of PXS5338K on Fibroblasts**	113
2.4.1	Isolation of cell lines and cell culture	113
2.4.1.1	Isolation of fibroblasts	113
2.4.1.2	Culture and passage conditions	115
2.4.1.3	Freezing and storing cells	116
2.4.2	Assessment of the effect of PXS5338K on collagen crosslinking in vitro	117
2.4.3	Scratch wound assay	117
2.4.4	Collagen contraction assay	118

2.5	**Statistical analysis and graphical representation**	119
3	**Results I: Testing PXS5303 and PXS5313, LOXL2 enzyme inhibitors, in models of liver fibrosis**	120
3.1.	**Introduction**	120
3.2	**Testing PXS5303, a LOXL2 enzyme inhibitor, in a Thioacetamide (TAA) model of liver fibrosis**	121
3.2.1	Assessment of inflammatory infiltrate	121
3.2.2	Assessment of liver fibrosis	122
3.2.3	Liver cell apoptosis, proliferation and differentiation in mice following TAA administration	127
3.2.4	Expression of lysyl oxidases in mice receiving I.P. TAA	131
3.3	**Testing PXS5313, a LOXL2 inhibitor in a rat model of Carbon tetrachloride-induced liver fibrosis**	132
3.3.1	Oral carbon tetrachloride thrice weekly for six weeks leads to hepatic injury and fibrosis in rats which is reduced by oral administration of PXS5153	133
3.3.2	The effect of oral CCl_4 in rats on inflammatory cell recruitment to the liver, apoptosis and cell differentiation	137
3.3.3	Manual counting of cleaved caspase 3 vs morphometric analysis of % area stained	140
3.4	**Discussion**	141
4	**Results 2: Exploring the effects of LOXL2 inhibition in a biliary model of fibrosis.**	145
4.1	**Introduction**	145
4.2	**Assessing the degree of fibrosis in FVB vs C57Bl/6 *Mdr2-/-***	147

4.3	**A pilot test of PXS5338K in FVB *Mdr2-/-* mice**	149
4.3.1	A pilot test of PXS5338K in FVB Mdr2-/- mice: Serum results	150
4.3.2	A pilot test of PXS5338K in FVB Mdr2-/- mice: Immunohistochemistry	150
4.3.2.1	Haematoxylin and Eosin	150
4.3.2.2	Picrosirius red	151
4.3.2.3	Alpha-smooth muscle actin	153
4.3.2.4	Cleaved caspase 3	154
4.3.2.5	CD45	155
4.3.2.6	SOX-9	156
4.3.3	Real time quantitative polymerase chain reaction	157
4.3.4	Conclusions: pilot study of PXS5338K in FVB *Mdr2-/-* mice	158
4.4	**Assessing the effects of PXS5338K in C57Bl/6 *Mdr2-/-* mice**	160
4.4.1	Assessment of liver injury	160
4.4.1.1	Serum analysis	161
4.4.2	Assessment of liver fibrosis	163
4.4.2.1	Assessment of liver fibrosis: immunohistochemistry	163
4.4.2.2	Assessment of liver fibrosis: protein expression by qPCR	166
4.4.3	Evaluation of cell differentiation and proliferation using IHC for SOX-9	169
4.4.4	Immune cell infiltration in C57Bl/6 *Mdr2*-/- mice treated with PXS5338K	171
4.4.4.1	Immune cell infiltration as measure by flow cytometry	171
4.4.4.2	Immune cell infiltration by IHC	178
4.5	**Discussion**	180
5	**Results 3: The assessment of PXS5338K in reducing liver injury and fibrosis in a TAA induced model of liver disease**	184
5.1	**Introduction**	184
5.2	**The effect of daily administration of PXS5338K P.O. for**	188

six weeks in healthy C57/Bl6 mice

5.3	**Therapeutic dosing of PXS5338K during TAA induced liver injury**	190
5.3.1	Assessment of liver injury	191
5.3.2	The effect of PXS5338K on liver fibrosis	195
5.3.2.1	Assessment of fibrosis via qPCR	198
5.3.3	The impact of PXS5338K on cell differentiation during TAA induced liver injury	200
5.3.4	The effect of PXS5338K on immune cell infiltration during TAA induced liver injury	203
5.3.4.1	Immune cell infiltration as measured by flow cytometry	203
5.3.4.2	Immune cell infiltration by IHC	208
5.3.5	Assessing the impact of PXS5538K on cell differentiation, inflammatory cell recruitment, and fibrosis resolution during recovery from liver injury	210
5.4	**Assessing the impact of the TAA resolution model on the health of mice according to animal weight over time**	211
5.4.1	Changes in liver serology during fibrosis resolution with and without PXS5338K following TAA induced liver injury	212
5.4.2	Assessing the impact of PXS5338K on fibrosis resolution following TAA induced liver disease	214
5.4.3	Examining the effect of PXS5338K on cell differentiation during fibrosis resolution	223
5.4.4	The effects of PXS5338K on immune cell infiltration during fibrosis resolution	224
5.4.4.1	Assessment of immune cell infiltration by flow cytometry	224
5.4.4.2	Assessment of immune cell infiltration by IHC	234
5.5	**Discussion**	238
6	**Results 4: In vitro effects of LOXL2 inhibition by PXS5338K in fibroblasts**	243
6.1	**Introduction**	243

6.2 **Attempted isolation of murine liver fibroblasts: a mixed cell population** 245

6.3 **The use of scratch wound assays to assess the impact of LOXL2 inhibition on fibroblast activity in the wound healing response** 247

6.4 **The effect of PXS5338K on collagen cross-linking by fibroblasts in vitro** 248

6.5 **The effect of PXS5338K on fibroblast activity and collagen contraction within a gel in vitro** 247

6.5.1 The effect of PXS5338K on LX2 cells within a collagen contraction assay 251

6.5.2 The effect of PXS5338K on 3T3 cells within a collagen contraction assay 252

6.5.3 The effect of PXS5338K on human fibroblasts within a collagen contraction assay 256

6.6 **Discussion** 260

7 **Discussion and conclusions** 263

List of References 272

Appendix 287

List of Figures

Chapter 1

Figure 1.1	The ductular reaction in liver injury	34
Figure 1.2	Mechanisms of liver injury and fibrosis	41
Figure 1.3	Fibrogenesis versus fibrosis resolution	46
Figure 1.4	The lysyl oxidases	54
Figure 1.5	Models of murine hepatic injury drive upregulation of LOX/L expression	70
Figure 1.6	Suggested mechanism for fibrosis reduction targeting LOXL2	74
Figure 1.7	Lysyl oxidases and mRNA are upregulated in chronic liver disease compared to normal liver controls	75-76

Chapter 2

Figure 2.1	TAA model in mice	89
Figure 2.2	CCl_4 model of fibrosis in rats	90
Figure 2.3	Study of PXS5338K in *Mdr2-/-* knock out mice	92
Figure 2.4	TAA model for liver fibrosis	94
Figure 2.5	Testing PXS5338K in fibrosis resolution	95

Chapter 3

Figure 3.1	TAA model in mice	121
Figure 3.2	LOXL2 inhibition has little effect on inflammatory markers in the TAA model	124
Figure 3.3	LOXL2 inhibition has minimal impact on fibrosis by IHC in the TAA model	126
Figure 3.4	LOXL2 inhibition has minimal impact on fibrosis by qPCR in the TAA model	127
Figure 3.5	LOXL2 inhibition had little effect on apoptosis, and no effect on proliferation or differentiation in the TAA model	130
Figure 3.6	Relative expression of LOX and LOX1-4 in 2 groups of	132

	BALB/c mice following a regimen of 12 weeks of TAA at a dose of 200 mg/kg via intraperitoneal injection (I.P.), in addition to vehicle orally (P.O.) from week 9, or PXS5303, using qPCR	
Figure 3.7	CCl_4 model of fibrosis in rats	133
Figure 3.8	Rats receiving oral CCl_4 develop fibrosis which is attenuated by LOXL2 inhibition	135
Figure 3.9	Expression of proteins upregulated during fibrogenesis were reduced with high and/or low dose PXS5153	136
Figure 3.10	Minimal changes in apoptosis and the ductular reaction were seen in rats receiving LOXL2 inhibitor following injury with CCl_4	139
Figure 3.11	Analysis of cleaved caspase via % positive staining versus manual counting of cleaved caspase positive cells did not affect the results	140
Chapter 4		
Figure 4.1	Fibrosis by PSR stain in two strains of *Mdr2-/-* mice	148
Figure 4.2	Model for testing PXS5338K in FVB *Mdr2-/-* mice	149
Figure 4.3	H&E staining of FVB *Mdr2-/-* demonstrated no differences between the groups receiving PXS5338K vs vehicle, and no areas of gross injury such as necrosis	151
Figure 4.4	Mild fibrosis was demonstrated in FVB *Mdr2-/-* mice but no benefit with PXS5338K.	152
Figure 4.5	PXS5338K had no effect on hepatic stellate cell activation	154
Figure 4.6	PXS5338K has no effect on apoptosis in the liver	155
Figure 4.7	Immune cell infiltration as measured by CD45 was similar in mice receiving PXS5338K and vehicle	156
Figure 4.8	Some FVB Mdr2-/- mice receiving PXS5338K displayed a different pattern of SOX-9 positive cells compared with those receiving vehicle, in whom biliary structures were	157

predominantly stained positive

Figure 4.9	No differences were seen in expression of ECM proteins or lysyl oxidases in a murine model of biliary fibrosis	158
Figure 4.10	Model for testing PXS5338K in C57Bl/6 *Mdr2-/-* mice	160
Figure 4.11	PXS5338K had no impact on body weight in C57Bl/6 mice	161
Figure 4.12	Serum biochemistry for liver injury were no different between animals administered with PXS5338K vs vehicle, or no gavage	162
Figure 4.13	PXS5338K did not improve fibrosis in C57Bl6/ *Mdr2-/-* mice for liver injury were no different between animals administered with PXS5338K vs vehicle, or no gavage	164
Figure 4.14	PXS5338K did not modulate expression of mRNA for proteins usually upregulated during fibrosis in C57Bl6/ *Mdr2-/-* mice	167
Figure 4.15	PXS5338K did not modulate expression of lysyl oxidase family genes in C57Bl/6 *Mdr2-/-* mice	169
Figure 4.16	Doses of PXS5338K at 3 mg/kg does not alter cell proliferation or differentiation according to SOX-9 IHC in C57Bl6/ *Mdr2-/-* mice	170
Figure 4.17	Comparison of lymphoid cell isolates from liver showed no differences between C57Bl/6 *Mdr2-/-* mice receiving 9 doses of PXS5338K or vehicle by oral gavage	170
Figure 4.18	Comparison of lymphoid cell isolates from liver showed no differences between C57Bl/6 *Mdr2-/-* mice receiving 9 doses of PXS5338K or vehicle by oral gavage	174
Figure 4.19	Comparison of myeloid cell isolates from liver showed no differences between C57Bl/6 *Mdr2-/-* mice receiving 9 doses of PXS5338K or vehicle by oral gavage	177
Figure 4.20	PXS5338K does not alter liver infiltration of B220 CD45 positive, F4/80 positive or LY6G positive cells during	179

liver injury

Chapter 5

Figure 5.1	Sixteen weeks of oral TAA in C57Bl/6 mice results in increased collagen deposition and fibrosis	185
Figure 5.2	Fibrosis resolution occurs following cessation of TAA induced liver injury in mice and improvement can be seen as early as day 14	187
Figure 5.3	PXS5338K was well tolerated by C57Bl/6 mice	189
Figure 5.4	3 mg/kg PXS5338K given daily by gavage for 6 weeks is well tolerated in mice	190
Figure 5.5	TAA model for liver fibrosis	191
Figure 5.6	PXS5338K had no effect on animal weight	192
Figure 5.7	TAA induced liver injury as defined by serum biomarkers was not ameliorated by PXS5338K dosing	194
Figure 5.8	16 weeks of TAA induced liver fibrosis in mice which was not ameliorated by PXS5338K	196
Figure 5.9	16 weeks of TAA induced liver fibrosis in mice which was not ameliorated by PXS5338K	198
Figure 5.10	SOX-9 expression is upregulated in TAA-induced liver injury but not reduced by inhibition of LOXL2 by PXS5338K	202
Figure 5.11	Comparison of lymphoid cell isolates from liver showed no differences in immune cell populations between mice receiving vehicle or PXS5338K by oral gavage	204
Figure 5.12	Comparison of myeloid cell isolates from liver showed no differences in immune cell populations between mice receiving vehicle or PXS5338K by oral gavage	207
Figure 5.13	Comparison of markers of inflammatory cells in the liver showed no differences in immune cell populations between mice receiving vehicle or PXS5338K by oral gavage	208

Figure 5.14	Testing PXS5338K in fibrosis resolution	211
Figure 5.15	Mice exposed to 16 weeks of TAA continue to gain weight and mice treated with either 7 or 14 days of vehicle or PXS5338K have similar weights at the end of treatment	212
Figure 5.16	PXS5338K did not alter serum markers of hepatocyte or biliary injury in mice recovering from TAA induced liver injury	213
Figure 5.17	PXS5338K may reduce collagen I expression in mice recovering from TAA induced liver injury	216
Figure 5.18	PXS5338K did not alter collagen III expression in mice recovering from TAA induced liver injury	217
Figure 5.19	PXS5338K did not alter fibrosis by collagen PSR stain in mice recovering from TAA induced liver injury	218
Figure 5.20	Reduced expression of α-SMA was demonstrated in mice receiving PXS5338K recovering from TAA induced liver injury	219
Figure 5.21	Administration of PXS5338K during the resolution phase did not alter mRNA expression for markers of fibrosis	220
Figure 5.22	An increase in the ductular reaction was observed in mice receiving PXS5338K recovering from TAA induced liver injury	224
Figure 5.23	Comparison of lymphoid cell isolates from liver showed no differences in immune cell populations between mice receiving vehicle vs PXS5338K by oral gavage	225
Figure 5.24	Comparison of lymphoid cell isolates from liver showed no differences in immune cell populations between mice receiving vehicle vs PXS5338K by oral gavage	228
Figure 5.25	Comparison of lymphoid cell isolates from liver showed no differences in immune cell populations between mice receiving vehicle vs PXS5338K by oral gavage	229

Figure 5.26	Comparison of myeloid cell isolates from liver showed no differences in immune cell populations between mice receiving vehicle or PXS5338K by oral gavage	231
Figure 5.27	Comparison of myeloid cell isolates from liver showed no differences in immune cell populations between mice receiving vehicle vs PXS5338K by oral gavage	232
Figure 5.28	Comparison of myeloid cell isolates from liver showed no differences in immune cell populations between mice receiving vehicle or PXS5338K by oral gavage	233
Figure 5.29	Administration of PXS5338K has no impact on B cell infiltration into the liver when delivered during fibrosis resolution	235
Figure 5.30	Administration of PXS5338K increases macrophage infiltration into the liver when delivered during fibrosis resolution	236
Figure 5.31	Administration of PXS5338K has no impact on granulocyte infiltration into the liver when delivered during fibrosis resolution	237

Chapter 6

Figure 6.1	Cells isolated from murine livers using a protocol for hepatic stellate cells were a mixed population	246
Figure 6.2	Administration of PXS5338K did not affect wound closure time in a scratch wound assay	248
Figure 6.3	PXS5338K does alter collagen crosslinking in vitro as measured by mass spectroscopy	250
Figure 6.4	Collagen plugs containing LX-2 cells, dosed with PXS5338K, TGF-β or endothelin in culture media did not contract	252
Figure 6.5	PXS5338K enhanced contraction of 3T3 cells within a collagen	254
Figure 6.6	High doses of PXS5338K inhibited contraction in	258

fibroblast populated collagen gels

List of Tables

Table 1.1	Selectivity of PXS5153 in vitro	79
Table 1.2	PK profiles of PXS5153 and PXS5338K in mice	81
Table 2.1	Antibodies used for flow cytometry	100
Table 2.2	Antibodies used in IHC with a summary of agents used	104
Table 2.3	Gene expression assays used for qPCR	112
Table 2.4	Cell culture media	116
Table 4.1	Serum analysis for the two mice receiving eight (M2) or nine (M3) doses of PXS5338K before becoming unwell	150

Abbreviations

AF	atrial fibrillation
AIH	autoimmune hepatitis
ALD	alcohol related liver disease
ALT	alanine aminotransferase
AMD	age related macular degeneration
aRA	active retinoic acid
αSMA	alpha smooth muscle actin
AST	aspartate aminotransferase
αvβ6	alpha v beta 6
β-APN	ß-aminopropionitrile
BA	bile acids
BALB/c	bagg albino
BDL	bile duct ligation
BEC	biliary epithelial cells
B2M	beta-2-microglobulin
BMP-1	bone morphogenic protein-1
BR	Bilirubin
CAF	cancer associated fibroblast

CCL	chemokine ligands
CCl_4	carbon tetrachloride
CK	cytokeratin
CLD	chronic liver disease
CPA	collagen proportionate area
CTGF	connective tissue growth factor
CXCL	chemokine (C-X-C motif) ligand
DAB	diaminobenzidine
DDC	3,5-diethoxycarbonyl-1,4-dihydrocollidine
DHLNL	dihydroxylysinonorleucine
DMN	dimethynitrosamine
DNA	deoxyribonucleic acid
dNTPs	Deoxynucleotide
DPD	deoxypyridinoline
ECM	extracellular matrix
EDTA	ethylenediaminetetraacetate
ELISA	enzyme-linked immunosorbent assay
EMT	epithelial mesenchymal transformation
EpCAM	epithelial cell adhesion molecule
ERK	extracellular signal-regulated kinase

FAK	focal adhesion kinase
FBS	fetal bovine serum
FGF	fibroblast growth factor
FOXP3	forkhead box P3
FVB	friend virus B
GFAP	glial fibrillar acidic protein
HBV	hepatitis B virus
HCC	hepatocellular carcinoma
HCV	hepatitis C virus
HIF	hypoxia-inducible factor
HIV	human immunodeficiency virus
HLNL	hydroxylysinonorleucine
Hnf4α	hepatocyte nuclear factor 4 alpha
HSC	hepatic stellate cells
IFN-γ	interferon gamma
IGF	insulin-like growth factor
IHC	immunohistochemistry
IL	interleukin
I.M.	intramuscular
IMC	isotype-matched control

I.P.	intraperitoneal
KW	Kruskal-Wallace
LOX	lysyl oxidase
LOXL	lysyl oxidase like
LTQ	lysyl tyrosylquinone
Ly6C	lymphocyte antigen 6 complex locus G6D
LPCs	liver progenitor cells
MAO	monoamine oxidase
MCD	methionine choline-deficient diet
MCP1	monocyte chemoattractant protein 1
MMP	matrix metalloproteinases
MO	mineral oil
M.O.M	mouse on mouse
MPO	myeloperoxidase
mRNA	messenger ribonucleic acid
MRS	magnetic resonance spectroscopy
MW	Mann-Whitney
NADPH	nicotinamide adenine dinucleotide phosphate oxidase
NAFLD	non-alcoholic fatty liver disease
NAS	NAFLD activity score

NASH	non-alcoholic steatohepatitis
NFκB	nuclear factor kappa-light-chain-enhancer of activated B cells
NK	natural killer
NKG2D	natural killer group 2D
NL	normal liver
PBC	primary biliary cirrhosis
PBS	phosphate buffered saline
PCR	polymerase chain reaction
PDGF	platelet derived growth factor
P.O.	per os
PPARγ	peroxisome proliferator-activated receptor gamma
PSR	picrosirius red
PSC	primary sclerosing cholangitis
PYD	pyridinoline
RNA	ribonucleic acid
RPMI	Roswell Park Memorial Institute
RT	reverse transcriptase
SASP	senescence associated secreted proteins
S.C.	subcutaneous
SCC	squamous cell carcinoma

SD	sprague dawley
SOX-9	sex determining region Y box 9
SRCR	scavenger receptor cysteine-rich
SSAO	semicarbazide-sensitive amine oxidase
STAT5	signal transducer and activator of transcription factor 5
TAA	thioacetamide
TBS	Tris-buffered saline
TBS-T	Tris buffered saline with 0.1% Tween-20
TIMP	tissue inhibitor of metalloproteinase
TG	transglutaminase
TGF-β	transforming growth factor beta
TLR	toll-like receptor
TNF	tumour necrosis factor
TRAIL	tumour necrosis factor related apoptosis-inducing ligand
VEGF	vascular endothelial growth factor
VM	vasculogenic mimicry
WLM	western lifestyle model

1. Introduction

1.1 The burden of liver disease

Liver disease is the third commonest cause of premature death in the UK (1) with over 90% of liver-related death occurring in individuals under the age of 70 (2). In addition to the social costs, this has significant implications for productivity; 62,000 years of working life are lost to liver disease annually (3). Worldwide, global burden of disease estimates suggest that cirrhosis and hepatocellular carcinoma now account for over 3.5% of all deaths (4).

Alcohol misuse, obesity and viral hepatitis are the leading causes of liver injury in the UK, (1), but the final common pathway for all chronic liver injury is a process known as fibrosis. Fibrosis is a wound healing response to chronic injury characterised by the accumulation of extracellular matrix (ECM) or “scar” tissue (5), which replaces damaged tissue and ultimately leads to cirrhosis and the sequelae of portal hypertension, liver failure and, in a small proportion of individuals, hepatocellular carcinoma (HCC) (1, 5, 6). Eliminating the chronic liver injury can lead to fibrosis regression and improvement in clinical course, as demonstrated in aetiologies such as hepatitis B, C, and iron overload (7-9). However, in the setting of more significant liver fibrosis (i.e. cirrhosis) there is minimal regression and often clinical progression despite removing the on-going injury. In conditions such as non-alcoholic fatty liver disease, chronic alcohol use, or primary sclerosing cholangitis (PSC), there is on-going injury for which treatment options are limited. For these patients, an intervention targeting fibrosis is needed, yet there is currently no approved pharmacotherapy targeting liver fibrosis, and liver transplantation is the only effective

treatment for patients with decompensated liver disease. Shortages of donor organs to meet demand has resulted in an increase of liver transplant waiting list mortality in North America and Europe to almost 20% (10).

1.2. Liver Injury and Fibrosis

Fibrosis is a highly coordinated and protective wound-healing response to tissue injury. It can be self-limiting and homeostatic or, in the presence of chronic liver injury, excessive, leading to accumulation of ECM (6). It can be broadly defined as either pan-lobular or biliary fibrosis, according to the mechanism of injury, but there is considerable overlap in pathogenesis. In pan-lobular fibrosis, normal hepatic architecture is replaced by a nodular structure of functional regenerative hepatocytes encapsulated by fibrous septa. An associated increase in vascular tone, maladaptive micro- and macro-circulatory changes results in liver failure (6). Biliary fibrosis is more poorly understood, but is characterised by chronic inflammatory duct damage and deranged homeostasis between epithelial and mesenchymal cells, eventually leading to progressive liver fibrosis, sharing pathological pathways with pan-lobular fibrosis (11).

1.2.1 Cellular mechanisms of liver fibrosis

During fibrogenesis, myofibroblasts are the primary effector cells and the major source of ECM, including fibril-forming collagens I, III, and V, and glycoproteins such as laminin and fibronectin. Hepatic stellate cells (HSC) are the principal precursor population for matrix-secreting myofibroblasts (12, 13). In healthy liver, HSCs are localized in the space of Disse, where they display a quiescent phenotype (qHSCs),

express neural markers such as glial fibrillar acidic protein (GFAP), synemin, and synaptophysin, and are the major storage sites of vitamin A in the body (5, 14). During liver injury, HSCs proliferate and differentiate into myofibroblast-like cells in response to locally increased cytokines such as platelet-derived growth factor (PDGF) and transforming growth factor-beta (TGF-β) (15). Activated HSCs are characterised by increased expression of cell surface markers such as collagenα1, vimentin and alpha smooth muscle actin (αSMA), down-regulated expression of lipogenic genes (including peroxisome proliferator-activated receptor gamma (PPARγ)), and the loss of intracellular vitamin A. Upon activation, HSCs move to sites of liver injury (5), synthesise large amounts of ECM, particularly collagen, and regulate degradation of ECM, primarily by secreting tissue inhibitors of metalloproteinases (TIMPs), specifically the myofibroblast-derived TIMP-1 (11). During liver injury, the myofibroblast-derived TIMPs drive fibrogenesis by inhibiting the hepatic matrix metalloproteinases (MMPs) from degrading the newly generated ECM. In fibrosis resolution, myofibroblasts either die or undergo a change to a non-fibrogenic phenotype, whereby they do not secrete ECM or TIMPs (4,9).

While HSCs contribute 90% liver myofibroblasts during fibrogenesis (16), other tissue-resident and bone marrow-derived fibroblasts, pericytes and epithelial cells are believed to contribute a smaller proportion to the pool, although their roles are not fully understood (16). Portal fibroblasts can also differentiate into myofibroblasts, and are believed particularly important in the early response to cholestatic liver injury (17) (see section 1.2.3).

1.2.2 Extracellular matrix in fibrosis

In health, the extracellular matrix in the liver is composed of collagen I and III, in equal amounts, distributed primarily in perivascular regions and in the liver capsule, and at the parenchyma the perisinusoidal ECM is non-electron dense and rich in type IV collagen and laminin (18, 19). During fibrogenesis, the expression of type III collagen initially dominates, but over time type I collagen emerges as the most prevalent component of the ECM. Other collagens, including collagen V, are also expressed and as the matrix load of the liver increases, other matrix components including elastin, are laid down and form a rich substrate for intermolecular crosslinking (19, 20).

Initially fibrillar matrix is deposited within the space of Disse and in a perisinusoidal distribution, probably due to their proximity to nearby resident HSCs. The presence of fibrillar collagen between the sinusoidal endothelium and hepatocytes, together with chemokines and cytokines produced by inflammatory cells and activated stellate cells, leads to a change in cell matrix interactions, the loss of endothelial fenestrae, a process known as “sinusoidal capillarization”; and in turn a loss of the normal hepatocyte brush border (19-21). Hepatocytes within a matrix rich in type I collagen deposit rapidly lose defining features of hepatocyte function, such as albumin secretion (22). This process of sinusoidal capillarization impairs the ability of the liver to exchange substances with the general circulation and diminishes metabolic function of both the diseased and remaining healthy hepatocytes (23). Ultimately the excess ECM bridges vascular structures including the portal and central veins leading to the architectural disruption that culminates in cirrhosis (24, 25).

1.2.3 Biliary fibrosis

Periportal, or biliary fibrosis, develops as part of the wound healing response to bile duct injury in chronic cholestatic liver diseases, such as primary biliary cholangitis (PBC), primary sclerosing cholangitis (PSC), and chronic cholestasis, and is less well understood compared to panlobular fibrosis. Injury triggers a process known as the ductular reaction, which drives both accumulation of myofibroblasts (and ECM) and biliary proliferation (17, 26). During this process the bile duct epithelial cells, derived from the ductular reaction (described below), will synthesize and release paracrine mediators, such as TGF-β, connective tissue growth factor (CTGF), PDGF-BB, and endothelin-1 (17) which stimulate myofibroblast transformation and activation. Studies have shown that portal fibroblasts may be the first to undergo myofibroblastic transition, which may later be taken over by HSCs that exhibit chemoattraction towards biliary structures (27). Severe or chronic injury and the associated periportal hepatocyte death is therefore believed to result in enhanced periportal matrix deposition and the portal-portal septa formation seen in biliary or portal fibrosis (27, 28).

1.2.4 Hepatocyte regeneration during liver injury

In healthy liver, axin2^{+} hepatocytes located around the central vein have a higher proliferative capacity than hepatocytes in the mediolobular or periportal areas (see Figure 1.1) (29). After a mild but chronic injury, the liver will predominately be repopulated by periportal hybrid hepatocytes. The name hybrid hepatocytes derives from the observation that these progenitor liver residential cells express both hepatocyte and biliary proteins, such as hepatocyte nuclear factor 4 alpha (Hnf4α)

and (sex determining region Y) box 9 (SOX-9) respectively, and are enriched in bile duct–specific genes and hepatocyte-specific transcription factors (30). Hybrid hepatocytes are able to reconstitute the liver mass after various chronic injuries but do not participate in normal liver homeostasis (30).

Severe chronic liver damage induces a ductular reaction in the periportal region, composed of ductal cells and liver progenitor cells (LPCs) (31). LPCs are a heterogeneous population of cells, expressing biliary markers, hepatoblast markers, and stem cell markers, and have the capacity to differentiate into hepatocytes and biliary cells. They are also capable of forming hepatocyte buds and repopulating the damaged parenchyma (32, 33). In chronic liver injury, the dialogue between LPCs and HSCs may promote fibrosis. HSCs secrete numerous growth factors, stimulating hepatocyte and LPC proliferation. In turn, LPCs express monocyte chemoattractant protein 1 (MCP1) and PDGF-β, which recruit activated HSCs, favouring fibrogenesis (34). LPCs were demonstrated inefficient in generating mature hepatocytes in patients with alcoholic hepatitis (35), which may contribute to the significant mortality associated with this condition.

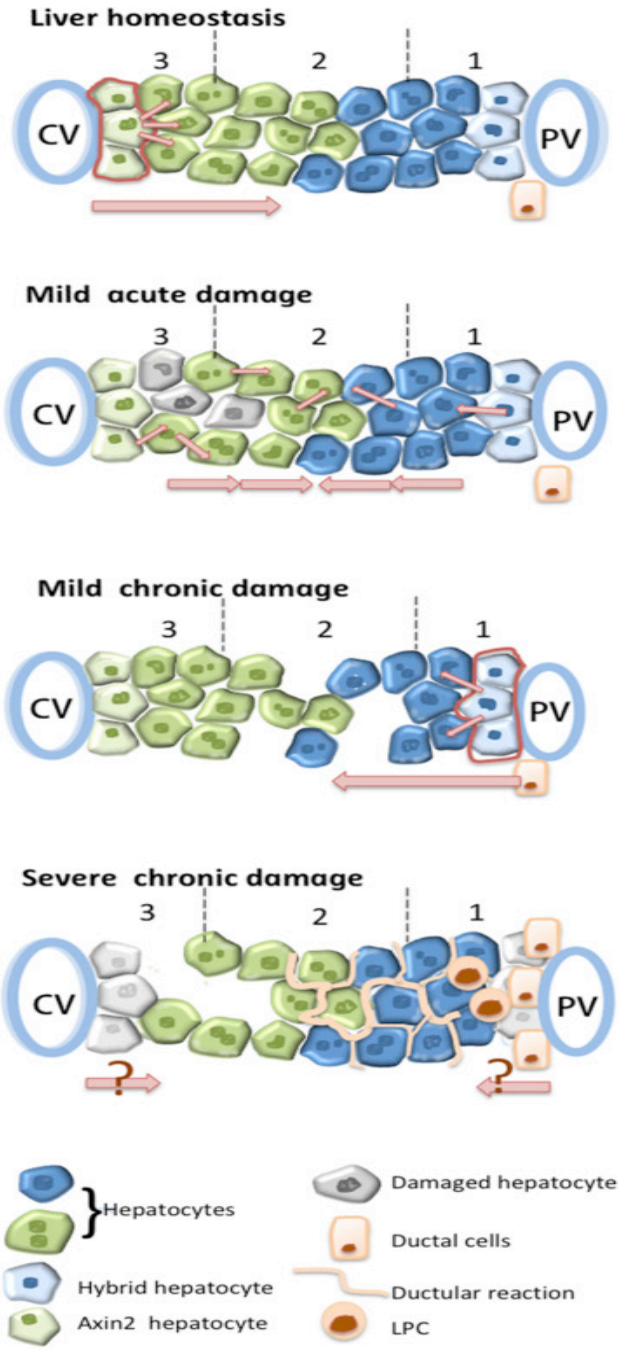


Figure 1.1 The ductular reaction in liver injury. In liver homeostasis, axin2^{+} hepatocytes located around the central vein have a higher proliferative capacity than hepatocytes located in mediolobular or periportal area. After a mild acute damage, healthy hepatocytes enter into the cell cycle and proliferate. After a mild chronic damage, hybrid hepatocytes located around the portal vein repopulate the liver. Severe chronic liver damage induces the ductular reaction composed of ductal cells and liver progenitor cells (LPCs). Zone 1 corresponds to the periportal region, zone 2 corresponds to the intermediate region, and zone 3 corresponds to the centrilobular region. CV, central vein; PV, portal vein. Adapted with permission from the *American Journal of Pathology* (34).

1.2.5 The immune system in liver disease

The immune system is implicated in the development of all liver diseases, regardless of aetiology. In some cases the response is specific to the insult, such as in autoimmune liver disease where Natural Killer T (NKT) cells activate other innate and adaptive immune cells within the liver to amplify and regulate subsequent immune responses (36), and in some HCV-infected individuals, where CD4 and CD8 T cell responses protect against viral persistence (37). However, there are also some common immune responses that occur independent of the initial cause of injury which will be discussed below (38).

In the initial immune response, the release of inflammatory mediators at the site of injury attracts leukocytes, which phagocytose dead or apoptotic cells, leading to the production of pro-inflammatory cytokines such as tumour necrosis factor (TNF), interleukin-6 (IL-6), IL-1β, and recruitment of T cells (5), amplifying the inflammatory response. Pro-inflammatory mediators also stimulate differentiation of mesenchymal cells into myofibroblasts, as discussed in 1.2.1, (38) which exacerbates the injurious process.

HSCs themselves have immune properties, producing nicotinamide adenine dinucleotide phosphate oxidase (NADPH), reactive oxygen species, pro-inflammatory cytokines and chemokine ligands (CCL) 3 and 4 (38), which activate and attract monocyte precursors to the site of injury. HSCs expressing Toll-like receptor 4 (TLR4) are also able to respond to bacterial components by expression of adhesion molecules and secreting chemokines, which attract resident macrophages (38).

Macrophages are critical in the response to tissue injury, and different subpopulations play functionally distinct roles. Macrophages can broadly be divided into resident Kupffer cells or monocyte-derived macrophages (39).

Kupffer cells are located in the hepatic sinusoids where they come into direct contact with antigens from the portal vein as well as circulating immune cells. They are therefore capable of inducing both immunogenic and tolerogenic immune responses, (40-42). Due to their hepatic location they provide a rapid response during liver injury by secreting pro-inflammatory cytokines and chemokines CCL2 and CCL5 (39). As hepatic inflammation and fibrogenesis evolve, the number of Kupffer cells decrease, and are later replenished once inflammation and fibrosis resolves where they produce anti-inflammatory mediators and take on a more restorative role (43, 44).

The number of monocyte derived macrophages increases in response to liver injury, specifically the $Ly6C^{hi}CD11b^{+}F480^{+}$ (lymphocyte antigen 6 complex locus G6D) hepatic macrophage population in mice, which are believed to be the key drivers in fibrogenic response. These cells secrete cytokines and chemokines, influencing the behaviour of HSCs and other myofibroblasts (45, 46). Specifically, TGF-β drives myofibroblast activation and ECM synthesis, and PDGF and the Type 2 helper cell (Th2)-produced cytokines interleukin-1 (IL-1) and IL-13, stimulate collagen synthesis (46). Chemokine secretion (including CCL7 and CCL8) recruits myofibroblasts, and CCL2, CCL3 and CCL5 facilitate leukocyte recruitment, perpetuating the pro-fibrotic environment (44).

In rodents, macrophages with high expression of Ly6C and Gr1 are pro-fibrogenic (45, 47), and are the dominant source of TGF-β, PDGF and insulin-like growth factor-1 (IGF1), which activate HSCs as well as providing nuclear factor kappa-light-chain-enhancer of activated B cells (NF-κB) -mediated survival signal to myofibroblasts (48). They also recruit other circulating inflammatory cells by secreting chemokines, cytokines and growth factors (44). Conversely, $CD11b^{neg}$ macrophages with low expression of Ly6C define a terminally differentiated, collagenase-secreting, phagocytic "restorative" macrophage responsible for the resolution of fibrosis (47, 49, 50). These produce MMPs, which break down ECM (see section above), and promote HSC apoptosis via caspase-9 and tumour necrosis factor related apoptosis-inducing ligand (TRAIL) (51). The equivalent "restorative" or M2 macrophage in humans has yet to be fully characterised, but is likely to be a subset of $CD14^{dim}CD16^{++}$ monocytes, with $CD14^{high}$ cells being the pro-inflammatory human counterpart to $Ly6C^{high}$ monocytes (43, 52).

This duality of macrophage function has been demonstrated in a range of murine models of fibrosis (carbon tetrachloride (CCl_4), dimethylnitrosamine (DMN), and thioacetamide (TAA)) (49, 53, 54), whereby macrophage depletion during chronic injury diminishes fibrogenesis, and macrophage depletion post-cessation of chronic injury abrogates the resolution of fibrosis (49).

1.2.5.1 Adaptive immune cells

The balance of type 1 T helper (Th1) and type 2 T helper (Th2) cells may influence the fibrotic response. Th2 cells are pro-fibrogenic; they secrete IL-13 which

stimulates TGF-β1 synthesis and upregulate expression of MMP-9, which in turn activates TGF-β1 (55). They also secrete IL-17 and IL-22; IL-17 induces type 1 collagen production in HSCs (56) and IL-22 promotes hepatocyte survival and proliferation, and has been demonstrated to be pro-inflammatory during Hepatitis B infection (57).

Conversely, a Th1 dominant response is associated wi_{th} IFN-γ production, which suppresses collagen deposition by regulation of MMPs and TIMPs, and decreases the production of profibrotic cytokines by Th2 cells, possibly in conjunction with IL-12. (55).

Regulatory T (T_{REG}) cells are a subset of $CD4^+$ cells characterised by expression of the transcription factor forkhead box P3 (FOXP3), signal transducer and activator of transcription factor 5 (STAT5), the cell surface marker CD25 (α-chain of the high-affinity IL-2 receptor), and production of IL-10. T_{REG} cells play a critical role in maintaining immunologic self-tolerance by actively suppressing self-reactive lymphocytes. Surprisingly, many investigators report an abundance of T_{REG} cells in parallel with effector immune cells in the livers of patients with autoimmune hepatitis (AIH) and primary biliary cholangitis (PBC); it seems likely that their function is defective in these conditions as their depletion or dysfunction leads to autoimmunity and inflammation in mice (58, 59). Conversely, T_{REGS} are significantly decreased in patients with alcoholic hepatitis compared healthy controls, and this is believed to contribute to the pronounced activation of the innate immune response observed in this condition (60). In chronic hepatitis C, FOXP3+CD4+ T_{REGS} have been identified

as an additional intrahepatic source of IL-8 acting on HSC, able to regulate fibrogenesis in addition to suppressing local immune responses (61).

Similarly, cytotoxic T cells ($CD8^+$ T cells) may have a pro-fibrogenic role in the liver (62), but their exact role is not fully understood. However, $CD8^+$ T-cells are the key effector cells that control viral infections via cytolytic activity and cytokine secretion. In HCV infection, $CD8^+$ T-cell cytolytic responses coincide with decreased HCV RNA titres in blood and a peak in alanine aminotransferase (ALT), a marker of hepatocyte injury. Interferon-gamma (IFN-γ) secreted by $CD8^+$ T-cells also directly suppresses viral replication in HCV replicon studies; CD8+ T cell depletion prior to HCV challenge in chimpanzees resulted in persistently elevated viral load until CD8+ T cells recovered and viral clearance was achieved (63, 64).

In mouse models of liver injury, CD8+ T-cell subsets were associated with increased HSC activation and fibrogenic stimulation, as assessed by expression of transforming growth factor (TGF)-β1, col1aI and α-SMA messenger RNA (mRNA) (62). However, other studies have shown no difference in CCl_4 induced liver fibrosis in CD8+ deficient mice compared with controls (65), and so it seems likely that their function may vary between disease aetiologies.

Natural Killer T cells (NKT cells) are a subset of T cells that share surface makers and functional characteristics of both the innate and adaptive arms of the immune system (66). They constitute about a third of hepatic lymphocytes in mice and 10–15% of rat and human liver lymphocytes, and yet their role in liver fibrosis remains unclear. NKT cells play an important role in regulating innate and adaptive immunity

via production of a variety of cytokines which enable them to respond quickly to remove invading pathogens, toxins, and food antigens from the portal venous blood via modulation of adaptive immune responses (67). A subset of NKT cells have been shown to patrol the liver sinusoids and become activated by the CXCR6 chemokine ligand CXCL16 during liver injury, secreting the cytokines interferon gamma (IFN-γ) and IL-4. This is believed to increase macrophage accumulation and perpetuate liver inflammation and fibrogenesis (68).

NK cells are lymphocytes of the innate immune system, abundant in the liver and play an important role in first-line defence against viral infection and tumour transformation (69). Their functions are believed to be mediated via production of cytokines such as IFN-γ or direct killing of target cells (67, 69). NK cells mediate apoptosis of activated HSCs via the retinoic acid early inducible natural killer group 2D (NKG2D)-dependent and the TRAIL-dependent mechanisms, thereby ameliorating liver fibrosis (70). NK cells also inhibit liver regeneration by producing IFN-γ and killing hepatocytes; however, their role in proliferation of liver progenitor cells remains controversial (67).

In summary, in the initial response to liver injury, pro-inflammatory cells activate myelofibroblast precursors (predominantly HSCs) through secretion of pro-inflammatory cytokines and chemokines (see figure 1.2). Differentiated myofibroblasts regulate the fibrotic response and are themselves controlled by a number of feedback mechanisms, including cytokine and growth factor production, cell-cell or cell-matrix interactions, and signals from macrophages and the adaptive

immune system. The balance of these factors determines whether tissue injury is limited and there is fibrosis resolution, or pathogenic liver scarring occurs.

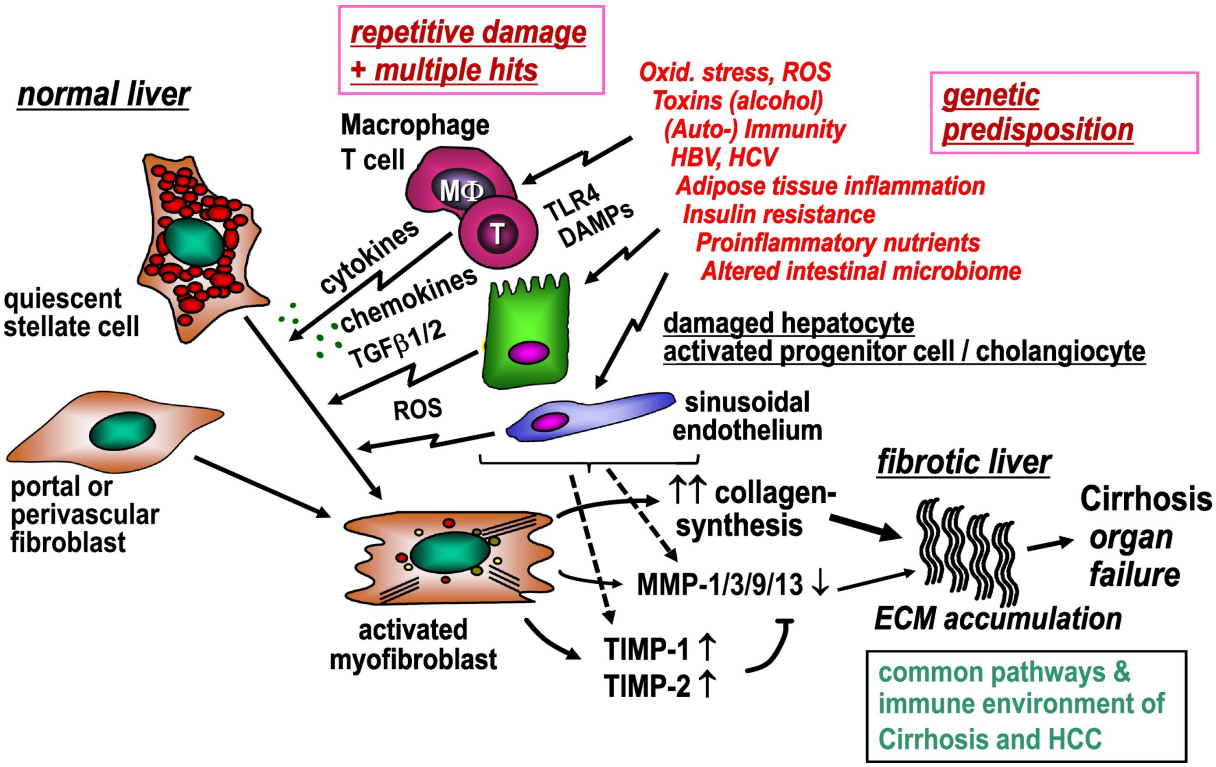


Figure 1.2 Mechanisms of liver injury and fibrosis. Factors inducing hepatic stellate cell transformation to fibrogenic myofibroblasts and mechanisms of resulting liver injury and fibrosis. The schematic highlights several major targets to treat liver fibrosis. Reproduced courtesy of *Matrix Biology* (71).

1.2.6 The role of lysyl oxidases and transglutaminases in liver fibrosis

Transglutaminases (TG) and lysyl oxidases both have a role in stabilisation and deposition of the ECM in the liver and are implicated in fibrosis (72).

TGs are a family of intracellular and extracellular enzymes that catalyze Ca^{2+} dependent acyl-transfer reactions between the γ-carboxamide group of peptide-bound glutamine residues and primary amines, including the ε-amino group of peptide-bound lysine. This leads to the formation of the N^{ε}(γ-glutamyl) lysine cross-

link, which is stable and resistant to proteolysis (73), thereby increasing resistance to chemical, enzymatic and mechanical degradation (72). TG2 is the most abundant and specifically found in the liver. Here it targets osteonectin, a calcium-binding glycoprotein, which is transiently produced at high levels in tissues undergoing remodeling as a consequence of injury or disease (74). Osteonectin expression is low in normal liver, but high during early fibrogenesis. It is prevalent at sites of inflammation and remodeling, but absent in dense fibrotic liver areas where remodeling no longer occurs (72, 74). TG2 is therefore thought to promote tissue repair in the early stage of fibrosis (75). Increased NF-kB transcription factor binding to TG promoter sites in the context of ongoing liver injury may represent one of the mechanisms by which cell injury induces TG transcription and thus potentiates the process of fibrogenesis (75). Despite theoretically holding therapeutic potential, $TG2^{-/-}$ mice exposed to carbon tetrachloride (CCl_4) or thioacetamide (TAA) induced liver injury showed no reduction of collagen crosslinking, levels of fibrosis-related transcripts, and no acceleration of fibrosis resolution compared to wildtype mice (76).

In contrast to transglutinaminases, lysyl oxidase-mediated cross-linking is thought to predominate later in the fibrotic process. In healthy tissues, collagens are a highly organised molecular structure in which three collagen chains are interwoven into a triple helix, and collagen fibrils are further strengthened by covalent crosslinks formed enzymatically between the collagen molecules (77, 78). Lysyl oxidases are responsible for initiating these modifications; specifically, they oxidatively deaminate lysine and hydroxylysine residues to form corresponding aldehydes in the telopeptide domains of the collagen molecule (77, 79). These aldehydes react spontaneously,

either with other aldehydes or with unmodified lysine or hydroxylysine residues, forming the crosslinks. This process results in the dimeric immature crosslinks dihydroxylysinonorleucine (DHLNL) and hydroxylysinonorleucine (HLNL). The reaction of immature crosslinks with an additional aldehyde results in the formation of the very stable trimeric, mature crosslinks pyridinoline (PYD) and deoxypyridinoline (DPD) (80, 81). During fibrosis, disproportionate collagen production and increased expression of lysyl oxidases leads to excessive maturation of crosslinks, resulting in the key characteristics of the disease: tissue stiffening, scarring and irreversibility.

1.2.7 Fibrosis resolution and regeneration

Liver fibrosis can be reversible after the removal of the causative agent; this has been demonstrated in both humans and in animal models of fibrosis (5, 82). The reversal of liver fibrosis is characterized by reduced inflammatory and fibrogenic cytokine levels, increased collagenase activity and disappearance of myofibroblasts and fibrous scars. During fibrosis resolution, activated HSCs (aHSCs) are susceptible to undergo apoptosis or senescence followed by death receptor-mediated cell death caused by deprivation of fibrogenic cytokines (7). The activation of death receptor-mediated pathways, decreased expression of pro-survival proteins, and increased expression of pro-apoptotic proteins results in a reduction in active myofibroblasts (83). In addition, NK cells will induce rapid killing of HSC following activation by IFN-γ (70) (as discussed in 1.2.5.1). Moreover, myofibroblasts and activated HSCs can also revert to an inactive phenotype during liver fibrosis regression, losing expression of Col1a1 and α-SMA, and returning to the space of Disse (7, 84). HSCs do not, however, revert fully to their quiescent state; genes such as glial fibrillary acidic

protein (GFAP), adiponectin receptor-1 (Adipor1), and D site of albumin promotor (albumin D-box) binding protein (DBP) are not re-expressed in inactivated HSCs (iHSCs), and may respond to recurring injury more effectively than naïve HSCs (13, 85).

HSCs may also enter senescence, primarily induced by the protein p53, as well as other cytokines and senescence associated secreted proteins (SASP), with resultant reduction in ECM production and increases in the level of ECM degrading enzymes.(86). Some studies have shown that within a stressful environment, HSCs increase their levels of p53, inducing senescence and reducing hepatic fibrogenesis, which may be a protective mechanism and have therapeutic potential (87, 88). Finally, rodent studies have demonstrated that during fibrosis resolution macrophages produce TRAIL, which has the ability to induce caspase-dependant apoptosis of activated HSC (89).

Macrophages play different roles during liver fibrosis progression and resolution (see Figure 1.3). Traditionally, these were referred to as pro-inflammatory M1 or pro-resolution, anti-inflammatory M2 macrophages; in mice these are well defined as either $Ly6C^{high}$ or $Ly6C^{low}$ cells (43), but they have yet not been so well characterised in humans, possibly because multiple intermediate phenotypes have been described, and cells may even have the ability to switch from one phenotype to another (43, 90). More recently, single cell RNA sequencing of human liver revealed two distinct populations of intrahepatic CD68+ macrophages; CD68+ macrophage population 1, characterized by enriched expression of LYZ, CSTA, CD7454, possibly representing

inflammatory macrophages, and CD68+ macrophage population 2, characterized by enriched expression of CD5L, MARCO, VSIG4, CPVL, CD163, CCDC88A, C5AR1, LIPA, LILRB5, MAF, CTSB, MS4A7, VMO1, RAB31, SLC31A2, TTYH3, VCAM1, KLF4, HMOX1, AIF1l, TMIGD3, which may have a tolerogenic function (91).

During liver injury and fibrogenesis, macrophages produce cytokines and growth factors to induce activation and proliferation of HSCs into ECM producing myofibroblasts (as outlined in 1.2.1). However, during fibrosis resolution, macrophages transform into a pro-resolution phenotype and no longer secrete fibrogenic or inflammatory factors, instead secreting matrix metalloproteases (MMPs), such as MMP-9, -12 and -13 (51, 92). MMPs are the major enzymes capable of ECM degradation, and can be secreted by many cell types, including macrophages, as pro-active enzymes and require post-translational modification for their function (13, 49). During fibrosis, TIMPs inhibit MMPs and provide an autocrine anti-apoptotic stimulus for myofibroblasts (13, 23), and thus a decline in TIMP levels is critical. A reduction in functional TIMP results in a reduced number of active ECM producing myofibroblasts, and facilitated unopposed action of MMPs to degrade fibrotic scar tissue (13).

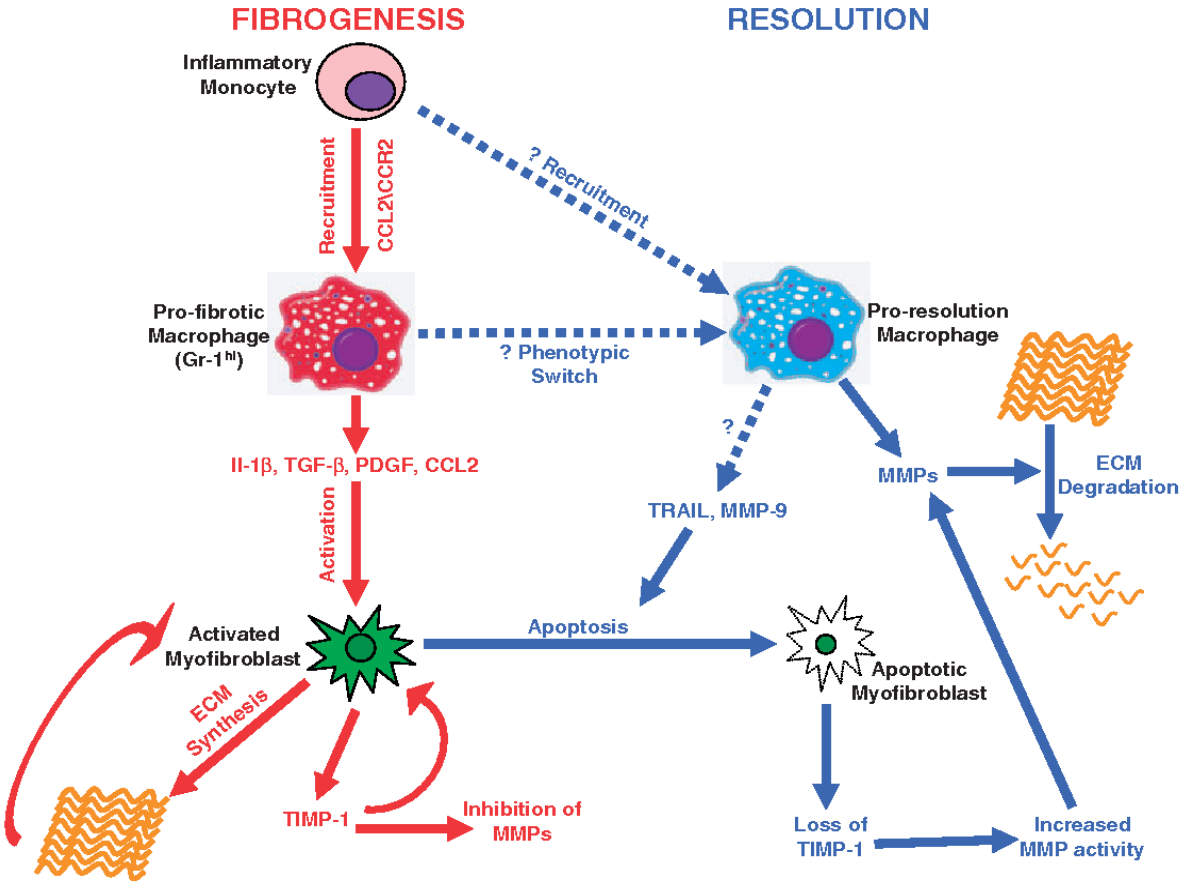


Figure 1.3 Fibrogenesis versus fibrosis resolution. During fibrogenesis, inflammatory monocytes are recruited to the inflamed liver via chemokine interactions, forming the pro-fibrotic macrophage population. Pro-fibrotic macrophages express mediators such as TGF-b, PDGF and CCL2, which promote activation of hepatic myofibroblasts. Activated myofibroblasts synthesise ECM and TIMP-1, a potent inhibitor of MMP activity. Both TIMP-1 and ECM interactions promote persistence of activated myofibroblasts. During fibrosis resolution, there is a change in macrophage phenotype, either from a phenotypic switch of pro-fibrotic macrophages or by separate recruitment of monocytes. Pro-resolution macrophages express MMPs that promote ECM degradation and express mediators that induce myofibroblast apoptosis, leading to a reduction in ECM synthesis, loss of TIMP-1 expression and enhanced MMP activity. Reproduced with permission from QJM (93).

1.2.8 Persistent liver fibrosis

Even if the injurious agent has been removed (eg. in treated Hepatitis C, cessation of alcohol misuse), fibrosis resolution does not always occur and may occasionally progress.

Persistent tissue injury results in pathological alterations in the quantity and the composition of the matrix (specifically an increase in fibrillar collagens). Furthermore the condition leads to biochemical modifications that render the fibrotic liver less susceptible to remodelling and repair. Mature scar ECM, composed of cross-linked collagen and elastin, is more resistant to proteases (94), and fibrils sequestered in deeper portions of a scar are inaccessible to degrading enzymes. The pattern and distribution of fibrosis can differ according to disease aetiology and is associated with varying degrees of angiogenesis and potential for reversibility (95).

Expression of MMPs and collagenases often remains high in the fibrotic liver, even once injury has been removed (7). A likely explanation for this is ongoing biomechanical signalling from increased liver stiffness, resulting in stimulation of myofibroblasts which retain a differentiated, contractile phenotype, and TGF-β, contributing to a sustained profibrotic environment (82).

In addition, acellular scars lack the endogenous sources of MMPs, which would have derived from the infiltrating inflammatory cells and myofibroblasts, and TIMP levels may remain high, further reducing the potential for MMP activity (94).

The result of this is that individuals with established cirrhosis may still develop decompensated liver disease (encephalopathy, HCC, complications related to portal hypertension) despite removal of injurious agents such as alcohol, hepatitis C.

1.3 Drug development targeting fibrosis

In the scenario where there is persistent fibrosis following treatment of the underlying condition, or there is no suitable treatment for the underlying liver injury, drug development has targeted key molecules and pathways of the fibrotic process.

Despite this the most effective method of reducing fibrosis is to remove or treat the causative agent. Treatments for HCV are now over 90% effective and will in time reduce the burden of viral liver disease (96). Treatment of iron overload in haemochromatosis can also improve fibrosis (97). In conditions such as longstanding HCV infection or chronic alcohol use, fibrosis can persist despite elimination of the causative agent; in others such as non-alcoholic fatty liver disease or PSC, no real treatment options exist, and so alternative solutions are sought.

1.3.1 Targeting early myofibroblast activation

Resveratrol is a polyphenol, found in skin of red grapes, and is thought to possess anti-inflammatory, anti-carcinogenic and lipid modulation properties. Studies in two different rat models of liver fibrosis demonstrated down-regulation of α-SMA, the marker of active HSCs, and an improved in liver biochemistry (98, 99). Resveratrol is currently in Phase II clinical trial in individuals with non-alcoholic fatty liver disease (NAFLD) (ClinicalTrials.gov Identifier: NCT02030977).

Emricasan is an irreversible pan-caspase inhibitor, and thus has been investigated in pathways of inflammation and apoptosis as a potential agent that may target key drivers of liver fibrosis. Steatotic hepatocytes are prone to apoptosis via both intrinsic and extrinsic pathways (100). Downstream apoptotic bodies are phagocytosed by Kupffer cells (101) and hepatic stellate cells (HSC) (102) in an environment that promotes inflammation and fibrogenesis. Reducing hepatocyte apoptosis by caspases inhibitors has been demonstrated to protect the liver in murine models of acute liver failure, and attenuates inflammation and fibrosis in murine models of cholestatic-, ethanol-, and methionine/choline deficient diet-induced liver injury (100). In a phase II placebo control trial performed with patients suffering from NAFLD, Emricasan reduced liver enzymes and markers of apoptosis, and in a different study in individuals with HCV related cirrhosis, Emricasan led to improved liver function (103, 104). There have as yet been no safety concerns despite its widespread and irreversible mechanism of action.

1.3.2 Targeting hepatic myofibroblast properties

Several drugs have been developed to directly target myofibroblast activity, and are being tested primarily in idiopathic pulmonary fibrosis (IPF). STX-100 is a monoclonal antibody directed against the alpha v beta 6 (αvβ6) integrin, which activates the cytokine TGF-β, and so STX-100 is being trialled as TGF-β inhibitors in idiopathic pulmonary fibrosis (105) (ClinicalTrials.gov Identifier: NCT01371305). Pirfenidone, another compound believed to have anti-inflammatory and anti-TGF-β properties (106), has also demonstrated efficacy in IPF (107, 108).

Asiatic acid has been demonstrated to inhibit collagen matrix production by HSC and keloid fibroblasts (isolated from keloid tissue) by blocking the autocrine effect of TGF-β *in vitro* and in animal models, but there are currently no plans for human trials (109). Although other compounds targeting TGF-β have been developed for other fibrotic disorders such as systemic sclerosis, renal sclerosis and renal fibrosis, as well as some cancers, results thus far have been underwhelming, possibly due to the widespread role of TGF-β across different tissues (110). It requires further investigation in the liver.

1.3.3 Increasing ECM degradation

Relaxin is a peptide hormone of the insulin superfamily. Despite a structural similarity to insulin, there is no common function. Its best documented role is in reproduction, where it inhibits uterine contraction and induces growth and softening of the cervix (111). More recently, in vitro experiments suggest that relaxin can reduce synthesis and/or increase the rate of degradation of extracellular matrix components in the skin, lung, liver, and kidney (112). Unemori *et al.* demonstrated that relaxin increases the synthesis of collagenase and decreased the synthesis of TIMP-1 in cultures of normal human dermal fibroblasts (113). The same group reported that in cultures of normal human lung fibroblasts, relaxin inhibits TGF-β -induced expression of interstitial collagen and fibronectin, as well as stimulating collagenase expression (114). In liver fibrogenesis, the addition of relaxin to activated hepatic stellate cells reduced collagen deposition and TIMP-1 and TIMP-2 secretion in cultures of activated hepatic stellate cells, and similar results have been seen in murine studies

(115, 116). In humans, clinical trials have demonstrated relaxin to be well tolerated but thus far have focused on reducing portal hypertension (117) (NCT02669875).

1.3.4 Cell therapy

Some preclinical studies suggested that injections of bone-marrow-derived cells reduce hepatic fibrosis and stimulate liver regeneration, thereby improving the synthetic function of the liver (118, 119). However, a recently published phase II clinical trial whereby granulocyte colony-stimulating factor with or without autologous CD133-positive stem-cells were given to individuals with liver cirrhosis showed no benefit with either therapy, and possibly an increase in adverse events (120).

The potential for macrophage therapy has also been demonstrated in several mouse models, where they have been shown to reduce myofibroblast levels and increase anti-inflammatory cytokine production (121). Macrophages are also able to stimulate proliferation and differentiation of hepatic progenitor cells proliferation, thus offering a potential treatment strategy for patients with cirrhotic liver disease to promote resolution of fibrosis and stimulate resolution (122). Indeed, inflammatory monocytes can contribute significantly to pathology, and a group in Edinburgh have developed a method of producing consistent, well-characterized pro-resolution CD14+ macrophages to be used as a therapy for cirrhosis, which is currently in phase 1 trial (123, 124).

1.3.5 Altering the balance of MMPs and TIMPs

Influencing the balance of MMPs versus TIMPs seems an obvious therapeutic target, and there have been multiple murine studies investigating various compounds targeting this axis (125). Despite many rodent studies demonstrating benefit, such as a study of mutant MMP-9 in CCl_4 induced liver fibrosis in rats (126), clinical trials have been disappointing (127). Antibodies targeting MMP-9 may have some potential; AB0041, AB0046 are highly selective allosteric inhibitors targeting the MMP-9 region close to the active site and has shown benefit for intestinal fibrosis in Ulcerative colitis, and another MMP-9 antibody was effective in reducing collagen deposition and hydroxyproline content in patients with fibrotic Crohns disease (128). Another therapeutic option being explored is the use of an inactive mutant of MMP-9 as a decoy. It has been shown to reduce fibrogenesis, transdifferentiation of HSCs and levels of α-SMA and TGF-β. Increased expression of MMP-2, MMP-9, and reduced accumulation of ECM have also been demonstrated, but thus far only in murine studies (126, 129, 130).

One factor affecting the use of targeting ECM proteases is their broad function throughout several different tissues resulting in unwanted side effects in non-pathological processes. Efforts have been made to take a more tissue specific approach with some success. In the fibrotic microenvironment, MMP-2 secreted by HSCs promotes the fibrotic cascade. A vitamin A coupled liposome has been developed to deliver MMP-2 siRNA directly to HSCs, and a reduction in α-SMA and collagen I protein expression was observed in vitro (131). Another liposome delivering siRNA against gp46 (heat shock protein 47), which mediates the pro-

collagen triple helix formation in the endoplasmic reticulum, has been developed in rats, and shows promise as an antifibrotic (132). Drugs directly targeting ECM formation such as the LOX family of enzymes have been developed in cancer models, and could be applied in fibrotic disease (127).

1.4. Lysyl Oxidase; role and function

Lysyl oxidase and Lysyl-like oxidases 1, 2, 3 and 4 are a family of five (LOX, LOXL1-4) copper dependent amine oxidase enzymes, each with related but discrete functions (133). Amine oxidases are enzymes that catalyse the oxidative cleavage of alkylamines such as neurotransmitters, histamine and xenobiotic amines, into aldehydes, releasing hydrogen peroxide and ammonia. There are two classes of amine oxidases, flavin-containing and copper-containing, the latter capable of being further subdivided into 3 families; lysyl oxidases, primary-amine oxidase, and diamine oxidase (134). Copper-containing amine oxidases are found in bacteria, fungi, plants and animals where they have a broad range of functions, including cell differentiation and growth, wound healing, detoxification and cell signalling (135).

The LOX protein family is characterised by a highly conserved amino acid sequence at their C terminal end that includes the copper binding site, residues for carbonyl co-factor formation, and a cytokine receptor like domain (136). All lysyl oxidase isoforms incorporate copper intracellularly, a process likely to be dependent on the copper chaperone ATP7a, and essential for optimal enzyme activity (137). Lysyl oxidases are expressed and secreted by fibrogenic cells into the extracellular environment predominantly in the heart, lung and kidneys, as well as the liver; one common

function being to oxidise lysine residues in collagens and elastin (79). This results in covalent crosslinking and stabilisation of structural components within the extracellular membrane, conferring the tensile strength of collagen and elastic fibres (79).Expression of LOX and LOXLs significantly overlap and expression of each member may be coordinated. In addition, each LOX-like protein has a unique N-terminal domain that determines its individual biological role. LOX and LOXL1 contain a highly basic propeptide that is cleaved by bone morphogenic protein-1 (BMP-1) to generate active enzyme (138, 139), whereas LOXL2, 3, and 4 contain four scavenger receptor cysteine-rich (SRCR) domains which are thought to mediate protein–protein interactions and cell adhesion (see Figure 1.4) (140).

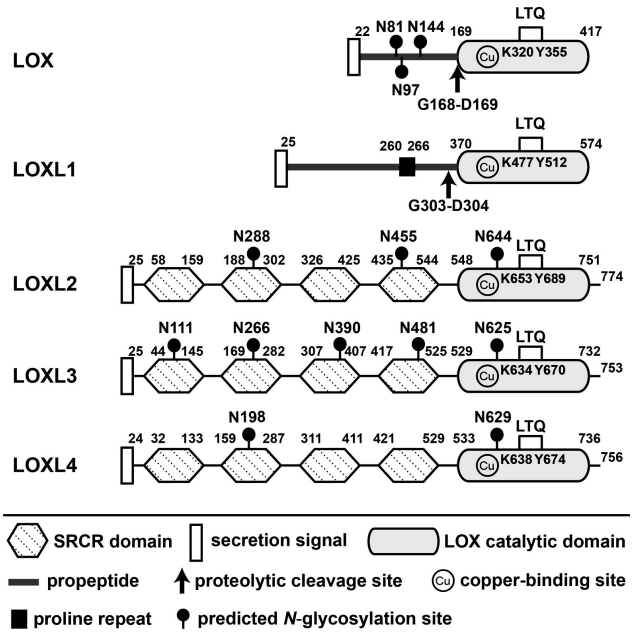


Figure 1.4 The lysyl oxidases. Diagrammatic representation of the LOX family of proteins. Each member retains a conserved C-terminal LOX catalytic domain, which encompasses a copper-binding site and an LTQ cofactor formed from conserved Lys and Tyr residues by post-translational modification. Each member also possesses an N-terminal secretion signal, and LOX and LOXL2-4 also contain predicted *N*-linked glycosylation sites. LOX and LOXL1 constitute one subfamily, possessing an N-terminal propeptide sequence, which is proteolytically removed by procollagen c-proteinase (BMP-1) at a conserved site (*black arrow*). LOXL2-4 constitute the other subfamily, with four SRCR domains instead of a propeptide. Reproduced with permission from *Archives of Biochemistry and Biophysics* (140).

1.4.1 The role of LOX

The roles of LOX are better understood than the other members of the LOX family. It is synthesized as a 50 kDa pre-proenzyme and, like all five isoforms, undergoes signal peptide removal and intracellular N-glycosylation in the endoplasmic reticulum. The proenzyme is secreted into the extracellularly as an inactive precursor and undergoes proteolytic processing by procollagen C-proteinases. This process releases the active enzyme (active LOX) and the lysyl oxidase propeptide (LOX-PP), each with independent biological functions.

1.4.1.1 Active LOX

LOX is required for the biosynthesis and maturation of collagen and elastin fibres, and is therefore widely expressed, particularly in vascular, mineralised and non-mineralised connective tissues. *Lox*-/- mice die at the end of gestation or as neonates, and have large aortic aneurysms, ruptured diaphragms and highly fragmented elastic fibres in the aortas, and discontinuity in the smooth muscle cell layers (141, 142). These animals also demonstrate disorganised collagen fibres in the lungs and skin (143), with immature collagen and elastin cross-linking (142), and poor development of the distal and proximal lung airways, associated with fewer and more disperse elastic fibres than in wild type mice (97).

LOX expression is consistently upregulated in fibrotic disease, where its enzymatic function renders collagen and elastin fibres more resistant to proteolytic degradation, leading to an accumulation of connective tissue and fibrosis (144-146). Lung, liver, heart, and skin fibrosis of all aetiologies are associated with elevated LOX levels, the

exception being phenytoin induced gingival over growth, which is accompanied by an increase in LOXL2 levels (147).

Elevated LOX levels are also associated with diabetic retinopathy, leading to uneven cross-linking and a thickened and distorted basement membrane, increased vascular permeability, bleeding and blindness (148, 149). LOX and LOXL2 levels are also elevated in murine models of age related macular degeneration (AMD), and LOX and LOXL2 antibodies successfully reduced fibrosis, α-1 type I collagen (*Col1a1*) expression, and inhibition of LOXL2 reduced angiogenesis and inflammation, and vascular endothelial growth factor expression in these models (150).

Studies have demonstrated a role for LOX in the development of myelofibrosis beyond cross-linking of collagen. LOX enzyme activity is essential for optimal PDGF signalling and cell proliferation during megakaryocyte differentiation, and reduced LOX levels over time permit differentiation of megakaryocytes into platelets. Persistently high LOX levels results in ECM accumulation and bone marrow fibrosis in mice (151). In human primary myelofibrosis, both LOX and the LOX-like enzymes (LOXL1-4) are elevated, and in myeloproliferative neoplasms, individual LOX isoforms are raised, suggesting a possible therapeutic role for enzyme inhibition in these conditions (151, 152).

Elevated LOX levels accompany and may even drive metastatic cancer via several mechanisms, making LOX a potential therapeutic target. Firstly, dysplastic tissue tends to be fibrotic and has increased stiffness. LOX-dependent collagen crosslinking

enhances fibrosis, integrin signalling, tumour cell intravasation and migration (153-156). Secondly, there is some evidence that LOX may localise at a site distant to tumours, forming a metastatic niche, then attracting tumour cells to their site (156). Identification of LOX at metastatic sites describe a 70-80 kDa protein, whereas pro-LOX is established to be only 48-50 kDa, suggesting a possible modification of the protein which should be examined (157). Finally, LOX may promote angiogenesis in tumours via platelet derived growth factor receptor β (PDGFRβ) stimulation, activation of Akt (Protein Kinase B), and increased vascular endothelial growth factor (VEGF) expression (158), particularly in hypoxic conditions, further facilitating tumour growth and progression (159, 160).

1.4.1.2 Lysyl oxidase propeptide (LOX-PP)

The best described role for LOX-PP, which is unique in sequence, is as a tumour growth inhibitor/tumour suppressor, and several targets for LOX-PP have been identified in breast and prostate cancer, in addition to lung and gastric cancers (161).

In breast cancer cells, LOX-PP is believed to attenuate fibronectin-stimulated focal adhesion kinase (FAK) signalling and extracellular signal-regulated kinase 1/2 (ERK1/2) activation, and inhibit Ras-signalling by direct targeting of c-raf and hsp-70 chaperone proteins (which have anti-apoptotic properties) leading to reduced ERK1/2 activation downstream, inhibiting proliferation and migration of breast cancer cells, and stimulating apoptosis (162, 163).

In prostate cancer, LOX-PP inhibits fibroblast growth factor 2 (FGF-2) binding to the DU145 prostate cancer cell lines, thereby inhibiting DNA synthesis and proliferation via the MEK/ERK and PI3K/AKT pathways (164, 165). Other studies have shown that LOX-PP is able to interact directly with, and inhibit nuclear DNA repair proteins rendering them more sensitive to the effects of ionizing radiation (166).

Although LOX-PP is generated extracellularly, the majority of molecular targets appear to be intracellular, particularly the Ras-Raf-MEK-ERK signalling pathway (163), and LOX-PP is being investigated in a variety of cell lines whereby uptake may block cancer growth and metastatic potential (157).

1.4.2 LOXL1

Lysyl-like oxidase protein 1 (LOXL1) is structurally similar to LOX; both are widely expressed and there are some similarities and overlap in enzyme function (167). LOXL1 is more specifically associated with elastogenesis and elastin maturation. It interacts closely with fibulin-5, a protein required for elastin development (168), and polymerizes tropoelastin monomers into growing elastin polymers. LOXL1 deficient mice develop pelvic organ prolapse, enlarged pulmonary alveoli and loose skin, all manifestations related to deficiency of elastic fibre formation. Vascular abnormalities are also seen but appear less severe than in LOX deficient mice (169, 170).

Genetic variants of the LOXL1 gene are prone to exfoliation syndrome/glaucoma. The true mechanism of this syndrome is poorly understood, but it is caused by excess of elastin and extracellular matrix in microscopic fibrils in numerous ocular

and non-ocular tissues and caused by excessive production and abnormal crosslinking of elastic fibres, which have been associated with polymorphisms of LOXL1 (171).

Other studies have suggested a role for LOXL1 in collagen II maturation. High expression of LOXL1 has been demonstrated in the growth plates of femurs, and significant deterioration of trabecular bone structure was seen in long bones and vertebrae of female *Loxl1*-/- mice, suggesting a role for LOXL1 in the organisation and maturation of collagen II in bones (172).

There is conflicting data for the role of LOXL1 in cancer. One study suggested that LOXL1 enhanced tumour metastases in lung cancer under hypoxic conditions (173), while another suggested that LOXL1 can inhibit Ras and ERK1/2 signalling in bladder cancer in a similar mechanism to that seen in breast cancer; more studies are required to define the role of LOXL1 in cancer (174).

1.4.3 LOXL2

LOXL2, -3 and -4 form a distinct group of LOX enzymes characterized by the presence of four scavenger receptor cysteine-rich (SRCR) domains within their N-terminal sequences (175). Although the function of these is poorly understood, they are commonly found on soluble and membrane-bound proteins, and may mediate protein-protein interactions and ligand binding (175, 176). The SRCR is attached to a highly conserved lysyl oxidase catalytic domain, the functions of which are better understood (177).

Interestingly, although the predicted mass of LOXL2 is about 84 kDa, a 100 kDa LOXL2 protein is found in both intracellular and extracellular compartments, suggesting post-translational modification (178). Similarly, a 65 kDa form of LOXL2 has been identified in the extracellular compartment of cultured cells and tissues, suggesting that proteolytic processing of the larger form may occur prior to enzyme activity (179-181), comparable to the BMP-1 cleavage of LOX and LOX-1 (138, 139). The functions of LOXL2 will be discussed in detail in 1.5.

1.4.4 LOXL3

Less is known regarding the functions of LOXL3, but it is likely to play an important role in collagen organisation and maturity, and possibly spinal development in utero. LOXL3 null mice are perinatal lethal and exhibit cleft palate and vertebral defects. Analysis of tissue demonstrated sparse collagen fibres in thoracic vertebrae, palate shelves and around columnar chondrocytes (cells essential to bone growth and development), as well as immature cross-linking of collagen in craniofacial bones and spines. Hearts, aortas, tracheae and diaphragms of mutant mice showed no apparent abnormalities, highlighting the difference in functions between members of the LOX/L enzymes (182).

In one family a missense mutation of LOXL3 has been found to cause stickler syndrome (SS), a collagenopathy characterized by arthropathy, cleft palate and vitreoretinopathy with myopia usually caused by mutations in the collagen genes *Col2a1*, *Col11a1* and *Col11a2*, suggesting a possible link between LOXL3 and collagen expression (183). Splice variants of LOXL3 have been identified; one is

initiated from a different promotor and has distinct catalytic activity and expression patterns compared with other variants. However, the relevance of these variants *in vitro* is yet to be determined; all are elevated in fibrotic disease but therapeutic agents to target LOXL3 are yet to be identified (184).

1.4.5 LOXL4

LOXL4, the last of the lysyl oxidases to be identified, is expressed in vascular tissues where it plays a role in ECM remodelling, and is regulated by the profibrotic cytokine TGF-β (185). In addition, LOXL4 expression is induced by active retinoic acid (aRA) during corneal injury, and is believed to be an essential component of the aRA dependent wound healing response (186).

Like LOXL3, LOXL4 exists in several isoforms, and there is evidence that LOXL4 splice variants have invasive and metastatic potential in some types of breast and ovarian cancer, possibly via upregulation of MMP-2 and improved ability of variant-expressing malignant cells to attach to ECM and basement membrane proteins (collagen IV and laminin (187)). In contrast, full-length LOXL4 reduces the metastatic potential of cells and delays tumour progression *in vivo*. Furthermore cells expressing full-length LOXL4 display lower MMP-2 activity and reduced attachment to matrix proteins than control cell (187).

LOXL4 expression is also upregulated in lymph node metastases and primary tissues of head and neck cancers (188, 189); the LOXL4 gene was detected in 71% of samples of mucosal head and neck carcinomas compared with only 9% of the

healthy mucosa (p=0.0002) in one study (189), and 92.7% of tumour and 97.8% lymph node tissue in another (188). While the role of LOXL4 in head and neck malignancy is not understood, in gastric cancer the protein has been shown to directly increase cell proliferation, migration and invasion, possibly via the focal adhesion kinase/steroid receptor coactivator (FAK/Src) pathway and enhancement of cell-matrix adhesion (190).

LOXL4 knock out mice have been generated, and it is hoped that their phenotype, once reported, will provide further insight into the physiological roles of LOXL4 (191).

1.5 A focus on the functions of LOXL2

Like its other family members, LOXL2 catalyses the oxidative deamination of peptidyl lysine residues, which promotes the formation of lysyl-derived cross-links in collagen and elastin (192). Primarily LOXL2 (as well as LOX) promotes cross-linking of fibrillar collagen I (79, 193), a major component of desmoplastic stroma and fibrosis, and as such has been implicated in tumour invasion and metastases, and fibrosis of the heart, lungs and liver (133, 194-196). In blood vessels and renal glomeruli, cross-linking of collagen IV by LOXL2 helps formation and stabilisation of basement membranes (181, 197, 198). In addition, LOXL2 has been involved in gene transcription, cell migration and adhesion, angiogenesis, and differentiation, demonstrating its ability to affect both extra and intracellular cell functions (180, 198-205).

Only about 50% of Loxl2-/- mice survive prenatally, and death is associated with severe heart defects such as disrupted ventricular septa and dilated hepatic vessels which were also found in 40% of surviving Loxl2-/- mice (206). Overexpression of LOXL2 caused male sterility due to inflammation, increased fibronectin, elastin and collagen deposition leading to epithelial disorganization, and fibrosis of the epididymis (206).

1.5.1 The role of LOXL2 in cancers

LOXL2 is widely overexpressed in skin cancer (206), oral cancer (207), squamous cell carcinoma (SCC) of the skin, head and neck (200, 206), cholangiocarcinoma (208), breast cancer (180, 199, 209), primary liver cancer (210) gastric (211) metastases, and in fibroblasts associated with colon cancer (212). Most of the studies in these cancers also show reduced metastases and tumour invasion with attenuation of LOXL2. Only one cancer, lung adenocarcinoma, has documented an association with downregulated LOXL2 expression (213). Numerous pathways have been highlighted as possible mechanisms for LOXL2 involvement, and it is possible that these may vary according to cancer type. It has been hypothesised that LOXL2 secreted from tumour and stromal cells may contribute to matrix stiffness, FAK activation and integrin signalling to promote cancer cell migration and aid metastasis (212, 214).

In head and neck, lung, and renal cancers, there is failure of LOXL2 downregulation, suggesting that regulatory pathways controlling expression of LOXL2 may drive metastatic disease (215-217). LOXL2 overexpression may repress the Notch1

signalling pathway, whose normal function is to reduce epidermal growth and differentiation. LOXL2 overexpression in mice was associated with increased squamous cell tumour (SCC) burden and malignant progression on exposure to chemical skin carcinogenesis, identifying LOXL2 as a potential target for SCC therapy (206).

A hypoxic tumour microenvironment is one of the most important characteristics shown to promote tumour metastasis, epithelial-mesenchymal transition and angiogenesis (218). Several studies have shown that in this environment, increased expression of Hypoxia-inducible factor 1-alpha (HIF-1α) induces upregulation of LOXL2, which represses E-cadherin responsible for mediating epithelial mesenchymal transformation (EMT) (218). This is associated with activation of vimentin and the subsequent promotion of EMT and vasculogenic mimicry (VM), both of which ultimately contribute to tumour progression (218, 219). Local invasion is thought to constitute the first event in the transition from premalignant to invasive malignant carcinomas, and this step requires tumour cells to disrupt the E-cadherin-mediated cell–cell adhesions and acquire motility, and it is frequently associated with EMT (220). Snail is a transcription factor also capable of repressing E-cadherin expression, and LOXL2 has been shown to interact directly with snail to downregulate E-cadherin and stimulate EMT and migration of cancer cells (200). In the same study, copper binding histidine residues were mutated to eliminate enzyme activity, and both active and inactive forms of LOXL2 were found to stimulate focal adhesion-associated protein kinase (FAK) driving cell migration and invasion. These studies also demonstrated a role for LOXL2 outside of its enzyme activity (200, 221),

highlighting possible functions for splice variants or proteolytic processed forms of LOXL2 which mediate intracellular activity.

There has been particular interest in LOXL2 inhibition in the treatment of breast cancer (222), where LOXL2 has been heavily implicated in tumour invasion (223) and metastases, although the mechanism is yet unclear (177). Selective inhibition of LOXL2 reduced growth of primary breast tumours *in vivo*, probably mediated by reduced angiogenesis and cancer associated fibroblast (CAF) activation (15). Dual inhibition of LOX and LOXL2 additionally reduced metastases in the lung and liver, but this effect was not achieved by LOXL2 inhibition alone (15).

LOXL2 promotes angiogenesis both within and outside the tumour microenvironment; organisation of endothelial cells into tubes requires LOXL2 expression but not enzyme activity whilst stabilisation of structures of the basement membrane and formed vessels is enzyme dependent (204, 224).

1.5.2 The role of LOXL2 in cartilage development

While LOX is demonstrated to be important in osteoblast differentiation (225), and LOXL1 implicated in organisation of collagen II fibres in bone during growth and development (170), LOXL2 knockdown studies *in vitro* show that LOXL2 expression is required for chondrocyte cell differentiation through regulation of transcription factors Snail and SOX-9 (226). In this setting, LOXL2 appears to repress Snail, a transcriptional repressor expressed at high levels during proliferative phases of chondrocyte development, with levels diminishing as type II collagen expression

increases. Overexpression of Snail blocks synthesis of type II collagen via transcriptional repression of an E box cis-acting element in its promoter (227). Thus inhibition of Snail by LOXL2 promotes collagen II synthesis during bone development and healing.

It is also believed that LOXL2, rather than Snail, promotes upstream expression of SOX-9, a master regulator of chondrogenesis which drives chondrocyte differentiation (226), highlighting a role for LOXL2 in cartilage formation, growth, and repair.

Interestingly, this study highlighted differences between LOXL2 interactions and Snail within the tumour microenvironment, and within ECM in the context of injury and fibrogenesis, which warrants further investigation.

1.5.3 Fibrosis

LOXL2 catalyses the oxidative deamination of peptidyl lysine residues, which promotes the formation of lysyl-derived cross-links in collagen and elastin, particularly collagen I. It is this catalytic activity that implicates LOXL2 in fibrotic disease, particularly that of the heart, lungs and liver. Some of its role in fibrogenesis however, may extend beyond enzyme activity, and some of the mechanisms described above may help us to understand a more complex role for LOXL2 in fibrosis.

1.5.3.1 Cardiac fibrosis

LOXL2 is upregulated in the interstitium of diseased mouse and human hearts, and results in increased TGF-β2 production through the PI3K/AKT intracellular signalling system. This triggers fibroblast to myofibroblast transformation, cell migration, and enhanced collagen deposition and crosslinking in the hypertrophic regions of stressed hearts (228) leading to interstitial fibrosis and cardiac systolic and diastolic dysfunction. In mice, antibody-mediated inhibition of LOXL2 reduced stress-induced cardiac fibrosis and chamber dilatation, improving systolic and diastolic functions (228), suggesting a therapeutic potential for individuals with heart failure of multiple aetiologies.

A similar mechanism is likely to be associated with the development of atrial fibrillation, (AF) a condition in which structural remodelling and fibrosis of the left atrium results in cardiac rhythm disturbance (229). Serum LOXL2 levels are found to be significantly elevated in individuals with AF, and correlate with the size of the left atrium (230).

Interestingly, a LOXL2 enzyme inhibitor (PXS5153, one of the compounds I investigate in liver fibrosis, see 3.2) was investigated in murine models of cardiac fibrosis, and demonstrated improvement in fibrosis by picrosirius red stain (PSR, a marker of collagen and surrogate marker for fibrosis), and mild improvement in ejection fraction in the treated mice (231). There have not yet been any clinical trials targeting LOXL2 or the LOX family in cardiac fibrosis.

1.5.3.2 Pulmonary fibrosis

Like other forms of fibrosis, pulmonary fibrosis is characterised by enhanced deposition and remodelling of the extracellular matrix (ECM), predominantly collagens I and III (232, 233). Treatment with the LOXL2 monoclonal antibody AB0023 in murine models of pulmonary fibrosis resulted in a significant reduction in both fibrosis and alveolar thickening, and was associated with a decrease in the number of activated fibroblasts in the lungs of mice. In addition, a significant reduction in the amounts of TGF-β1, endothelin-1, chemokine (C-X-C motif) ligand 2 (CXCL12) and LOXL2 was observed, as well as TGF-β signalling as measured by immunohistochemistry or tissue-based ELISA (133). A subsequent clinical trial using the same antibody in patients with idiopathic pulmonary fibrosis was halted early due to lack of efficacy (234), and has prompted another group to re-examine the role of the lysyl oxidase family in pulmonary fibrosis (235). One key finding of this study was that both LOXL1 and LOXL2 are upregulated in subjects with pulmonary fibrosis, and that expression of both proteins correlated positively with fibrillary collagen organisation (235). In addition, the use of a pan-LOX enzyme inhibitor, ß-aminopropionitrile (β-APN), reduced TGF-β induced collagen remodelling and stiffening of the ECM in vitro, but a selective LOXL2 enzyme inhibitor did not. This further supports the data that LOX family enzymes other than LOXL2 are key drivers of ECM remodelling in pulmonary fibrosis, and ongoing investigation of LOX enzymes as a potential therapeutic target.

1.5.3.3 Liver fibrosis

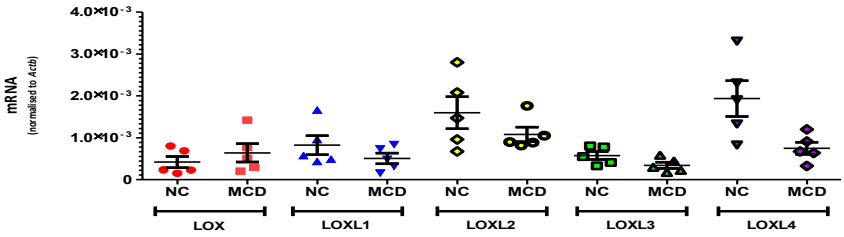
There is as yet no medical therapy which targets liver fibrosis, and so interest in LOXL2 for its potential as anti-fibrotic has grown over the years.

Early work by Vadasz *et al*. described over expression of LOX and LOXL2 in hepatocytes of patients with Primary Biliary Cholangitis (PBC) and Wilsons disease (193) (an autosomal recessive disease in which mutations of the ATP7b-copper transporter lead to excess accumulation of copper in the liver causing fibrosis and cirrhosis if left untreated (236)). This compared with little or no expression of LOX enzymes in healthy controls, and increased expression of LOX and LOXL2 was associated with collagen deposition around hepatocytes, confirming that the key role for LOXL2 in liver fibrosis was oxidation of lysine residues to form collagen cross-links (193).

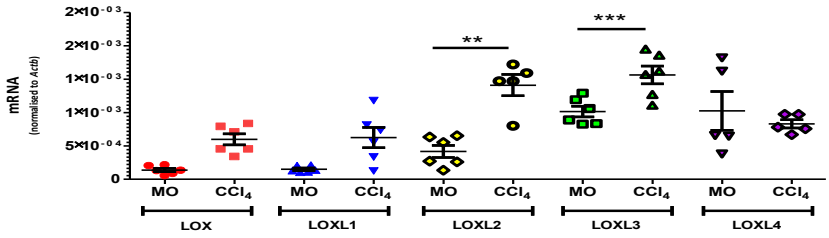
1.5.3.3.1 LOXL2 in liver fibrosis: findings from preclinical studies

Studies at Birmingham University have demonstrated consistent upregulation of LOXL2 mRNA across a spectrum of murine models of liver disease (CCl_4 and TAA induced liver injury, western lifestyle model (WLM)), except the methionine choline-deficient (MCD) diet (see Figure 1.5)

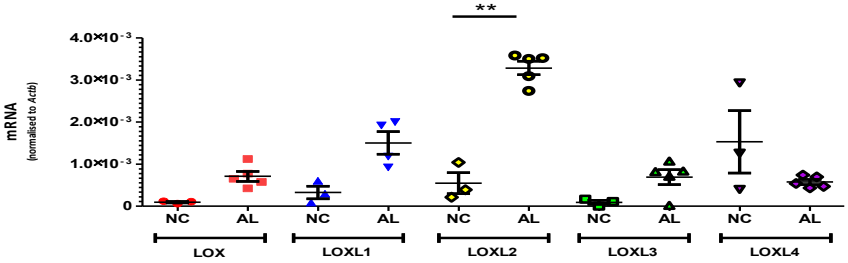
(A) MCD diet (6 weeks)



(B) CCl_4 (8 weeks)



(C) WLM (9 months)



(D) TAA (16 weeks)

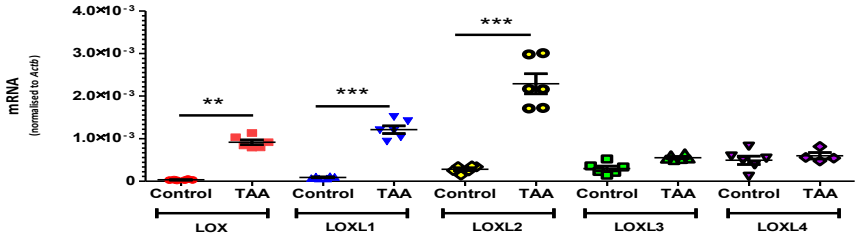


Figure 1.5 Models of murine hepatic injury drive upregulation of LOX/L expression. Expression of mRNA for LOX family members relative to beta actin housekeeping gene was performed in triplicate on groups of 3-5 mice for each model. Mice were fed an MCD diet (MP Biomedicals) ad lib for 6 weeks (A). Mice were injected twice weekly 6 weeks with either CCl_4 (1.0 mL/kg CCl_4 diluted 1:4 in mineral oil (MO) or MO alone (B). Mice were fed a diet with 45% of calories obtained from fat and 30% of the fat in the form of partially hydrogenated vegetable oil (Custom Research Diet TD.06303; Harlan Laboratories) in conjunction with fructose-supplemented drinking water (55% fructose, 45% glucose by weight at a concentration of 42 g/L) *ad lib* for 9 months. Control animals received normal chow (NC) and non-supplemented drinking water (C). Mice were given TAA diluted in orange squash (prediluted 1:5 with water) in escalating doses up to 600 mg/L by day 9 and maintained on this dose *ad lib* for 16 weeks; control mice were given squash only (D). Data were calculated by 1-way ANOVA using Dunn's Multiple Comparison Test. ** P<0.01, *** P< 0.001. Figure courtesy of Dr Emma Shepherd at the University of Birmingham.

In work by Barry-Hamilton *et al.* the expression of LOX and LOXL2 in multiple human pathological environments, including lung and liver fibrosis and the cancer microenvironment (133) was investigated. Both LOX and LOXL2 expression was demonstrated at the fibrotic disease interface in human lung fibrosis and in liver diseases such as steatohepatitis and active hepatitis C infection.

The same study showed that in CCl_4–induced liver fibrosis in mice, LOXL2 expression was associated with activated fibroblasts along fibrotic tracts. Inhibition of LOXL2 using the non-competitive allosteric LOXL2 antibody AB0023 led to reduced portoportal and portocentral bridging fibrosis using the METAVIR fibrosis scoring system, and a reduction in α-SMA+ myofibroblasts in the portoportal septa (133). Mechanistically, the levels of intracellular signal transduction molecule p-Smad3, but not TGF-β, were reduced using AB0023. TGF-β signal induction in hepatic stellate cells has been characterized as a p-Smad3–dependent process, whereby p-Smad3 transmits TGF-β signals from the cell surface to the nucleus (237). However, p-Smad3 may have additional roles related to collagen expression that are independent of TGF-β during liver injury (238), and LOXL2 may target p-Smad3 independent of TGF-β leading to enhanced fibrosis.

A later study by Liu *et al.* used the irreversible (but less specific) pan-LOX inhibitor β-APN to explore the role of CCl_4 induced liver fibrosis in mice, and demonstrated wider fibrotic septae and collagen fibrils which were loosely organized in the mice receiving β-APN compared to control mice, suggesting a more favourable pro-resolution environment (146). A reduced proportion of mature, highly cross-linked

collagen was found in the β-APN group, and there was reduced hepatic stellate cell activation measured by immunohistochemistry (IHC) for α-SMA. Gene expression of fibrosis markers *Tgfb1, Col1a1, Timp* was also reduced by pan-LOX inhibition and increased F4/80+ macrophage infiltration was seen along fibrotic septae, further confirming the role of LOX in collagen stabilization and limiting fibrosis reversal, in addition to being a potential target for pharmacological therapy (146).

The functions of LOX and LOXL2 may well overlap, as both promote cross-linking of fibrillary collagen I and are present in similar pathological microenvironments (133). However, LOXL2 is a more attractive therapeutic target, as it is more frequently associated with the pathological microenvironment, whereas LOX is widely expressed in healthy tissue (133). It is likely that for this reason that the LOXL2 targeting antibody AB0023 has been favoured for *in vitro* and *in vivo* testing, and early phase 2 trials to assess efficacy in reducing both lung (see 1.5.3.3.2) and liver fibrosis. In a 12 week model of thioacetamide (TAA) induced fibrosis in mice, the treatment group receiving 6 weeks of AB0023 from week six showed a significant reduction in fibrosis as measured by IHC for collagen I and α-SMA, picrosirius red staining, and hydroxyproline assay (195). Insoluble, highly crosslinked collagen was also reduced by LOXL2 inhibition (195). In a six week TAA model where LOXL2 antibody was given for 12 weeks at the end of injury in order to assess effects on fibrosis reversal, increased disruption of bridging and widening of fibrotic septa with splitting of fibrils was observed at 4 weeks in the group receiving AB0023 compared with vehicle, suggesting a LOXL2 blockade as a potential tool for promoting fibrosis resolution (195). Interestingly, a group receiving LOX inhibitor (M64) showed reduced

liver collagen content by hydroxyproline assay, but none of the other changes seen with AB0023 treatment.

Similar results were observed following antibody blockade of LOXL2 in models of biliary fibrosis (*Mdr2*-deficient mice or 3,5-diethoxycarbonyl-1,4-dihydrocollidine (DDC) animals) where AB0023 treatment led to significant reduction in hepatic collagen content and picrosirius red staining following morphometric analysis. These changes were not seen in mice receiving the LOX inhibitor M64. In addition to a reduction in biliary-type fibrosis, the authors suggested a possible role for LOXL2 in the ductular reaction and regulation and differentiation of hepatic progenitor cells (195). Specifically, *in vitro* and *in vivo* experiments demonstrated a preference of epithelial cell adhesion molecule (EpCAM) positive hepatocytes to differentiate towards a functional hepatocyte lineage rather than cytokeratin-19 (CK19+) fibrogenic cholangiocytes in the presence of AB0023 (195), with inhibition of the ductular reaction and myofibroblast activation (239). This study suggested that inhibiting this process may have the potential to reduce biliary fibrosis through modulation of LOXL2 in addition to reduced collagen crosslinking (see Figure 1.6).

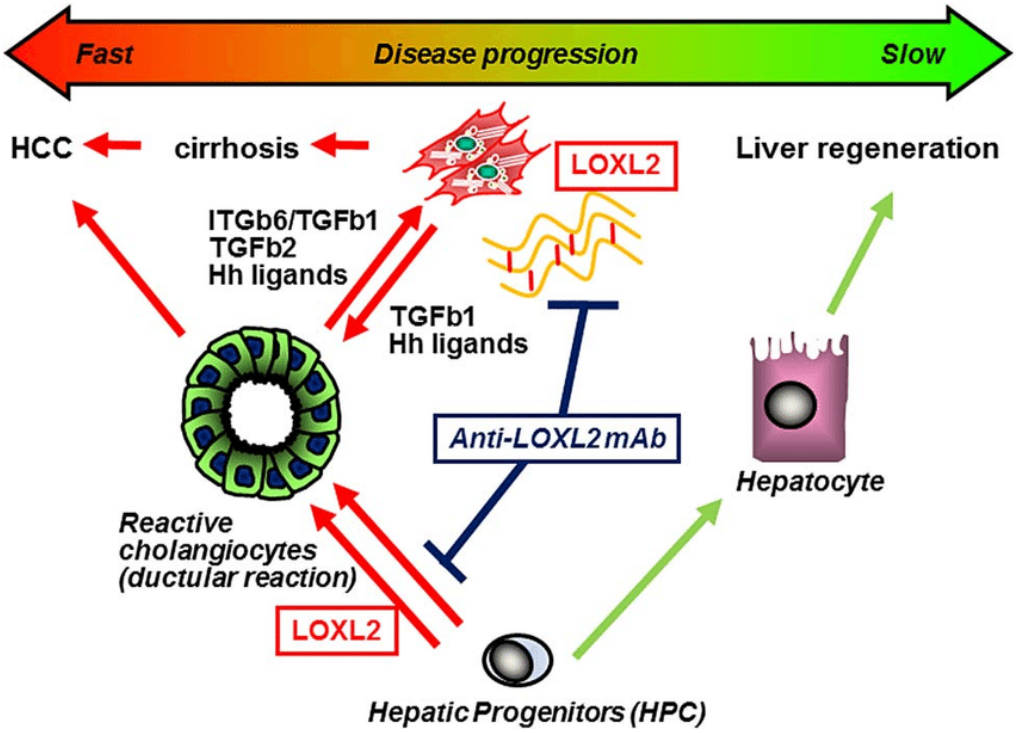
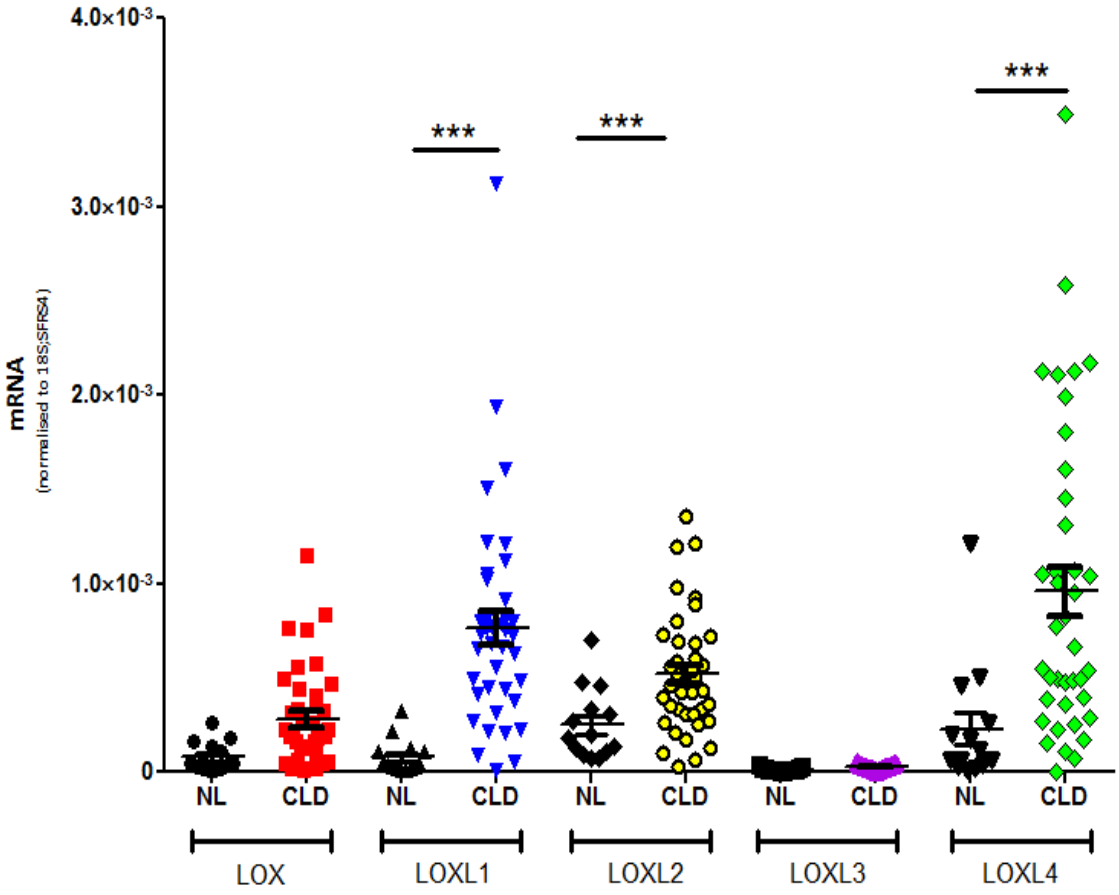


Figure 1.6 Suggested mechanism for fibrosis reduction targeting LOXL2. In addition to reduced collagen crosslinking, studies by Ikenaga *et al* suggest that hepatic progenitor cells preferentially differentiate towards a hepatocyte lineage rather than the profibrogenic cholangiocytes in the presence of LOXL2 inhibition with an monoclonal antibody Reproduced with permission from *GUT* (195).

1.5.3.3.2 Targeting LOXL2 in human liver fibrosis

LOXL2 protein expression has been demonstrated to correlate with liver fibrosis in biopsy samples of patients with Wilson's disease, PBC (193), steatohepatitis and hepatitis C (133), serum LOXL2 levels are elevated in individuals with NAFLD (240) and chronic hepatitis C, and correlate to fibrosis severity (241). Our own laboratory has demonstrated upregulated LOXL1, 2 and 4 mRNA expression across a spectrum of human liver disease and increased lysyl oxidase protein expression in liver tissue in chronic liver disease (see Figure 1.7).

A


4.0×10-3
3.0×10-3
2.0×10-3
1.0×10-3
0
mRNA
(normalised to 18S;SFRS4)
***
***
***
NL
CLD
NL
CLD
NL
CLD
NL
CLD
NL
CLD
LOX
LOXL1
LOXL2
LOXL3
LOXL4

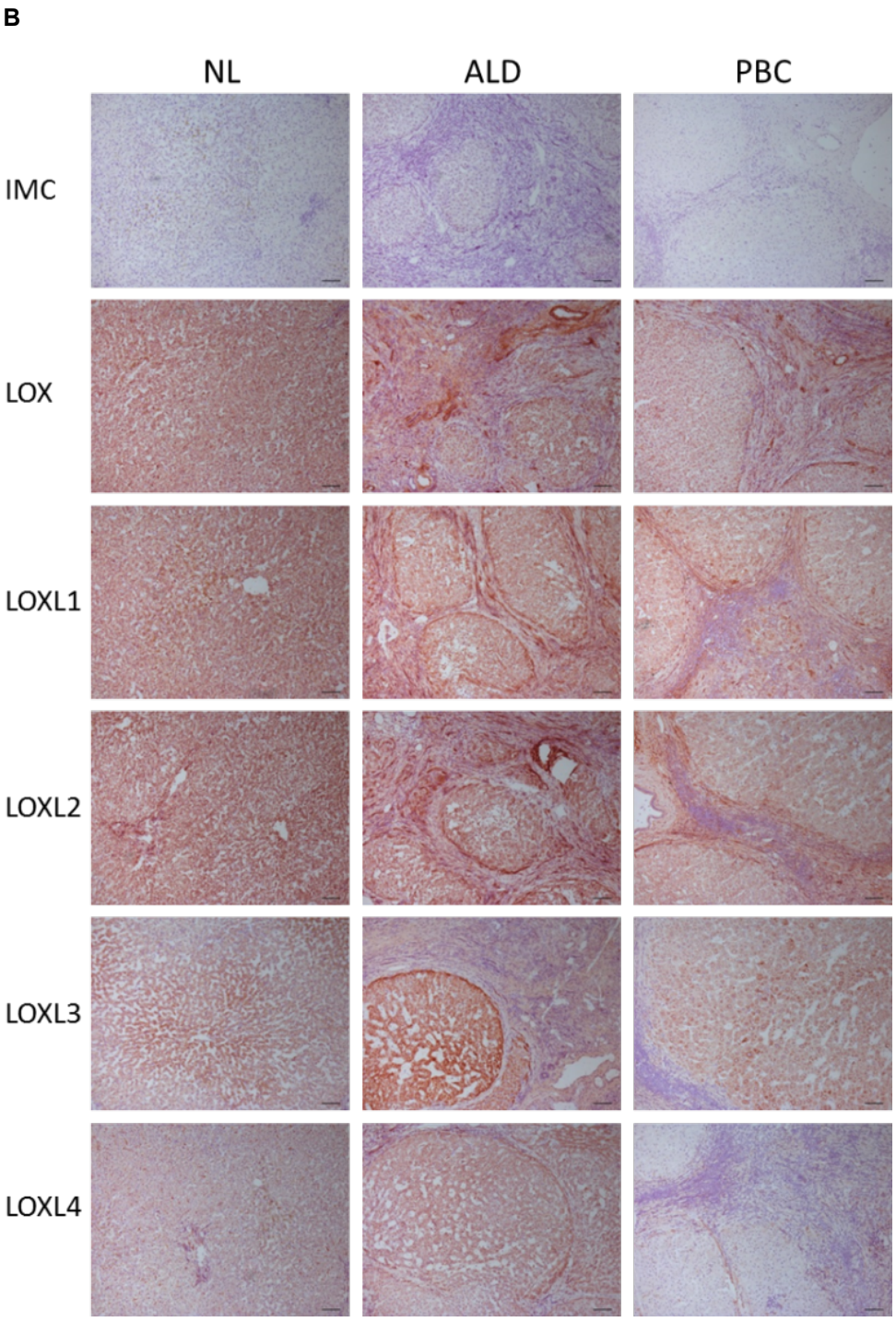


Figure 1.7 Lysyl oxidases and mRNA are up-regulated in chronic liver disease compared to normal liver controls. (A) Expression of LOXL2, 3 and 4 mRNA relative to two housekeeping genes (SRSF4 and 18S) was up-regulated in chronic liver disease (CLD) compared to normal liver controls. Data were calculated by 1-way ANOVA using Dunn's Multiple Comparison Test. *** P< 0.001. (B) The expression of lysyl oxidase proteins (stained red) was more intense in chronic liver disease (representative images from ALD and PBC tissue) than that detected in normal liver (NL). Images courtesy of Dr Emma Shepherd.

These findings, together with preclinical data, have prompted interest in targeting LOXL2 in human fibrotic disease. A human version of AB0023, a therapeutic antibody targeting LOXL2 (Simtuzumab) has now been tested in Phase II trials in patients with both PSC (NCT01672853) and non-alcoholic steatohepatitis (NASH) related fibrosis (NCT01672866). In NASH it has also been tested in subjects in combination with Selonsertib (an anti-apoptotic agent) (NCT02466516), and also in subjects with NASH related cirrhosis (NCT01672879). Used in combination with Selonsertib, no additional benefit was gained from Simtuzumab (242). The trials in NASH were terminated early due to lack of efficacy (243), and a study in PSC study also showed no benefit (243). Trials in individuals with HCV and HIV (244), myelofibrosis (245) and pancreatic (246) and colorectal cancer (247) were also negative.

Several mechanisms as have been suggested for the inefficacy of Simtuzumab. Firstly, although Simtuzumab has been demonstrated to effectively bind LOXL2 (248), its inhibitory activity may be insufficient to affect collagen cross-linkage *in vivo*, and there is as yet no marker for clinical evaluation of LOXL2 inhibition on which to test this. Secondly, LOXL2 inhibition alone may be insufficient to reduce fibrosis due to other concomitant pathways that mediate collagen cross-linkage, such as the other LOX isoforms and tissue transglutaminase. Finally, it is possible that the fibrosis in the patients studied in these trials may have been too advanced for the inhibition of collagen cross-linking to be effective or to be amenable to ECM remodelling (243).

While these outcomes in human studies are disappointing, it is possible that targeting the enzyme function of LOXL2 rather than antibody blockade will have greater potency in reducing collagen cross-linking in liver fibrosis. Given that the non-enzymatic functions of LOXL2 are yet fully understood, selective targeting of LOXL2 may be the safest option and reduce the risk of unwanted long-term side effects.

To this end, the pharmaceutical company Phamaxis (Sydney, Australia) have developed mechanism based, selective LOXL2 enzyme inhibitors, that have shown potential in limited rodent models of liver fibrosis. One of these compounds, PXS5153, has been designed to selectively inhibit LOXL2 and LOXL3, and has shown efficacy in reducing collagen content and collagen cross links in two murine models of liver fibrosis (Pharmaxis, personal communication).

PXS5153 interacts with the lysyl tyrosylquinone (LTQ) cofactor on the enzymatic pocket of LOXL2 and LOXL3 and leads to a covalently bound enzyme-inhibitor complex, irreversibly blocking enzymatic function with an apparent binding constant (Ki) 1.01 μM and a rate of inactivation (k_{inact}) of 0.2 min^{-1}. Further characteristics of PXS5153 were time dependent potency (increased inhibition with longer incubation with the enzyme), substrate competition (increasing substrate concentrations leads to reduced enzyme inhibition), and irreversible inhibition demonstrated by jump dilution experiments (231). The half maximal inhibitory concentration (IC_{50}) of PXS5153 for LOXL2 across all mammalian species was <30nM, but also inhibited LOXL3 with an IC_{50} of 45nM (see table 1). These properties are favourable compared with other

commonly used monoamine inhibitors (249, 250). A possible shortfall of the inhibitor is its short half-life, estimated at 0.6 hours in rats and 1 hour in mice (231).

Assay	IC50 (nM)
Recombinant human LOXL2	21
Recombinant mouse LOXL2	21
Recombinant rat LOXL2	15
Recombinant dog LOXL2	9
Native human LOXL2	38
Native human LOX	1790
Recombinant human LOXL1	1325
Recombinant human LOXL3	45
Recombinant human LOXL4	104
SSAO, MAO-A and MAO-B	>30000

Table 1.1: Selectivity of PXS5153 in vitro. Each value is an average of at least three experiments. Semicarbazide-Sensitive Amine Oxidase, SSAO, Monoamine oxidase-A,MAO-A, Monoamine oxidase-B, MAO-B. Table courtesy of Dr S Schilter at Pharmaxis.

To further interrogate the ability of the enzyme to inhibit oxidation of collagen lysine residues, collagen was incubated with recombinant human LOXL2 (rhLOXL2) with or without increasing concentrations of PXS5153, and the ability of the enzyme to catalyse cross-links in collagen was measured by mass spectrometry. As expected, rhLOXL2 increased collagen crosslinking, while treatment with PXS5153 prevented all crosslink formation (mature crosslinks dihydroxylysinonorleucine (DHLNL) and hydroxylysinonorleucine (HLNL), and immature crosslinks pyridinoline (PYD) and deoxypyridinoline (DPD) (231).

In a 6 week CCl_4 induced model of liver fibrosis in rats, PXS5153 was given in escalating doses and reduced collagen content by hydroxyproline assay, picrosirius red stain, and mRNA expression of collagen I. Low dose enzyme inhibitor also reduced immature and mature collagen cross-links, as measured by ELISA or mass spectrometry, presumably by inhibiting oxidation of lysine residues, rendering collagen in the fibrotic environment more prone to degradation (231, 251). I also performed tissue analysis from this model and the data is included in this thesis (see section 3.3)

Similar findings were made with the same compound in a mouse model of non-alcoholic steatohepatitis (NASH) induced by streptozotocin/high fat diet. Collagen cross-linking was less convincingly reduced, but hepatocyte ballooning was significantly reduced using the NAFLD activity score (NAS) according to the Kleiner criteria, and fibrosis was reduced using collagen staining with PSR (231).

Interestingly, PXS5153 was also investigated in murine models of cardiac fibrosis and demonstrated improvement in fibrosis by PSR and mild improvement in ejection fraction in the treated mice (231)

Another LOXL2 enzyme inhibitor, PXSS2B, produced by Pharmaxis has been tested in mouse models of diabetic nephropathy, which is characterised by excess ECM in glomeruli and the tubulointerstitial space. Treatment with PXSS2B reduced albuminuria, expression of glomerular fibronectin and tubulointerstitial collagen I, and

ameliorated glomerulosclerosis highlighting a possible role for LOXL2 in diabetic nephropathy (252).

The same company have developed other selective LOXL2 enzyme inhibitors and are being investigated in preclinical trials for NASH, pulmonary, and kidney fibrosis, the results of which are as yet unavailable.

One of these compounds has been modified to improve bioavailability from oral administration (PXS5153 and PXS5338K, see table 2, equivalent data in rats also available). Previous versions of this compound, and the LOXL2 antibody AB0023, could be delivered only by intravenous injection, and so the new compound is a more attractive therapeutic option. I have examined the efficacy of this latest compound, PXS5338K, in addition to two related compounds, in reducing liver fibrosis across a variety of murine models.

PK parameter	PXS5153 (mouse, oral 5 mg/kg)	PXS5338K (mouse, oral 10 mg/kg)
$AUC_{0\text{-}last}$ (hr*ng/mL)	158	82
C_{max} (ng/mL)	114	84
$T_{1/2}$ (h)	0.6	Not available
Oral bioavailability, F (%)	41	4

Table 1.2: PK profiles of PXS5153 and PXS5338K in mice. Data courtesy of Pharmaxis

1.6. Murine models of liver fibrosis

1.6.1 Pan-lobular fibrosis

Several murine models of liver fibrosis have been developed for experimental purposes. Administration of the hepatotoxin carbon tetrachloride (CCl_4), by intramuscular (I.M.), intraperitoneal (I.P.), subcutaneous (S.C.) injection, or the oral route, induces perivenular ballooning of hepatocytes at six hours, inflammatory infiltration, and centrilobular necrosis at 24–72 hours, followed by collapse of existing collagen architecture, leading to *de novo* collagen synthesis and early fibrosis after one week (82, 253). Following twice weekly injections for 4 weeks, mature collagen fibrils bridging vascular structures are observed, mimicking the advanced human fibrosis that occurs in conditions such as alcohol-related liver disease, haemachromatosis or non-alcoholic liver disease (82). Criticisms of this model, however, are manifold; firstly, the response to the same dose of CCl_4 in individual animals can be variable, impeding assessment of responses to intervention; secondly, mortality can be as high as 60% within the first 2 weeks of treatment; thirdly, only mice (not rats) administered with CCl_4 are prone to developing HCC, the reason for which is unknown. Finally, any model where centrilobular necrosis is the predominant feature is a poor model for biliary diseases in which periportal fibrosis dominate (253).

Administration of thioacetamide (TAA), either via I.P. injection, or orally, is believed to be a safer method of inducing liver fibrosis in both rats and mice than CCl_4, being associated with less mortality, and resulting in regenerative nodules and fibrosis which may be more representative of human fibrosis (76, 254, 255). TAA is a

hepatotoxin which is converted into toxic oxygenized metabolites by cytochrome P450 (CYP) enzymes in the liver (256, 257), triggering the production of reactive oxygen species (ROS), oxidative stress and hepatocyte damage, and activation of hepatic stellate cells (256). Oral or I.P. administration for 12 weeks results in macronodular cirrhosis separated by thick connective septa (5) with the oral route facilitating absorption via the gut and direct delivery to the liver via the portal system, potentially limiting extrahepatic effects. An additional benefit of *ad libitum* delivery is that hepatotoxicity may be self-limiting; those animals with severe injury have a reduced appetite and thereby reduce their own exposure to TAA in drinking water, with the benefit of reduced mortality (255). The caveat to *ad libitum* delivery is that results between animals can be more variable (255).

A less commonly used model is induced by dimethynitrosamine (DMN), a hepatocarcinogen that causes fibrosis within four weeks of twice weekly I.P. injection, with activation of HSCs, Kupffer cells and expression of profibrotic cytokines (258). However, DMN has mutagenic and carcinogenic properties, and so interpretation and analysis of fibrosis experiments may be complicated by involvement of mutated signalling pathways (259).

1.6.2 Biliary Fibrosis

Models for biliary fibrosis are even more limited; ligation of the common bile duct (BDL) is one commonly used model. Bile duct obstruction results in increased biliary pressure, inflammation and cytokine secretion, thus generating cholestasis, proliferation of biliary epithelial cells, increased expression of fibrogenic markers, and

accumulation of B cells and T cells in the portal tracts (260). The applicability of this model is limited by early mortality due to perforation of the bilioperitoneum (261), rupture of biliary cysts or the gall bladder, which tends to occur 5–6 weeks after BDL, favouring short-term experiments only (262). The rapidly progressive nature of the biliary fibrosis seen in BDL is also associated with substantial proliferation of bile ducts rarely seen in man (263).

Feeding mice a diet supplemented with 3,5-diethoxycarbonyl-1,4-dihydrocollidine (DDC) feeding can be used to study Mallory body formation (seen in alcoholic liver disease), but cholestatic serum markers also become significantly elevated in these mice and a strong ductular reaction can be observed. Histologically, a pericholangitis is observed, with infiltration of inflammatory mononuclear cells and activation of periductal myofibroblasts, causing biliary fibrosis that resembles sclerosing cholangitis in humans (264).

Multi-drug resistant 2 (*Mdr2-/-)* mice are deficient in the canalicular phospholipid flippase, and spontaneously develop liver injury due to the absence of phospholipid from bile, causing disruption in tight junctions and basement membranes in bile ducts, leakage of bile into the portal tract, and periportal biliary fibrosis (263). By 4 weeks of age, picrosirius red staining demonstrates accumulation of peribiliary extracellular matrix and peribiliary α-SMA immunoreactivity in portal fibrotic regions (263). By 8 weeks, BALB/c *Mdr2-/-* mice demonstrate moderate bridging fibrosis and by 12 weeks this becomes severe with thickened collagen septa. However, there is significant variability between species whereby the FVB strain develops significantly

less fibrosis and never truly develops bridging of collagen septa; hydroxyproline content reaches only ~25 µg per 100 mg liver compared with ~ 90 µg/100 mg liver in BALB/c mice (265). The Birmingham liver laboratory has previously demonstrated that C57Bl/6 mice develop similar fibrosis to BALB/C animals, data that I have revalidated (see chapter 4), and so this model was used to explore the potential of LOXL2 inhibition in biliary fibrosis on a C57Bl/6 background.

1.6.3 Diet–induced fibrosis

Other commonly used models are the methionine-deficient and choline-deficient (MCD) diet, the high fat, fructose, and cholesterol and cholate diets, which tend to mimic non-alcoholic steatohepatitis (NASH) and take a long time to develop fibrosis.

Given the expectation that the compound being tested would have an antifibrotic effect, the models used to assess the effect of LOXL2 enzyme inhibition were those in which fibrosis is the predominant histological feature, and were accessible, reproducible, and most closely reflect the diseases that the drug is expected to target.

1.7. Hypothesis

LOXL2 enzyme inhibition reduces liver fibrosis in mice.

1.8. Aims and Objectives

The aim of my research was to assess the efficacy of selective LOXL2 enzyme inhibitors on liver fibrosis and regeneration, to determine the potential of LOXL2 inhibition as a treatment option for patients with advanced liver disease.

Two murine models of liver fibrosis were developed on which to test selective LOXL2 inhibitors designed by Pharmaxis Inc. (Sydney, Australia; PXS5303 and PXS5153). Both models were developed under contract at Pharmalegacy (Shanghai, China) and for each model (CCl_4 in rats and TAA in mice), tissue was sent for analysis and preliminary data collection (results in this report). A later developed compound, PXS5338K, also a LOXL2 enzyme inhibitor, is then retested in our own models of liver fibrosis, using *Mdr2-/-* mice, thioacetamide (TAA) induced liver injury and during in-vitro studies. My objectives were to:

- Establish the degree of liver fibrosis achieved in the mouse models (those completed at Pharmalegacy and in our own murine models). This will be achieved primarily by:
  - Measurement of collagens using IHC on paraffin and frozen sections of liver tissue
  - Measuring expression of proteins upregulated during fibrogenesis
- Examine the effect of LOXL2 inhibition on liver injury, cell differentiation, fibrosis and fibrosis resolution, in two models of murine liver fibrosis; thioacetamide (TAA) induced liver injury, and *Mdr2-/-* mice. The following methods are used:

- Comparison of liver biochemistry from serum of treated mice vs mice receiving vehicle at sacrifice
- IHC of liver sections from mice treated with PXS5338K or vehicle
- Expression of fibrosis associated genes by qPCR.

• Establish whether the compound has any effect on inflammatory cell recruitment to the liver. This is achieved by:
  - Isolation of lymphoid and myeloid cells at sacrifice and comparison of populations using flow cytometry.
  - Identification of inflammatory cells using IHC on paraffin sections of liver tissue.
• Assess the effect of PXS5338K on fibroblast activation and migration in vitro, via:
  - Scratch wound assays
  - Collagen contraction assays
  - Magnetic resonance spectroscopy (MRS) of extracellular matrix from fibroblasts exposed to PXS5338K to quantify the degree of collagen crosslinking.

This will consolidate current understanding of the role of LOXL2 inhibition in liver fibrosis, and establish whether it may have potential in treatment of human liver disease.

2. Materials and Methods

2.1 Murine models for preliminary analysis, developed by Pharmalegacy (Shanghai, China): the use of thioacetamide and carbon tetrachloride to induce liver fibrosis

Two murine models of liver fibrosis were developed on which to test PXS5303, a compound designed to inhibit LOXL2. The models were developed by Pharmalegacy (Shanghai, China) and run according to local and international industry standard, as described in their report to Pharmaxis (read, not published). Samples were shipped to Birmingham for further analysis.

2.1.1 Thioacetamide (TAA) induced liver fibrosis in mice

20 eight-week old BALB/c mice were administered with 200 mg/kg TAA thrice weekly via intraperitoneal injection (I.P.) for 12 weeks. From week 9, ten mice additionally received vehicle orally (P.O.), and 10 mice received PXS5303 P.O. once daily for the remaining 3 weeks. Livers were sectioned, snap frozen in liquid nitrogen, and placed at -80˚C for later processing, or fixed in 10% neutral formalin (Sigma-Aldrich®) for paraffin embedding and sectioning.

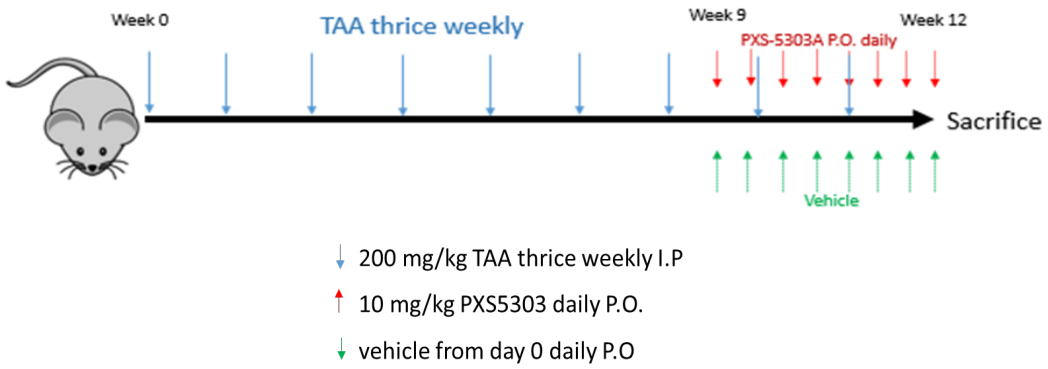


Figure 2.1: TAA model in mice. BALB/c mice were given a regimen of 12 weeks of TAA at a dose of 200 mg/kg via intraperitoneal injection (I.P.), in addition to vehicle orally (P.O.) from week 9 (group 4B), or PXS5303 (group 4C), orally from week 9.

2.1.2 Carbon tetrachloride (CCl_4) induced liver fibrosis in rats

From day 0, 4-6 week old Sprague Dawley (SD) rats were orally administered with CCl_4 0.25 µL/g (formulated as 2.5 µL/g of CCl_4 olive oil solution), 3 times per week for 6 weeks, to induce liver fibrosis. Thereafter, concurrent to the same regimen of CCl_4, rats were administered with vehicle P.O, low dose PXS5153 at 3 mg/kg daily for 6 weeks, or from week 4, high dose PXS5153 at 10 mg/kg daily for 2 weeks. 15 rats received each of the above regimens and in addition 6 rats received sham control. Once rats had been sacrificed the liver was dissected and one lobe submerged in RNA later (Thermo Fisher Scientific) solution as quickly as possible. Samples were stored at 4°C overnight and frozen afterwards at -80°C. The remaining livers were perfused, sectioned and snap frozen in liquid nitrogen and placed at -80°C for further storage. The right liver lobe was fixed in 10% neutral formalin (Sigma-Aldrich) for paraffin embedding and sectioning.

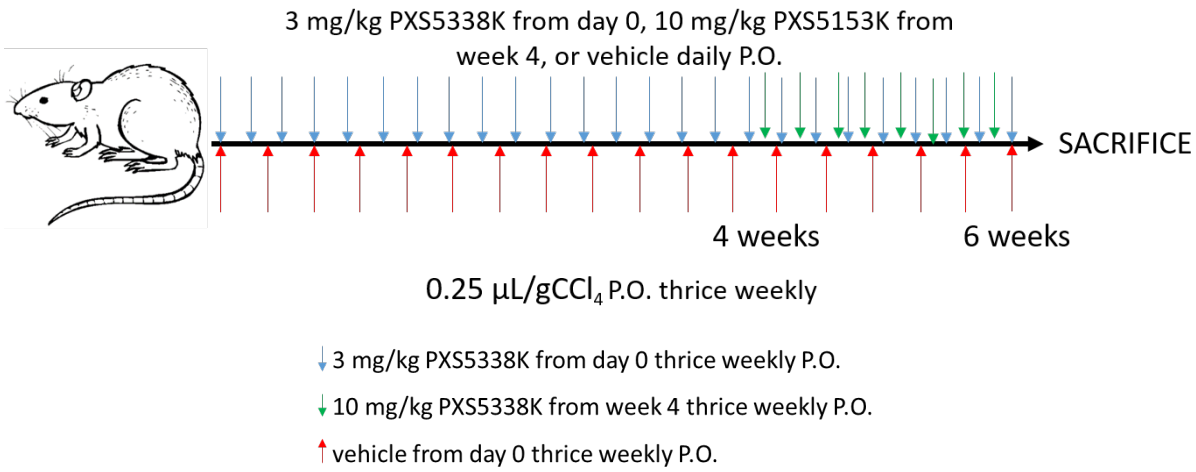


Figure 2.2 CCl_4 model of fibrosis in rats. Sprague Dawley rats were orally administered with vehicle or 0.25 µL/g CCl_4 from day 0, 3 times per week for 6 weeks, in addition to either vehicle, low dose PXS5153, or high dose PXS5153 from week 4.

2.2 Development of murine liver injury models in Birmingham for use in testing the efficacy of LOXL2 inhibitors

Two models of liver fibrosis that have been previously established locally and induce liver fibrosis in mice, namely TAA administered orally *ad libitum*, and *Abcb4*$^{-/-}$, known more commonly as *Mdr2-/-* mice, were used to test PXS5338K as a potential anti-fibrotic, and to assess its effect during fibrosis resolution.

2.2.1 Animal Husbandry

Male C57Bl/6 mice were purchased from Jackson Laboratory and acquired at an age of 6-8 weeks. *Mdr2*-/- C57Bl/6 mice originated from embryos (gifted from Professor Lohse; Austria) which had been transferred into the uterus of wild-type C57Bl/6 females and stock derived from offspring. Homozygotes were exclusively used, so genotyping was not deemed necessary. Friend virus B (FVB) *Mdr2*-/- mice were bred from the C57Bl/6 strain at the University of Birmingham Biomedical Services Unit.

All mice were housed and cared for at the University of Birmingham Biomedical Services Unit by standard care protocols. All procedures were carried out in accordance with the Animals (Scientific Procedures) Act 1986, UK, under the Home Office licence held by Patricia Lalor, P2DF9DB6E, and underwent ethical review prior to approval and enactment. Male only C57Bl/6 mice were used for experiments using TAA, which started at age 8-10 weeks.

2.2.2 A study of PXS5338K in *Mdr2* knock out mice

Both FVB and C57Bl/6 strains of *Mdr2-/-* mice develop progressive liver injury and fibrosis. A pilot study using 6 FVB *Mdr2*-/- was undertaken to assess the tolerability of 10 mg/kg PXS5338K in 6 FVB *Mdr2*-/- mice. Because this dose was poorly tolerated, a further study was carried out to assess a lower dose of 3 mg/kg which was tested in 14 healthy C57Bl/6 mice aged 6-8 weeks, and found to be better tolerated.

Subsequently, the experiment was repeated using 41 C57Bl/6 *Mdr2*-/- mice, which have a tendency to develop more advanced fibrosis than the FVB strain (265). The methods used to assess PXS5338K in *Mdr2*-/- mice was otherwise the same for both experiments, and are discussed in this chapter.

Thirty-six male and female C57Bl/6 *Mdr2*-/-, aged 9 weeks, received either PXS5338K at a dose of 3 mg/kg thrice weekly (from a stock solution of 0.6 mg/ml), or vehicle (phosphate-buffered saline, Sigma-Aldrich) thrice weekly, for 3 weeks. The number of gavages that could be performed in this model was restricted to a total of

9 under the animal licence used. Both vehicle and PXS5338K was administered using a 1 ml syringe and 20 gauge x 30 mm disposable plastic feeding tubes (Harvard Apparatus). Five age-matched mice were used as a control to assess any unexpected impact of gavage on the mice. Two mice were culled before nine gavages could be administered; one mouse appeared to aspirate at gavage (instantly unwell following administration of compound) and a second mouse bit off the plastic gavage needle and so was immediately culled. The mice were clinically assessed prior to each gavage procedure, and weighed daily to instruct correct dosing and monitor health. Mice had access to normal chow diet and drinking water *ad libitum* during the full 12-week period. Weight loss of up to 20% was deemed acceptable in the absence of other clinical signs of distress.

Mice were sacrificed age 12 weeks, 3 days after their final dosing (gavage took place on Monday, Wednesday and Friday of each week, and mice were culled on the following Monday after the final dose on Friday, see Figure 2.3). Tissue was harvested for analysis as described in section 2.2.5.

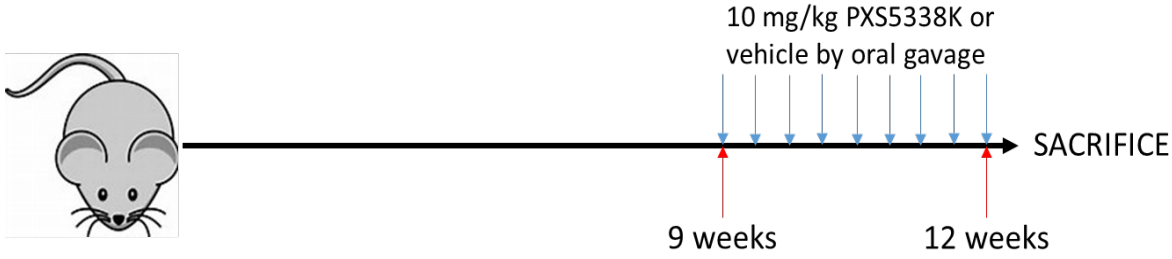


Figure 2.3: Study of PXS5338K in *Mdr2-/-* knock out mice. Nine week old *Mdr2-/-* mice were gavaged with either vehicle or inhibitor thrice weekly for 3 weeks, receiving a total of nine gavages before sacrifice.

2.2.3 PXS5338K in TAA induced liver fibrosis

A model of TAA-induced hepatic fibrosis has been developed at the University of Birmingham Biomedical Services; for this reason, a pilot study was not undertaken. This model demonstrated safe and reproducible liver fibrosis following 16 weeks of TAA *ad libitum* in drinking water. Despite the limitations associated with a lengthier animal model, a shorter duration of injury such as 12 weeks was believed to demonstrate a less consistent liver injury, with no added mortality associated with a longer 16 week model. This method of injury was replicated in two separate experiments, firstly to assess PXS5338K during liver injury, and in a second experiment, to assess its efficacy in promoting fibrosis resolution once liver injury has ceased.

2.2.3.1 Method 1: Model of chronic hepatic injury induced by 16 weeks of *ad libitum* TAA in drinking water and administration of PXS5338K from week 10.

Mice were housed and provided chow as per usual Biomedical Services Unit protocols, but their drinking water was substituted for thioacetamide (TAA, Sigma-Aldrich) solution. To acclimatise the mice to the change, mice were given TAA in 1:5 diluted fruit squash (Robinson's orange, single strength, no added sugar) at a dose of 100 mg/L for 3 days, and then 300 mg/L for 3 days, followed by 600 mg/L for the rest of the duration. TAA stock solution was prepared at a concentration of 20 mg/ml.

From week 10, 15 mice received PXS5338K via oral gavage at a daily dose of 3mg/kg (from stock solution made up to 0.6 mg/ml), and 15 mice received vehicle (PBS); an equivalent volume of PBS according to weight was given. Daily gavage

was given for 6 weeks, concurrent to ongoing ad libitum access to TAA in drinking water, and animals were sacrificed at week 17. Mice were weighed and clinically assessed for signs of distress daily; a weight loss of up to 20% was deemed acceptable in the absence of other clinical signs of distress. Upon sacrifice, tissue was collected for analysis as described in section 2.2.5.

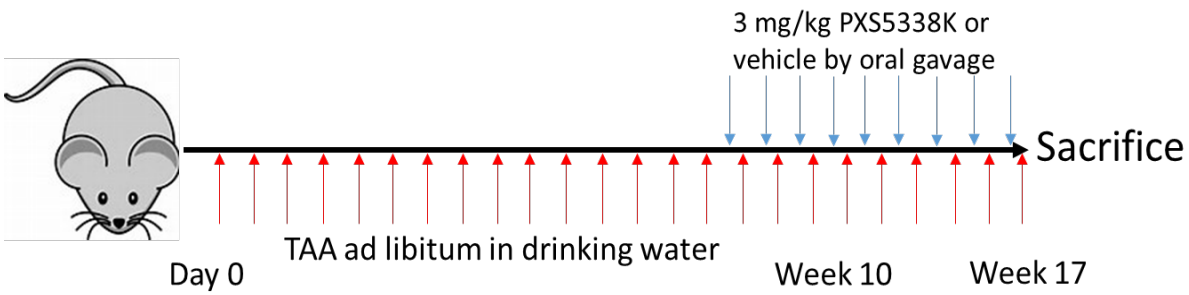


Figure 2.4 TAA model for liver fibrosis. TAA was given for 16 weeks to induce liver fibrosis, and 3 mg/kg PXS5338K or vehicle was administered by oral gavage for the final 6 weeks.

2.2.3.2 Method 2 (fibrosis resolution): Chronic hepatic injury was induced following 16 weeks of *ad libitum* TAA in drinking water, after which TAA was withdrawn and PXS5338K was administered for 2 weeks.

30 mice were housed and provided normal chow, but their drinking water was substituted for TAA solution, slowly escalating the concentration up to 600 mg/L, as described in section 2.2.2. At the beginning of week 17, orange squash containing TAA was replaced with drinking water, and 15 mice received PXS5338K via oral gavage at a daily dose of 3mg/kg, as described in 2.2.3.1, while the remaining 15 mice received an equivalent volume of vehicle (PBS). Daily gavage was given for 2 weeks, and animals were sacrificed at week the beginning of week 19. Mice were weighed and clinically assessed for signs of distress daily; a weight loss of up to 20% was deemed acceptable in the absence of other clinical signs of distress.

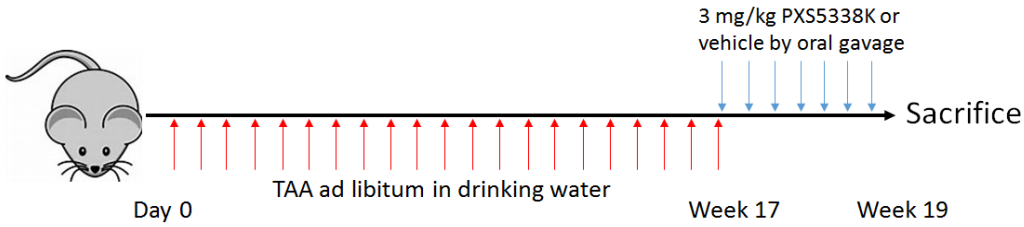


Figure 2.5: Testing PXS5338K in fibrosis resolution. TAA was given for 16 weeks then exchanged for normal drinking water; PXS5338K or vehicle was given for 2 weeks to assess efficacy in fibrosis resolution.

2.2.4 Power calculations

Analysis of results from the TAA-induced model of liver injury permitted power calculations estimating the number of mice to be used in each experiment. Calculations showed that 14 mice were required (7 to receive compound and 7 vehicle) to show a median 25% reduction of % area PSR stain from 4 to 3% ($p = 0.05$). Given that a higher % PSR was expected in our TAA model and some deaths were expected (either TAA or gavage induced), a total of 30 mice were used for the experiments of TAA induced liver injury, and up to 40 for the *Mdr2-/-* model of fibrosis (given that a lower concentration of compound was to be given over a shorter period of time).

2.2.5 Mouse sacrifice and collection of tissue for analysis

Upon completion of an experiment, mice were subject to cardiac puncture under terminal anaesthesia by isofluorane, by which up to 1000 µl of blood was aspirated through a 23-25-gauge needle with an appropriate syringe, and collected in a 1.5 ml Eppendorf tube. The mice were immediately sacrificed by cervical dislocation, and death confirmed. Abdominal contents were exposed by sleeve laparotomy and

reflection. The portal vein was cut to allow subsequently flushed contents to escape the circulation. The thorax was then exposed by carefully incising through the rib cage, avoiding damage to underlying organs. The heart was identified and injected slowly with 10ml of phosphate buffered saline using a 26-gauge needle in order to flush the liver. Swelling and pallor of the liver confirmed adequate flushing. The liver was subsequently surgically dissected from the abdomen, and the gallbladder surgically removed. The left lateral lobe of the liver was placed in Roswell Park Memorial Institute (RPMI, Gibco®) culture media containing 2% fetal bovine serum (FBS, Life Technologies®), the right lateral lobe was placed in formaldehyde, to be subsequently prepared for formalin-fixed paraffin embedded tissue sectioning. The other lobes were snap frozen in liquid nitrogen for various subsequent uses: the right median lobe was used for preparing acetone fixed frozen sections on glass slides, and the other lobes for molecular biology including RNA isolation and Western Blotting.

The clotted blood was spun on a bench-top micro-centrifuge at maximum speed for 10 minutes. The serum supernatant was aspirated and re-spun under the same settings to clarify the supernatant from any cell debris. 200 µL of serum was then diluted at a ratio of 1:5 with 0.9% normal saline for immediate measurement of markers of liver injury aspartate aminotransferase, alanine aminotransferase, bilirubin and bile acids. The remaining serum was stored at -80°C.

2.2.5.1 Extraction of leukocytes from mouse liver and flow cytometry

2.2.5.1.1 Isolation of murine hepatic leukocytes using Optiprep

The previously isolated left lobe (see methods section 2.2.5) was macerated through a 70 µm strainer using a 5ml syringe plunger and the homogenate transferred into a 15 ml falcon tube and made up to 15 ml RPMI on ice. The samples were centrifuged at 800 x *g* at 4°C for 5 minutes. The resulting pellet was resuspended 10 ml prepared cold RPMI, divided equally into 5 ml and then overlayed onto 7 ml Optiprep solution (240 ml made up from 63.9 ml Optiprep (60% solution of iodixanol in sterile water, Sigma-Aldrich) made up with 176.1 ml sterile PBS). The tubes were centrifuged at 1000 x *g* for 25 minutes at RT (with no brake).

To isolate cells (lymphocytes and monocytes) at interface, 3 ml of fluid containing cells was carefully removed from the interface of both tubes using a sterile plastic pipette, and transferred into a new 15 ml tube, pooling cells from the same liver that had been separated. The sample was topped up to 15 mls with prepared cold RPMI and then centrifuged at 800 x *g* at 4°C for 5 minutes. The cells were washed by resuspension in PBS and spinning at 2000 x *g* 4°C for 5 minutes.

The cell pellet was resuspended in 500 µl cold, sterile PBS. 100 µl cell suspension from each sample was transferred into a clean Eppendorf and the total volume divided equally for unstained and live/dead isotype controls. 50% of the total volume to be used for live/dead stain was transferred to a Grant QBT2 heat block for 4 minutes at 65°C before mixing back with the total volume to be used for live/dead staining. The unstained cells suspension sample was fixed with 200 µl 1% formalin

(2.7 ml of 37% Sigma stock formaldehyde in 100 ml PBS) and stored in a cold room until analysis. The remaining samples were added to a curved bottomed Sarstedt™ 96 well plate, and 200 μl/well added per liver sample for both lymphoid and myeloid staining panels). The plates were spun at top speed for 3 minutes in a plate centrifuge.

To each sample (except isotype controls, IMCs), 50 µL live dead fixable viability dye (1:1000 in PBS, Thermo Fisher Scientific) was added under darkened conditions, and the suspension mixed. The plate was covered to protect it from light and left on ice for 30 minutes.

The cells were washed twice with sterile MACS buffer solution (made up of PBS, 1mM ethylenediaminetetraacetate (EDTA) and 2% FBS) by centrifuging at 1000 x *g* for 3 min in the plate centrifuge. 50 µL of previously prepared master mix containing antibodies (see table 2.2 below) was added to cells from each liver sample for both the lymphoid and myeloid panels, and 50 µL isotype control mastermix for both the lymphoid and myeloid panels was added to the appropriate mixed sample cells. The plate was incubated on ice for 30 minutes in the cold room. Finally, 150 μl cold MACS buffer was added to all tubes and the cells washed twice, as before, and fixed in 200 μl 1% formalin until analysis.

2.2.5.1.2 Preparation of compensation beads for single colour staining for both lymphoid and myeloid panels

1 μl of relevant antibody was added to one drop of Aqua compensation beads (Thermo Fisher Scientific) for each antibody, the suspension pulse vortexed, and then the beads were covered with foil to protect them from light, and incubated on ice in the cold room for 30 minutes**.**

Finally, 1-2 ml cold MACS buffer was added to each suspension of beads and antibody prior to washing twice by centrifuging at 2000 *x g* 4°C for 5 minutes, and resuspended in 400-500 μl MACS buffer prior to use.

The following day, after gentle vortexing, the samples were centrifuged, resupended in 400μl cold MACS buffer, and filtered prior to analysis. (CyAn ADP 3-laser, 9-colour flow cytometer; Beckman Coulter Inc, USA). Unlabelled cells were used to define appropriate forward- and side-scatter voltages/gain, and single-colour antibody labelling using compensation beads permitted colour compensation. Data analysis was performed using Summit software v.4.3 (Dako, USA).

Antibody	Supplier	Catalogue No.	Concentration	Source	Isotype	Working dilution
Lymphoid Panel						
Brilliant Violet 510™ Anti-Mouse CD3 Antibody	BioLegend	100233	0.2 mg/ml	Rat	IgG2b, κ	1:25
Anti-Mouse CD4 APC	eBioscience	17-0041-81	0.2 mg/ml	Rat	IgG2b, κ	1:100
Anti-Mouse CD8a PerCP-Cy5.5	eBioscience	45-0081-80	0.2 mg/ml	Rat	IgG2a, κ	1:100
Brilliant Violet 421™ Anti-Mouse CD19	BioLegend	115537	0.2 mg/ml	Rat	IgG2a, κ	1:100
PE/Dazzle™ 594 Anti-Mouse CD25	BioLegend	102047	0.2 mg/ml	Rat	IgG1, κ	1:40
Alexa Fluor(R) 488 Anti-Mouse CD49b (pan-NK cells)	BioLegend	108913	0.5 mg/ml	Rat	IgM. κ	1:200
Myeloid Panel						
PE Anti-Mouse F4/80	BioLegend	123109	0.2 mg/ml	Rat	IgG2a, κ	1:20
Anti-Mouse CD11b Alexa Fluor® 488	eBioscience	53-0112-80	0.5 mg/ml	Rat	IgG2b, κ	1:100
Brilliant Violet 421™ Anti-Mouse Ly-6C	BioLegend	128031	0.2 mg/ml	Rat	IgG2c, κ	1:40
APC Anti-Mouse Ly-6G/Ly-6C (Gr-1)	BioLegend	108411	0.2 mg/ml	Rat	IgG2b, κ	1:200
CD45 mAb PerCP-cyanine 5.5	eBioscience	45-0451-82	CLR067	Rat	IgG2b, κ	1:200
Isotype Controls						
Isotype Control, Brilliant Violet 510™	BioLegend	400645	0.2 mg/ml	Rat	IgG2b, κ	-
Isotype Control, APC	eBioscience	17-4031-82	0.2 mg/ml	Rat	IgG2b, κ	-
Isotype Control, PerCP-Cyanine5.5	eBioscience	45-4321-80	0.2 mg/ml	Rat	IgG2b, κ	-
Isotype Control Brilliant Violet 421™	BioLegend	400536	0.2 mg/ml	Rat	Rat IgG1, κ	-
Isotype Control PE/Dazzle™ 594	BioLegend	400446	0.2 mg/ml	Rat	Rat IgG1, κ	-
Isotype Control Alexa Fluor 488	BioLegend	400811	0.5 mg/ml	Rat	IgM. K	-
Isotype Control PE	BioLegend	400508	0.2 mg/ml	Rat	IgG2a, κ	-
Isotype Control Alexa Fluor 488	eBioscience	53-4031-80	0.5 mg/ml	Rat	IgG2b, κ	-
Isotype Control Brilliant Violet 421™	BioLegend	400725	0.2 mg/ml	Rat	IgG2c, κ	-

Table 2.1: Antibodies used for flow cytometry

2.3 Assessment of liver fibrosis and inflammation

A combination of staining techniques and quantitative real-time polymerase chain reactions (qPCR) was used to assess the degree of liver fibrosis and inflammation as described below.

2.3.1. Haematoxylin and Eosin Staining

Liver tissue sections embedded in paraffin wax were cut to a thickness of 3 μm and mounted onto glass microscope slides (X-tra adhesive, Leica) using a heated water bath and stored at room temperature until subsequently required. The slides were de-waxed by serial rinsing in xylene thrice, followed by 99% ethanol thrice, and rehydrated in water twice. Each rinse/wash was undertaken for 3 minutes.

Slides were placed in Harris haematoxylin stain (PFM Medical) for 4 minutes, then in water for 2 minutes, and differentiated in 1% acid alcohol for 30 seconds. They were then washed in water for 2 minutes, then Scott's Tap Water (PFM Medical) for 30 seconds and then in water again for a further 2 minutes before being stained in 1% eosin aqueous (PFM Medical) for 1 minute. The slides were then washed in water for 4 minutes before being serially dehydrated in 99% ethanol for 3 minutes thrice, followed by clearing in xylene for 3 minutes thrice. The slides were mounted with coverslips using non-aqueous DPX mountant (Sigma-Aldrich).

2.3.2. Immunohistochemistry

Paraffin embedded sections were de-waxed by serial rinsing in xylene thrice, followed by 99% ethanol thrice, and washed in water twice. Each rinse/wash was

undertaken for 3 minutes. Frozen sections were air dried for 20 minutes at room temperature and fixed in acetone for 5 minutes. A wax pen was used to draw a boundary around the sections on each slide, and the slides placed in a humidified chamber. Endogenous peroxidase activity was blocked by incubating sections with 150 µl of peroxidase blocking solution (Dako REAL) for 20 minutes in the humidified chamber, with constant rocking. Slides were then washed twice in Tris-buffered saline (TBS, Sigma-Aldrich) or in phosphate-buffered saline (PBS, Fisher Scientific) containing 0.1% Tween-20 (Sigma-Aldrich) (TBS-T/PBS-T). Washing was performed by applying enough TBS-T or PBS-T to cover the sections, and leaving to incubate for 5 minutes, with constant rocking. Antigen retrieval was then undertaken for paraffin embedded sections: 10 ml of concentrated high pH antigen unmasking solution (0.5 M EDTA and sodium hydroxide; pH 8) was mixed with 990 ml of deionised water in a plastic bucket and pre-heated at high power in a microwave oven for 5 minutes. The slides were immersed in the pre-warmed solution, and heated at high power in the microwave for 15 minutes. The slides were then allowed to passively cool at room temperature for 20 minutes. The slides were then twice washed in buffered saline (TBS-T or PBS-T) as described above. Non-specific antibody binding was then blocked by applying 150 µl of x1 casein buffer solution (from x10 stock casein buffer (Vector) diluted in TBS/PBS) to the sections, and incubating in a humidified chamber for 20 minutes with constant rocking. The casein buffer solution was then tipped off. When staining for α-SMA, a separate protocol was subsequently followed using a mouse on mouse blocking reagent (see below). For all others, at this stage, the primary antibody (150-200 µl), diluted to the required concentration in either PBS or TBS (according to which was being used for wash

steps), was added to the section, and left to incubate at room temperature in a humidified chamber for 1 hour, with constant rocking.

The sections were then washed twice in buffered saline as previously described, followed by incubating with the relevant horseradish peroxidase conjugated (ImmPRESS Peroxidase Anti-Rat (mouse adsorbed) IgG (Vector)) secondary antibody for 30 minutes at room temperature in a humidified chamber for 30 minutes. The sections were then washed twice in buffered saline as previously described. The peroxidase substrate used was either diaminobenzidine (DAB), or NovaRed peroxidase solution (Vector Laboratories). The sections were incubated with 200 µl of either DAB or NovaRed substrate long enough to stain the positive control brown, or deep red, before washing rapidly in water. The sections were then counterstained by incubating with 200 µl of filtered Mayer's haematoxylin for 15-20 seconds. The sections were then washed in a cold-water bath for 2 minutes with agitation, and then in a warm-water bath for 2 minutes with agitation. The slides were serially dehydrated in 99% ethanol thrice, followed by clearing in xylene thrice. Each rinse was undertaken for 3 minutes. The slides were mounted with coverslips using non-aqueous DPX mountant (Sigma-Aldrich).

ntibodies used in IHC with a summary of agents used.

Supplier	Catalogue No.	Concentration	Source	Paraffin / Frozen	Isotype	Working dilution	Antigen retrieval (pH)	Wash	Substrate	Not
eBioscience	14-0415	0.5 mg/ml	Rat	Paraffin	IgG2b	1/200	HIGH	TBS	DAB	
Bio-Rad	MCA497G	1.0 mg/ml	Rat	Paraffin	IgG2b	1/200	HIGH	TBS	DAB	
Sigma-Aldrich	A5228	0.5 mg/ml	Mouse	Paraffin	IgG2a	1/200	HIGH	TBS	DAB	MOM kit used - blocking steps
BD Bioscience	553084	0.5 mg/ml	Rat	Paraffin	IgG2aκ	1/200	LOW	TBS	Nova-Red	
Abcam	Ab34710	1.0 mg/ml	Rabbit	Paraffin	IgG	1/200	LOW	TBS	Nova-Red	
Abcam	Ab7778	1 mg/ml	Rabbit	Frozen	IgG	1/200	LOW	TBS	DAB	
Abcam	Ab9535		Rabbit	Paraffin	IgG	1/25	LOW	TBS	DAB	
Cell Signalling	#9661		Rabbit	Paraffin	-	1/300	HIGH	PBS	DAB	
Abcam	Ab71916	1 mg/ml	Rabbit	Paraffin	IgG	1/100	HIGH	PBS	DAB	
Abcam	Ab185966	1.197 mg/ml	Rabbit	Paraffin	IgG	1/1000	HIGH	PBS	Nova Red	
Millipore	AB9260		Rabbit	Paraffin	IgG	1/1000	LOW	TBS	DAB	Additional block horse serum; p antibody resusp & 2.5 %Goat se
Abcam	Ab27478	0.2 mg/ml	Rabbit	Paraffin	-	-				
eBioscience	14-4031	0.5 mg/ml	Rat	Paraffin	-	-				
Dako	X0942	0.1 mg/ml	Mouse	Paraffin	-	-				

2.3.2.1 Staining for α-SMA

The use of a mouse α-SMA antibody to stain murine liver tissue slices necessitated addition of a mouse blocking agent to reduce non-specific binding of the antibody to the sections. The protocol described above was followed until addition of primary antibody as indicated. At this stage, the sections were washed in TBS-T twice. Endogenous biotin, biotin receptors, and avidin binding sites were blocked using an Avidin/Biotin blocking kit (Vector Laboratories) according to the manufacturer's instructions. Endogenous mouse antibody was then blocked using a Mouse on Mouse Blocking Reagent (Vector Laboratories Mouse on Mouse Kit). Two drops of Mouse on Mouse (M.O.M) Immunoglobulin Blocking Reagent were added to 2.5 ml of TBS and 100 µL of the final solution was added to each slide and incubated for 1 hour. The sections were twice washed in TBS-T, then incubated for 5 minutes in M.O.M diluent (prepared by adding 600 µL protein concentrate to 7.5 ml TBS). Excess M.O.M diluent was removed from the slides by tapping them gently on their sides, and the primary antibody was added to each slide (diluted in M.O.M diluent to the appropriate concentration) and allowed to incubate for 40 minutes. The slides were washed twice in TBS-T. The secondary antibody, M.O.M Biotinylated Anti-Mouse IgG Reagent (prepared by adding 10 µL stock solution to 2.5 ml M.O.M diluent) was added to each slide and left to incubate for 10 minutes. The sections were twice washed in TBS-T, and Vectastain Elite ABC reagent (Avidin and Biotinylated horseradish peroxidase [HRP] Complex, Vector Laboratories), was added to bind the primary/secondary antibody complex, and left to incubate for 5 minutes. Preparation of Vectastain Elite ABC reagent was by adding 2 drops of reagent A (Avidin DH) to 2.5 mls of TBS and gently mixing. Two drops of reagent B

(biotinylated enzyme) were added to the preparation, which was gently mixed and allowed to stand for 30 minutes prior to use.

After 5 minutes incubation, the sections were twice washed in TBS-T. The NovaRed peroxidase solution (Vector Laboratories) was prepared, added to the sections and left to incubate long enough for staining to develop (5-10 minutes). The sections were then counterstained with Mayer's haematoxylin, washed, then dehydrated and mounted as described previously.

2.3.3. Staining for collagens with picrosirius red (PSR)

Formalin-fixed paraffin embedded sections cut to 3 μm were used. The slides were de-waxed by serial rinsing in xylene thrice, followed by 99% ethanol thrice, and washed in water twice. Each rinse/wash was undertaken for 3 minutes. Enough distilled water was applied to each section to cover, using a plastic Pasteur pipette. The water was then tipped off, and replaced with 200 μl of 0.5% phosphomolybdic acid (Sigma-Aldrich), and left to incubate in the humidified chamber for 5 minutes with rocking at room temperature. The slides were then transferred to a slide rack and bathed in picrosirius red solution (100 mg of Direct Red 80 (Sigma-Aldrich) in 100 ml of saturated picric acid (Sigma-Aldrich)), with rocking at room temperature for 90 minutes. The slide rack was then removed from the picrosirius red, and serially rinsed in 2 baths of acidified water (0.5% glacial acetic acid (Sigma-Aldrich)) with agitation for 30 seconds each, followed by a bath of 0.1% (w/v in acidified water) fast green FCF (Sigma-Aldrich) for 1 minute (not used for rat slides), followed by 2 further serial rinses in acidified water (15 seconds each). Serial bathing in fresh 99% ethanol

thrice then rapidly dehydrated the slides – 30 seconds in each ethanol bath with agitation. The slides were finally transferred to xylene for 5 minutes before being mounted with coverslips using non-aqueous DPX mountant (Sigma-Aldrich).

2.3.4. Morphometric analysis of PSR and IHC stained liver tissue sections

Stained sections on slides were scanned and captured in their entirety by Axio Scan Z1 slide scanner (Zeiss), and acquired in a stitched format at a 10x objective. For PSR, collagen I and collagen III, several low and high resolution images were taken and results compared. Each .czi file generated by this process was then opened in Zen 2 Blue (Zeiss) Image processor, and zoomed in to show approximately 70% of the whole slide at 85x magnification (each slide containing one liver lobe) on the screen. This image was then captured using the snippet tool on Microsoft Windows 10, which would allow any aberrant staining, or large white vascular trunk areas, to be excluded. This provided a representative image to process, which was saved as a .png file. The resolution was sufficient to differentiate stained from negative control samples. The .png file was then opened in Image J (NIH/Fiji) software, and converted to an RGB stack image. The image was then set to the green channel for PSR stained slides, and the blue channel for DAB stained slides. An automatic colour threshold was obtained, and adjusted to ensure no aberrant positive areas were demarcated. The positive area was then calculated by the software as a % area of the total field of view and recorded. An arithmetic mean of the values estimated the overall % area covered. The same process was repeated using 5 random images from each slide taken at higher, 120x magnification; the two methods were compared and no difference in results was observed.

For EpCAM, SOX-9 and myeloperoxidase, quantitative analysis was performed by manually counting the number of stained cells within a fixed area. Gridlines were applied to the image captured on Zen 2 Blue (Zeiss) Image processor, and stained cells were counted within five fixed area squares chosen at random, and the mean number of cells per square calculated.

2.3.5. Real time quantitative polymerase chain reaction (qPCR)

Real time quantitative polymerase chain reaction was used to assess expression of genes related to liver inflammation or fibrosis, and the house-keeping gene glyceraldehyde-3-phosphate dehydrogenase (*Gapdh*, mice) or beta-2-microglobulin (*B2m*, rats).

2.3.5.1 RNA extraction

The RNeasy Mini Kit (Qiagen) was used to extract RNA from frozen murine hepatic tissue. All instruments were pre-treated with UV-light for 20 minutes prior to use. 20-30 mg of supplied mouse liver tissue was placed into a sterile GentleMACS M tube (Miltenyi Biotec) containing 600 µl of RLT buffer supplemented with 10 µl/ml of 2-mercaptoethanol (Sigma-Aldrich). Samples were then mechanically homogenised and disrupted on a GenleMACS-processor (Miltenyi Biotec) using program RNA.01_01. The homogenate was transferred to a 1.5 ml Eppendorf tube, and spun at top speed in a bench-top micro-centrifuge for 3 minutes. The supernatant was extracted (the debris discarded) and mixed with one volume (approximately 600 µl) of 70% ethanol. The sample was then transferred to an RNAeasy Spin Column and centrifuged at 21,000 *x* g for 20 seconds. The flow through collected in the collection

tube was discarded, and 350 µl of RW1 buffer was added to the spin column and centrifuged at 21,000 *x* g for 20 seconds. The flow-through was discarded and 80 µl of RNase-free DNase solution (Qiagen) was carefully added to the spin column membrane and left to incubate for 15 minutes at room temperature. On completion, 350 µl of RW1 buffer was added to the spin column and centrifuged at 21,000 *x* g for 20 seconds. The flow-through was discarded. 500 µl of RPE buffer was then added to the spin column and centrifuged at 21,000 *x* g for 20 seconds. This was then repeated, with the flow through being discarded on each occasion. The spin column was then transferred to a new collection tube and centrifuged for 2 minutes at 21,000 *x* g. Upon completion the spin column was transferred to a sterile UV treated 1.5 ml Eppendorf tube, and 50 µl of sterile nuclease free (pre-warmed to 37^{o}C in a water bath) was added to the spin column membrane and centrifuged at 21,000 *x* g for 1 minute. The eluate was then replaced on to the spin column membrane and re-centrifuged at 21,000 *x* g for 1 minute. The spin column was then discarded, leaving the eluate (RNA) for analysis and use. The purity and yield of RNA was subsequently analysed using a Nanophotometer, and the RNA stored at -80°C.

2.3.5.2 cDNA synthesis

All instruments were pre-treated with UV-light for 20 minutes prior to use. Total RNA (4.5 µg) from each sample was made up to 10.5 µl with sterile nuclease-free water in a mini Eppendorf tube. 0.5 µl of random primers (Promega) and 1 µl of dNTPs (Bioline) were then added to each sample, and the sample tubes transferred to a pre-heated plate and heated for 5 minutes in a bench-top thermo-cycler at 65°C. The sample tubes are then transferred to ice, and 4 µl of 5x First Strand Buffer

(Invitrogen), 2 µl of dithiothreitol (Invitrogen) and 1 µl of nuclease free water was added to each sample. The samples were left to incubate for 2 minutes at 25°C, before transferring the tubes back to ice. Finally 1 µl of SuperScript-II (Invitrogen) was added to each sample, and mixed gently before using a bench-top thermo-cycler to heat samples to 45°C for 50 minutes, and then 70°C for 15 minutes. The samples were then stored at -80°C until ready for use. Control samples were also prepared in which either the RNA or reverse transcriptase enzyme were omitted from the reaction mixture (RT controls).

2.3.5.3 Real time quantitative polymerase chain reaction (qPCR)

All instruments were pre-treated with UV-light for 20 minutes prior to use. Taqman gene expression assays (see table 2.3 below) were used for qPCR, and results analysed by relative quantification of gene yields against reference house-keeping gene (*Gapdh* for mice, *B2m* for rats). Lightcycler 384 well multi-well plates (Roche) were used for qPCR, with a total working volume of 10 µl for each well. Each well consisted of 0.3 µl of Taqman gene probe (Thermo Fisher Scientific), 5.0 µl of 2x reaction Taqman MasterMix II (Applied Biosciences), 3.7 µl of nuclease free water and 1 µl of cDNA. Each sample and gene was tested in either triplicates or quadruplicates, and control reactions which contained PCR grade water in place of cDNA, or RT controls (prepared as described above) were also run. The plates were processed using a LightCycler 480 Instrument II (Roche). The PCR acquisition program consisted of polymerase activation (95°C for 10 minutes), then denaturing and annealing over 40 cycles (95°C for 15 seconds, 60°C for 1 minute), with the fluorescence being recorded at the end of each cycle.

The cycling curves for each reaction were analysed, and sample results with obvious errors (high background noise, or no discernible curve) were discarded. A threshold to analyse cycling threshold (Ct) was manually set in the bottom third of the curve, above any background noise. These Ct values were used to measure relative differences between samples using the ΔΔCt method, where:

- Target = gene of interest
- Reference = control house-keeping gene
- Treatment = intervention of interest
- ΔCt (sample) = Ct (target) – Ct (reference);
- ΔΔCt = (ΔCt (target, untreated) – Ct (reference, untreated)) – (Ct (target, treated) – Ct (reference, treated))

The ratio of the target gene in sample of interest against a control sample was calculated by taking $2^{-\Delta\Delta Ct}$.

Table 2.3: Gene expression assays used for qPCR

Target gene (mouse)	Gene expression assay
Col1a1	Mm00801666_g1
Col3a1	Mm01254476_m1
Acta2	Mm00725412_s1
Eln	Mm00514670_m1
Mmp2	Mm00439498_m1
Mmp3	Mm00440295_m1
Mmp9	Mm00442991_m1
Mmp13	Mm00439491_m1
Timp1	Mm01341361_m1
Cxcl2	Mm00436450_m1
Tnfa	Mm00443258_m1
Il1rn	Mm00446186_m1
Sox-9	Mm00448840_m1
Tgfb1	Mm01178820_m1
Lox	Mm00495386_m1
Loxl1	Mm01145738_m1
Loxl2	Mm00804749_m1
Loxl3	Mm00442953_m1
Loxl4	Mm00446385_m1
Gapdh	Mm99999915_g1
Target gene (rat)	**Gene expression assay**
Co1a1	Rn01463848_m1
Col3a1	Rn01437681_m1
Acta2	Rn01759928_g1
Elastin	Rn01499782_m1
Mmp2	Rn01538170_m1
Mmp3	Rn00591740_m1
Mmp9	Rn00579162_m1
Mmp12	Rn00588640_m1
Timp1	Rn01430873_g1
Timp2	Rn00573232_m1
Tgfb1	Rn00688966_m1
Pdgfrb	Rn00709573_m1
Loxl2	Rn01466080_m1
B2m	Rn00560865_m1

2.4 In vitro assessment of the effect of PXS5338K on fibroblasts

2.4.1 Isolation of cell lines and cell culture

The human hepatic stellate cell (HSC) line LX2 was a gift of S. Friedman, Mount Sinai School of Medicine, New York, New York, USA. The Murine 3T3 cell line was purchased from Sigma-Aldrich. Cells were screened routinely for mycoplasma contamination.

2.4.1.1 Isolation of fibroblasts

A slice of human liver explant tissue (approximately 30 g) was finely chopped and mixed with 20 ml sterile PBS and 5ml collagenase (10 mg/mL, Sigma-Aldrich). The mixture was incubated 37° C for 25-45 minutes depending on texture of tissue. The digest was the strained through fine mesh into a fresh sterile beaker and washed several times with PBS. It was made up to a total volume of 200 ml using PBS, aliquoted between 8 sterile universal containers, and centrifuged at 2000 x g for 5 minutes.

The 8 resulting pellets were re-suspended into 4 universal containers and centrifuged again at 2000 x g for 5 minutes. The 4 pellets were re-suspended into 2 universal containers and centrifuged at 2000 x g for 5 minutes, finally re-suspending the pellets into a single universal container in 24 mls PBS.

Next, 3ml of 33% Percoll, Sigma-Aldrich, (33ml of stock + 67ml 1x PBS) was added to each of eight 15ml conical bottomed tubes, followed by 3ml of 77% Percoll (77ml of stock + 23ml 1x PBS) underneath the 33%. 3 mls of cell suspension was layered

onto the Percoll gradients and centrifuged at 2000 x g or 25 minutes with brake speed set at 0. The top layer of cells was removed and discarded, and the band of cells at the interface of the Percoll gradient was removed and combined with another aliquot into 1 universal (4 universals in total). The volume in each universal was made up to 25 ml with PBS, mixed well, and centrifuged at 2000 x g for 5 minutes. The supernatant was tipped off 2 pellets combined into 1 universal container, the total volume made up to 25 mls with PBS and again centrifuged at 2000 x g for 5 minutes.

The resulting pellets were combined into a 15 ml conical bottom tube, made up to 14 mls with PBS and centrifuged as previously. The pellet was resuspended in 500ul PBS, 50 µL anti-human epithelial antigen (HEA, ProGen®, 10ug/mL stock) 125 was added, and the solution incubated at 37°C for 30 minutes with intermittent agitation.

The solution was then made up to a volume of 14 mls with PBS and centrifuged at 2000 rpm for 5 minutes. The pellet was resuspended in 500 µL ice cold PBS, and 10 µL cold Goat-anti-mouse IgG Dynabeads were added (Thermo Fisher Scientific), and the mixture incubated at 4 °C for 30 minutes with constant agitation.

6 ml of ice cold PBS was added, the solution mixed, and placed in a magnet for 2 minutes. With the tube still in the magnet the supernatant was removed and transferred to a second 15 ml conical bottom tube (tube 2) for endothelial and fibroblast isolation. The remaining cells that were attracted to the magnet by means of the Dynabeads were processed further for biliary epithelial cells (BEC).

Tube 2 was then placed in the magnet for a further 2 minutes to remove any residual beads. While the tube was still in the magnet the supernatant was removed into a fresh conical bottom tube and made up to a volume of 14 ml with PBS. The mixture was centrifuged at 2000 x g for 5 minutes, the supernatant removed and the pellet resuspended into 500ul of PBS. 10 µL of anti-CD31 coated Dynabeads was added and the mixture incubated at 4^{o}C for 30 minutes with continual agitation.

6 ml of cold PBS was added, mixed, and the tube was placed in a magnet field for approximately 2 minutes. With the tube still in proximity to the magnet the supernatant was removed and decanted into a clean conical bottomed tube for fibroblast isolation. The volume was made up to 14 mls with PBS and the sample was centrifuged at 2000 x g for 5 minutes. The supernatant was removed and the pellet subsequently resuspended in fibroblast medium and left to incubate at 37 °C and 5% CO_2 in a Corning® 75 cm^2 flask.

2.4.1.2 Culture and passage conditions

Culture media varied according to cell types and are shown in table 2.4. All cultures were examined daily by and cell morphology, the colour of medium and density of cells was observed. Once the cells became densely populated they were separated and divided into two or three 75 cm^2 flasks, depending on the estimated population. Adherent cells were passaged using an appropriate volume of Thermo Fisher Scientific TrypLE (2-4 mL according to the cell type and size of flask). Specifically, old media was discarded and adherent cells washed with PBS before adding warm (37^{o}C) TrypLE. The flask was then agitated gently by hand to enable cellular

detachment. Once detachment was complete, sterile PBS was added to the suspension, and the final mixture collected and centrifuged at 1000 x *g* for 5 minutes. The cell pellet was then re–suspended in appropriate media before reseeding for further culture. Generally 3T3 and LX2 cells were used up to passage 10, and primary human fibroblasts up to passage 3.

Cell viability was assessed when necessary using Trypan–blue (Life Technologies) exclusion and cells counted using a haematocytometer (MerckMillipore, UK).

2.4.1.3 Freezing and storing cells

If cells were not being used for experiments, they were preserved in liquid nitrogen. Once pelleted, cells were resuspended at a density of 106/mL in freezing media (95% FBS+5% DMSO (Sigma-Aldrich, UK)) and transferred to cryovials and placed in a MrFrost freezing container (Wessington Cryogenics, UK) for a 24 hours at –80oC to permit gradual cooling and prevent crystal formation within the cytoplasm. Cells were transferred to liquid nitrogen for long-term preservation. When needed, cells were removed from storage, thawed, washed in media, centrifuged to remove cellular debris and resuspended in appropriate media.

Cell type	Base media	Supplementation
Primary human fibroblasts	DMEM*	16% FBS + 1% PSG
3T3	DMEM*	10% FBS + 1% PSG
LX2	DMEM*	2% FBS + 1% PSG

Table 2.4 Cell culture media

2.4.2 Assessment of the effect of PXS5338K on collagen crosslinking in vitro

LX2 cells, 3T3 cells, and primary human fibroblasts were detached from tissue culture flasks using TrypLE (Thermo Fisher Scientific), then resuspended in appropriate media and plated at concentrations of 125 000, 150 000 or 250 000 cells/well in uncoated 6-well plates. The volume was adjusted to 3 ml using the appropriate cell culture media (see table 2.4) in the absence or presence of 30 nM or 3000 nM PXS5338K in triplicate. Cells were incubated at 37°C and 5% CO_2 for one, two, or three weeks.

At the end of each time period, the media was carefully removed from each well, the cells were washed with PBS, and the cells and ECM removed from the well using a cell scraper (Costar®), in 1 ml of distilled water. Cells were stored in cryovials at -80°C and later dry frozen using a ScanVac (LaboGene™) for shipment and further analysis. Further analysis was carried out by Pharmaxis to assess the presence of immature and mature collagen crosslinks; quantitation of the immature crosslinks dihydroxylysionorleucine (DHLNL), the trivalent mature crosslinks pyridinoline (PYD) and deoxypyridinoline (DPD) in the prepared samples was measured by ultra-performance liquid chromatography-electrospray ionization tandem mass spectrometry (UPLC-ESI-MS/MS). Quantification of hydroxylysinonorleucine (HLNL) was not possible which precluded calculation of the collagen maturity ratio.

2.4.3 Scratch wound assay

Prior to commencing, the lid of the Cell-IQ (CMTechnologies) plate was sterilised and placed in a UV box with irradiation for 20 minutes.

Cells (human fibroblasts and human LX2 stellate cells) were trypsinised and resuspended to a concentration of $1x10^5$ cells/mL in appropriate media, as above. Cells were seeded into a 24 well plate using 1mL/well, equivalent to 100,000 cells/well.

Plates were left in an incubator overnight at 37ºC and 5% CO_2 to permit cell adhesion and formation of a confluent monolayer. The following day, the center of the well was scratched from top to bottom using a 10 uL pipette tip, using a fresh tip for each well to avoid 'carry-over' of debris. The media was then removed from each well and replaced with 1 mL PBS, pipetted onto the wall of the well so as not to disturb the scratch created. The PBS in the plate was gently swirled to suspend the dead and/or damaged cells, and removed, one row at a time to avoid the cells drying out.
1 mL of media containing 0 nM, 300 nM, 1000 nM or 3000 nM of PXS5338K, or PDGF-BB (Peprotech, UK) was transferred into each well, and then PBS added into the spaces between the wells (to reduce evaporation in the Cell-IQ). The Cell-IQ lid was secured in place with electrical tape and the plate placed into the Cell-IQ system (CM Technologies) for 24 hours at 37^{o}C, 5% CO_2. Real-time cell images were captured every 15 minutes using Imagen software version 2.8.12.0 and analyzer version 3.3.0.

2.4.4 Collagen contraction assay

LX2, murine 3T3 fibroblasts, or human fibroblasts, were trypsinised and resuspended to a concentration of 3 x 10^5 cells/mL in appropriate culture media (see above). Bovine collagen (Thermo Fisher Scientific) was diluted to a concentration of 3mg/mL

using PBS, and 200 µL per well was added to a 400 µL per well cell suspension. Sterile, filtered 1M NaOH was promptly added (6 µL per well) and the solution gently mixed. 500 µL of this solution was seeded into 24-well plates (or 250 µL for 48-well plate) and allowed to set at 37°C. After 30 minutes, the gel was released from the edges of the well using a 10 µL pipette tip and 500uL appropriate culture media either alone, or containing increasing concentrations (1000-1000000 nM) of PXS5338K, 10 nM endothelin-1, 10 ng/ml PDGF-BB (Peprotech), or 10 mM 2,3-Butanedione monoxime (Sigma-Aldrich) was added to the wells. Gels were photographed at various time-points and ImageJ used to measure gel area and assess contraction.

2.5 Statistical analysis and graphical representation

The distribution of continuous variables was assessed via the Kolmogorov-Smirnov method. Non-parametric data are presented using the median values unless otherwise specified. The Mann-Whitney (MW) test was conducted when comparing between two independent groups, and analysis of variance through Kruskal-Wallis (KW) test with Bonferroni-Dunn post-hoc correction for multiple groups using GraphPad Prism version 7.02.

3. Results I: Testing PXS5303A, a LOXL2 enzyme inhibitor in a Thioacetamide (TAA) model of liver fibrosis

3.1 Introduction

The thioacetamide (TAA) model of liver fibrosis is believed to mimic more closely chronic liver injury such as NAFLD, compared with CCl_4 or biliary models; injury is induced over a longer period of time and animals gradually develop regenerative nodules and bridging fibrosis (255), as discussed in 1.6.1. For this reason, it was chosen as a model on which to test PXS5303A, one of the compounds developed by Pharmaxis designed to inhibit LOXL2 enzyme activity. Liver tissue was obtained from mice treated according to fibrosis models developed by Pharmalegacy (Shanghai, China), as described in 2.1. All mice had received TAA with or without LOXL2 enzyme inhibitor; no tissue was available from TAA untreated mice as a control.

The primary aim was to evaluate whether there had been any reduction in liver fibrosis in PXS5303 treated mice, but the effect of PXS5303 on inflammatory cell recruitment, cell apoptosis, proliferation and differentiation was also interrogated, primarily because the potential effect of LOXL2 inhibition, and specifically these compounds, on these processes, was not yet known.

3.2 Testing PXS5303, a LOXL2 enzyme inhibitor, in a Thioacetamide (TAA) model of liver fibrosis

Immunohistochemistry and qPCR was used to determine the extent of liver injury and fibrosis achieved by 12 weeks I.P. injection of TAA was assessed and compared with the same injury induced in animals that also received vehicle or PXS5303 daily for the last 3 weeks (Figure 3.1).



Figure 3.1: TAA model in mice. BALB/c mice were given a regimen of 12 weeks of TAA at a dose of 200 mg/kg via intraperitoneal injection (I.P.), in addition to vehicle orally (P.O.) from week 9, or PXS5303, orally from week 9

3.2.1. Assessment of inflammatory infiltrate

Paraffin embedded sections of liver tissue were stained using haematoxylin and eosin (H&E) and demonstrated perivascular inflammatory infiltrate, which was confirmed using IHC for immune cell markers CD45, F4/80, Ly-6C and myeloperoxidase (MPO) (Figure 3.2). Expression of the pro-inflammatory cytokines tumour necrosis factor alpha (TNFα), involved in the acute phase reaction and chemokine ligand 2 (Cxcl2), which is secreted by monocytes and macrophages and is chemotactic for polymorphonuclear leukocytes and hematopoietic stem cells, in addition to an inhibitor of the immune response, interleukin-1 receptor antagonist (IL1RN) was also assessed by qPCR (Figure 3.2). There was noticeable infiltration of inflammatory cells perivascularly, particularly F4/80+ and CD45+ cells for both

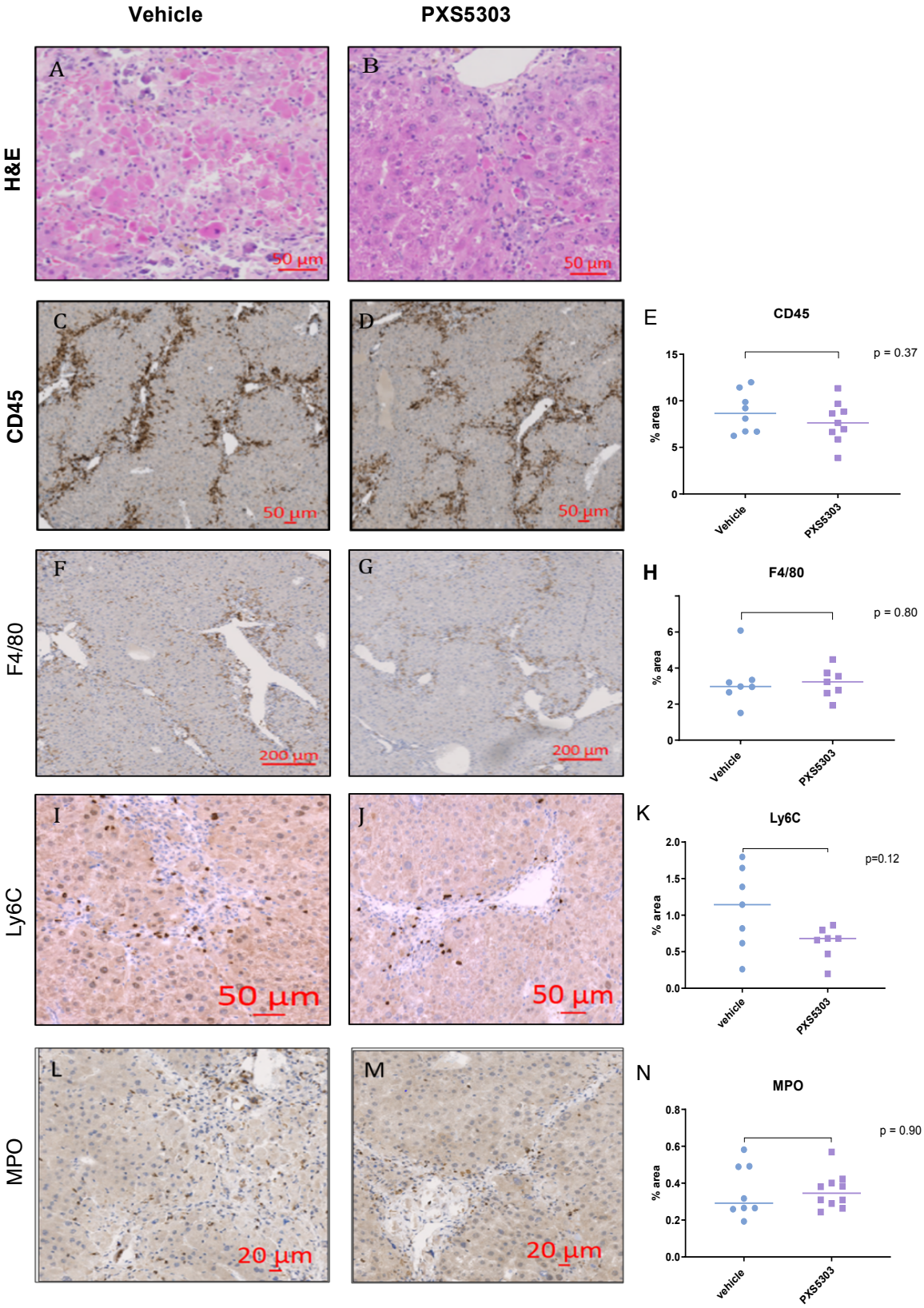
groups of mice, and less so for Ly6C+ and MPO+ cells. Although there was evidence for inflammatory cell infiltration in mice receiving TAA plus vehicle and in mice receiving TAA in combination with PXS5303, no differences were seen between the two groups in the pattern of staining or on quantitative analysis of the IHC (see Figure 3.2). Percentage area was used as a method of identifying positively stained cells rather than cell count as it permitted identification of positive staining over a larger surface area of tissue than manual cell counting, and positive cells were deemed to be adequately detected and differentiated from background using Image J (NIH/Fiji) software (as discussed in 2.3.4).

A small but statistically significant increase in expression of pro-inflammatory genes on qPCR data was seen in the mice receiving PXS5303, (Tnfa, $p = 0.046$, Cxcl2 $p = 0.026$, IL1RN $p = 0.011$) using the Mann-Whitney (MW) test to compare median values between the two groups.

3.2.2 Assessment of liver fibrosis

Liver fibrosis was compared between mice receiving PXS5303 and vehicle by staining paraffin embedded liver sections with PSR and fast green to detect collagen (as described in section 2.1.1). In addition, IHC was performed to detect Collagen I and Collagen III, the expression of which is upregulated to produce scar tissue in fibrosis, and α-SMA, which is expressed on activated hepatic stellate cells. The expression of pro-fibrogenic genes *Col1a1, Col3a1, Acta-2* (the gene for α-SMA), and the growth factor *Tgfb1* was assessed using and qPCR as surrogate markers to measure and compare fibrogenesis between the groups. Morphometric analysis of

the % stained area was used to compare the group that received I.P. TAA for 12 weeks to that receiving TAA in addition to PXS5303 for 3 weeks. No significant differences between the two groups were observed for PSR ($p = 0.11$), collagen I ($p = 0.72$), collagen III ($p = 0.16$) or α-SMA ($p = 0.96$) (Figure 3.3). Some subtle widening of the fibrous septa was seen in the group that received LOXL2 inhibitor compared with those animals that received vehicle alone (Figure 3.3, (A) and (B)). This may suggest more disorganised collagen fibres which have immature crosslinking of collagen, but this was not formally measured. No differences between the groups were seen for gene expression of *col1a1* ($p = 0.11$), *col3a1* ($p = 0.74$), *Tgfb1* ($p = 0.12$) or *Acta2* ($p = 0.25$).


Vehicle
PXS5303
H&E
CD45
F4/80
Ly6C
MPO
A
B
C
D
E
F
G
H
I
J
K
L
M
N
50 µm
200 µm
20 µm
CD45
p = 0.37
% area
Vehicle
PXS5303
F4/80
p = 0.80
Ly6C
p=0.12
vehicle
MPO
p = 0.90

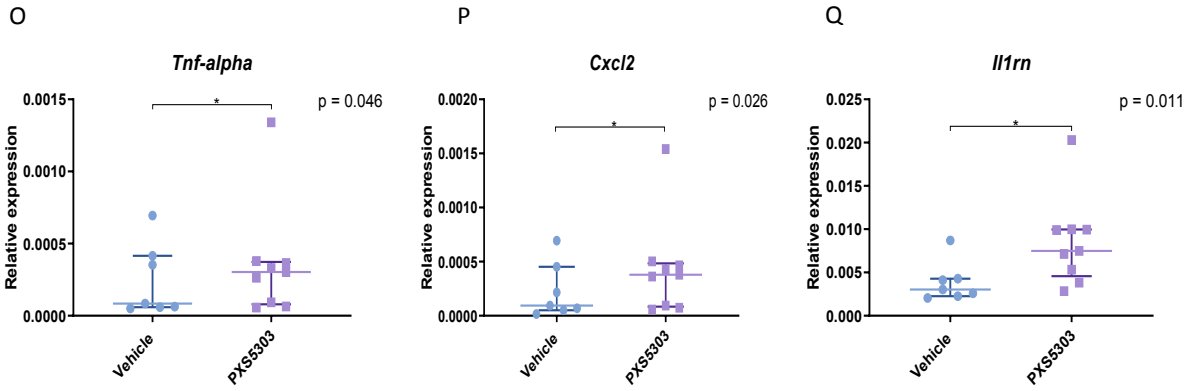


Figure 3.2 LOXL2 inhibition has little effect on inflammatory markers in the TAA model. BALB/c mice received a regimen of 12 weeks of TAA at a dose of 200 mg/kg via I.P. injection, with vehicle, or PXS5303 administered orally from week 9. Animals were subsequently culled at week 12. H&E staining of paraffin embedded slides cut at 3µm is shown for the group receiving vehicle (A), and the group receiving PXS5303 (B). IHC with morphometric analysis was performed with graphs demonstrating median % positive staining for CD45 (C-E), F4/80 (F-H), Ly6C (I-K), and MPO (M-O) for vehicle, and PXS5303 respectively. RNA was extracted and expression of *Tnfa* (O), *Cxcl2* (P), and *Il1rn* (Q) was calculated relative to that of *Gapdh* by RT-qPCR.

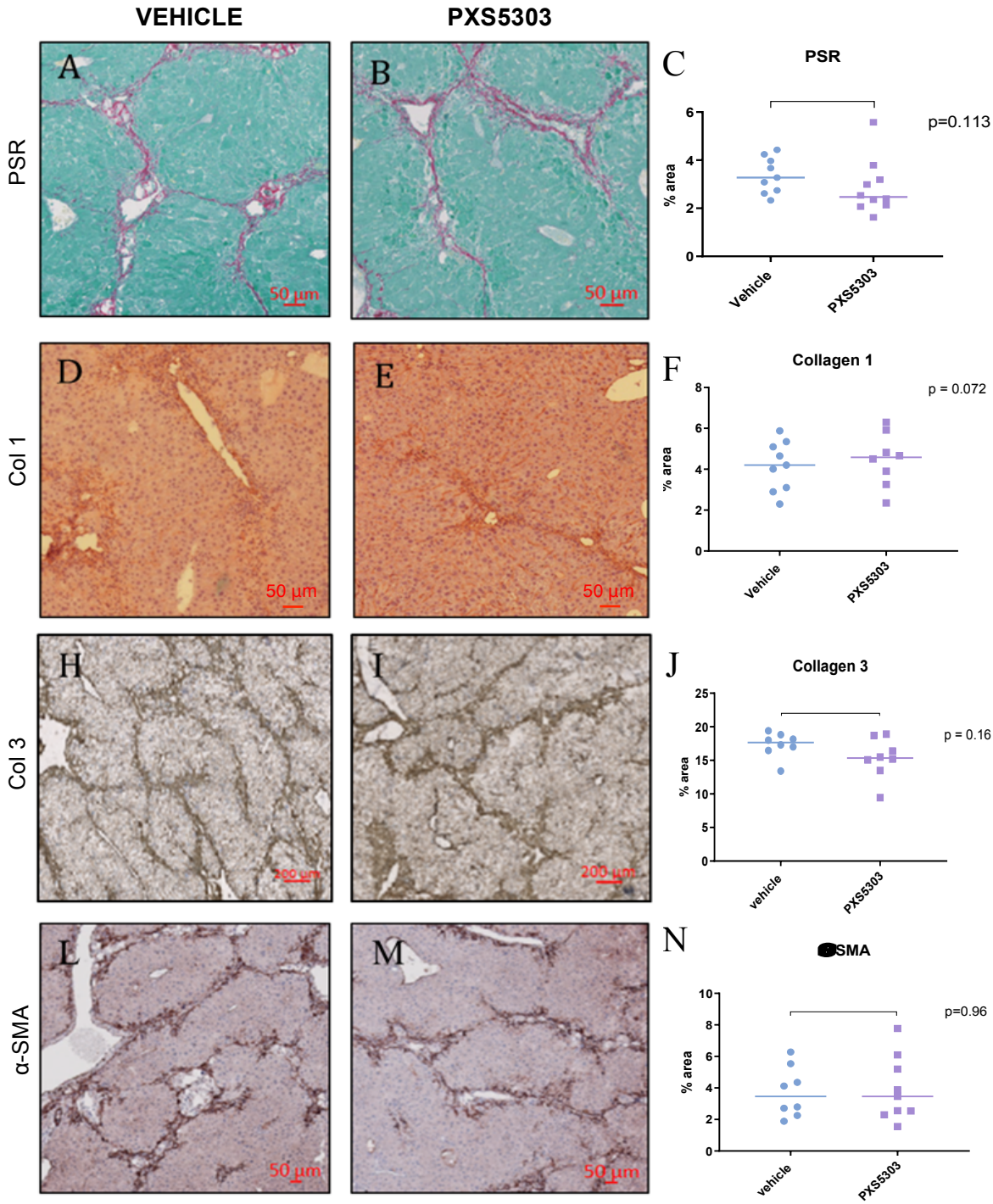


Figure 3.3 LOXL2 inhibition has minimal impact on fibrosis by IHC in the TAA model. BALB/c mice received 12 weeks of TAA at a dose of 200 mg/kg via I.P. injection in addition to vehicle or PXS5303 orally from week 9, and were culled at week 12. Paraffin embedded sections were stained for picrosirius red and fast green for the untreated (A), and treated group (B) respectively, and morphometric analysis of the % area for the two groups was performed (C). Similarly, IHC with morphometric analysis of % positively stained area for treated and untreated mice is shown for Collagen I (D-F) Collagen III (H-J) and α-SMA (L-N), with graphical representation of median values, compared using the MW test (*p<0.05).

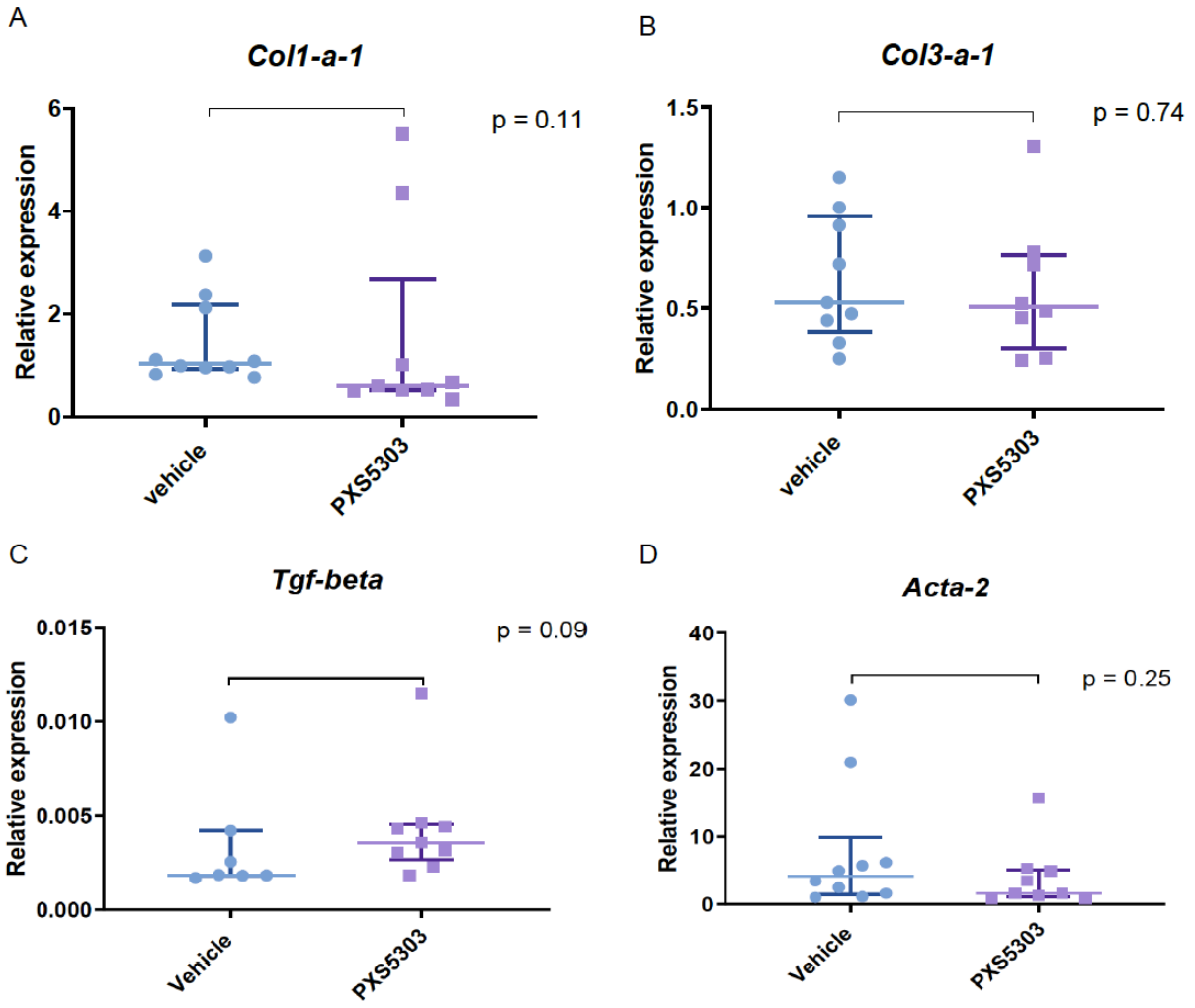


Figure 3.4 LOXL2 inhibition has minimal impact on fibrosis by qPCR in the TAA model. BALB/c mice received 12 weeks of TAA at a dose of 200 mg/kg via I.P. injection in addition to vehicle or PXS5303 orally from week 9, and were culled at week 12. RNA extraction and qPCR from frozen liver tissue was performed for the untreated and treated groups to assess and compare expression of *Col1a1* (A) *Col3a1* (B), *Tgfb1* (C), and *Acta-2* (D). Graphical representation demonstrates median values with interquartile ranges, values were compared using the MW test.

3.2.3 Liver cell apoptosis, proliferation and differentiation in mice following TAA administration

There is some evidence to suggest that LOXL2 may play a role in liver regeneration following liver injury, influencing the proliferation of hepatic cell differentiation in preference to the ductal lineage (195). The effect of 12 weeks I.P. TAA on liver cell

apoptosis, proliferation and differentiation was assessed using IHC, and the group receiving vehicle were compared with those that received 3 weeks of PXS5303. Morphometric analysis was performed to calculate the percentage area stained, or number of positive structures stained within a given area for each slide and comparisons were drawn to the median value for each group (as previously described). A higher number of cells expressing cleaved caspase 3, a marker of apoptosis, was seen in the group receiving PXS5303 (Figure 3.5 A-C), (0.098 vs 0.061, p = 0.013). Analysis was also performed by manual counting of positive cleaved caspase 3 cells within 10 fixed fields of view for each animal, calculating a mean for each and then comparing the two for each group. Apoptosis by cleaved caspase 3 remained higher in the group receiving PXS5303 using this method (8.4 vs 6.2, p = 0.038).

No significant differences in cell proliferation were seen between the two groups as determined by IHC for Ki67, the nuclear protein expressed during proliferation (median 0.514 vs 0.677, p = 0.274, for vehicle vs inhibitor, respectively, (Figure 3.5 D-F). The presence and pattern of staining for SRY-related HMG box transcription factor 9 (SOX-9) and the transmembrane protein, epithelial cell adhesion molecule (EpCAM), was also used as a measure of cells proliferating following liver injury in the ductular reaction (Figure 3.5 G-I). Both SOX-9 and EpCAM are present on progenitor cells originating from the ductular reaction following chronic liver injury, but tend to persist primarily on biliary cells rather than hepatocytes (30, 266, 267). These markers were therefore used to assess whether LOXL2 inhibition with PXS5303 had any effect on the distribution of SOX-9/EpCAM-positive cells, or whether a reduction

in biliary-type (SOX-9 or EpCAM positive) cells was present, suggestive of a tendency for differentiation toward hepatocytes rather than biliary cells arising from the ductular reaction (as demonstrated for the LOXL2 antibody in a previous study (195)). However, there were no differences in either the pattern of staining or the number of positively stained biliary structures for SOX-9 (median 102.5 vs 102, $p = 0.559$) or EpCAM (median 1.7 vs 2.1, $p = 0.500$).

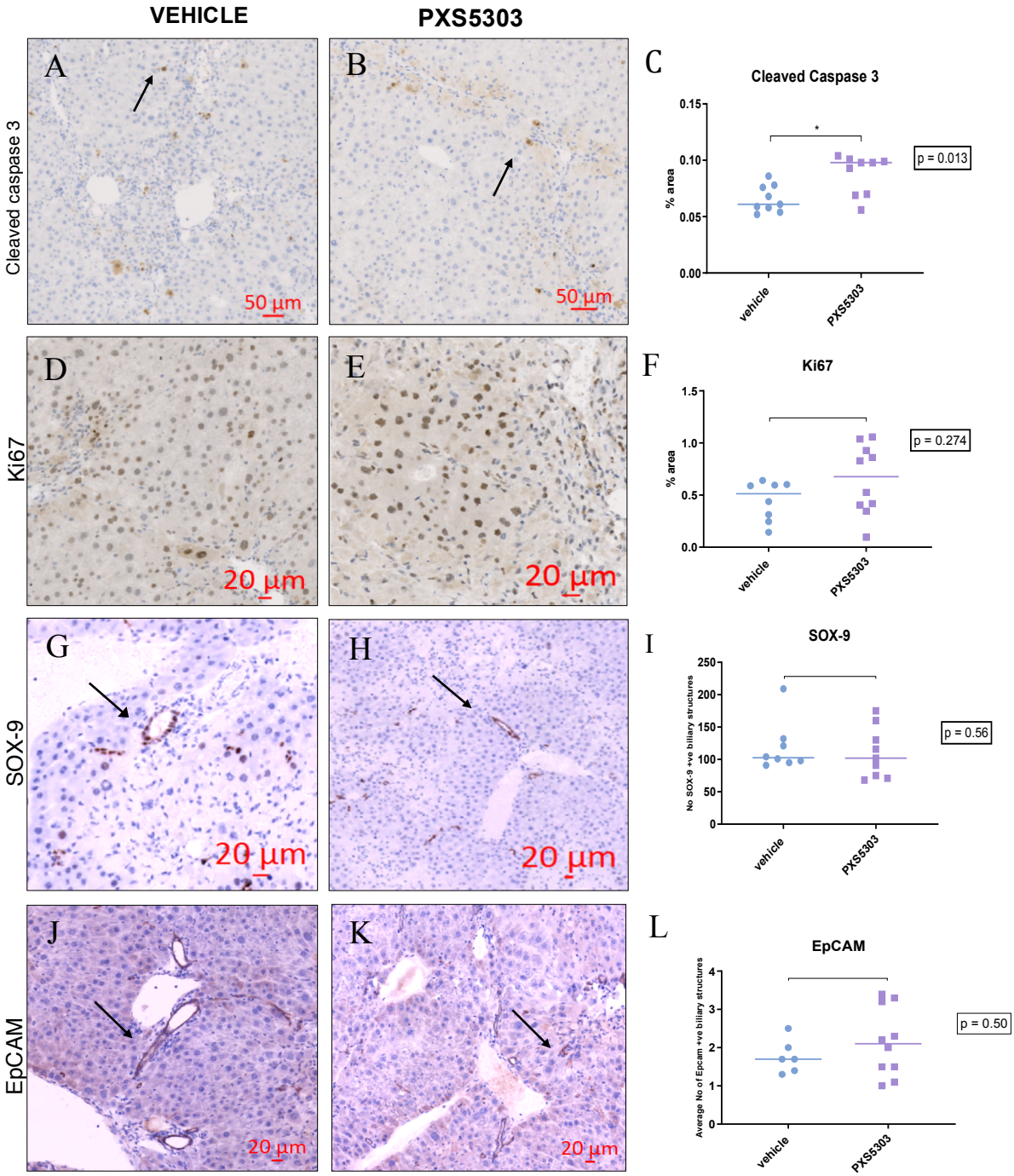
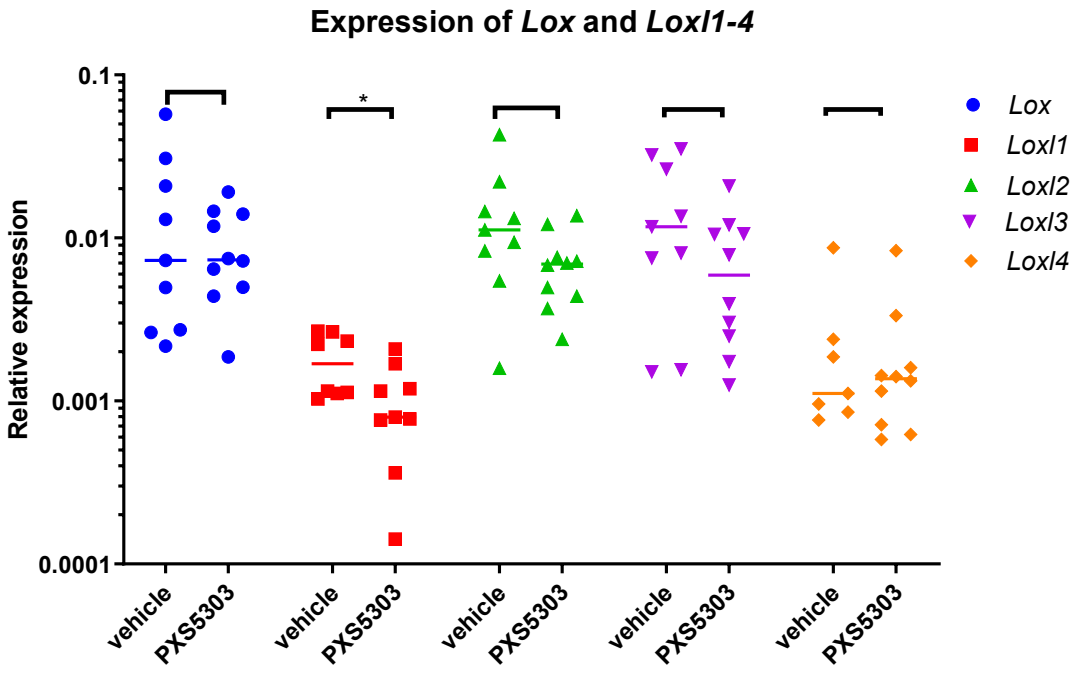


Figure 3.5 LOXL2 inhibition had little effect on apoptosis, and no effect on proliferation or differentiation in the TAA model. BALB/c mice received 12 weeks of TAA at a dose of 200 mg/kg via I.P. injection in addition to vehicle or PXS5303 orally from week 9, and were culled at week 12. Apoptosis, proliferation and differentiation were assessed using IHC for cleaved caspase 3 in the untreated (A) and treated group, (B) respectively, and morphometric analysis of the % area for the two groups was performed (C). Proliferation was assessed using Ki67 in the untreated (D) and treated group (E) and the two groups compared following morphometric analysis (F). Cell differentiation towards biliary lineage was assessed with IHC for SOX-9 and EpCAM in the untreated (G,J) and treated group (H,K) with the median number of SOX-9 or EpCAM positive cells within a 5mm^2 area used to compare the two groups (I). Arrows indicate positive staining. Data (C,F,I,L) is presented as median values, with capped lines and asterisks indicating statistically significant differences (MW test, *p = <0.05).

3.2.4 Expression of lysyl oxidases in mice receiving I.P. TAA

Messenger RNA for LOX and the lysyl oxidases 1-4 was measured by qPCR to assess whether the expression of other members of the lysyl oxidase family are differentially regulated by LOXL2 inhibition with PXS5303, perhaps reflecting the extent of injury or regeneration, or the presence of a feedback mechanism. All five members of the lysyl oxidase family of enzymes were expressed in murine liver tissue. A significant reduction in LOXL1 expression was observed in animals receiving PXS5303 compared with the control group (median 0.0017 vs 0.0080, p = 0.0495, vehicle vs PXS5303); a trend for reduced expression of LOXL2 and LOXL3 was observed, but did not reach significance (median 0.0112 vs 0.0069, p = 0.079 and median 0.0117 vs 0.0059, p = 0.242 respectively). However there was no significant reduction in expression of LOX (median 0.0072 vs 0.0073, p = 0.904 for vehicle vs PXS5303 or LOXL4 (median 0.0011 vs 0.0014, p = 0.813) using MW test to compare median values. It is possible that reduced expression of LOXL1, 2 and 3 represents reduced severity of injury and fibrosis in these animals, mediated by LOXL2 inhibition by PXS5303. Certainly not all lysl oxidases may be upregulated, and expression may vary according to animal species and model used. It is also possible that the findings for LOXL1 are due to chance, particularly given that the findings for LOXL2 and -3 do not reach significance.



Relative expression of LOX and LOX1-4 in 2 groups of BALB/c mice following a regimen of 12 weeks of TAA at a dose of 200 mg/kg via intraperitoneal injection (I.P.), in addition to vehicle orally (P.O.) from week 9, or PXS5303A, using qPCR.

Figure 3.6 Relative expression of *Lox* and *Lox1-4* in 2 groups of BALB/c mice following a regimen of 12 weeks of TAA at a dose of 200 mg/kg via intraperitoneal injection (I.P.), in addition to vehicle orally (P.O.) from week 9, or PXS5303, using qPCR. A small insignificant reduction in *Loxl2* and *Loxl3* were seen, and a significant reduction of LOXL1 expression was demonstrated in mice receiving PXS5303 compared with those receiving vehicle. Data is represented as median values, capped lines with asterisks indicate statistically significant values (MW test), *p<0.5.

3.3. Testing a LOXL2 inhibitor in a rat model of Carbon tetrachloride-induced liver fibrosis.

A second compound, PXS5153 has been developed to inhibit LOXL2 enzyme activity and required preliminary safety and efficacy testing. As for the TAA model, liver tissue was sent from Shanghai Laboratories where the model was developed and carried out, and tissue was processed and analysed as outlined in 2.1.2 to assess the degree of liver injury induced in the CCl_4 –induced model of liver fibrosis, and determine whether there was any difference between the groups of rats. Secondary

outcomes were the effect on neutrophil recruitment, apoptosis, and cell proliferation and differentiation.

Sprague Dawley rats were orally administered with 0.25 µL/g CCl_4 from day 0, 3 times per week for 6 weeks, to induce liver fibrosis, as described in section 2.2.3. Concurrent to the same regimen of CCl_4, rats were administered with either vehicle, low (3 mg/kg), or high (10 mg/kg) dose LOXL2 inhibitor PXS5153 P.O. from week 4. A control group of 4 rats received vehicle only for 6 weeks.

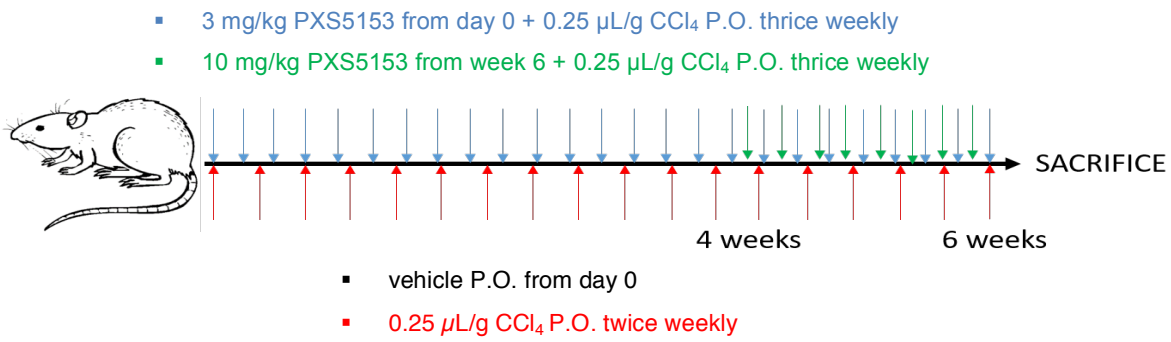


Figure 3.7 CCl_4 model of fibrosis in rats. Sprague Dawley rats were orally administered with vehicle or 0.25 µL/g CCl4 from day 0, 3 times per week for 6 weeks, in addition to either vehicle, low dose PXS5153, or high dose PXS5153 from week 4.

3.3.1. Oral carbon tetrachloride thrice weekly for six weeks leads to hepatic injury and fibrosis in rats which is reduced by oral administration of PXS5153.

Rats receiving 6 weeks of CCl_4 demonstrated significant liver injury with mild to moderate fibrosis and some bridging of fibrotic septae, and a median area of 2.84% with PSR stain ("CCl_4" group), compared with those receiving vehicle and no CCl_4 ("vehicle") for 6 weeks (Figure 3.8). Significant steatosis was also seen on H&E staining which may be a result of CCl_4 dilution in olive oil (Figure 3.6, A-D). Rats

receiving low (“low”) and high (“high”) dose LOXL2 inhibition with PXS5153 demonstrated a reduction in fibrosis in a dose dependent manner when compared with those receiving CCl_4 only, demonstrated by PSR staining for collagen (CCl_4 vs CCl_4 plus low dose PXS5153, median 2.84% vs 1.94%, p = 0.072, CCl_4 vs CCl_4 plus high dose PXS5153, median 2.84 % vs 1.90 %, p = 0.020, using the Mann-Witney test). The medians of each group were compared for unpaired data of a non-Gaussian distribution using the Kruskal Wallace and one way ANOVA tests and these results did not show significance (p = 0.061, see Figure 3.6). No significant reduction in IHC staining for collagen I (Figure 3.6, J-N) was demonstrated. Expression of profibrogenic markers was reduced in rats receiving 2 weeks of either low or high dose PXS5153 which was more marked in the high dose group (see Figure 3.8).

Although only the results for PSR and high dose PXS5153 were significant using the Mann-Witney test for direct comparison of groups, a trend for reduced fibrosis was observed for in the PSR and collagen I IHC in both high and low dose groups. Expression of fibrosis markers by qPCR was consistently reduced by PXS5153, and it was hoped that similar results would be later seen using the compound PXS5338K; this compound was expected to be a more specific and efficacious LOXL2 enzyme inhibitor than PXS5153. In addition, a greater degree of fibrosis was expected in our own TAA-induced fibrosis model in mice, and it was believed that LOXL2 inhibition would be more effective in the latter stages of fibrosis, during collagen cross-linking.

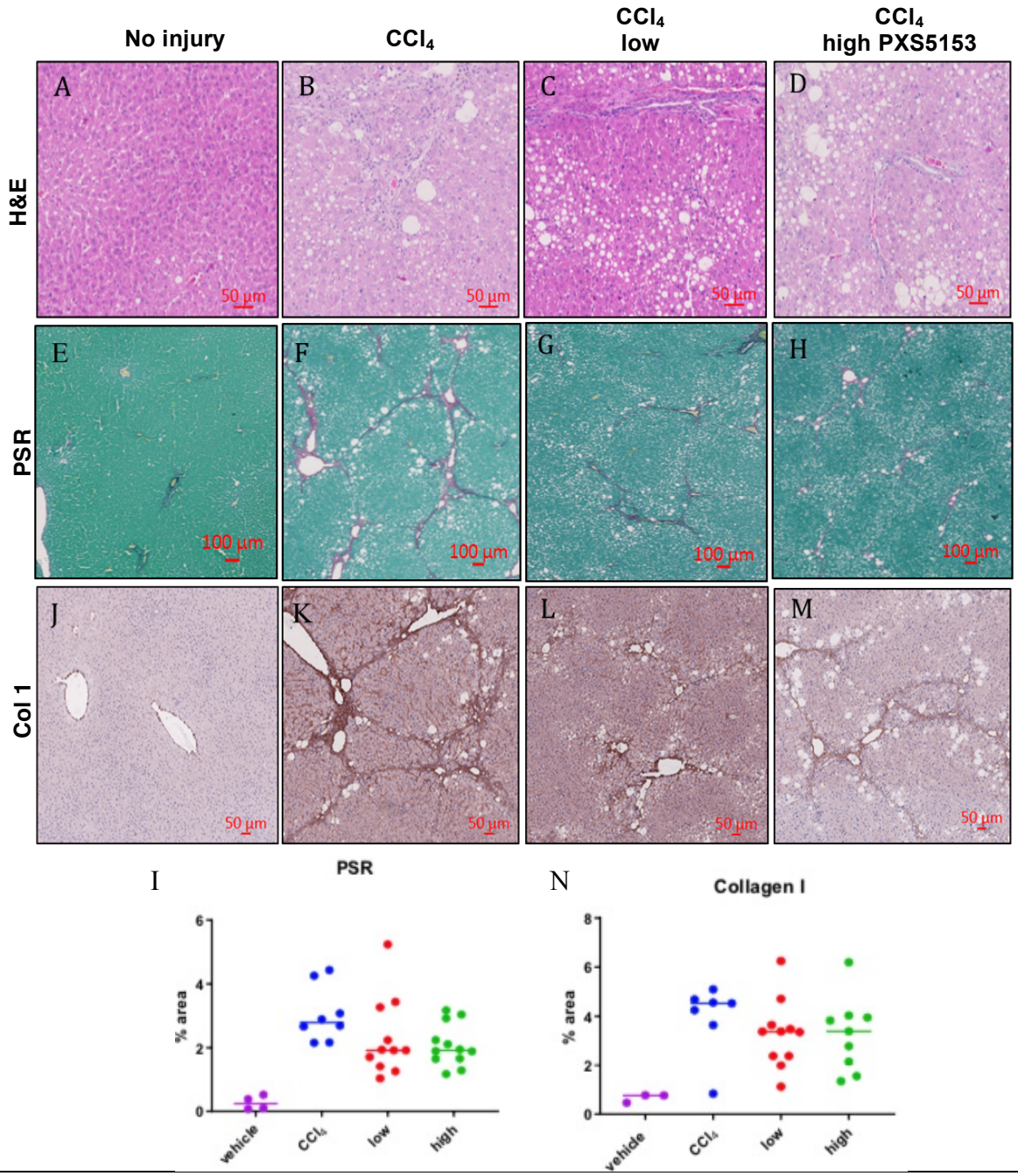


Figure 3.8 Rats receiving oral CCl_4 develop fibrosis which is attenuated by LOXL2 inhibition. Sprague Dawley rats were administered with vehicle (vehicle), or 0.25 µL/g CCl_4 orally 3 times per week for 6 weeks (CCl_4). In addition to CCl_4, 15 mice received low dose (low) PXS5153 from day 0, or high dose (high) PXS5153 from week 4. At week 6 the rats were sacrificed and dissected liver tissue was sectioned, frozen, and later cut for paraffin embedded slides. These were stained using haematoxylin and eosin (H&E) (A-D), picrosirius red (PSR) (E-H), and immunohistochemistry for Collagen-1-alpha (J-M). Morphometric analysis of proportionate staining for PSR demonstrated reduced fibrosis in rats receiving high dose inhibitor and a lesser, non-significant reduction for low dose inhibitor (I). Likewise, a trend for a reduction in collagen I was seen with both low and high dose inhibitor but this did not meet statistical significance (N). Graphs represent median values, capped lines and asterisks indicate statistical comparisons using KW test and Bonferroni-Dunn post-hoc correction.

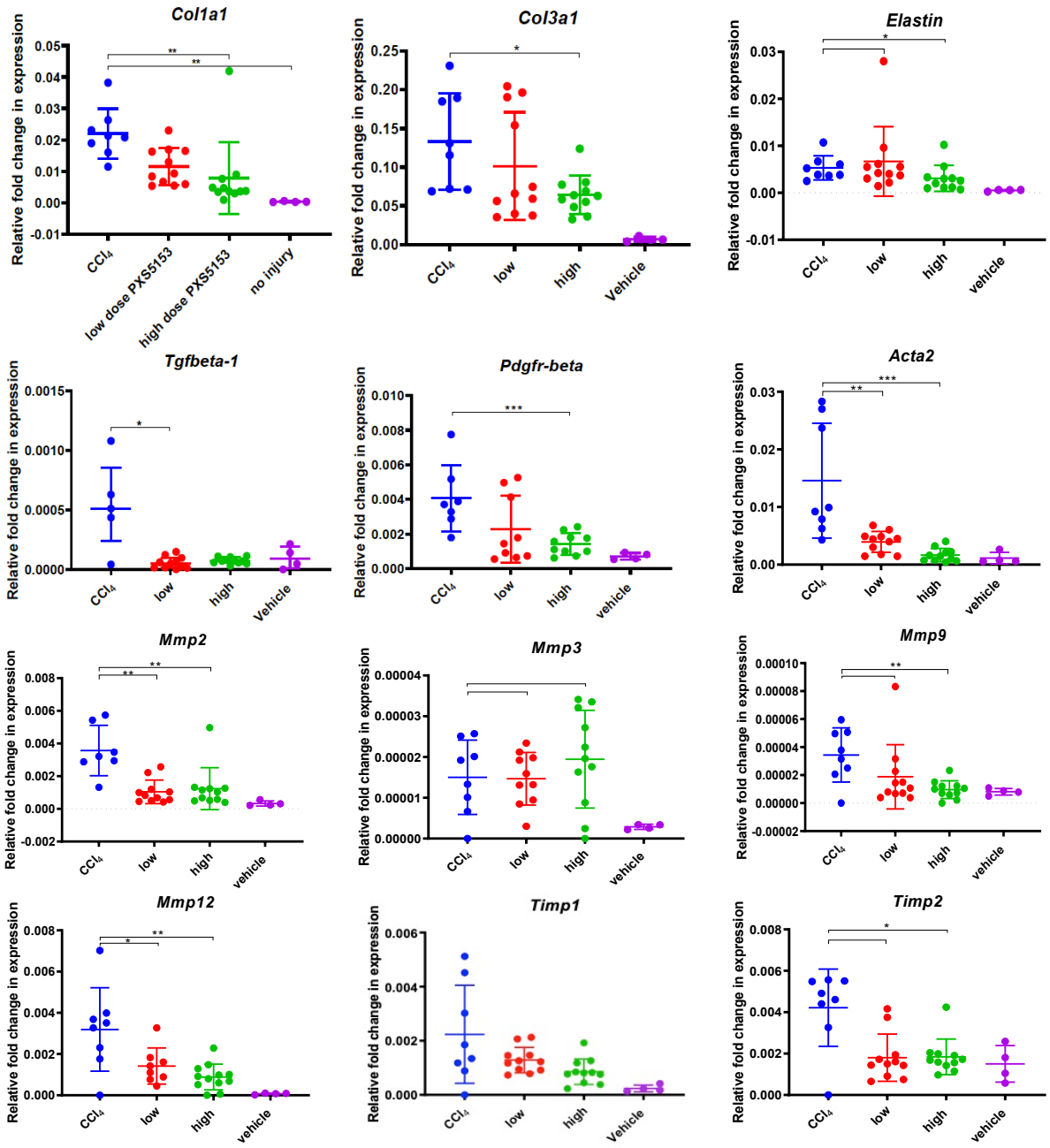


Figure 3.9. Expression of proteins upregulated during fibrogenesis were reduced with high and/or low dose PXS5153. RNA was extracted from frozen liver tissue and the relative expression of *Col1a1* and *-3*, *elastin, β-actin, Tgf1, Pdgfrb, Timp1* and *2*, and *Mmp 2, 3, 9* and *12*, was calculated after qPCR against the expression of a house keeping gene (B2M). Significant downregulation of these genes was demonstrated in mice receiving CCl_4 – induced liver injury in addition to low ("low") and/or high ("high") dose of PXS5153 compared with those receiving CCl_4 alone, except for *Mmp3*. A control group of mice received vehicle only ("vehicle"). *p <0.05, **p <0.005, ***p <0.0005 using KW test and Bonferroni-Dunn post-hoc correction. Graphs represent median values with an interquartile range.

3.3.2. The effect of oral CCl_4 in rats on inflammatory cell recruitment to the liver, apoptosis and cell differentiation.

Preliminary assessment on the effect of 6 weeks CCl_4 P.O. in rats on inflammatory cell recruitment to the liver was performed by IHC for myeloperoxidase (MPO), commonly expressed by neutrophils. A significantly higher proportion of cells expressed MPO in the CCl_4 injured rats when compared with uninjured rats, using both % area MPO positive staining and manual counting of MPO positive cells (median % area, 0.087 vs, 0.045, $p = 0.024$). There was no significant reduction in neutrophils using either low or high inhibitor, although overall the number of neutrophils seen was low (see Figure 3.7).

IHC for cleaved caspase 3 was used to assess apoptosis, with no significant differences seen between uninjured and injured rats, ($p = 0.15$), or injured rats receiving LOXL2 inhibition (CCl_4 vs CCl_4 + low dose PXS5153, $p = 0.46$, CCl_4 vs CCl_4 + high dose PXS5153, $p = 0.08$), although a trend toward reduced apoptosis uninjured mice and mice receiving inhibitor was demonstrated.

A preference for cells from the ductular reaction to differentiate towards a biliary lineage was assessed using IHC for EpCAM and SOX-9. CCl_4 injury led to an increase in both SOX-9 and EpCAM positive biliary cells which appeared ductular (vehicle vs CCl_4 –induced injury compared for number of positively stained biliary structures for SOX-9 and EpCAM, respectively, $p = 0.03$, and $p = 0.01$). Compared with rats receiving CCl_4 only, there were reduced staining of biliary structures in mice receiving low dose of inhibitor for SOX-9 (median 24.7 vs 7.2 $p<0.0001$) and in mice

receiving high dose inhibitor for EpCAM (median 22.36 vs 16.09, p = 0.0494), respectively, although the overall trend was for reduced biliary staining in those mice receiving inhibitor. This may represent reduced injury severity represented by the ductular reaction (268), or reduced differentiation towards a ductular lineage in those mice receiving LOXL2 inhibition (and therefore less expression of EpCAM or SOX-9).

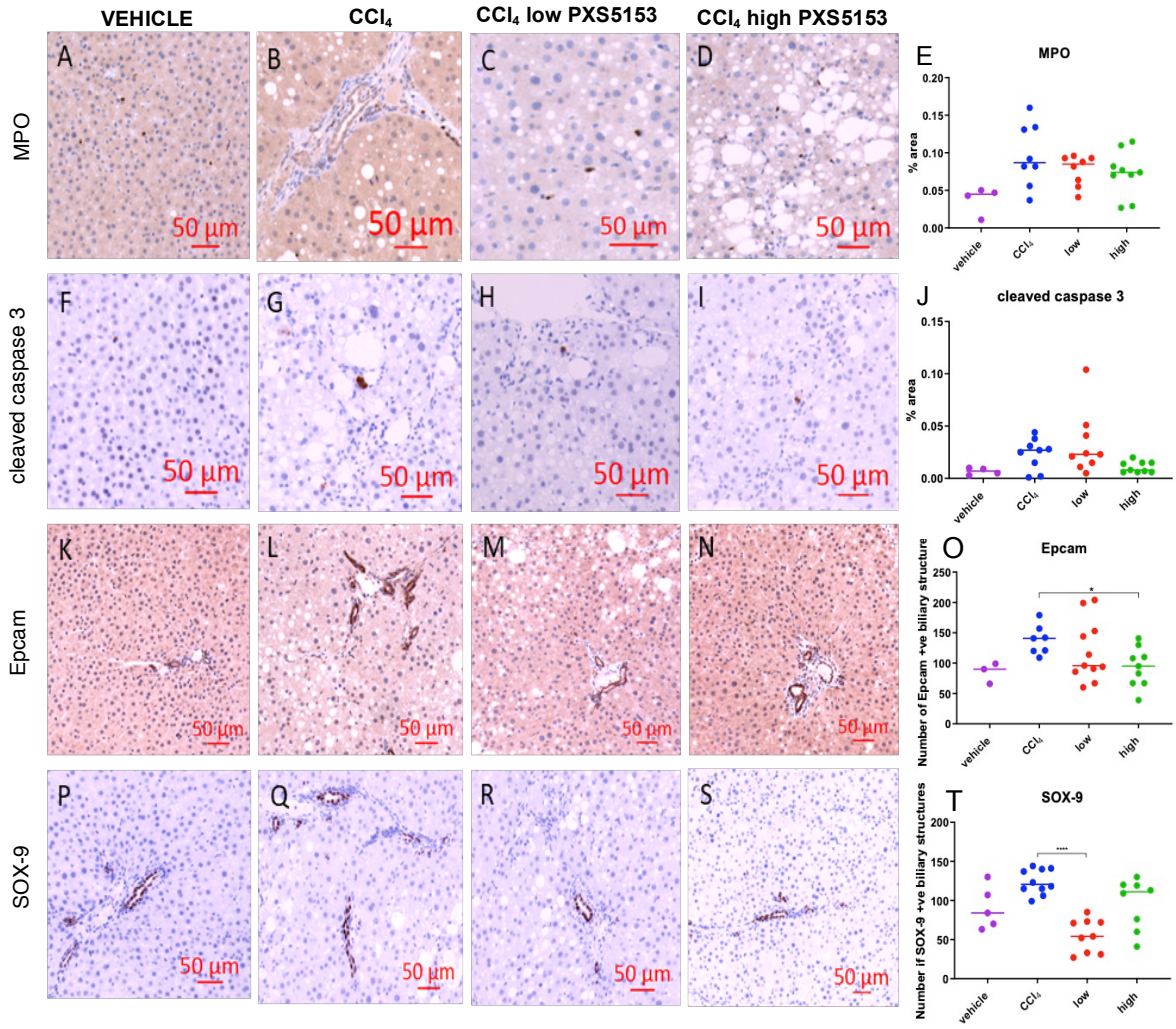


Figure 3.10 Minimal changes in apoptosis and the ductular reaction were seen in rats receiving LOXL2 inhibitor following injury with CCl_4. Sprague Dawley rats were administered with vehicle, or 0.25 µL/g CCl_4 P.O. 3 times per week for 6 weeks. In addition, 15 mice received low dose PXS5153 from day 0 or high dose PXS5153 from week 4. At week 6 the rats were sacrificed and dissected liver tissue was sectioned, frozen, and later cut for paraffin embedded slides. These were stained using immunohistochemistry for MPO, cleaved caspase 3, EpCAM and SOX-9 (A-D). Morphometric analysis of proportionate staining described in 2.2.4) permitted comparison between rats subjected to CCl_4 liver injury and rats receiving low and high dose PXS5153 in addition to CCl_4 induced liver injury, and uninjured rats as a control. Neutrophil recruitment was increased by CCl_4 injury (median % area CCl_4 only group, 0.087 vs median % area vehicle group, 0.045, p = 0.024) but was unaffected by PXS5153 (A). Apoptosis appeared to increase in the injured group but the differences between the groups were not statistically significant (B). The ductular reaction, assessed by EpCAM positive biliary structures was increased in rats subject to CCl_4 injury (vehicle vs CCl_4 group, p = 0.01) and was reduced with PXS5153 (CCl_4 vs CCl_4 plus high dose PCS5153, p = 0.008). Differentiation towards a biliary lineage, demonstrated with IHC for SOX-9, was increased in CCl_4 injured rats (vehicle vs CCl_4 only, p =0.03) and this was attenuated by PXS5153 (CCl_4 only vs CCl_4 and low dose PXS5153 p<0.0001). Graphs represent median values, capped lines and asterisks indicate statistical comparisons using KW test and Bonferroni-Dunn post-hoc correction, *p <0.05, **p <0.005, ***p <0.0005.

3.3.3 Manual counting of cleaved caspase 3 vs morphometric analysis of % area stained

Where some IHC is positive but has high background staining, it can be difficult to assess the accuracy of morphometric analysis using the method outlined in 2.3.4 (where positively stained structures are detected against background). For this reason, the analysis of cleaved caspase 3, SOX-9 and EpCAM was performed both by calculating % area using ImageJ, and also by manually counting cells/biliary structures. This had no overall effect on results.

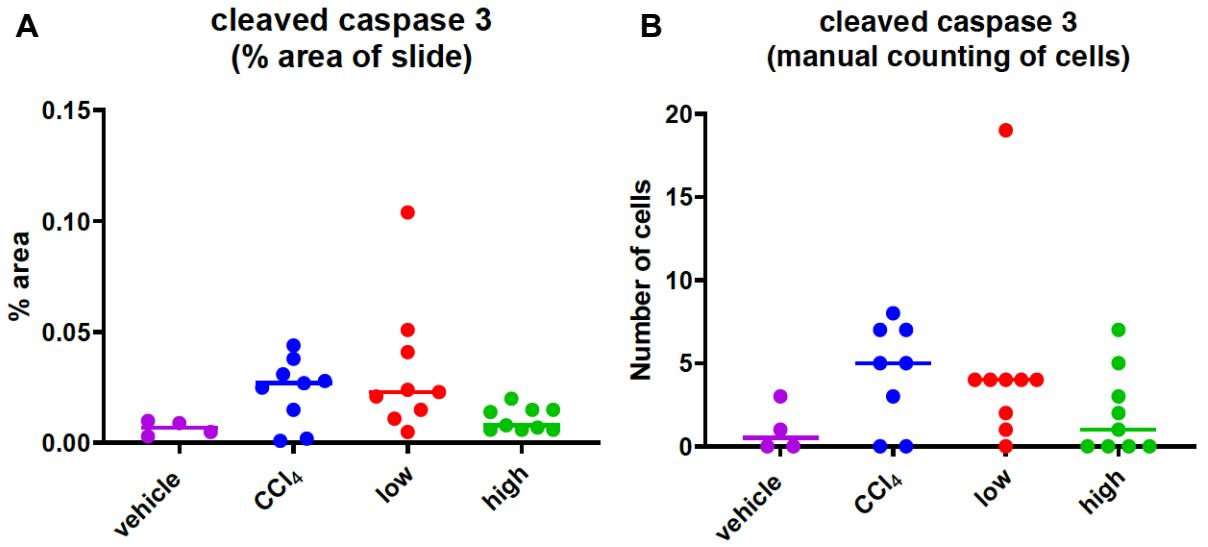


Figure 3.11 Analysis of cleaved caspase via % positive staining versus manual counting of cleaved caspase positive cells did not affect the results. IHC was performed for cleaved caspase 3 to assess apoptosis; analysis was performed by using image J to identify % positive area (A) and by manual counting of cells (B). The results were similar for both types of analysis with no differences seen between the groups (KW test). Graphs represent median values.

3.4 Discussion

The aim of these studies were twofold: firstly, to assess the safety and tolerability of two early stage compounds in the commonly used CCl_4 model of liver injury in rats, as well as the less commonly used model using I.P. injection of TAA, and secondly to assess the potential role of LOXL2 inhibition in these models.

Data from Pharmalegacy confirmed only one death in twenty of the mice receiving TAA, and one out of 46 rats receiving CCl_4. This falls within the expected numbers of deaths for animals undergoing interventions such as I.P. injections where vital organs can be accidentally injected, and bleeding or thromboembolic events can occur (253, 255). Likewise, animal weight remained stable throughout both TAA and CCl_4 models, with only a noticeable difference seen in rats receiving sham control (CCl_4), who gained more weight than those receiving CCl_4. Therefore one can conclude that the compound is well tolerated and had no immediate or concerning side effects.

Both animal models promoted the development of mild to moderate fibrosis, with bridging of fibrotic septae demonstrated with immunohistological staining for PSR and Collagen I and, in rats receiving CCl_4, increased expression of genes associated with a profibrogenic phenotype. There was reduction in fibrosis markers in both models using a LOXL2 inhibitor, but the differences were only found to be significant in the CCl_4 model. This may be due to subtle differences in the potency of the two inhibitors, or variation in the distribution or efficacy of the compounds in different species (discussed in detail in 1.5.3.3.2). The mildness of injury incurred in the TAA model was unexpected; with a less fibrotic response there may be fewer mature

collagen crosslinks being formed and so less of a role for LOXL2 inhibition. Other models of injury may induce a more florid fibrosis, demonstrating % PSR stain closer to 5% and thicker bridging collagen fibres seen. Unpublished work in this laboratory has demonstrated a robust fibrotic response to TAA when administered in the drinking water, with PSR between 4 - 6 %, and this route will be explored in subsequent studies (see chapter 5).

There is little or no data published on the possible effect of LOXL2 on inflammatory cell recruitment to the liver and apoptosis, and so this was examined using IHC for common immune cell markers and by comparing expression of inflammatory proteins in treated and untreated mice in the TAA model of fibrosis; cleaved caspase 3 was used as a marker of apoptosis in both models. Although I observed a tendency for increased expression of inflammatory marker in the mice receiving PXS5303, there was no evidence for increased infiltration of immune cells in the liver tissue using IHC. Immune cell recruitment and inflammation was poorly examined in the rat model of fibrosis, primarily due to lack of specific antibodies, and so conclusions could not be made. Flow cytometry is used in later experiments to interrogate the potential effect of LOXL2 inhibition in fibrosis more robustly.

Likewise, conflicting data was found for apoptosis. While cleaved-caspase 3 was found to be increased in liver tissue of mice receiving PXS5303, this was not reproduced in the rats receiving PXS5153. Apoptosis was increased in CCl_4 injured rats compared to uninjured rats and there was a tendency for reduction in the PXS5153 treated group; this is in keeping with known data that liver injury leads to

hepatocyte apoptosis (43, 70), therefore severity of injury is likely to be related to the degree of apoptosis and concurrently, attenuation of liver injury with the inhibitor may have led to a reduction in apoptosis. It is important to note that these findings in rats were not statistically significant, in addition to not being supported in the TAA mouse data. It is possible that discrete variance between the compounds used in the two models account for the difference in effect. It is also possible that the mild nature of the liver injury may have limited the magnitude of the effect of LOXL2 inhibition which was not observable within the noise of the experimental conditions.

Previous studies suggest that antibody blockade of LOXL2 may supress the ductular reaction and promote hepatic progenitor cells towards the hepatocyte lineage (195). In the CCl_4 induced liver injury, there was a trend for reduced EpCAM and SOX-9 positive biliary staining in animals receiving the LOXL2 enzyme inhibitor, supporting the hypothesis that this mechanism may be dependent on LOX/L enzyme activity. These preliminary findings require further exploration and validation, as they have important implications for hepatic regeneration. Given the variation between models, the use of additional mouse models will help to assess whether these results can be replicated. Although expression of LOX and LOXL proteins was demonstrated in the TAA model, LOXL2 expression was not markedly elevated compared to that seen in humans. This could also account for the lack of efficacy seen in this model.

In the following chapters I explore LOXL2 inhibition in a more robust and extensive fibrotic TAA model, in a cholestatic liver disease model, during in-vitro study, in

addition to the impact on liver regeneration in a resolution model. I will also investigate for any effect on inflammatory cell recruitment using flow cytometry.

4 Results 2: Exploring the effects of LOXL2 inhibition in a biliary model of fibrosis.

4.1 Introduction

Biliary fibrosis is predominant in numerous conditions, the commonest being primary biliary cholangitis and primary sclerosing cholangitis (11). Currently there are no pharmacological therapies targeting biliary fibrosis, but animal models have been developed on which to test compounds and to better understand the pathophysiology of these conditions. One such model is the use of *Abcb4*$^{-/-}$mice, more commonly known as *Mdr2*$^{-/-}$ mice. These mice are deficient in a canalicular phospholipid flippase, and spontaneously develop liver injury due to the absence of phospholipid from bile, causing disruption in tight junctions and basement membranes in bile ducts, leakage of bile into the portal tract, and periportal biliary fibrosis (263).

During analysis of the preliminary CCl_4 and TAA experiments, the results of studies using AB0023, a LOXL2 monoclonal antibody, were published suggesting that inhibition of LOXL2 may attenuate the ductular reaction and reduce differentiation of biliary cells, with the potential to reduce biliary fibrosis in this manner (195). Specifically, in the presence of LOXL2 inhibition, progenitor cells have a tendency towards hepatocyte rather than biliary lineage, with potential consequences for reducing fibrosis. Those cells that become hepatocytes may contribute to liver regeneration while reactive ductular cells promote fibrosis by secretion of growth factors, or growth factor like proteins, ECM, and attract fibroblasts (269). The ductular reaction is believed to be particularly important in the development of biliary fibrosis,

and for this reason I wished to test the efficacy of LOXL2 enzyme inhibition in a biliary model of fibrosis.

The *Mdr2-/-* model was chosen as a reproducible model accessible at Birmingham laboratory. Previous work at Birmingham and other published data demonstrated that by 9 weeks *Mdr2*-/- mice have moderate bridging fibrosis (265), and so gavage of compound was commenced at that age.

Mdr2-/- mice on both FVB and C57Bl/6 backgrounds develop progressive liver injury and fibrosis, although there can be subtle variation in phenotype between the strains (263, 265, 270). Previous data have shown fibrosis to be more advanced in the C57Bl/6 strain (see 1.6.2) and so this was the preferred strain on which to explore the effects of LOXL2 inhibition by PXS5338K. First of all, I wished to assess the fibrosis in these two strains of mice independently before proceeding. Once I established that fibrosis was more marked in the C57Bl/6 background, I planned to evaluate the dose of PXS5338K to be used in this strain. However, FVB knock out mice were readily available and were therefore used in a pilot study to assess the safety and tolerability of PXS5338K, while C57Bl/6 *Mdr2*-/- mice were bred.

The effect of 10 mg/kg PXS5338K administered orally was assessed in 6 nine week old FVB *Mdr2*-/- mice. The intention was to give 9 doses over three weeks on alternate days (Monday, Wednesday, Friday). Unfortunately this dose was poorly tolerated in the pilot study using FVB *Mdr2-/-* mice, and so the dose was reduced to 3

mg/kg which was still expected to provide coverage of the target molecule. This dose was tolerated by C57Bl/6 *Mdr2*-/- mice, with no safety concerns.

In this study 36 nine week old C57Bl/6 *Mdr2*-/- mice each received 9 doses of either vehicle or 3 mg/kg PXS5338K over three weeks (Monday, Wednesday, Friday) and were culled 72 hours following the 9th dose. The extent of fibrosis and the impact of LOXL2 inhibition were assessed by IHC for PSR, α-SMA, and collagen with morphometric analysis, and by measuring expression of pro-fibrogenic genes by qPCR. IHC for SOX-9 was also used to assess proliferation and biliary differentiation of cells. Detailed analysis of the inflammatory infiltrate was facilitated by flow cytometry of hepatic digests, with the inclusion of lymphoid, myeloid and granulocyte populations, as well as the use of IHC to detect immune cell markers.

4.2 Assessing the degree of fibrosis in FVB vs C57Bl/6 *Mdr2-/-*

It has been previously suggested that there may be variation in the type of injury that occurs between strains of *Mdr2-/-* mice. To establish the pattern of fibrosis that occurs in both FVB and C57Bl/6 *Mdr2-/-* mice (the two strains available at Birmingham), paraffin embedded liver tissue from both strains of mice culled at different ages were stained for collagen using PSR and the % area calculated (see Figure 4.1). Representative images are shown in A-D. Periductular staining representing collagen deposition and fibrosis is seen as expected in the FVB and C57/Bl6 strains with additional bridging fibrosis seen only in the FVB strain. Fibrosis appeared to regress over time in the FVB strain, but this may be due to random

sampling, as it has not been demonstrated elsewhere (265). There is a trend towards increasing fibrosis with age in C57Bl/6 *Mdr2-/-* mice.

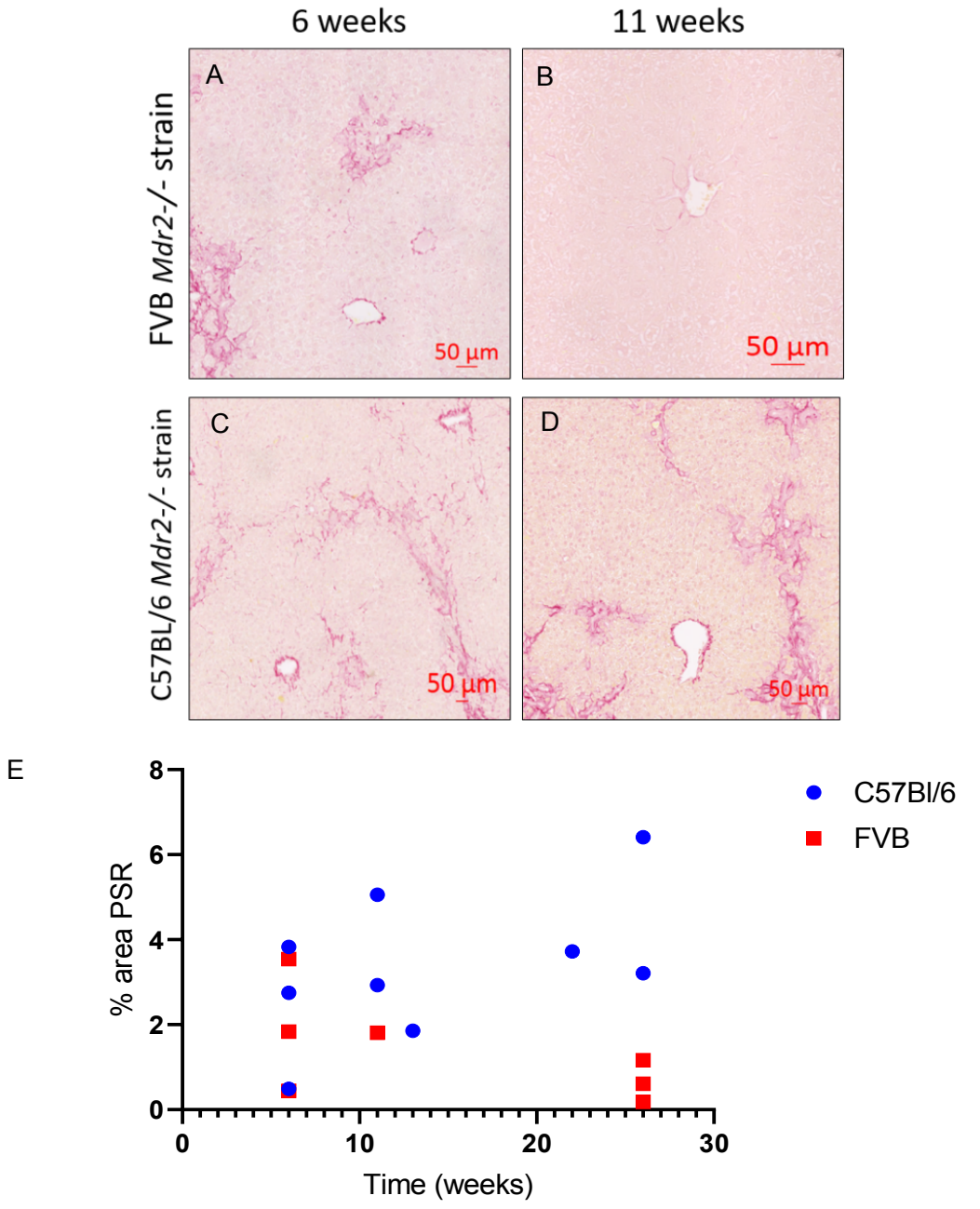


Figure 4.1 Fibrosis by PSR stain in two strains of *Mdr2-/-* mice. Sample PSR staining of paraffin embedded liver sections cut at 3 µm showing liver from both FVB and C57Bl/6 *Mdr2-/-* mice aged 6 and 11 weeks (A-D). Morphometric analysis was performed to calculate the mean % area of PSR stain from 5 different fields of view for each strain at various ages for both strains (E).

4.3 A pilot test of PXS5338K in FVB *Mdr2-/-* mice

The safety and efficacy of 10 mg/kg PXS5338K administered orally was assessed in 6 male nine-week-old FVB *Mdr2-/-* mice. A maximum of 9 gavages per animal was permitted for the *Mdr2-/-* strain according to our animal licence, and so dosing was planned over three weeks on alternate days (Monday, Wednesday, Friday), to allow the compound to take effect alongside natural progression of fibrosis in the aging mice.

Six male 9-week-old FVB *Mdr2*-/- mice received oral gavage of vehicle or PXS5338K at a dose of 10 mg/kg thrice weekly for up to 3 weeks, according to the planned model described in 2.2.2 (Figure 4.2). A total of 9 gavages were administered, as was permitted by the animal licence P2DF9DB6E, see 2.2.1. One mouse was culled following likely aspiration (immediate deterioration following the 5th gavage of PXS5338K), one after it became unwell (demonstrating weight loss, lethargy and poor grooming) following 8 gavages of PXS5338K, and the remaining mice after 9 gavages of either PXS5338K or vehicle due to a third mouse becoming unwell following the 9th gavage. In all cases serum samples were extracted via cardiac puncture under terminal anaesthesia and the liver was dissected for analysis as outlined in 2.2.5.

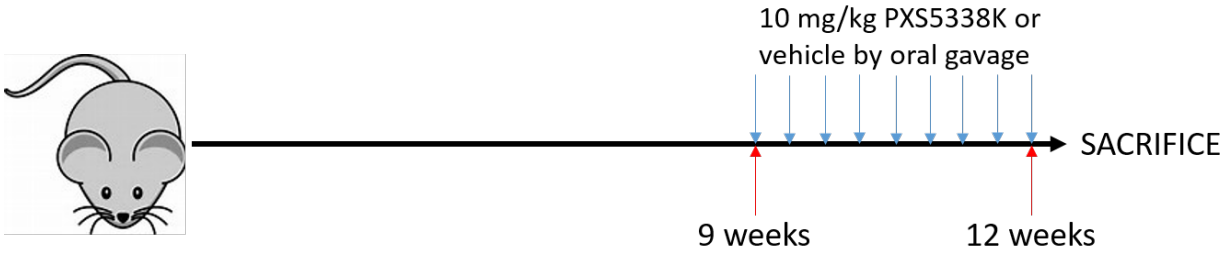


Figure 4.2 Model for testing PXS5338K in FVB *Mdr2-/-* mice. Six 9 week old FVB *Mdr2-/-* mice received 9 doses of PXS5338K at 10 mg/kg by oral gavage over 3 weeks.

4.3.1 A pilot test of PXS5338K in FVB Mdr2-/- mice: Serum results

Unfortunately only two serum samples were able to be analysed due to clotting of the sample in the syringe, and so the results shown in Table 4.1 are difficult to interpret without control samples (mice given vehicle) but are comparable to published data in other *Mdr2-/-* models (265, 271). Low phospholipid-associated cholelithiasis has been reported in *Mdr2-/-*mice, and this may account for the elevated bile acids in mouse 3 (M3, see table 4.1 below) (272). However, the liver, gallbladder, and bile ducts of all mice that became unwell were examined and no gallstones were found.

Animal	AST (U/l)	ALT (U/l)	Bile acids
M2 (8 doses of PXS5338K)	45	41	3
M3 (9 doses of PXS5338K)	70	132	251

Table 4.1: Serum analysis for the two mice receiving eight (M2) or nine (M3) doses of PXS5338K before becoming unwell.

4.3.2 A pilot test of PXS5338K in FVB Mdr2-/- mice: Immunohistochemistry

4.3.2.1 Haematoxylin and Eosin analysis

Haematoxylin and eosin staining was performed on paraffin-embedded liver sections for all 6 FVB *Mdr2-/-* mice from the pilot study. The slides were assessed for gross liver injury such as necrosis, inflammatory cell infiltrate and tissue architecture (Figure 4.3). The extent of injury was similar between groups receiving vehicle or PXS5338K, and in those mice that became sick compared to those that were well at week 12 (following 9 gavages). There was evidence of early bridging fibrosis in all

mice, and no gross necrosis or inflammatory infiltrate in those animals that became unwell.

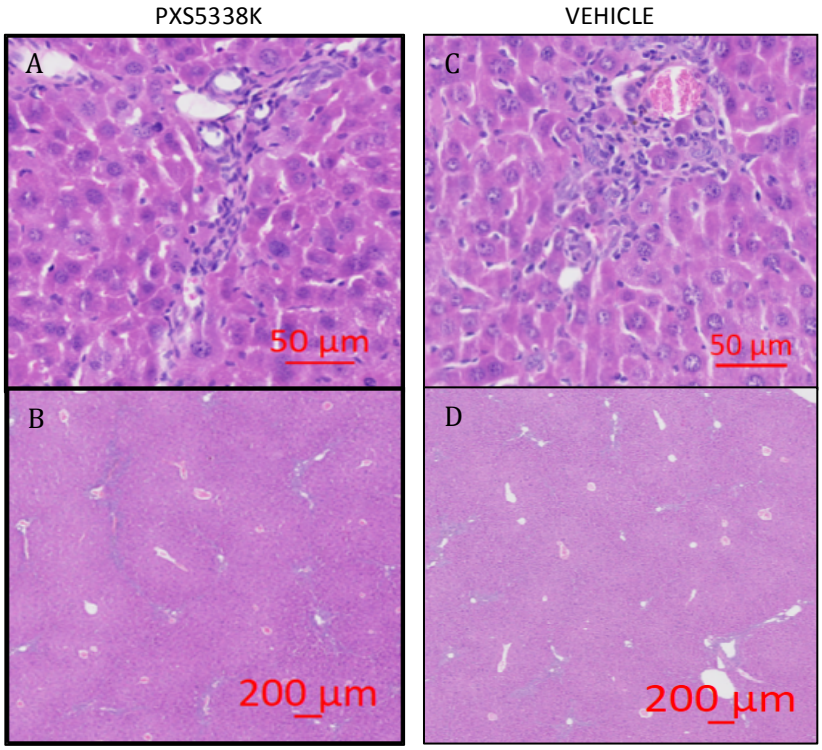


Figure 4.3 H&E staining of FVB *Mdr2-/-* demonstrated no differences between the groups receiving PXS5338K vs vehicle, and no areas of gross injury such as necrosis. H&E staining of paraffin embedded slides cut at 3 µm showing liver from FVB *Mdr2-/-* mice following nine gavages of either PXS5338K (A and B, high and low power, respectively) at 10 mg/kg, or vehicle (C and D). The extent of injury was similar between groups with evidence of early bridging fibrosis in all mice, and no gross necrosis in those animals that became unwell.

4.3.2.2 Picrosirius red

While the primary aim of this study was to evaluate the impact of PXS5338K on animal health, PSR stain was used to assess fibrosis and showed only mild bridging and up to 4 % area of collagen for all mice. Minimal fibrosis was seen in mouse 1 (M1), aged 10 weeks (aspirated after 5 doses of PXS5338K), with collagen representing only 1.2 % area using morphometric analysis of PSR stain. Slightly more fibrosis was seen in the 11-week-old mice receiving either PXS5338K or

vehicle, with median % collagen at 2.62 % and 3.34 % respectively. There was no significant differences in fibrosis between mice receiving vehicle and those receiving PXS5338K both with (E) and without inclusion of the mouse killed after only 5 doses of PXS5338K (aged 11 weeks) (F) (median 3.34 % vs 2.31 %, p = 0.700 and median 3.34 % vs 2.62 %, p = 0.800 respectively). Statistical analysis was not performed for the remaining IHC given the small numbers of animals in each group.

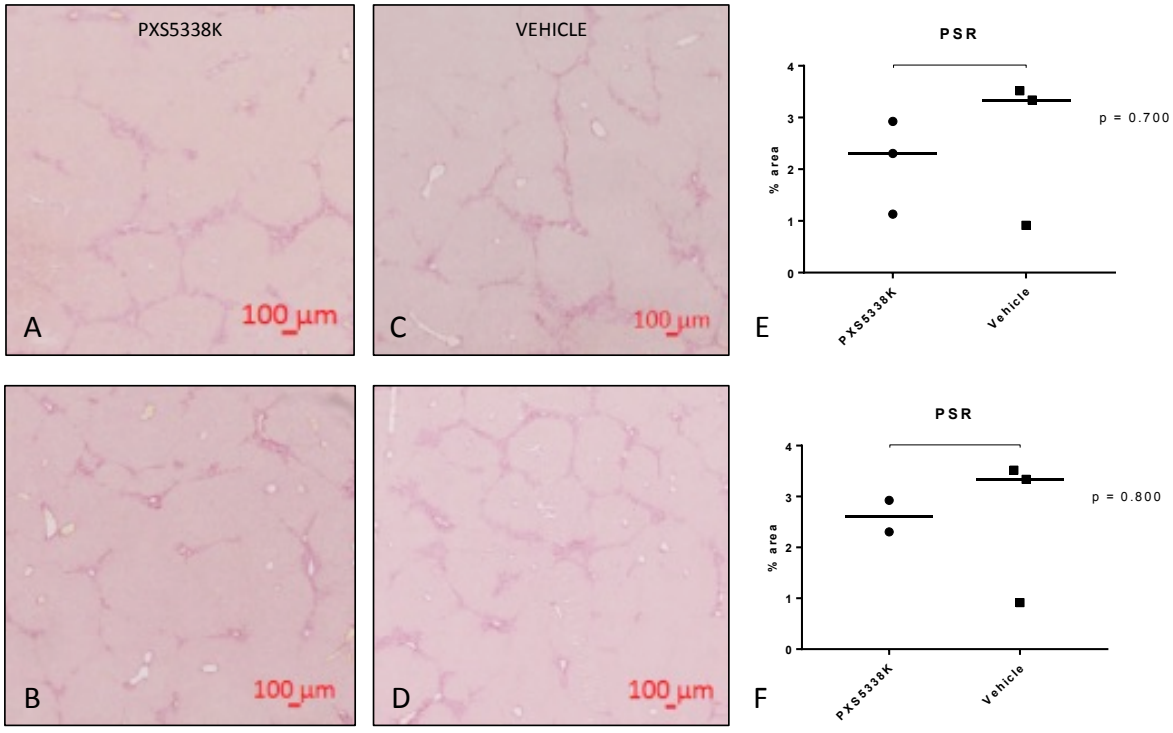


Figure 4.4 Mild fibrosis was demonstrated in FVB *Mdr2-/-* mice but no benefit with PXS5338K. PSR staining of paraffin embedded slides cut at 3 µm showing liver from 12 week old FVB *Mdr2-/-* mice following eight or nine gavages of PXS5338K (A and B respectively) at 10 mg/kg, or 9 gavages of vehicle (C and D). Morphometric analysis was performed to calculate the % area stained. There was no significant differences seen when median values for the two groups were compared both with (E) and without inclusion of the mouse killed after 5 doses of PXS5338K (F) (MW test).

4.3.2.3 Alpha-smooth muscle actin

Alpha-smooth muscle actin (α-SMA) is a marker of active hepatic stellate cells and is often used as surrogate marker for fibrosis severity. In liver fibrosis the pattern of staining usually mimics that of collagen deposition, or PSR stain. IHC for α-SMA was therefore used to assess the degree of fibrosis in the FVB *Mdr2-/-*mice and whether there was any difference in the pattern or severity of fibrosis in mice that received PXS5338K, despite not being the primary aim of this study.

However, the liver sections demonstrated less α-SMA positive staining than expected, even accounting for the FVB strain, and it was primarily at the site of blood vessels rather than at periportal or fibrotic areas. This raised suspicion that the antibody was detecting vessels rather than active HSCs. Nevertheless, % area of tissue stained following morphometric analysis was calculated but statistical comparison not carried out given the small number of animals and doubt regarding the IHC.

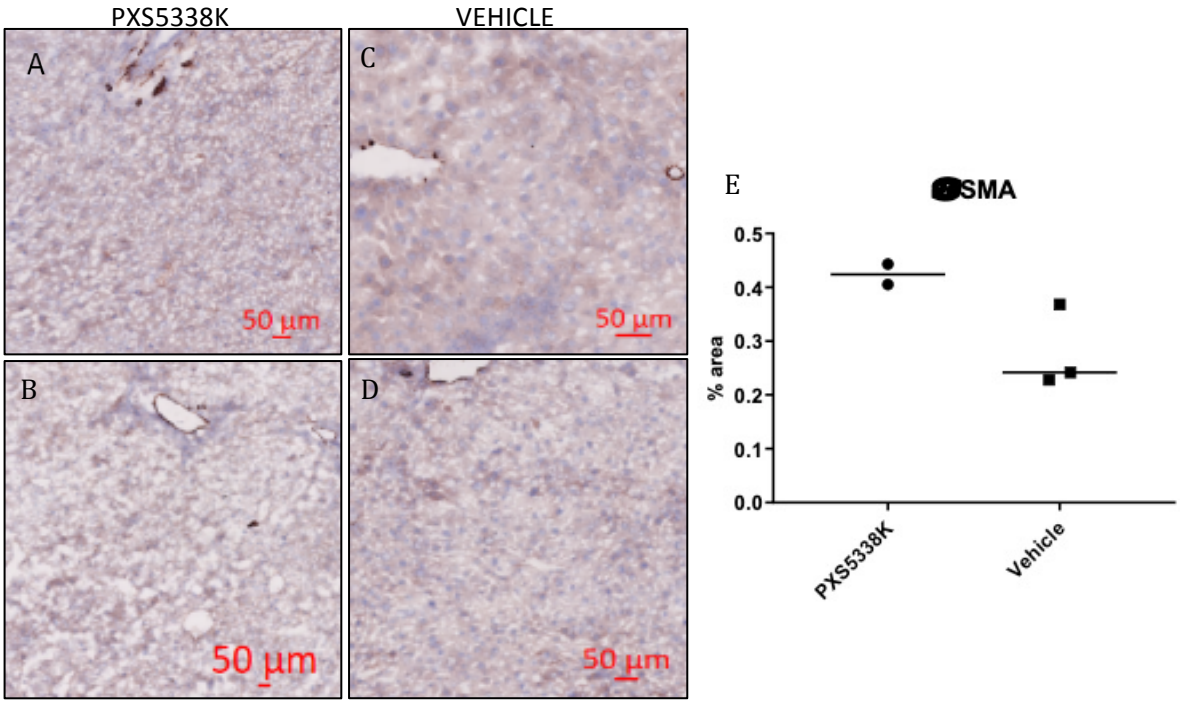


Figure 4.5 PXS5338K had no effect on hepatic stellate cell activation. Immunohistochemistry was performed on liver tissue cut on frozen slides from FVB *Mdr2-/-* mice receiving eight or nine gavages of either PXS5338K (A and B respectively) at 10 mg/kg, or 9 gavages of vehicle (C and D), for α-SMA. Morphometric analysis was performed to calculate the % area stained.

4.3.2.4 Cleaved caspase 3

IHC for cleaved caspase 3 was performed as a marker for apoptosis; I was specifically interested to see if there was increased apoptosis in those mice receiving PXS5338K, as a marker of increased liver injury induced by PXS5338K (given that compound had been poorly tolerated), but there was no evidence for increased apoptosis in these animals (Figure 4.6). Positively stained cells were few, with no fixed distribution, at no particular site of injury, and appeared consistent with lobular hepatocytes. The number of cells within five fixed fields of view were counted and the average number calculated for each mouse.

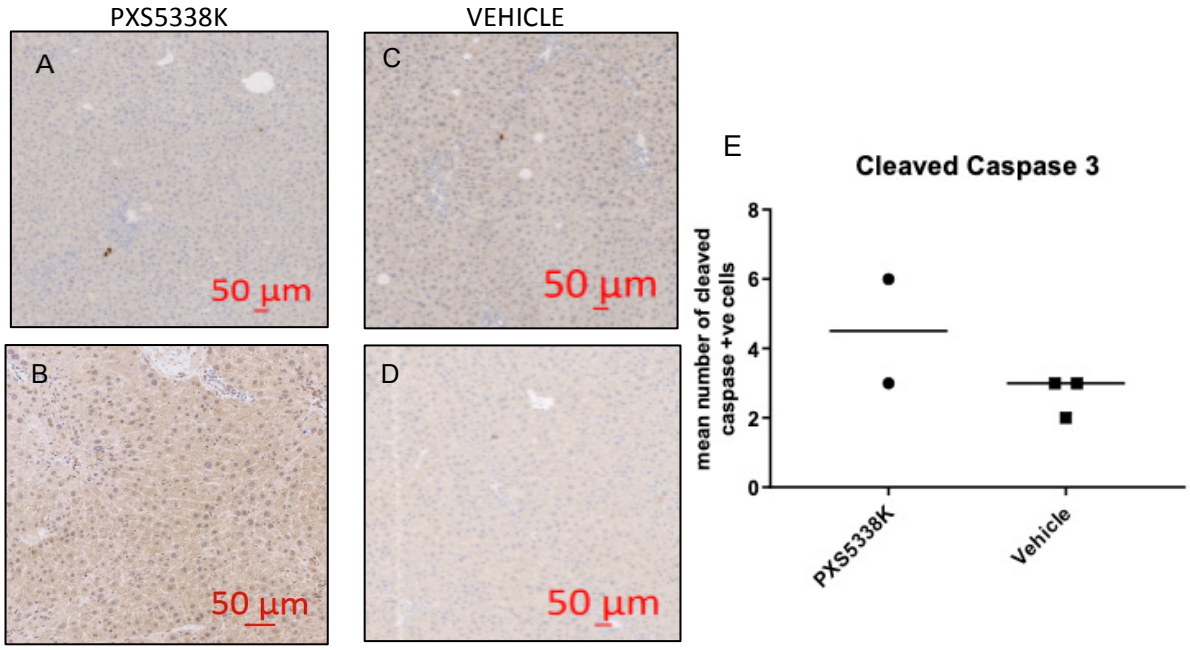


Figure 4.6 PXS5338K has no effect on apoptosis in the liver. Immunohistochemistry was performed on liver tissue cut on paraffin slides from FVB *Mdr2-/-* mice receiving eight or nine gavages of either PXS5338K (A and B respectively) at 10 mg/kg, or 9 gavages of vehicle (C and D), for cleaved caspase 3. The mean number of stain positive cells from 10 fields of view within a fixed area are demonstrated graphically for interest.

4.3.2.5 CD45

Fibrosis is typically driven by an immune response, therefore CD45 was used as a marker of immune cell infiltration. As for cleaved caspase 3, there was particular interest in assessing liver inflammation given the poor tolerability of PXS5338K. Staining was distributed around vessels and periportally in all 6 mice, and no pattern of injury or increase in staining were apparent in the mice that were unwell. Immune cell infiltration as measured by CD45 positive cells appeared similar in both groups.

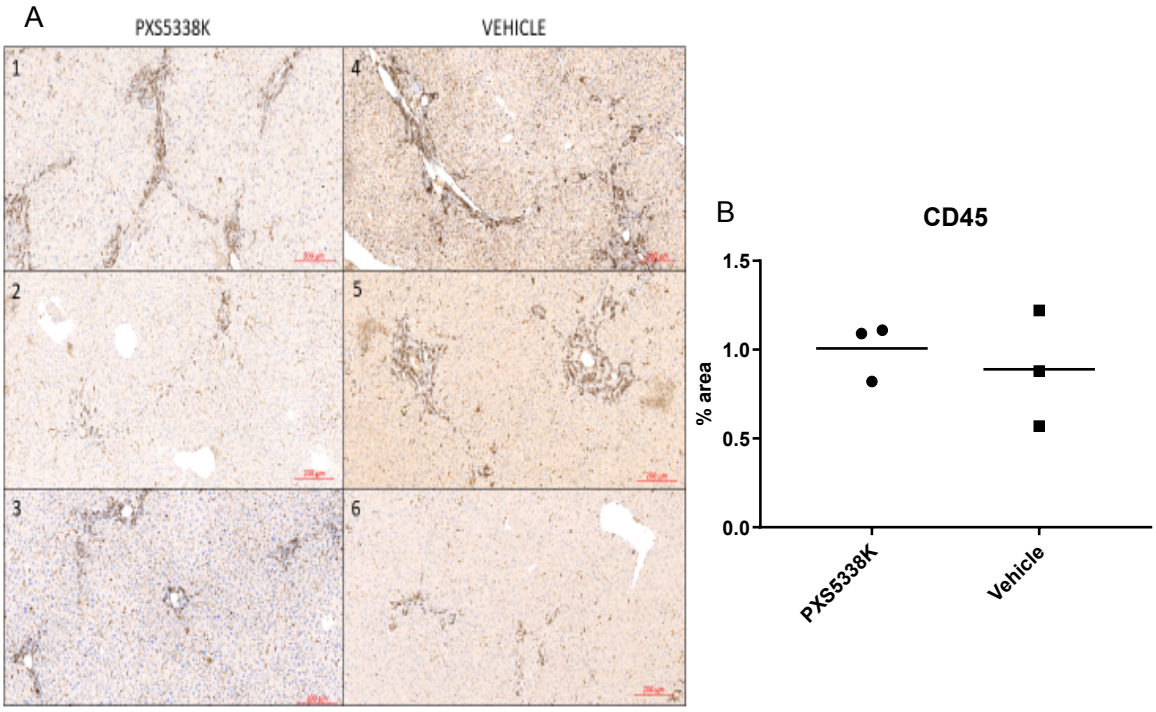


Figure 4.7 Immune cell infiltration as measured by CD45 was similar in mice receiving PXS5338K and vehicle. Immunohistochemistry was performed on liver tissue cut on paraffin slides from FVB *Mdr2-/-* mice receiving five, eight or nine gavages of either PXS5338K (mice 1, 2 and 3 respectively) at 10 mg/kg P.O., or 9 gavages of vehicle P.O. (mice 4-6), for CD45. % area positive stain for CD45 is demonstrated graphically.

4.3.2.6 SOX-9

Despite the absence of any differences in fibrosis or immune infiltration, inhibition of LOXL2 may have an impact on the ductular reaction. I therefore used IHC to detect SOX-9 positive cells in order to assess the severity of the ductular reaction, and to assess for differences in pattern of staining or epithelial differentiation of cells. In the group receiving PXS5338K, particularly mouse 2 (see Figure 4.8) there appeared to be a more lobular rather than biliary pattern of staining. This was unexpected given that the other IHC including H&E and PSR for this animal appeared similar to mouse 1 and 3. This pattern of staining could be interpreted as fewer cells differentiating toward a biliary lineage in the presence of PXS5338K.

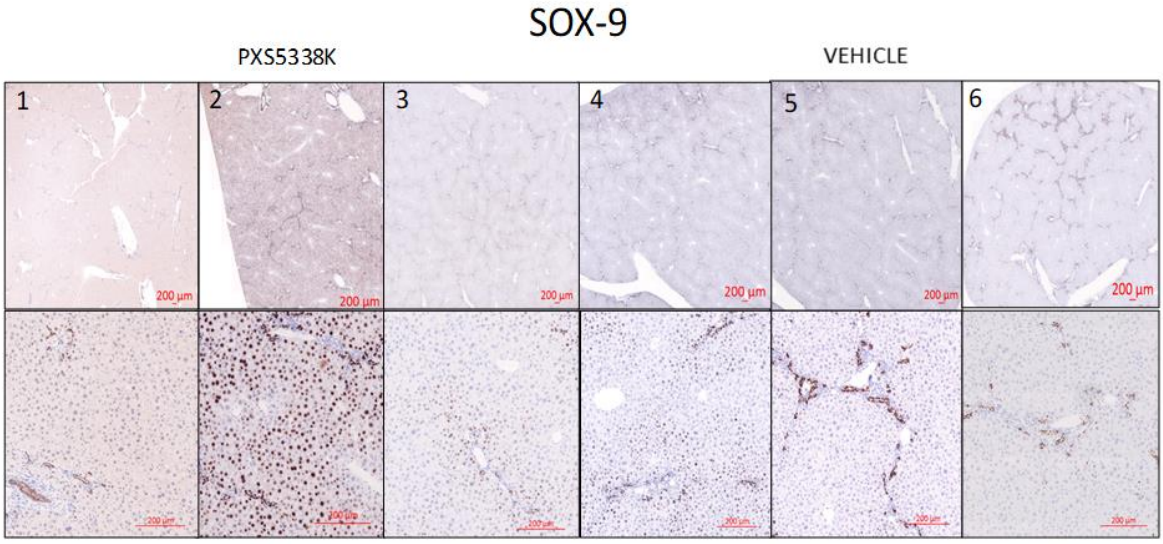


Figure 4.8 Some FVB *Mdr2-/-* mice receiving PXS5338K displayed a different pattern of SOX-9 positive cells compared with those receiving vehicle, in whom biliary structures were predominantly stained positive. Immunohistochemistry was performed on liver tissue cut on paraffin slides from FVB *Mdr2-/-* mice receiving gavage of either PXS5338K (1-3) at 10 mg/kg, or 9 gavages of vehicle (4-6), for SOX-9. Liver tissue from all 6 animals are shown at low and high magnification; those mice receiving PXS5338K (5, 8 and 9 doses for animals in 1, 2 and 3 respectively), and 9 doses of vehicle in animals 4, 5 and 6. A pattern of lobular rather than biliary SOX-9 positive cells was seen in the mice receiving PXS5338K compared with vehicle.

4.3.3 Real time quantitative polymerase chain reaction (qPCR)

As surrogate markers of fibrosis severity, expression of mRNA for collagen I, III and elastin were measured by extraction of mRNA and qPCR. The expression of LOX and the lysyl oxidase family was also assessed, as there is little published data for this model and strain. Unfortunately RNA could not be extracted for the animal that received only 5 doses of PXS5338K and became unwell unexpectedly. I was unable to obtain accurate expression of LOXL2 or LOXL3, which may reflect low levels of expression, or may be due to experimental error.

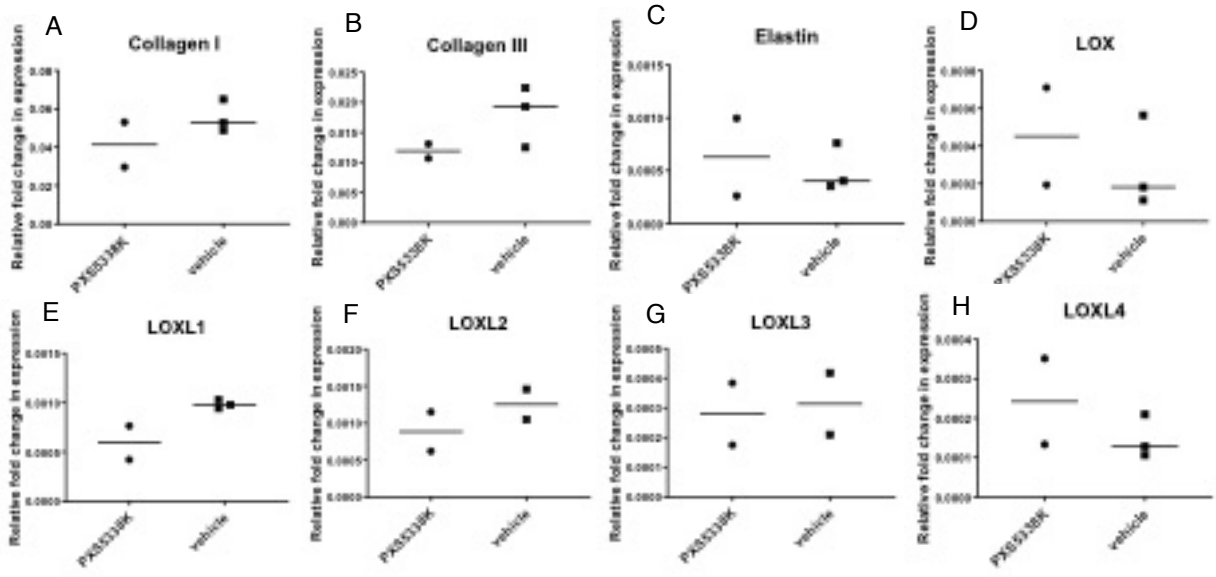


Figure 4.9 No differences were seen in expression of ECM proteins or lysyl oxidases in a murine model of biliary fibrosis. RNA was extracted from the livers of FVB *Md2-/-* mice receiving eight or nine gavages of PXS5338K, or nine gavages of vehicle, and qPCR was performed to assess the expression of collagen 1 alpha 1 (A), collagen 3 alpha 1 (B), elastin (C), LOX (D) and LOXL1-4 (E-H) relative to the expression of *Gapdh*..

4.3.4 Conclusions: pilot study of PXS5338K in FVB *Mdr2-/-* mice

This was a small pilot study assessing the impact and tolerability of PXS5338K in the knock out *Mdr2-/-* model of biliary fibrosis using the FVB strain of mice. Evidence of early bridging fibrosis was seen on PSR stain in all mice which was associated with CD45-positive inflammatory infiltrate. Some trend toward reduced PSR stain and expression of collagen I and III was seen in the group receiving PXS5338K compared with vehicle, but with such small numbers of mice, the differences did not meet statistical significance, and no real conclusions can be drawn. However, this pilot study permitted investigation of the impact of the inhibitor on liver histology, and aided in the design of a more robust study of the effects of the inhibitor.

As previously discussed, studies have suggested a potential role for LOXL inhibition to influence differentiation of cells arising from the ductular reaction; specifically that in the presence of LOXL2 inhibition, progenitor cells have a tendency towards a hepatocyte rather than biliary lineage, with potential consequences for ameliorating fibrosis. The results for SOX-9 may support this theory but require further investigation.

The compound was administered thrice weekly and tolerated well until the eighth and ninth dose at days 17 and 19, respectively. Analysis of serum results, H&E, and cleaved caspase 3 results did not reveal a clear cause for the deterioration. *Mdr2*-/- mice are known to develop gallstones, albeit more commonly in females (272), and so it is possible that the two mice becoming unwell developed such complications, despite a lack of stones at PM. It is also possible that PXS5338K is not excreted or metabolised as efficiently in *Mdr2-/-* mice when compared to wild-type animals that apparently exhibited no adverse events at this dose previously (Pharmaxis, personal communication). I had, however, received data that other laboratories had similar problems with wild type mice at the 10 mg/kg dose. The compound was further tested in wild-type mice with no liver injury at the lower dose of 3 mg/kg, administered daily P.O., and confirmed tolerability. Thereafter, the experiment was repeated in a larger cohort of C57Bl/6 *Mdr2-/-.*

4.4 Assessing the effects of PXS5338K in C57Bl/6 *Mdr2-/-* mice

A follow up experiment to the pilot was devised where 36 nine week old C57Bl/6 *Mdr2-/-* mice each received 9 doses of either vehicle or 3 mg/kg PXS5338K over three weeks and were culled 72 hours following the 9th dose (see Figure 4.10). A small group of 5 mice received no intervention by gavage and were used as control to observe any effect elicited by this intervention.

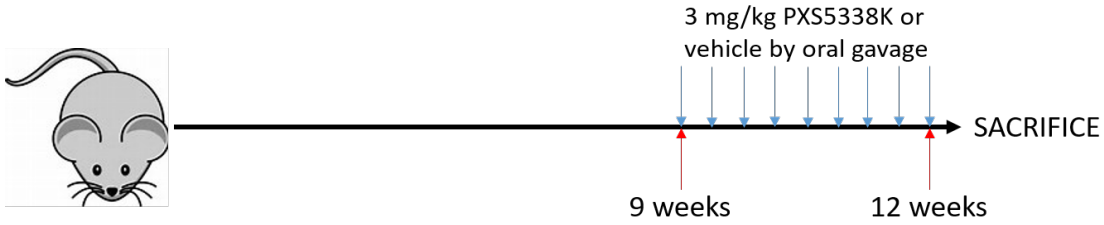


Figure 4.10 Model for testing PXS5338K in C57Bl/6 *Mdr2-/-* mice. Six 9 week old C57Bl/6 *Mdr2-/-* mice received 9 doses of PXS5338K at 10 mg/kg by oral gavage over 3 weeks (Monday, Wednesday, Friday) and were culled 72 hours following the 9th gavage.

4.4.1 Assessment of liver injury

PXS5338K was well tolerated by C57Bl/6 *Mdr2-/-* mice at this dose and no mice were culled due to weight loss or becoming sick. Some serum results were unavailable for analysis due to haemolysis of the blood sample following cull. There was no difference in weight change between the group receiving vehicle vs PXS5338K, or the group that had no intervention (median change 7.4 % vs 6.9 % vs 6.4 %, p = 0.89) using the KW test and post hoc Bonferroni–Dunn correction to compare median % change (see Figure 4.11).

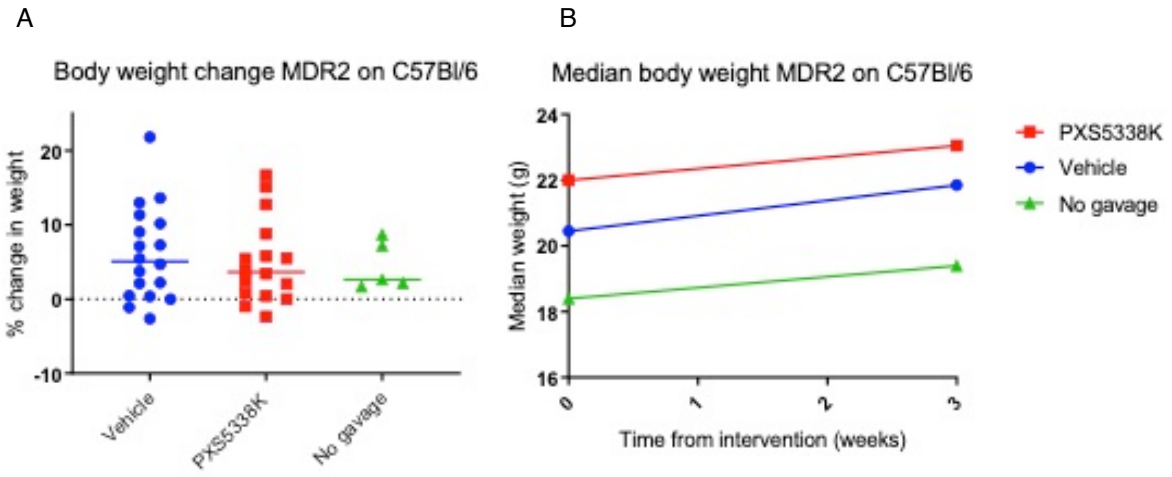


Figure 4.11 Model for testing PXS5338K in C57Bl/6 *Mdr2-/-* mice. Six 9 week old C57Bl/6 *Mdr2-/-* mice received 9 doses of PXS5338K at 10 mg/kg by oral gavage over 3 weeks (Monday, Wednesday, Friday) and were culled 72 hours following the 9th gavage. Graph (A) demonstrates median % change in weight from start of gavage to end of gavage at 3 weeks. No significant differences were seen using KW test and post analysis Bonferroni-Dunn correction. Graph (B) demonstrates mean weight of the mice for each group during the 3-week experiment.

4.4.1.1 Assessment of liver injury: Serum analysis

Terminal cardiac puncture facilitated analysis of serum at the end of the three week treatment period. Serum AST and ALT levels appear slightly lower than other published data and previous data from Birmingham (265, 271), as for the FVB strain. No differences were seen for biochemical markers of liver injury between mice receiving vehicle compared with those receiving compound, or no gavage (Figure 4.12; mean rank 17.19 vs 13.08 vs 20.5, p = 0.247 respectively for AST, and mean rank 16.38 vs 18.05 vs 9.70, p = 0.214, for ALT using the KW), except for a small increase in bile acids in those animals not undergoing oral gavage (mean rank 15.27 vs 12.96 vs 25.80, p = 0.021). This confirms no liver injury induced by the oral gavage itself. Oddly, the mouse with the outlying result for bile acids in the no gavage group had unremarkable AST and ALT; likewise, mice in the PXS5338K and vehicle group had concurrently high AST and ALT but normal bile acids, suggesting possible

variation in liver injury between individual C57Bl6 *Mdr2-/-* mice; it is worth noting, however, that AST and ALT were not particularly elevated above normal range.

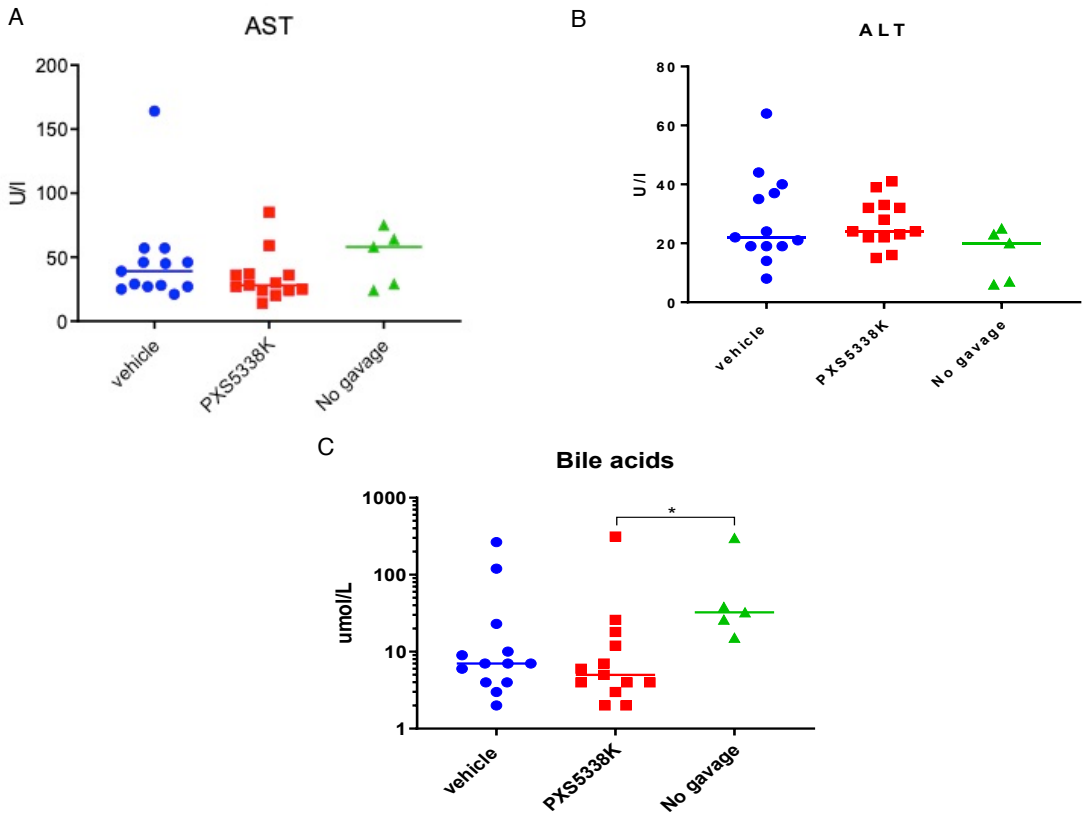
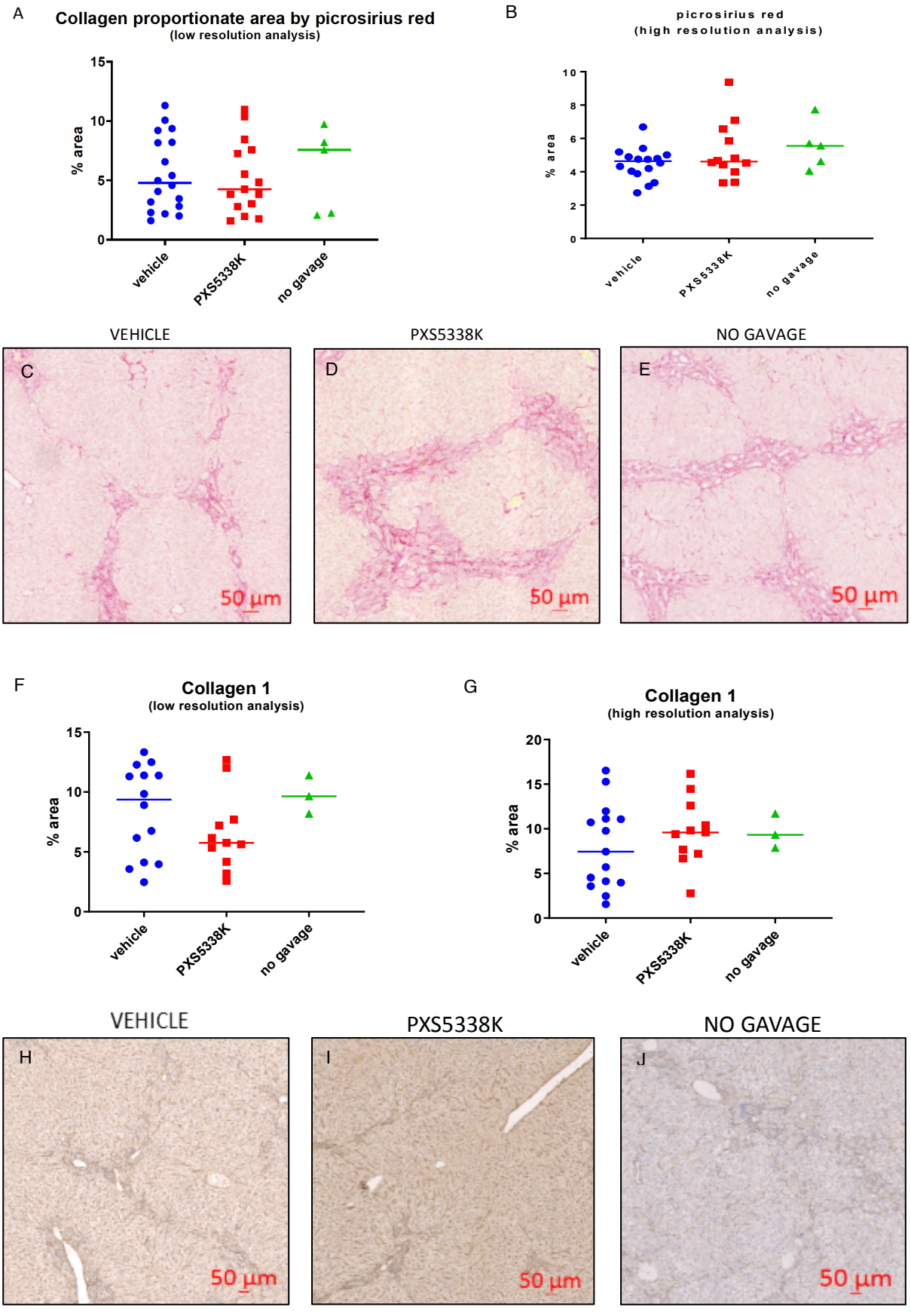


Figure 4.12 Serum biochemistry for liver injury were no different between animals administered with PXS5338K vs vehicle, or no gavage. 41 nine-week-old C57Bl/6 *Mdr2-/-* mice received 9 doses of vehicle (n = 13), 3 mg/kg PXS5338K (n = 13), or nil by oral gavage (n = 5). Serum biochemistry was evaluated at cull and showed no differences between the groups using KW test and post analysis Bonferroni-Dunn correction.

4.4.2 Assessment of liver fibrosis

4.4.2.1 Immunohistochemistry

Fibrosis was assessed by detecting collagens using the PSR stain and collagen I, collagen III and α-SMA with IHC. Periportal and bridging fibrosis was observed in a similar pattern to that seen in previously in the C57Bl/6 strain, but again the bridging fibrosis was much more marked. The % area stained using PSR was between 3 and 7 %, and no differences were observed comparing mice receiving vehicle, PXS5338K, or no gavage with the KW test (Figure 4.13; mean ranks 14.78, 17.88, 22.00, p = 0.320). Similarly, assessment of fibrosis with IHC for collagen I and collagen III demonstrated moderate fibrosis in all groups but no reduction in collagen with PXS5338K (mean ranks 15.68, 11.86, 18.67, KW test p = 0.335 for collagen I, and mean ranks 16.0, 12.7 and 18.0, p = 0.561, for collagen III). Picrosirius red and collagen I were analysed in two ways, firstly at low magnification, whereby an image is captured to include as much of the slide (and liver lobe) as possible and then the % positively stained area is calculated. Secondly, the same liver sections were reanalysed by taking 5 images for each slide at higher magnification, where the detail of fibrils were more closely captured, and the mean % positive staining calculated for each slide. Although a small increase was seen for collagen in mice receiving PXS5338K, when they were analysed at high resolution differences between the groups were not significant. The intention was again to detect activated hepatic stellate cells by IHC for α-SMA as a surrogate for active fibrosis, but the antibody seems to have detected vasculature rather than aHSCs. However, no differences were seen for mice receiving vehicle, PXS5338K, or nil (mean ranks 0.39, 0.46, 0.42, respectively, KW test 0.578).


A
Collagen proportionate area by picrosirius red
(low resolution analysis)
% area
15
10
5
0
vehicle
PXS5338K
no gavage
B
picrosirius red
(high resolution analysis)
% area
10
8
6
4
2
0
vehicle
PXS5338K
no gavage
VEHICLE
PXS5338K
NO GAVAGE
C
D
E
50 µm
50 µm
50 µm
F
Collagen 1
(low resolution analysis)
% area
15
10
5
0
vehicle
PXS5338K
no gavage
G
Collagen 1
(high resolution analysis)
% area
20
15
10
5
0
vehicle
PXS5338K
no gavage
VEHICLE
PXS5338K
NO GAVAGE
H
I
J
50 µm
50 µm
50 µm

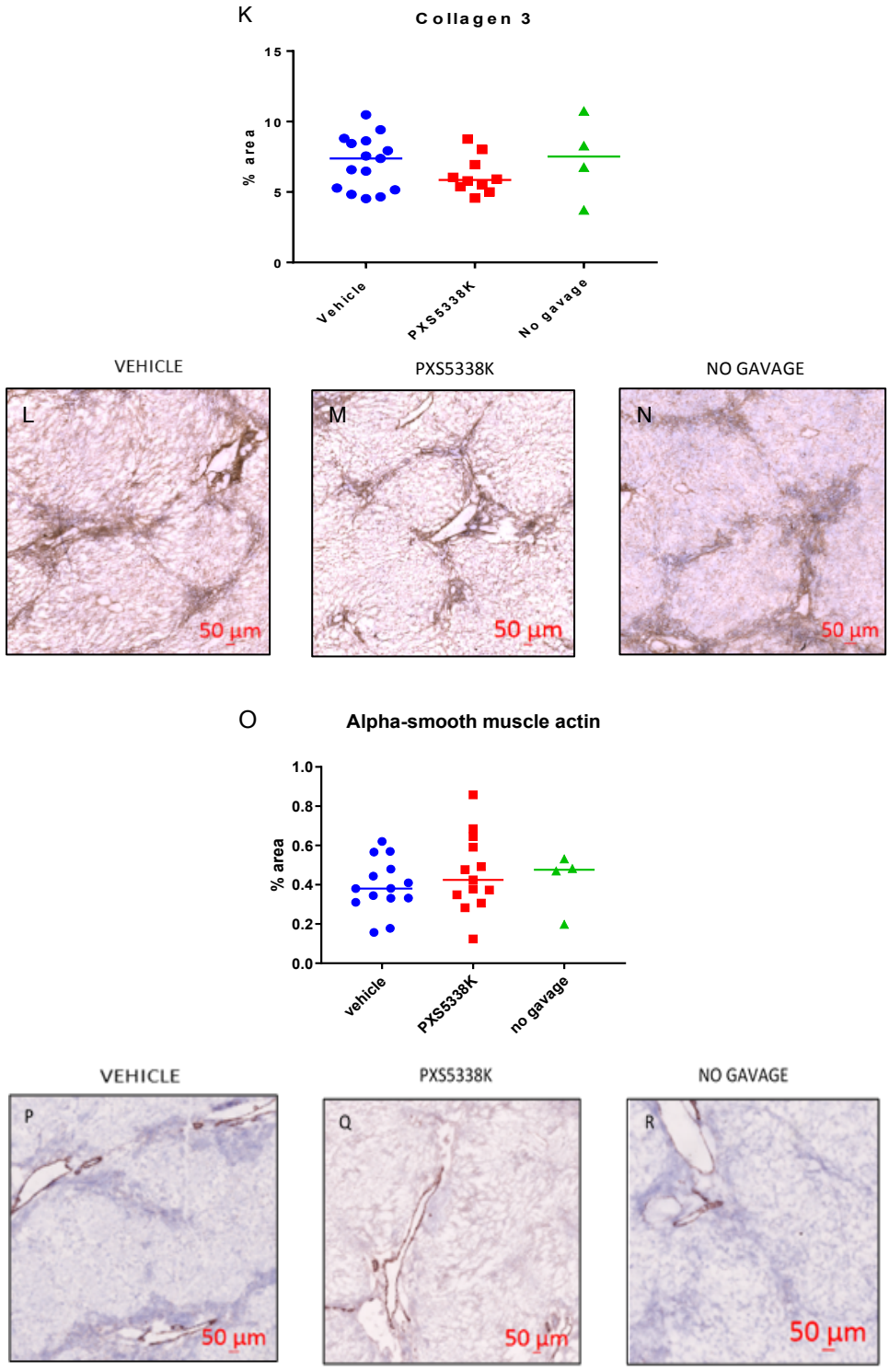
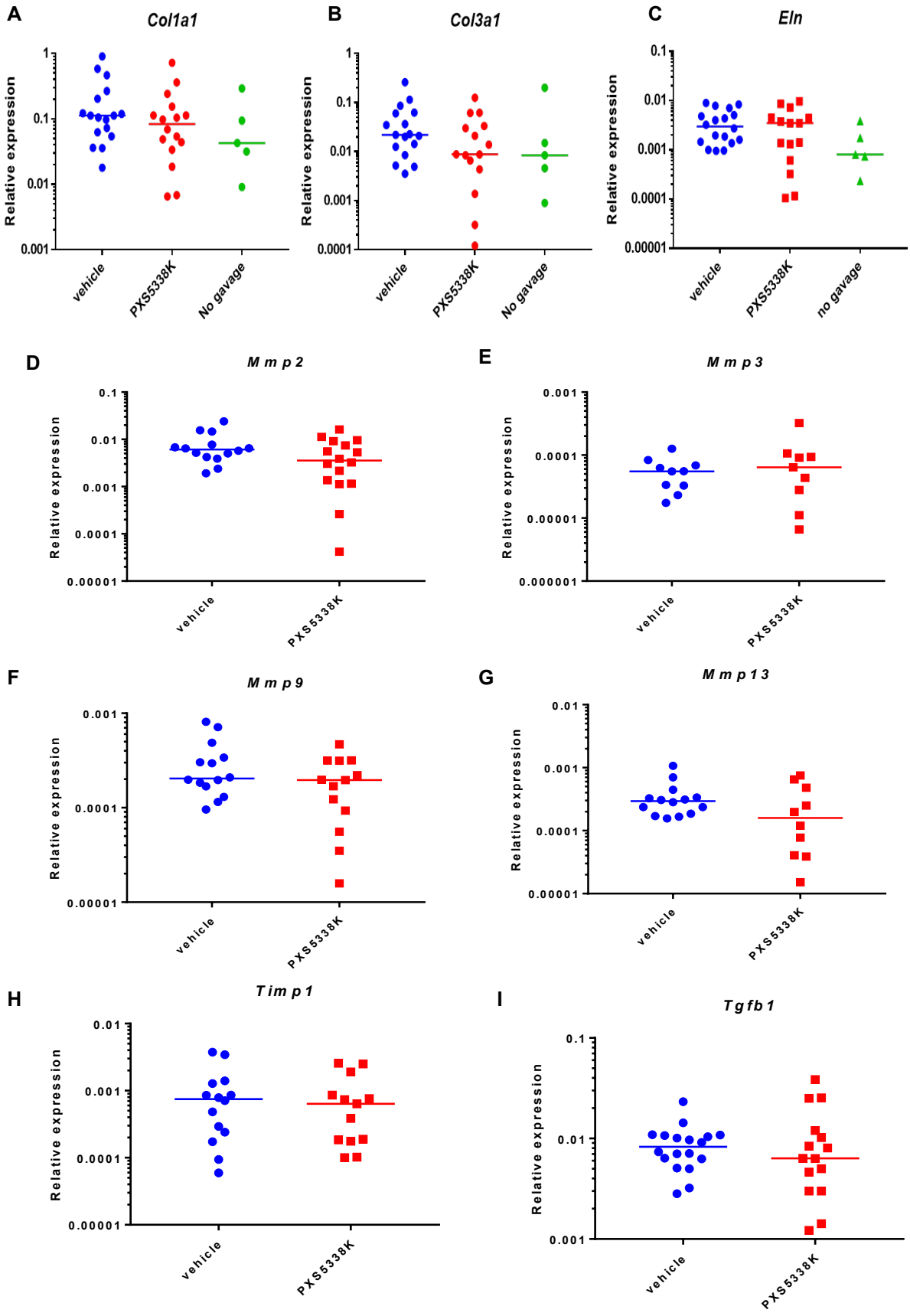


Figure 4.13 PXS5338K did not improve fibrosis in C57Bl6/ *Mdr2-/-* mice for liver injury were no different between animals administered with PXS5338K vs vehicle, or no gavage. 41 nine week old C57Bl/6 *Mdr2-/-*mice received 9 doses of vehicle, 3 mg/kg PXS5338K, or nil by oral gavage. Paraffin embedded, or frozen, slides were cut at 3 µm and IHC with morphometric analysis was performed for PSR (A-E) and collagen I (F-J) (analysis at low and high resolution), collagen III (K-N) and α-SMA (O-R). Graphs represent median values for % area positive staining.

4.4.2.2 Assessment of fibrosis: protein expression by during qPCR

Real-time polymerase chain reaction (qPCR) was used to assess expression of proteins upregulated during fibrosis. There were no differences in gene expression of ECM proteins between mice receiving vehicle, PXS5338K, or no gavage for collagen I using the KW test to compare mean ranks (mean rank 22.41, 18.13, 14.00, p = 0.268), collagen III (22.18, 16.60, 15.40, p = 0.252) or elastin (22.22, 18.87, 11.60, p = 0.161) (Figure 4.14). Given that gavage appeared to have no impact on liver injury or fibrosis in the mice, only the groups receiving vehicle or PXS5338K are compared hereafter. No differences in expression of matrix metalloproteinases or *Timp1* were found between these two groups using MW test to compare median value for gene expression compared with the housekeeping gene (*Mmp2* median 0.0061 vs 0.0036, p = 0.131, *Mmp3* median 0.0005 vs 0.0006, p = 0.719, *Mmp9* medians 0.0002 vs 0.0002, p = 0.254, *Mmp13* median 0.0003 vs 0.0002, p = 0.186 and *Timp1* median 0.0007 vs 0.0006, p = 0.756 for vehicle vs PXS5338K, respectively). Expression of *Tgfb1* and *Acta2* were also measured but no differences were seen for vehicle vs PXS5338K (*Tgfb1*, median 0.008 vs 0.006, p = 0.514 and *Acta2* 0.0006 vs 0.0005, p = 0.976). *Sox9* expression was measured as a surrogate marker of the ductular reaction and possible epithelial differentiation, and no differences were seen between the two groups (median 0.0045 vs 0.0033, p = 0.174).


A
Col1a1
Relative expression
1
0.1
0.01
0.001
vehicle
PXS5338K
No gavage
B
Col3a1
Relative expression
1
0.1
0.01
0.001
0.0001
vehicle
PXS5338K
No gavage
C
Eln
Relative expression
0.1
0.01
0.001
0.0001
0.00001
vehicle
PXS5338K
no gavage
D
M m p 2
Relative expression
0.1
0.01
0.001
0.0001
0.00001
vehicle
PXS5338K
E
M m p 3
Relative expression
0.001
0.0001
0.00001
0.000001
vehicle
PXS5338K
F
M m p 9
Relative expression
0.001
0.0001
0.00001
vehicle
PXS5338K
G
M m p 1 3
Relative expression
0.01
0.001
0.0001
0.00001
vehicle
PXS5338K
H
T i m p 1
Relative expression
0.01
0.001
0.0001
0.00001
vehicle
PXS5338K
I
T g f b 1
Relative expression
0.1
0.01
0.001
vehicle
PXS5338K

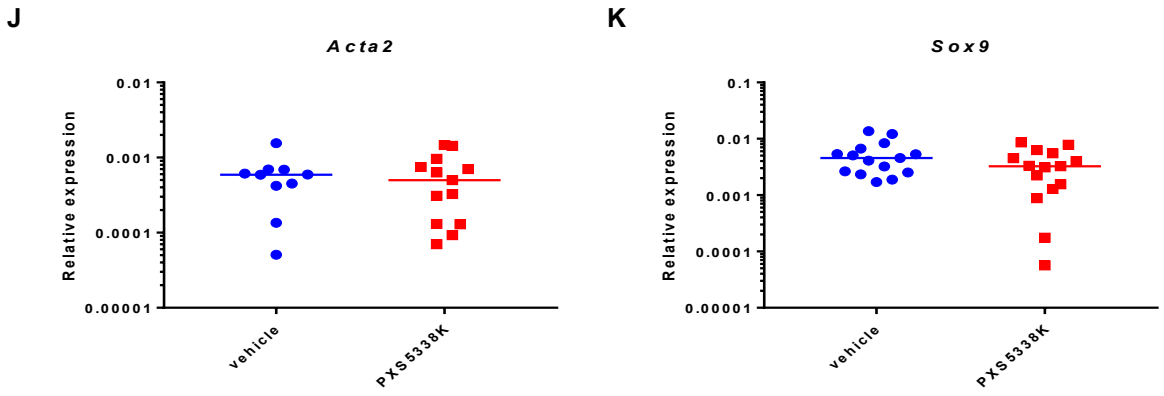


Figure 4.14 PXS5338K did not modulate expression of mRNA for proteins usually upregulated during fibrosis in C57Bl6/ *Mdr2-/-* mice. 36 nine-week-old C57Bl/6 *Mdr2-/-* mice received 9 doses of vehicle, or 3 mg/kg PXS5338K, by oral gavage. RNA was extracted from frozen liver tissue and relative expression of mRNA was quantified against expression of the housekeeping gene *Gapdh*. No differences were seen comparing median values of the groups for mRNA expression of *Col1a1*, *Col3a1, Eln, Mmp2, Mmp3, Mmp9, Mmp13, Timp1, Tgfb1, Acta2 or Sox9* (A-K).

Expression of Lysyl oxidases

Expression of the lysyl oxidase family, particularly LOX and LOXL2 are demonstrated to be elevated in the TAA mouse model of liver injury (see 1.5.3.3.2). It is possible that inhibition of LOXL2 may induce upregulation of other members of the LOX/L family as a compensatory mechanism. I therefore wanted to assess expression in C57Bl/6 *Mdr2-/-* with and without PXS5338K (Figure 4.15). No differences were seen for expression of any of the lysyl oxidase enzymes using the MW test (LOX median 0.0011 vs 0.005, p = 0.130, LOXL1 median 0.0007 vs 0.006, p = 0.841, LOXL2 median 0.0015 vs 0.0016, p = 0.592, LOXL3 median 0.0003 vs 0.0002, p = 0.213, LOXL4 median 0.0008 vs 0.0004, p = 0.237 for vehicle vs PXS5338K, respectively).

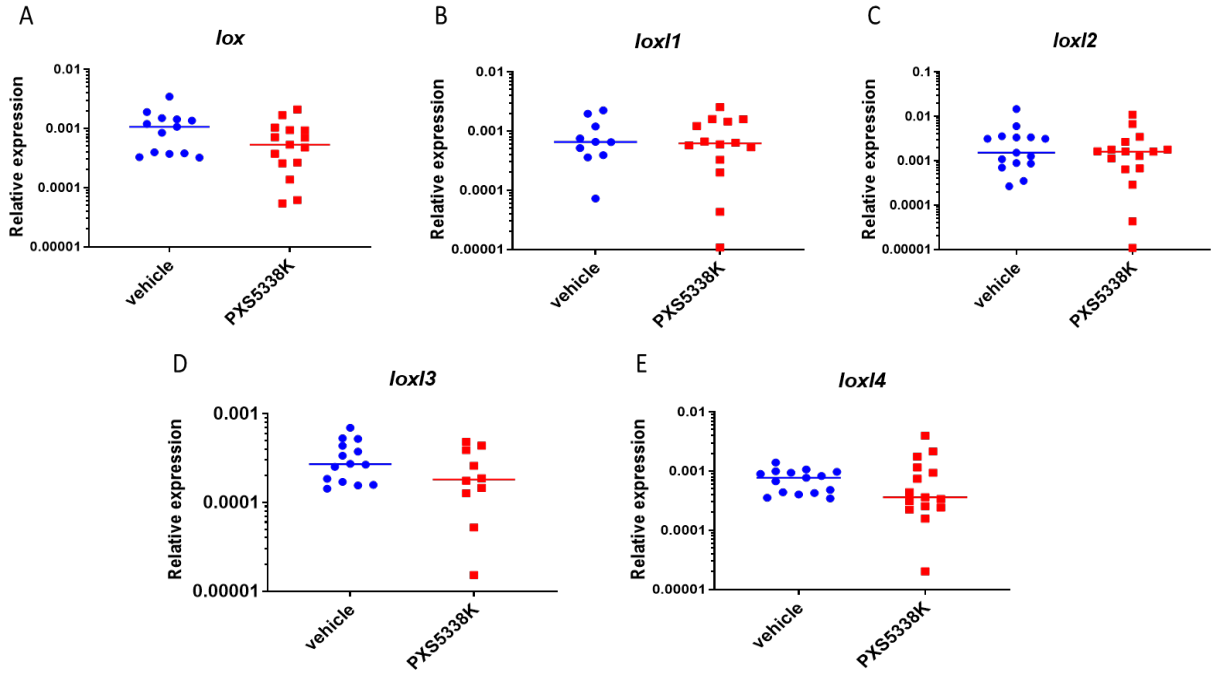


Figure 4.15 PXS5338K did not modulate expression of lysyl oxidase family genes in C57Bl6/ *Mdr2-/-* mice. 36 nine week old C57Bl/6 *Mdr2-/-*mice received 9 doses of vehicle, or 3 mg/kg PXS5338K, by oral gavage. RNA was extracted from frozen liver tissue and relative expression of mRNA was quantified against expression of the housekeeping gene *Gapdh*. No differences between the groups were seen for expression of mRNA for proteins *Lox, Loxl1, Loxl2, Loxl3 or Loxl4* (A-E) with MW test. Graphs represent median values.

4.4.3 Evaluation of cell differentiation and proliferation using IHC for SOX-9

There was particular interest in evaluating the effect of PXS5338K on cell differentiation and proliferation given the altered pattern of staining in at least one of the FVB *Mdr2*-/- in the pilot study. Unfortunately due to poor quality staining (faded) on some slides, not all could be analysed for % area of staining. However the pattern of staining was more in keeping with biliary or epithelial cells in all animals (receiving vehicle, PXS5338K, or no gavage), rather than the scattered, pan-lobular appearance that was seen in the pilot study. There was no difference in the % area of SOX-9 staining, suggesting no difference between groups in cell proliferation or fibrosis severity, comparing mean ranks using the KW test (mean ranks 9.38, 10.25, 11.00, p = 0.91 for vehicle vs PXS5338K vs no gavage, respectively).

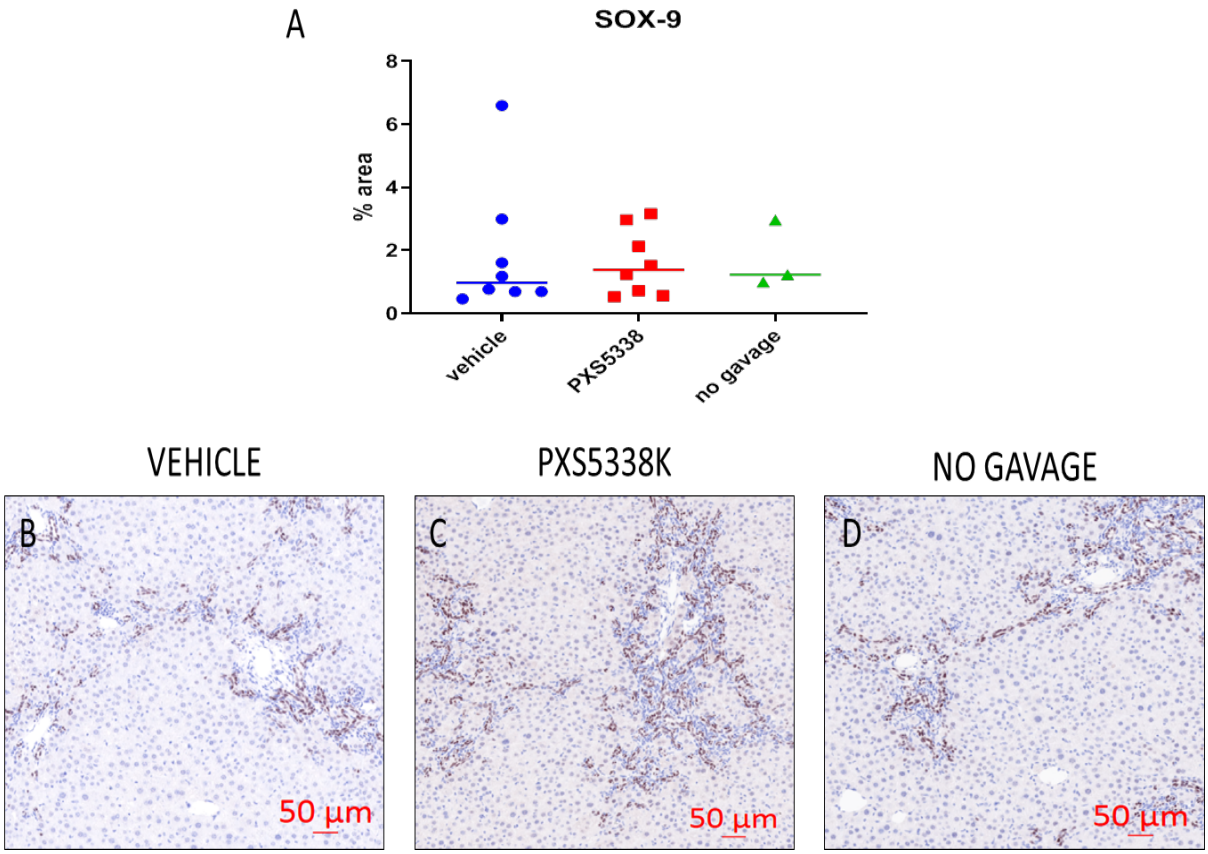


Figure 4.16 Administration of PXS5338K at 3 mg/kg does not alter cell proliferation or differentiation according to SOX-9 IHC in C57Bl/6 *Mdr2-/-* mice. 36 nine week old C57Bl/6 *Mdr2-/-* mice received 9 doses of vehicle, or 3 mg/kg PXS5338K, by oral gavage, with 5 C57Bl/6 receiving no gavage. Paraffin-embedded liver tissue was used to assess presence of SOX-9 and demonstrated no changes in the distribution or volume of SOX-9 positive cells in mice receiving PXS5338K.

4.4.4 Immune cell infiltration in C57Bl/6 *Mdr2-/-* mice treated with PXS5338K

The immune system is known to have an important role during liver injury, as detailed in 1.2.5. Isolation of lymphoid and myeloid cells for flow cytometry and assessment of liver sections using IHC facilitated assessment of whether inhibition of LOXL2 affects immune cell infiltration during liver injury and fibrogenesis. Following cull by cervical dislocation, the liver is flushed *in situ* so that intrahepatic immune cell populations are observed as much as possible, with minimal contribution from peripheral blood leukocytes. Unfortunately because the experiment was carried out over months (C57Bl/6 mice reaching 9 weeks of age as they were bred at different time points), and because the flow panel had not been fully optimised, data from only a few experiments could be used resulting in a smaller cohort of results. This was less of a problem for the myeloid panel.

4.4.4.1 Immune cell infiltration as measured by flow cytometry

Populations of NKT cells and B lymphocytes

CD49b+ NKT cells comprise approximately a third of lymphocytes and secrete the cytokines IFNγ and IL-4 which attracts profibrogenic macrophages (68). CD19+ B cells have a T cell-independent role in fibrosis (fibrosis being attenuated in B cell deficient mice) possibly through mediation of CD4+ and NKT cell activity, but also by production of soluble factors that directly stimulate collagen production in hepatic stellate cells (65).

To assess the population of CD49b+ NKT and CD19+ B cells, lymphoid cells were isolated from C57Bl/6 *Mdr2-/-* mice receiving either vehicle or 9 doses of either

PXS5338K, and fluorescently labelled as described in 2.2.5.1. The frequency of each population of lymphocytes was examined by flow cytometry, in which the total lymphocyte population cloud was subject to gating on the live cells, and subsequently gated on expression of CD3 and co-receptors (Figures 4.17). No differences were seen in the % of CD3- CD49b+ NKT cells calculated as a proportion of live cells comparing median % for individual mice in each group the MW test (median 21.21% vs 19.42%, p = 0.556 for vehicle and PXS5338K, respectively). Likewise, CD3- CD19+ B cells were calculated as a % of live CD3+ cells, but no differences were seen for vehicle vs PXS5338K (196.1% vs 100.4%, p 0.162 using the MW test).

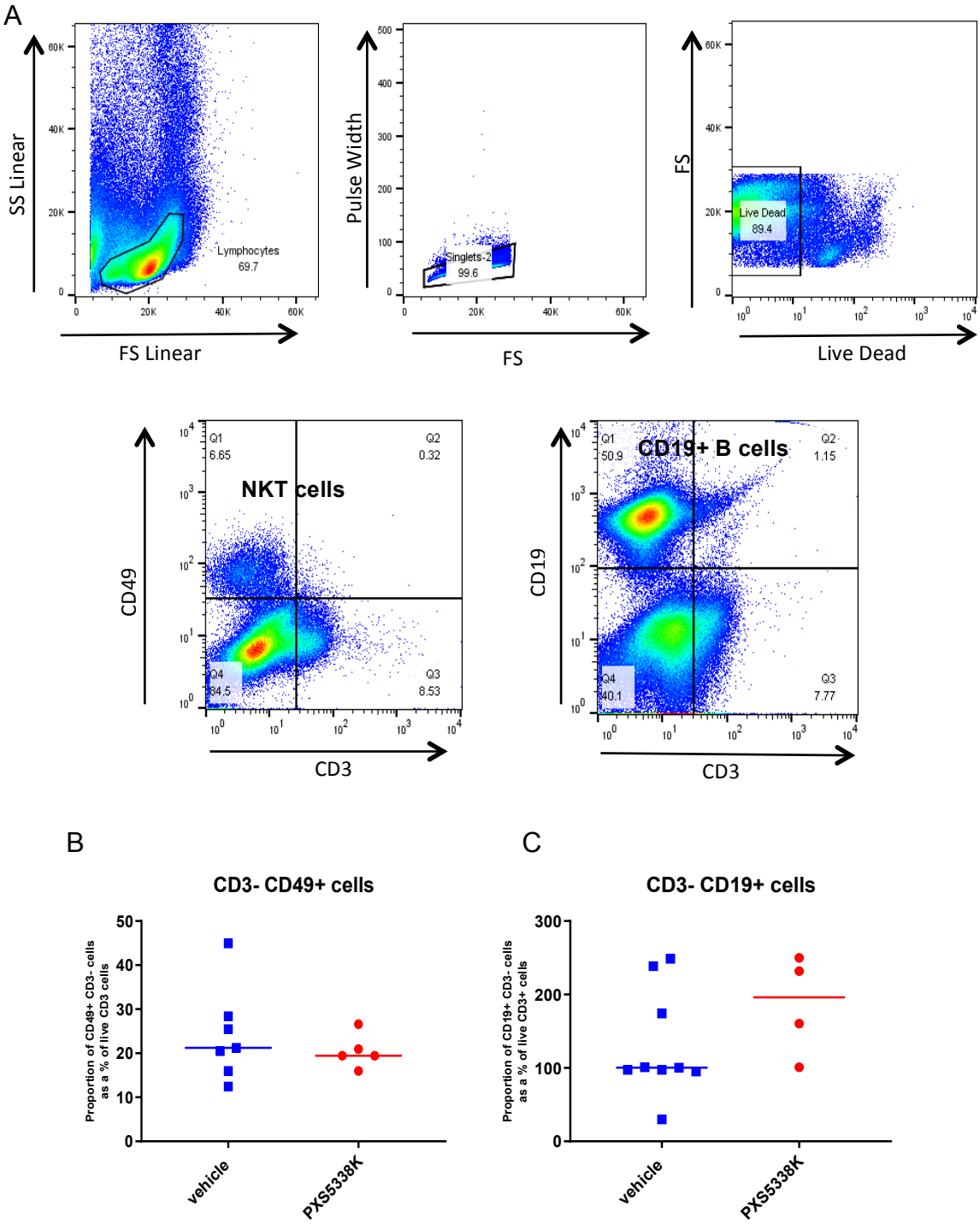
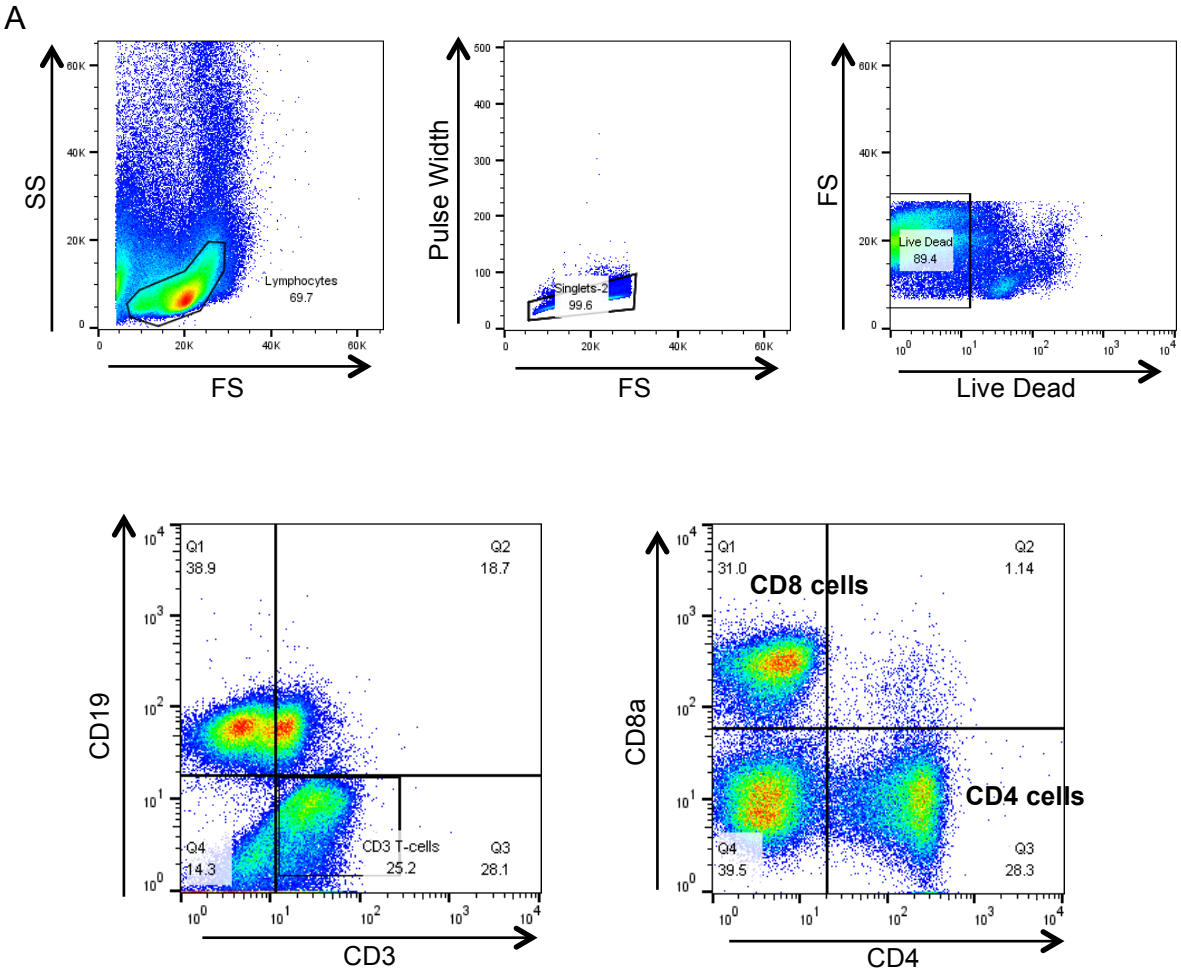


Figure 4.17 Comparison of lymphoid cell isolates from liver showed no differences between C57Bl/6 *Mdr2-/-* mice receiving 9 doses of PXS5338K or vehicle by oral gavage. The standard flow cytometry gating strategy used to identify tissue-infiltrating lymphocyte populations is illustrated in (A): forward and side light scatter (FS and SS, respectively), and absence of dead cell staining defined live singlet lymphocytes. This population was further subdivided into CD3- CD49b+ cells, and CD3- CD19+ cells. No differences were seen in mice receiving PXS5338K or vehicle comparing median % of cells for these populations (presented in B and C) using the MW test.

CD4 and CD8 positive T cells

CD45+ leukocytes initiate the inflammatory response at the site of injury and recruit CD3+ T cells (5, 44). CD4+ T helper cells and CD8+ cytotoxic T cells are also upregulated in liver disease, although their role is not fully understood (38, 61, 62). The population of CD4+ and CD8+ T cells was assessed by isolation of lymphocytes and fluorescent labelling of CD4+ and CD8+ cells; the population was calculated as a proportion of live CD3+ cells. No differences were seen for % of CD4 cells (median 29.8% vs 33.3%, p = 0.486) or CD8 cells (median 17.7% vs 21.1%, p = 0.081) using the MW test to compare medians % for mice receiving vehicle vs PXS5338K, respectively.



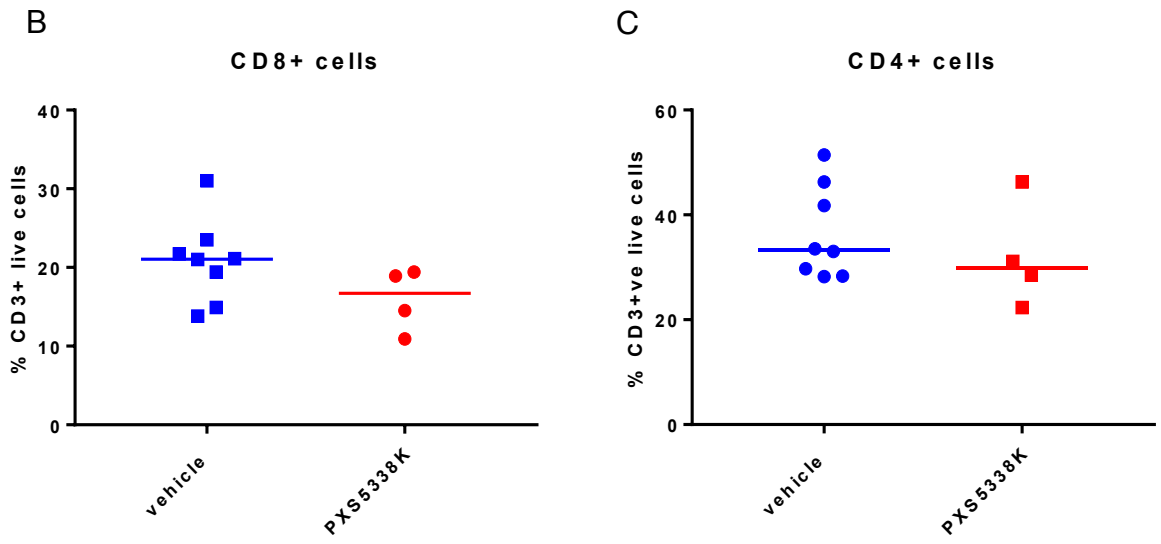


Figure 4.18 Comparison of lymphoid cell isolates from liver showed no differences between C57Bl/6 *Mdr2-/-* mice receiving 9 doses of PXS5338K or vehicle by oral gavage. The standard flow cytometry gating strategy to identify tissue-infiltrating lymphocyte populations is illustrated in (A): forward and side light scatter (FS and SS, respectively), and absence of dead cell staining defined live singlet lymphocytes. This population was further subdivided into CD3+ CD19- cells, and CD4 and CD8 expressing cells. No differences were seen in mice receiving PXS5338K or vehicle comparing median % of cells (presented in B and C) using the MW test.

Myeloid panel

CD11b+ F4/80+ macrophages are believed to be key drivers in the fibrotic response, and secrete pro-inflammatory cytokines and chemokines (39). GR1+ macrophages are also profibrogenic, and secrete TGF-β, PDGF and insulin-like growth factor-1 (IGF1), which activate HSCs as well as providing an NF-κB-mediated survival signal to myofibroblasts (47, 48). Conversely, Ly6G+ neutrophils, have been demonstrated to promote fibrosis resolution, probably through production of MMP8 and MMP9 (273)

Intrahepatic myeloid cells were isolated from the livers of C57Bl/6 *Mdr2-/-*mice receiving 9 doses of either vehicle or PXS5338K and incubated with appropriate

fluorochrome-labelled antibodies, as described in 2.2.5. The frequency of monocytes was examined by flow cytometry, in which the total myeloid cloud was subject to gating on the live CD45+ population of cells, and subsequently gated on expression of CD11b and co-receptors F4/80, Ly6C and GR-1 (Figure 4.19). CD11b + F4/80+ macrophages are calculated as a % of CD45+ live cells and the median % of cells compared for mice receiving vehicle vs gavage, showing no differences between the groups using the MW test (4.3% vs 3.6%, p = 0.792, respectively). Likewise, CD11b+ Ly6G+ granulocytes were calculated as a % of CD45+ live cells, and showed no difference between the groups (4.7% vs 4.9%, p = 0.678). A similar lack of effect was observed for CD11b+ GR-1+ neutrophils as a % of CD45+ live cells (2.9 % vs 2.7%, p = 0.571) when comparing mice receiving vehicle vs compound, respectively.

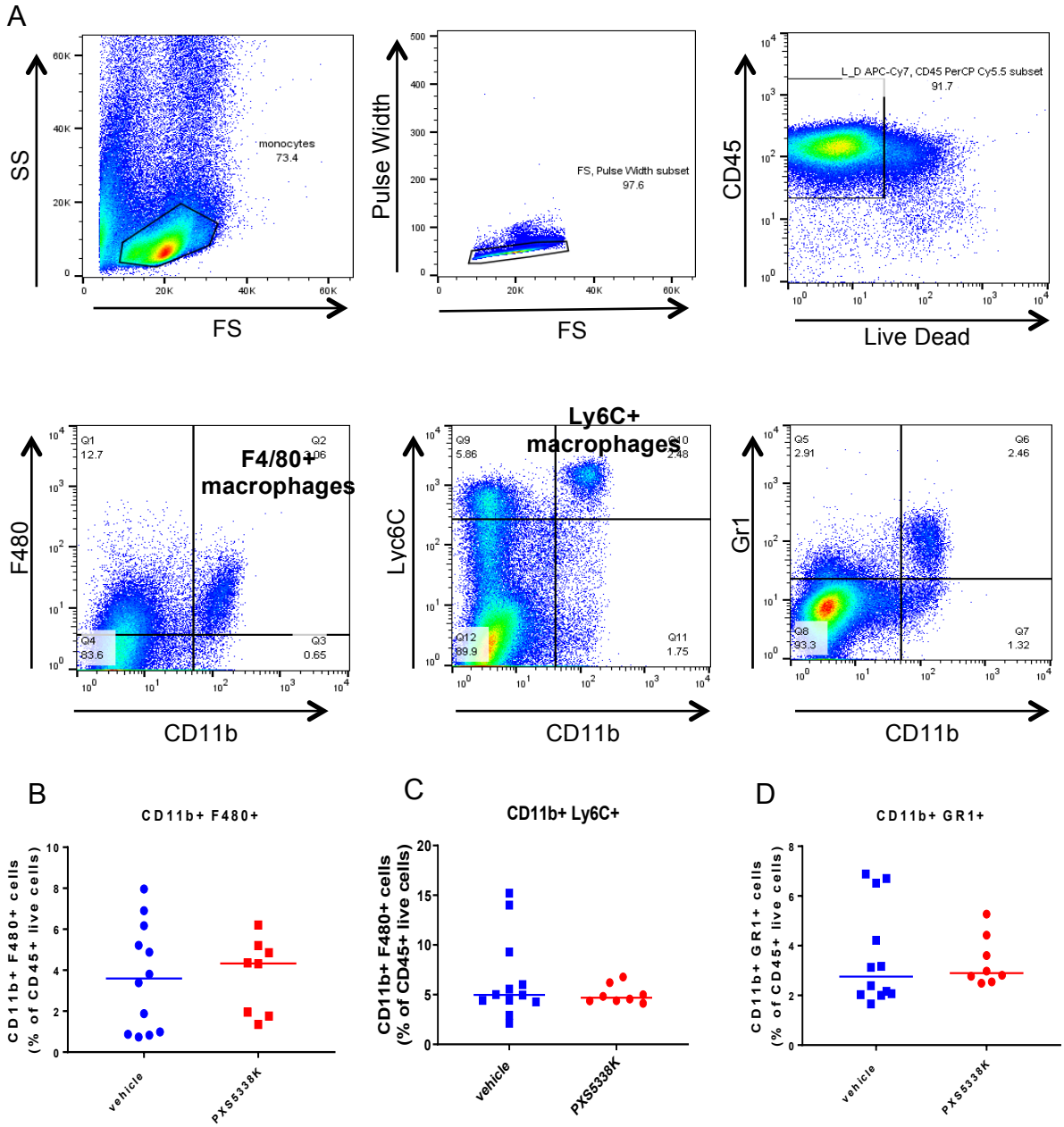
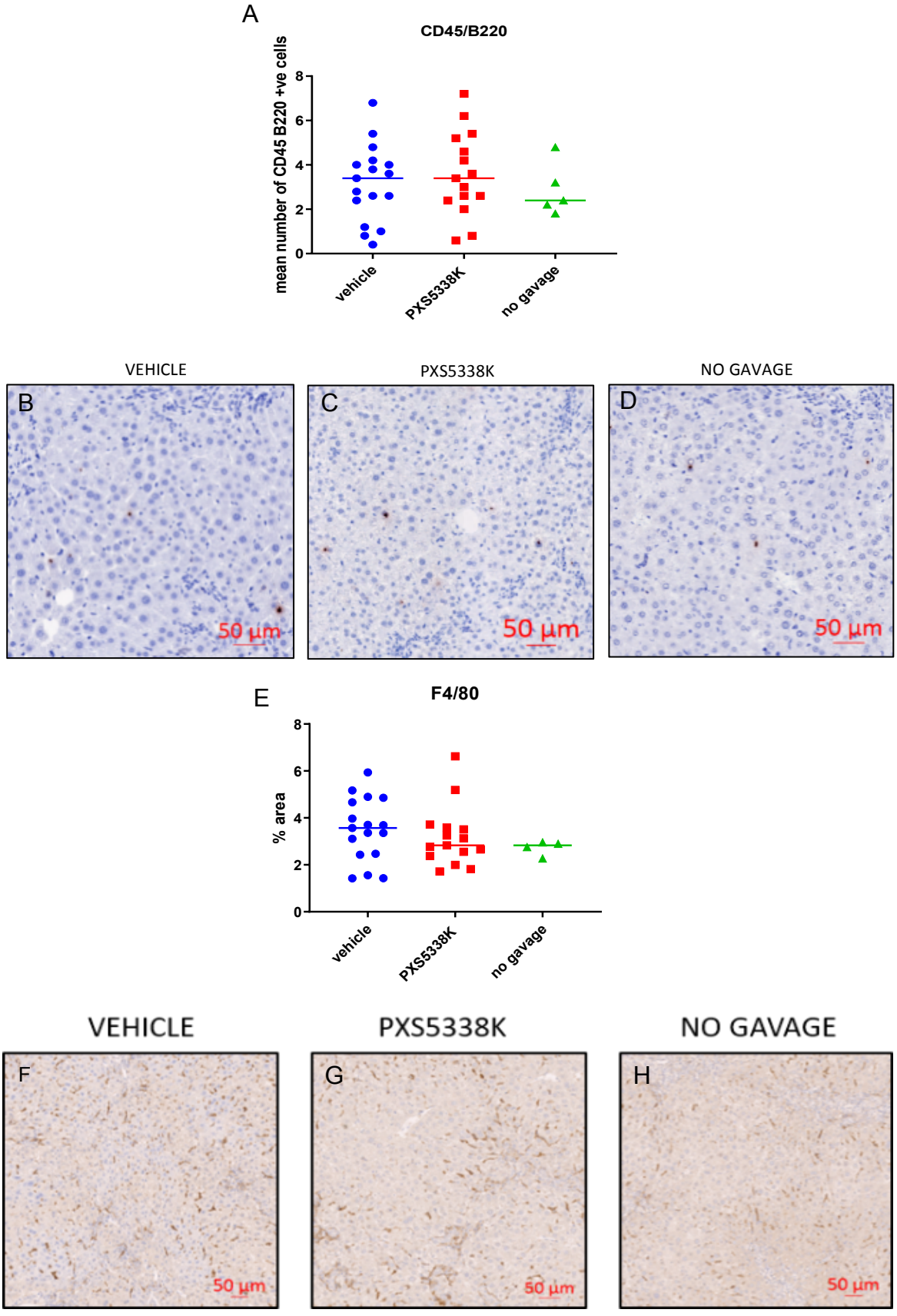


Figure 4.19 Comparison of myeloid cell isolates from liver showed no differences between C57Bl/6 *Mdr2-/-* mice receiving 9 doses of PXS5338K or vehicle by oral gavage. The standard flow cytometry gating strategy to identify tissue-infiltrating myeloid populations is illustrated in (A): forward and side light scatter (FS and SS, respectively) and cell surface expression of CD45 with absence of dead cell staining defined live singlet myeloid cells. This population was further subdivided into CD11b+ F4/80+ cells, CD11b+ Ly6C+ and CD11b+ GR1+ cells. No differences were seen between the two groups comparing median % of cells (presented in B-D) using the MW test.

4.4.4.2 Immune cell infiltration by IHC

To consolidate data from flow cytometry, IHC was performed to assess the volume and distribution of immune cell infiltration into the liver in the presence of LOXL2 inhibition. An antibody for the B220 isoform of CD45 was used to assess the presence of B cells, F4/80 to assess macrophage infiltration, given their importance during fibrogenesis and fibrosis resolution, and Ly6G to assess neutrophil and eosinophil infiltration (Figure 4.20). CD45 and F4/80 positive cells were dispersed equally across the tissue with only a hint of aggregation around sites of fibrosis for F4/80 positive cells. Ly6G was seen in more densely populated periportal regions and areas of fibrosis. PXS5338K had no effect on immune cell inflammation compared with vehicle, or no gavage for B220 CD45 (mean number of B220 CD45 positive cells taken from an average of 5 fixed areas) using the KW test (mean ranks 20.57, 18.71, 15.30, $p = 0.633$, respectively). Likewise, no differences were seen in the F4/80 positive population for vehicle vs PXS5338K vs no gavage (mean ranks 20.76, 17.33, 13.25, $p = 0.375$) or the Ly6G+ population (mean ranks 14.43, 17.23, 20.4, $p = 0.444$) respectively using the KW test and post hoc Bonferroni-Dunn correction.


A
CD45/B220
mean number of CD45 B220 +ve cells
0
2
4
6
8
vehicle
PXS5338K
no gavage
VEHICLE
PXS5338K
NO GAVAGE
B
C
D
50 µm
50 µm
50 µm
E
F4/80
% area
0
2
4
6
8
vehicle
PXS5338K
no gavage
VEHICLE
PXS5338K
NO GAVAGE
F
G
H
50 µm
50 µm
50 µm

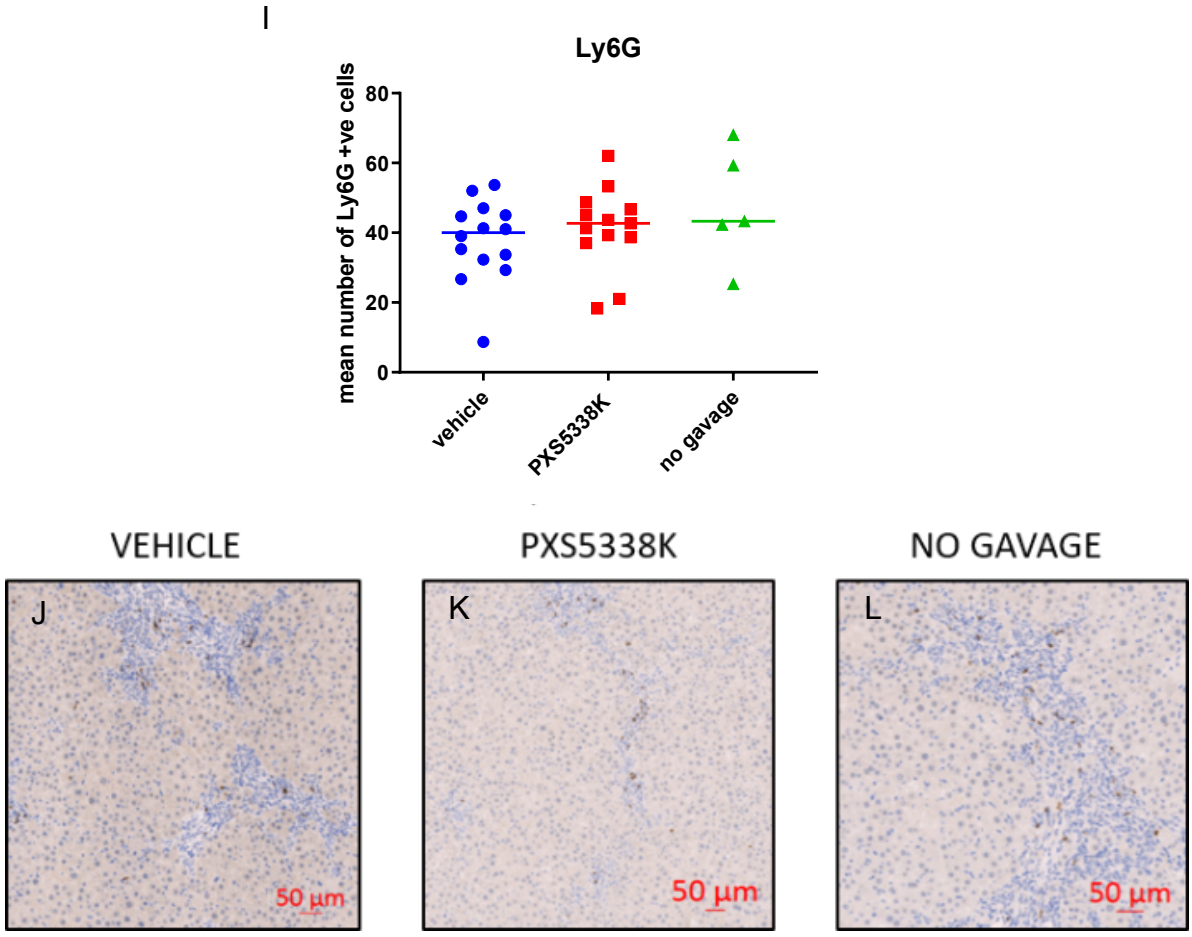


Figure 4.20 PXS5338K does not alter liver infiltration of B220 CD45 positive, F4/80 positive or LY6G positive cells during liver injury. 36 nine week old C57Bl/6 *Mdr2-/-*mice received 9 doses of vehicle, or 3 mg/kg PXS5338K, by oral gavage, with 5 C57Bl/6 receiving no gavage. Paraffin-embedded liver tissue was used to assess presence of B220 CD45+ (A-D), F4/80+ (E-H) and Ly6G+ cells (I-L). No significant differences were observed between the groups receiving PXS5338K, vehicle, or no gavage for mean number of cells (B220 CD45 and Ly6G) or % area with morphometric analysis using the KW test.

4.5 Discussion

In conclusion, PXS5338K was poorly tolerated by 9 week old FVB *Mdr2-/-* mice administered at a dose of 10 mg/kg, but no clear cause for this could be determined. A reduced dose of 3 mg/kg was well tolerated in 9 week old C57Bl/6 *Mdr2-/-* mice, each receiving received 9 doses of the compound over three weeks. At this dose, PXS5338K had no effect on liver injury or fibrosis, expression of lysyl oxidases, or immune cell infiltration into the liver. While there was some suggestion that SOX-9+

cells in FVB mice receiving 10 mg/kg PXS5338K had a more lobular and less ductular pattern, this finding was not replicated in the C57Bl/6 mice administered with 9 doses of the lower 3 mg/kg dose.

It is possible that the dosing strategy could account for the lack of benefit with compound that was observed. The half-life of PXS5338K is not known but the similar compound PXS5153 has a half-life of only 36 minutes, and that if PXS5338K is likely to be similar. In the context of progressive injury in this strain of mice, the reduced dose of compound administered on alternate days (Monday, Wednesday and Friday for 3 weeks), with cull at 72 hours following the final dose, full coverage of the target may have been difficult to achieve, with loss of impact on fibrosis, inflammation and the ductular reaction.

Conversely, a total of 18 mice received vehicle and 16 received compound, and so even small changes in injury for fibrosis achieved by the small and infrequent dose of PXS5338K could have been detected, although the study was not accurately powered. However, previous power calculations based on a median 25% reduction of % PSR stain from 4 to 3 % using statistics generated from the Shanghai I.P. TAA model of fibrosis suggested that 7 mice in each groups should be adequate. In addition, realistically, there was no convincing trend for reduced fibrosis in the mice receiving PXS5338K and so greater numbers would have been extraneous.

The stain for PSR and collagen I was analysed at two magnifications; the idea being that at lower magnification the majority of the liver lobe could be assessed, avoiding

random sampling of areas with less or more fibrous septa. However, this method can miss the smaller fibrils of collagen seen at higher magnification, hence a higher magnification at which these could be visualized was also used, and 5 fixed areas chosen at random to measure the % area covered by collagen; this method was not fully validated to assess exactly how many fixed areas should be used, but given that there was very little difference in the % area using each method, and the % area looked comparable between the treated and untreated groups, so a change in methodology was not explored further.

The results were disappointing given the results seen with PXS5153A in the CCl_4 rat model. This could be due to subtle differences in the compound pharmokokinetics, different efficacy according to species, or differences in the pathophysiology between species or disease models (CCl_4 vs *Mdr2-/-* model). Unfortunately I was unable to look for LOXL2 protein expression in liver tissue due to absence of an effective murine antibody, but LOXL2 mRNA expression was not markedly elevated in this model making it unlikely that enzyme inhibition will be effective. The theory that other LOX/Ls compensated for inhibited LOXL given that their expression was no more elevated in animals receiving PXS5338K than those receiving vehicle. However, it is a widely held view in the field that the levels of the LOX/Ls measured by PCR may not be a reflection of the levels of protein and so identifying the presence of LOX/LOXLS in liver tissue or even serum would be beneficial in these models. Unfortunately antibodies against human are likewise poor and so qPCR remains commonly used to detect their expression.

My results also contrast with those of Ikenaga *et al*, who demonstrated a change in differentiation of cells and suppression of the ductular reaction in the presence of a LOXL2 antibody using the *Mdr2-/-* model of biliary injury. Reduced collagen deposition and promotion of fibrosis reversal was also seen in the TAA model of fibrosis. I hope to demonstrate similar results but improved efficacy using direct enzyme inhibition using PXS5338K in a model of TAA induced fibrosis.

5 Results III: The assessment of PXS5338K in reducing liver injury and fibrosis in a TAA induced model of liver disease

5.1 Introduction

TAA induced liver injury results in a pan-lobular fibrosis (255), similar to that seen in NAFLD, ALD and hepatitis C (274, 275). At the University of Birmingham Biomedical Services Unit we have developed a 16 week model whereby mice have *ad libitum* access to TAA in drinking water sweetened with sugar free Robinsons™ orange squash. Animals develop moderate bridging fibrosis by 16 weeks, but mortality is reduced probably because the injury is self-limiting; those mice that become unwell drink less TAA in drinking water, but also mortality associated with I.P. injection is avoided. The disadvantage of this model is that there is variability in the severity of fibrosis induced (measured by PSR stain and hydroxyproline assay, see Figure 5.1), presumably at least partially due to differences between mice in oral intake of the TAA diluted in drinking water, but also individual response to the toxin. In preliminary experiments, extending TAA exposure form 12 to 16 weeks at least partially reduced the variability in fibrosis readouts (see Figure 5.1), and so this is the model I chose to use.

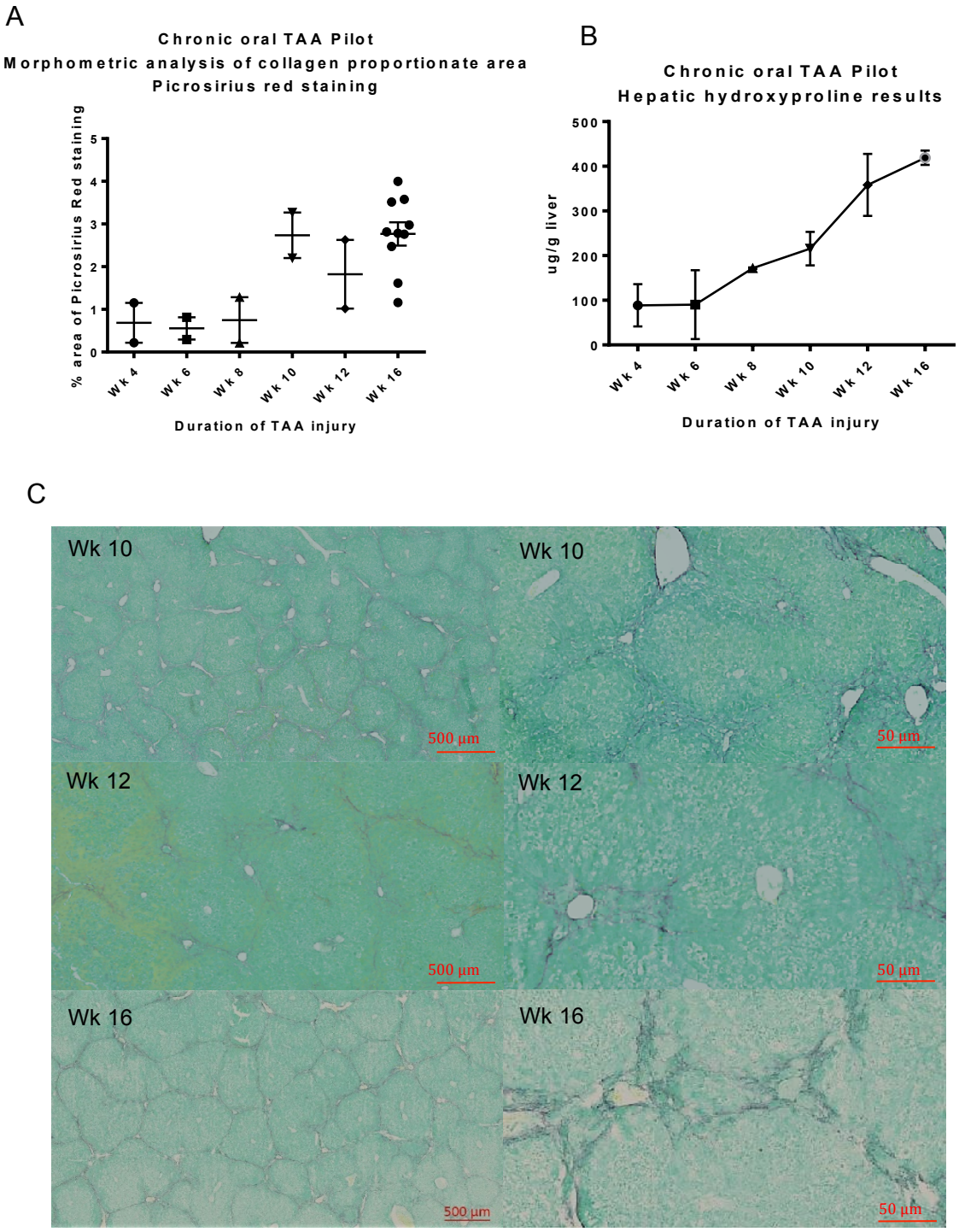


Figure 5.1 Sixteen weeks of oral TAA in C57Bl/6 mice results in increased collagen deposition and fibrosis. Mice were given TAA diluted in orange squash (prediluted 1:5 with water) in escalating doses up to 600mg/L by day 9 and maintained on this dose ad libitum for up to 16 weeks. All 10 mice given 16 weeks of TAA survived and had a median % area PSR of 2.8% (A+C). Collagen content measured by hydroxyproline assay also steadily increased, reaching a median of 422 µg/g liver (B). Data courtesy of Dr D Halder, University of Birmingham.

Lysyl oxidases are widely believed to have a role in ECM remodelling, and so there was interest in whether LOXL2 inhibition may have a role during fibrosis resolution. This would have implications in a number of conditions, just one being treated HCV-related cirrhosis, whereby liver injury has ceased but where the burden of fibrosis persists.

Previous studies using the 16 week TAA liver injury model had shown that fibrosis resolution can begin rapidly within two weeks of injury cessation (see Figure 5.2). For this reason, to test LOXL2 inhibition during fibrosis resolution, mice were exposed to 16 weeks of ad libitum TAA followed by normal drinking water for up to two weeks, during which time half the group received compound and the remaining half were given vehicle. Interim analysis of 7 mice receiving vehicle or compound was performed at day 8 in case differences between the groups were missed (see methods 2.2.3.2).

In this chapter I investigate the effect of PXS5338K on liver injury, fibrosis, and inflammatory cell recruitment during TAA induced liver injury and following that, during a two week period of recovery to assess any benefit of the compound in fibrosis resolution.

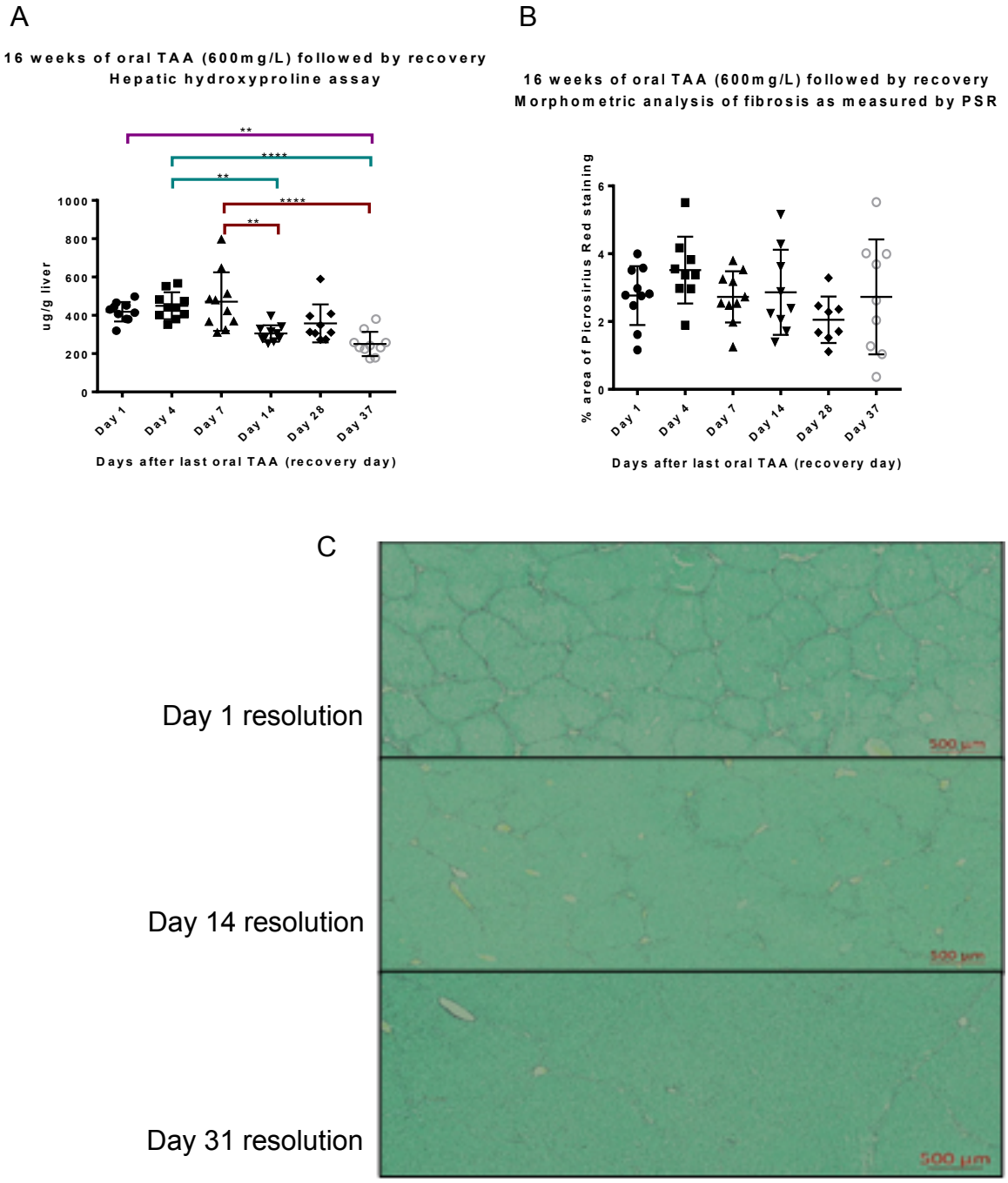


Figure 5.2 Fibrosis resolution occurs following cessation of TAA induced liver injury in mice and improvement can be seen as early as day 14. Mice were given TAA diluted in orange squash (prediluted 1:5 with water) in escalating doses up to 600mg/L by day 9 and maintained on this dose ad libitum for up to 16 weeks. During recovery, mice were culled at different time points and liver tissue assessed for collagen content by hydroxylproline assay and PSR stain. Median % area by PSR stain showed variability and between groups but a downward trend for reduced collagen was seen (A+C)), and significant reductions were seen for hydroxyproline assay using Shapiro-Wilk test, **p<0.005, ***p = 0.001 (B). Data courtesy of Dr D Halder, University of Birmingham.

5.2 The effect of daily administration of PXS5338K P.O. for six weeks in healthy C57/Bl6 mice

As described in the previous chapter, a dose of 10 mg/kg PXS5338K was poorly tolerated in FVB *Mdr2-/-* and so a further pilot study was carried out to assess the tolerability of 3 mg/kg PXS5338K daily for 6 weeks in C57Bl/6 mice, in the absence of TAA induced liver injury. As the key outcome was to assess the safety of the compound, the mice were compared with mice receiving no gavage, and a direct control of gavage with vehicle was not performed.

From a total groups size of 15 mice, one animal bit off the clear plastic end of the needle and was immediately culled to avoid further distress. The remaining 14 mice survived 6 weeks of 3 mg/kg PXS5338K daily by oral gavage with no overt signs of distress. Mice gained a mean weight of 3.7g, or 16 % total body weight; (see Figure 5.3), and none of these animals lost weight overall. Serum results were unremarkable and no different when compared with animals receiving no gavage using the MW test (AST median 14.0 vs 19.5, $p = 0.217$, ALT median 10.5 vs 4.5, $p = 0.118$, bilirubin 2.0 vs 2.0, $p = 0.999$, 2.5 vs 1.0, $p = 0.531$ for no gavage vs gavage with PXS5338K, respectively).

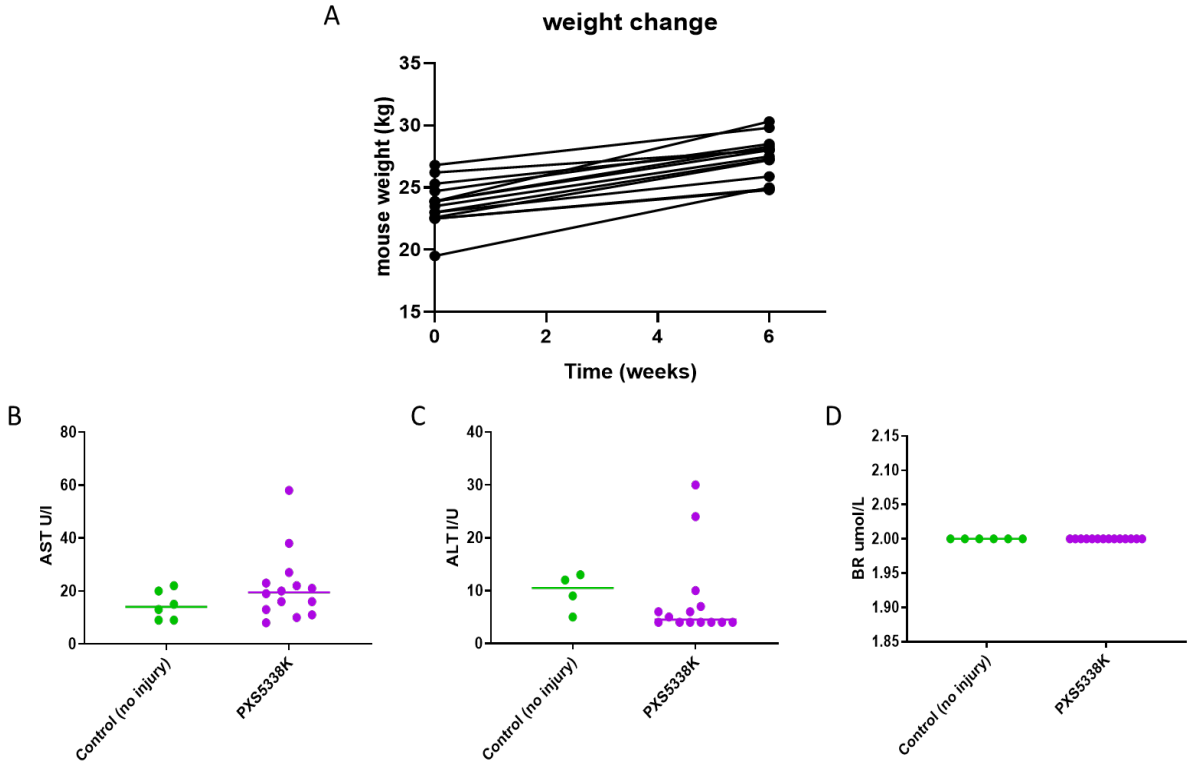


Figure 5.3 PXS5338K was well tolerated by C57Bl/6 mice. Fourteen 6-8 week old mice received 6 weeks oral gavage of 3 mg/kg PXS5338K and gained a mean body weight of 3.7 g (A). Serum results aspartate aminotransferase, AST (B), alanine aminotransferase, AST (C), and bilirubin (BR) did not differ from uninjured control mice that received no PXS5338K.

Haematoxylin and eosin staining of paraffin embedded sections of the liver, small and large intestines, lungs and spleen demonstrated no evidence of injury as defined by areas of necrosis, inflammation and normal tissue architecture, and are demonstrated in Figure 5.4.

This dose was tolerated by the mice, and so I proceeded to test the compound in mice exposed to 16 weeks of TAA, firstly assessing the effect of PXS5338K during liver injury, and then during fibrosis resolution.

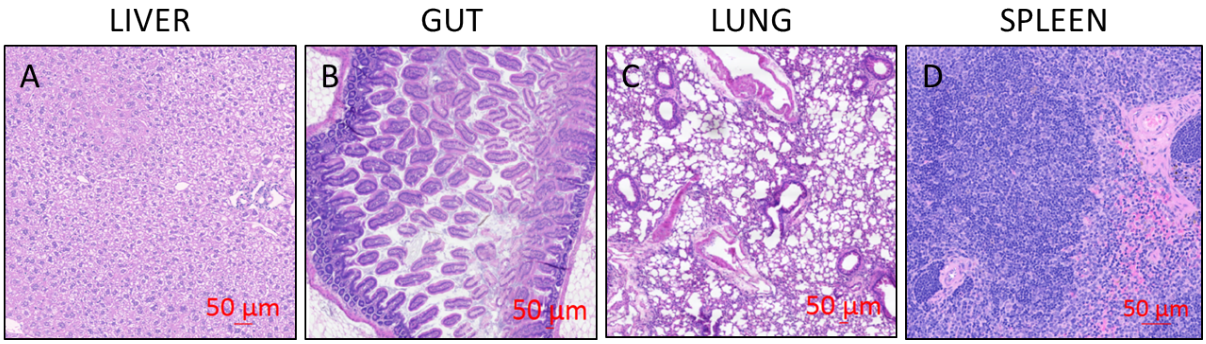


Figure 5.4 3mg/kg PXS5338K given daily by gavage for 6 weeks is well tolerated in mice. C57Bl/6 mice received oral gavage of 3 mg/kg of PXS5338K daily for 6 weeks. Animals were culled and dissected for organ retrieval. Gross examination and H&E stain of tissue demonstrated normal tissue architecture.

5.3 Therapeutic dosing of PXS5338K during TAA induced liver injury

Having demonstrated that the mice tolerated the inhibitor for a total of 6 weeks, I sought to determine whether administration of the compound to mice experiencing TAA-induced liver injury have a reduced burden of disease.

For 16 weeks, mice were housed and provided chow as per usual Biomedical Services Unit protocols, but their drinking water was substituted for TAA solution in incremental doses up to 600 mg/L by day nine, as described in 2.2.3.1. From week 10, 15 mice received PXS5338K via oral gavage at a daily dose of 3mg/kg, as described in methods 2.2.3.1, and 15 mice received vehicle (PBS); an equivalent volume to those receiving PXS5338K according to weight was given. Daily gavage was for 6 weeks, concurrent to ongoing ad libitum access to TAA in drinking water (the same duration as the pilot experiment described above), and animals were sacrificed at the beginning of week 17, 24 hours following their last gavage (Figure 5.5).

Upon sacrifice, tissue was collected for analysis as described in section 2.2.5. Liver injury and fibrosis was assessed by serum biochemistry, immunohistochemistry and expression of fibrotic markers by qPCR. The ductular reaction was assessed by IHC for SOX-9, and immune cell infiltration was assessed by IHC and extraction of lymphocytes and monocytes for multi-colour flow cytometry.

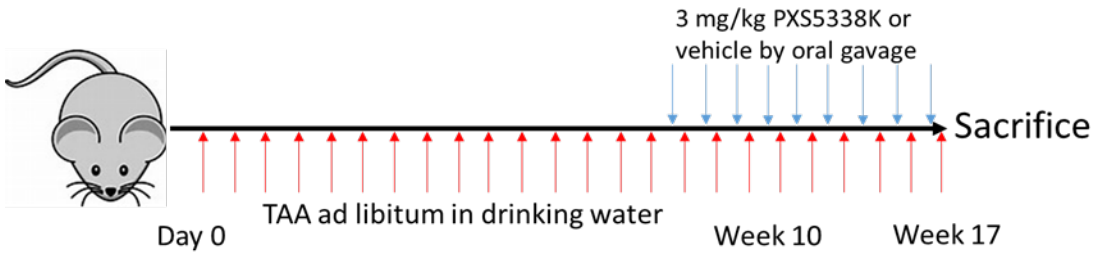


Figure 5.5 TAA model for liver fibrosis. TAA was given for 16 weeks to induce liver fibrosis, and 3 mg/kg PXS5338K or vehicle was administered by oral gavage for the final 6 weeks.

5.3.1 Assessment of liver injury

30 mice were commenced on TAA therapy and were gavaged from week 10. One mouse became unwell (weight loss, poor hair condition) at week 13 having received 3 weeks of daily gavage of PXS5338K. 14 mice received 6 weeks of compound and 15 received vehicle. A control group received no TAA and no gavage and these groups were also compared with the mice receiving PXS5338K and no TAA.

No differences in percentage weight gain were observed between the groups exposed to prolonged oral gavage, but a negative effect of gavage on weight gain was demonstrated using the KW test to compare mean ranks (mean ranks 20.2, 18.1, 46.5, 28.0, for TAA + vehicle, TAA + PXS5338K, no injury or gavage and no injury + PXS5338K, respectively, $p < 0.001$ for comparison of both groups of injured

mice against the uninjured control). The effect of oral gavage on weight gain is demonstrated more clearly in Figure 5.6.

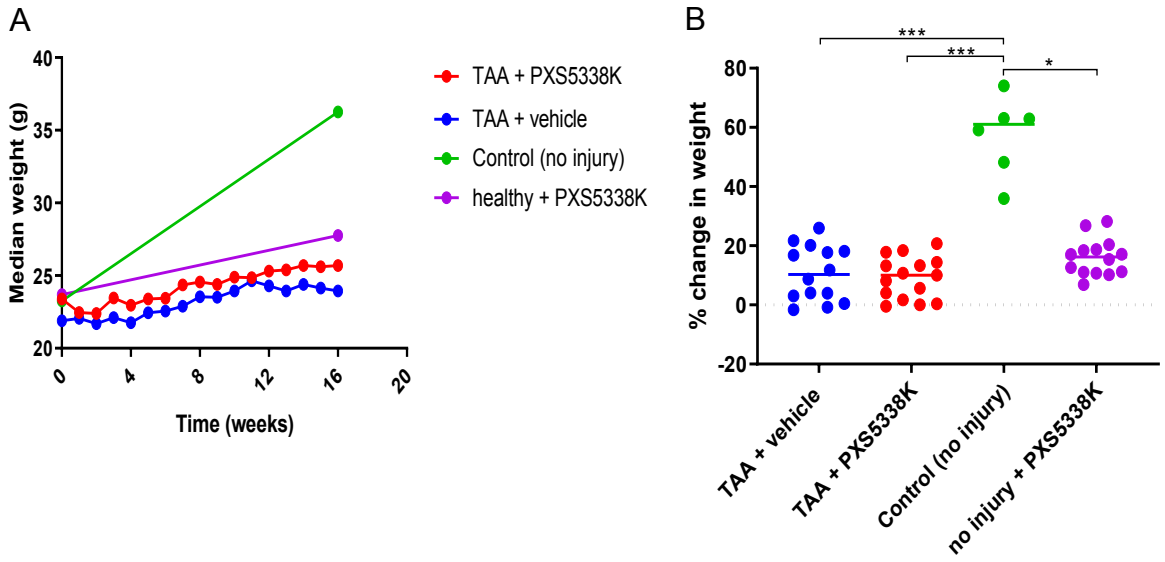


Figure 5.6 PXS5338K had no effect on animal weight. Mice received 16 weeks of TAA with 6 weeks daily gavage of either vehicle or PXS5338K during the final 6 weeks, or were not exposed to TAA or gavage. (A) demonstrates incremental weight over 16 weeks and (B) shows % weight change over 16 weeks for mice receiving TAA + vehicle, TAA + PXS5338K, no intervention control, and for healthy mice receiving 6 weeks of PXS5338K; capped lines with asterisks indicate statistically significant differences using the KW test with Dunn's post-hoc correction, p values *<0.05,***<0.001.

Serum markers for hepatic injury were measured and are shown in Figure 5.7. Measurement of AST revealed an increase in the two groups of mice exposed to TAA when compared with control mice (no TAA or gavage) using KW with post-hoc correction via the Bonferroni-Dunn method (mean ranks 21.9, 18.0, 3.9, p = 0.007, TAA + vehicle, TAA + PXS5338k and no injury/gavage mice, respectively).

A similar trend was seen for ALT, but this was only significantly different for TAA + vehicle vs control mice using the same test (20.8, 14.9, 4.25, p = 0.004, as before). As the no TAA injury, no gavage group are not a true control group for observing the effect of TAA (this would be no TAA injury plus 6 weeks of gavage with vehicle), the

two groups receiving TAA with either PXS5338K or vehicle were directly compared using the MW test; no differences were observed between the groups. For results hereafter, the KW test was used to compare the two groups receiving TAA and the control group with no TAA or gavage (as this provides a baseline uninjured measurement), and these results were further validated by comparison of two groups receiving TAA only (vehicle vs compound) using the MW test, so that differences between these were not missed. These results were did not show significant differences (vehicle vs compound) and so are not presented here. The group of healthy mice receiving PXS5338K were not analysed further.

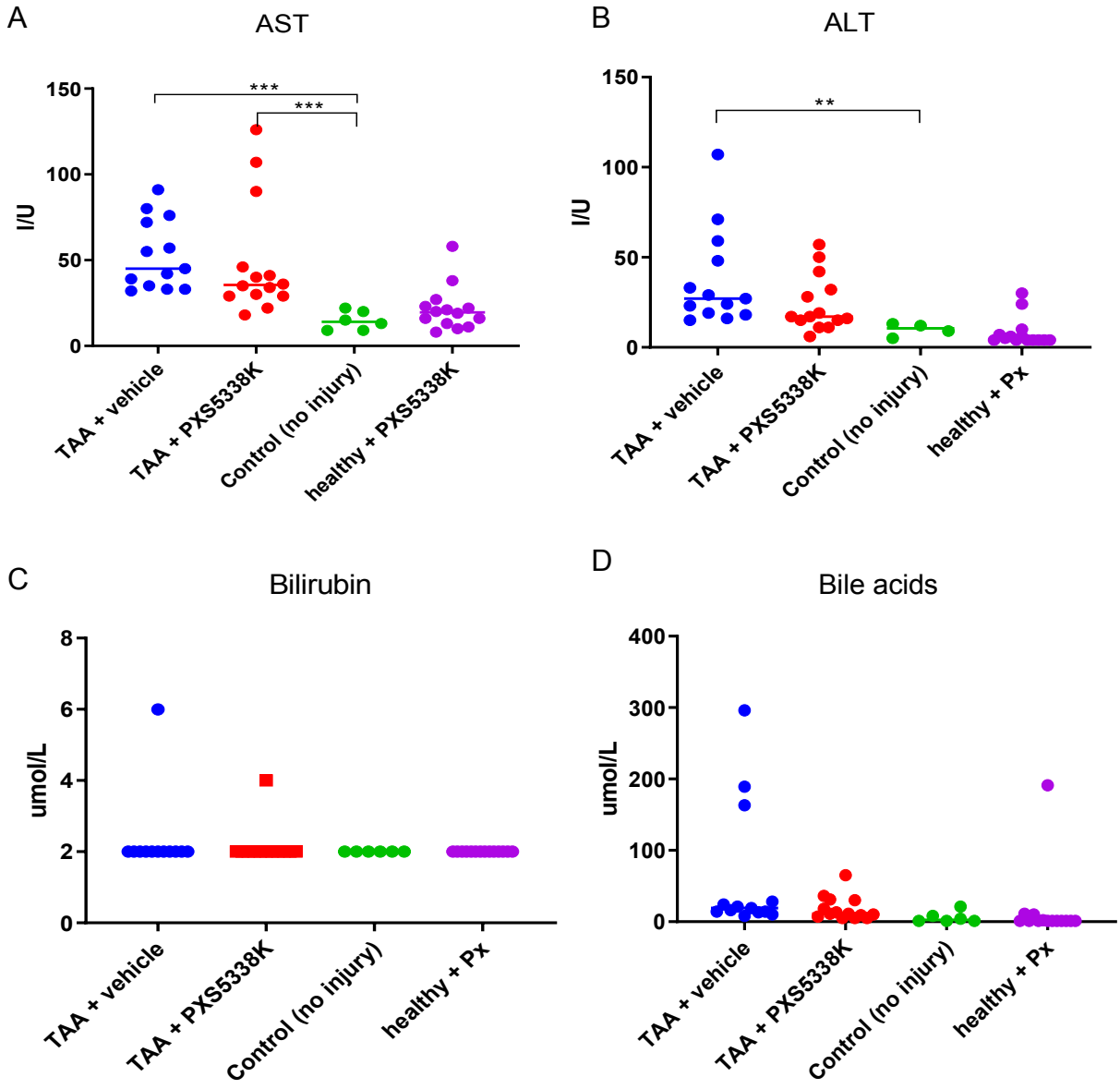


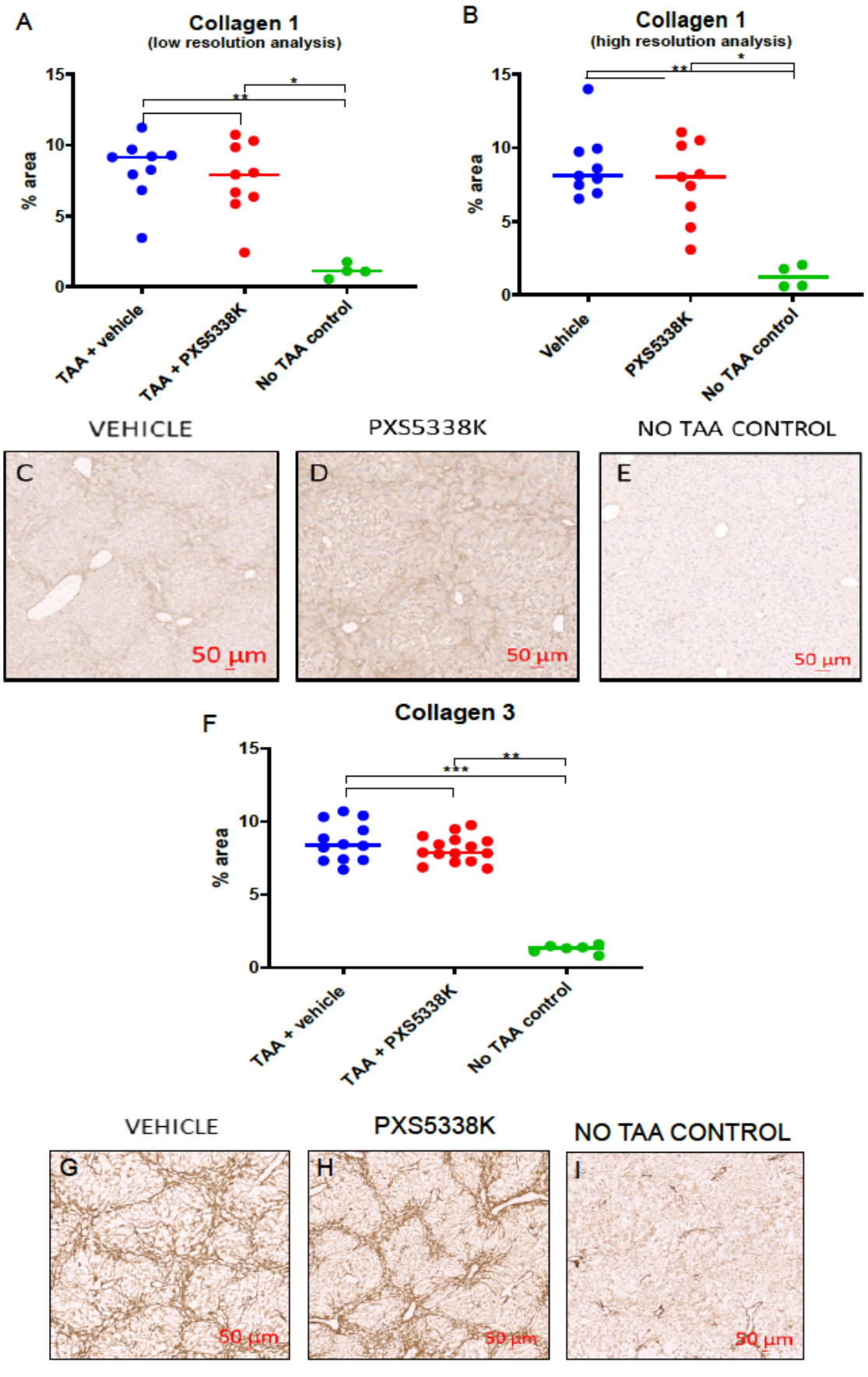
Figure 5.7 TAA induced liver injury as defined by serum biomarkers was not ameliorated by PXS5338K dosing. Mice received 16 weeks of TAA with 6 weeks gavage of either vehicle or PXS5338K, or were not exposed to TAA or gavage. AST was elevated in mice that were given TAA in drinking water (A), compared with mice that did not. ALT was elevated in mice on TAA that received 6 weeks gavage with vehicle but not those receiving 6 weeks PXS5338K (B). Markers of biliary injury were similar for all groups (C+D). Groups receiving TAA + vehicle, TAA + PXS5338K, and no intervention control, were compared using the KW test with Dunn's post-hoc correction; capped lines with asterisks indicate statistically significant differences p values **<0.01, ***<0.001.

5.3.2 The effect of PXS5338K on liver fibrosis

Next, I examined whether 6 weeks gavage of PXS5338K at 3 mg/kg had any impact liver fibrosis induced by 16 weeks of TAA liver injury in mice, by immunohistochemistry for collagen I and III, collagens with PSR stain, and α-SMA for HSC activity.

As described in 2.3.4 collagen I IHC was analysed in two ways; firstly by analysis of images at low magnification which permits analysis of approximately 70% of the liver lobe, and then at high magnification which permits detection of smaller collagen fibrils. IHC was not easily measureable for all slides, particularly for collagen III, for which the antibody did not work well, and so the results shown are only for those that could be accurately analysed.

In mice receiving TAA, there was an increase in collagen I, collagen III, total collagen by PSR stain, and α-SMA compared with uninjured mice, but no differences between the groups receiving TAA in addition to vehicle vs compound, using the KW with Bonferroni Dunn post-hoc correction (Figure 5.8). The MW test was also used to assess for differences between the groups receiving compound vs vehicle in the mice receiving TAA, but no differences were seen (results not shown). In summary, this model of TAA induced liver injury resulted in fibrosis, with % mean PSR area at 8-10%, but PXS5338K showed no benefit on fibrosis.


A
Collagen 1
(low resolution analysis)
% area
15
10
5
0
**
*
TAA + vehicle
TAA + PXS5338K
No TAA control
B
Collagen 1
(high resolution analysis)
% area
15
10
5
0
**
*
Vehicle
PXS5338K
No TAA control
VEHICLE
PXS5338K
NO TAA CONTROL
C
50 µm
D
50 µm
E
50 µm
F
Collagen 3
% area
15
10
5
0
***
**
TAA + vehicle
TAA + PXS5338K
No TAA control
VEHICLE
PXS5338K
NO TAA CONTROL
G
50 µm
H
50 µm
I
50 µm

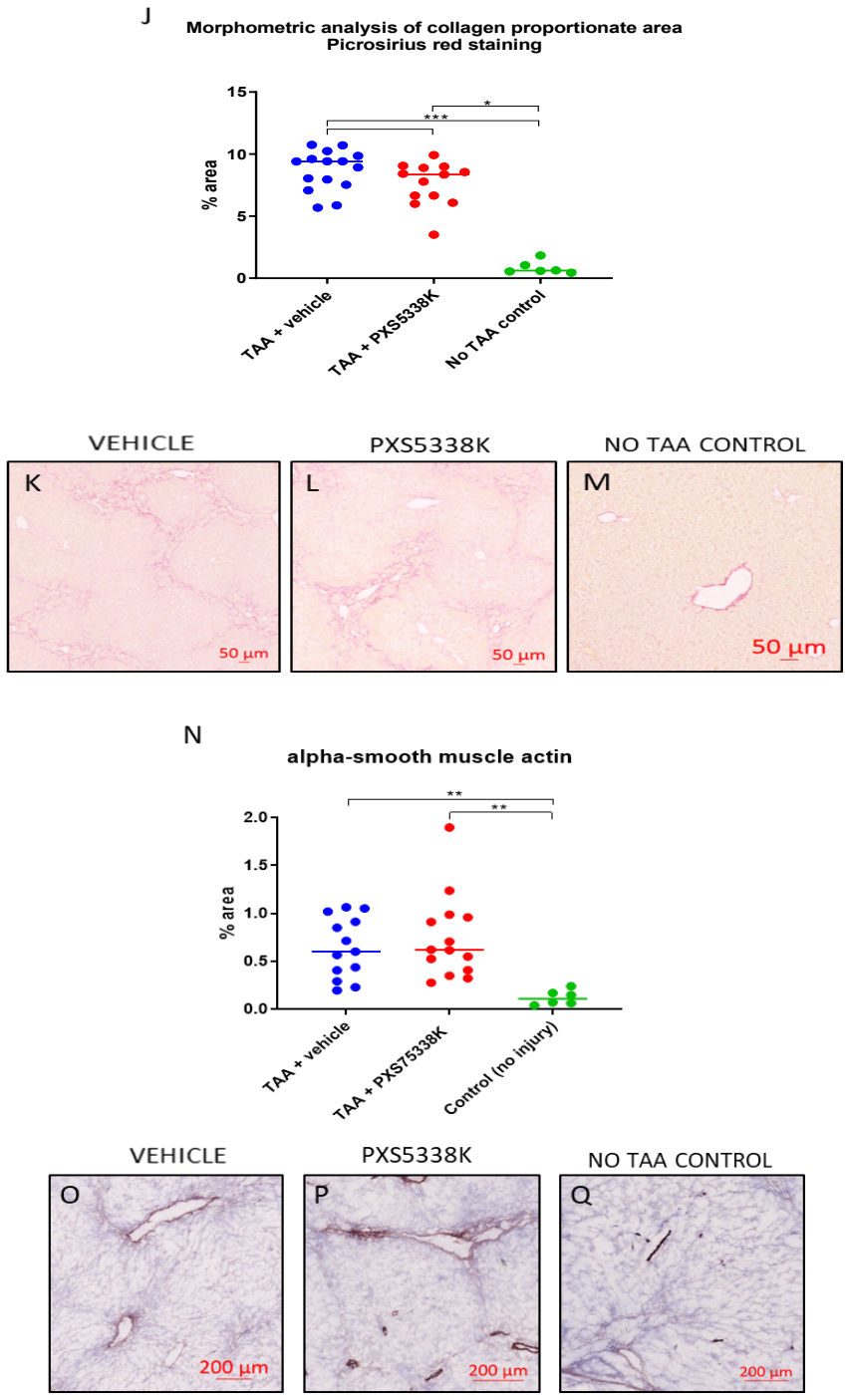
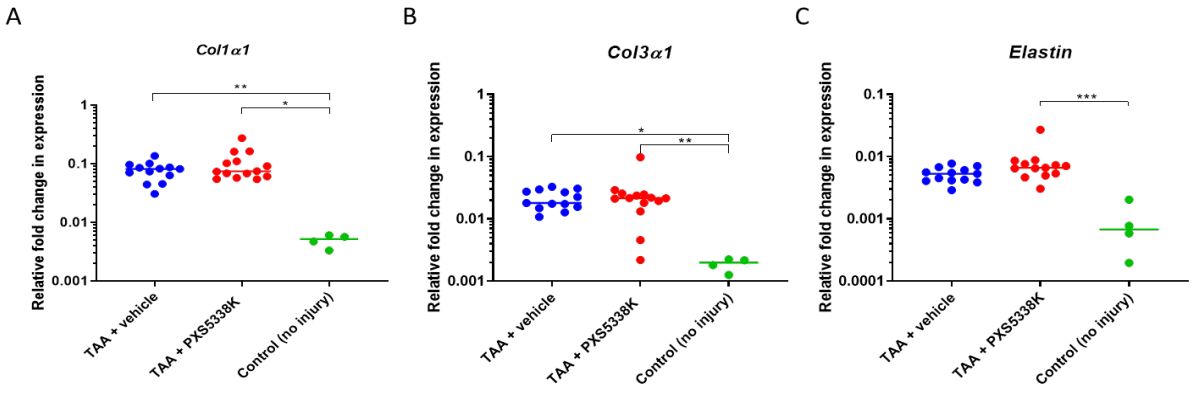
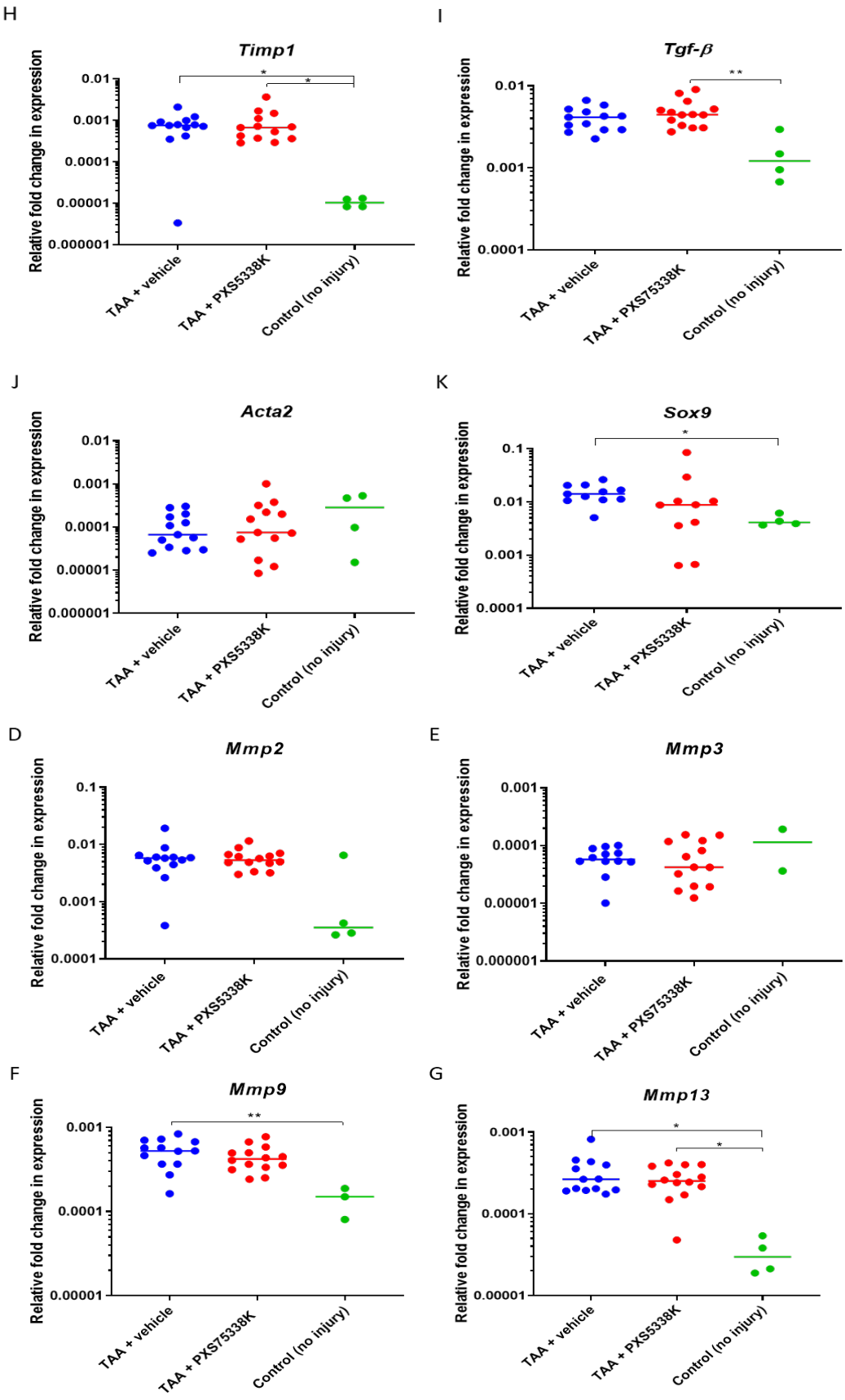


Figure 5.8 16 weeks of TAA induced liver fibrosis in mice which was not ameliorated by PXS5338K. Mice were exposed to 16 weeks of TAA ad libitum in drinking water with 6 weeks gavage of either vehicle or PXS5338K from week 10. A comparison group received no TAA. IHC was performed on paraffin embedded liver sections. Fibrosis was no different between the injured mice receiving vehicle or PXS5338K, but increased compared with the uninjured control group for Collagen I ((A-E) mean ranks 14.4, 12.6, 2.5, p = 0.003, using KW test and post hoc analysis with Bonferroni-Dunn correction) collagen III (F-I, mean ranks 21.6, 18.7, 3.5 p = 0.0006, collagen by PSR ((J-M) mean ranks 22.9, 17.8, 3.5, p = 0.0003) or α-SMA ((N-Q) 19.3, 20.5, 3.8, p = 0.001). Capped lines with asterisks indicate statistically significant differences, p values *<0.05,**<0.01, ***<0.001.

5.3.2.1 Assessment of fibrosis via qPCR

Expression of genes usually upregulated during fibrosis was assessed by qPCR and are shown in Figure 5.9. The relative expression of mRNA for ECM components were upregulated in TAA injured mice, but no differences were seen between groups receiving vehicle vs compound (collagen 1α1, mean ranks for uninjured mice, injured mice receiving vehicle, and injured mice receiving PXS5338K were 16.9, 18.9, and 2.5 respectively, p = 0.005, using the KW test with Bonferroni-Dunn correction; likewise for collagen 3α1, mean ranks were 18.0, 17.9, 2.8, p = 0.008 and for elastin, mean ranks were 14.4, 20.6, 2.5, p = 0.001) (Figure 5.9 A-C). Similarly, gene expression for proteins that control matrix remodelling such as matrix metalloproteinases (MMPs) and tissue inhibitor of metalloproteinases 1 (TIMP1), and the pro-fibrotic factor TGF-β were increased injured mice but the expression level was not reduced by PXS5338K. Likewise, expression of the LOX family transcripts was increased in the TAA injured group (although this did not reach significance for mice receiving PXS5338K in LOXL3 or mice receiving vehicle in LOXL4), but no significant differences were seen between the two groups for vehicle vs compound. Activation of HSC was also similar between groups as indicated by mRNA expression for *Acta2* (gene encoding the α-SMA protein).




H
Timp1
Relative fold change in expression
0.01
0.001
0.0001
0.00001
0.000001
*
*
TAA + vehicle
TAA + PXS5338K
Control (no injury)
I
Tgf-β
Relative fold change in expression
0.01
0.001
0.0001
**
TAA + vehicle
TAA + PXS75338K
Control (no injury)
J
Acta2
Relative fold change in expression
0.01
0.001
0.0001
0.00001
0.000001
TAA + vehicle
TAA + PXS5338K
Control (no injury)
K
Sox9
Relative fold change in expression
0.1
0.01
0.001
0.0001
*
TAA + vehicle
TAA + PXS5338K
Control (no injury)
D
Mmp2
Relative fold change in expression
0.1
0.01
0.001
0.0001
TAA + vehicle
TAA + PXS5338K
Control (no injury)
E
Mmp3
Relative fold change in expression
0.001
0.0001
0.00001
0.000001
TAA + vehicle
TAA + PXS75338K
Control (no injury)
F
Mmp9
Relative fold change in expression
0.001
0.0001
0.00001
**
TAA + vehicle
TAA + PXS75338K
Control (no injury)
G
Mmp13
Relative fold change in expression
0.001
0.0001
0.00001
*
*
TAA + vehicle
TAA + PXS5338K
Control (no injury)

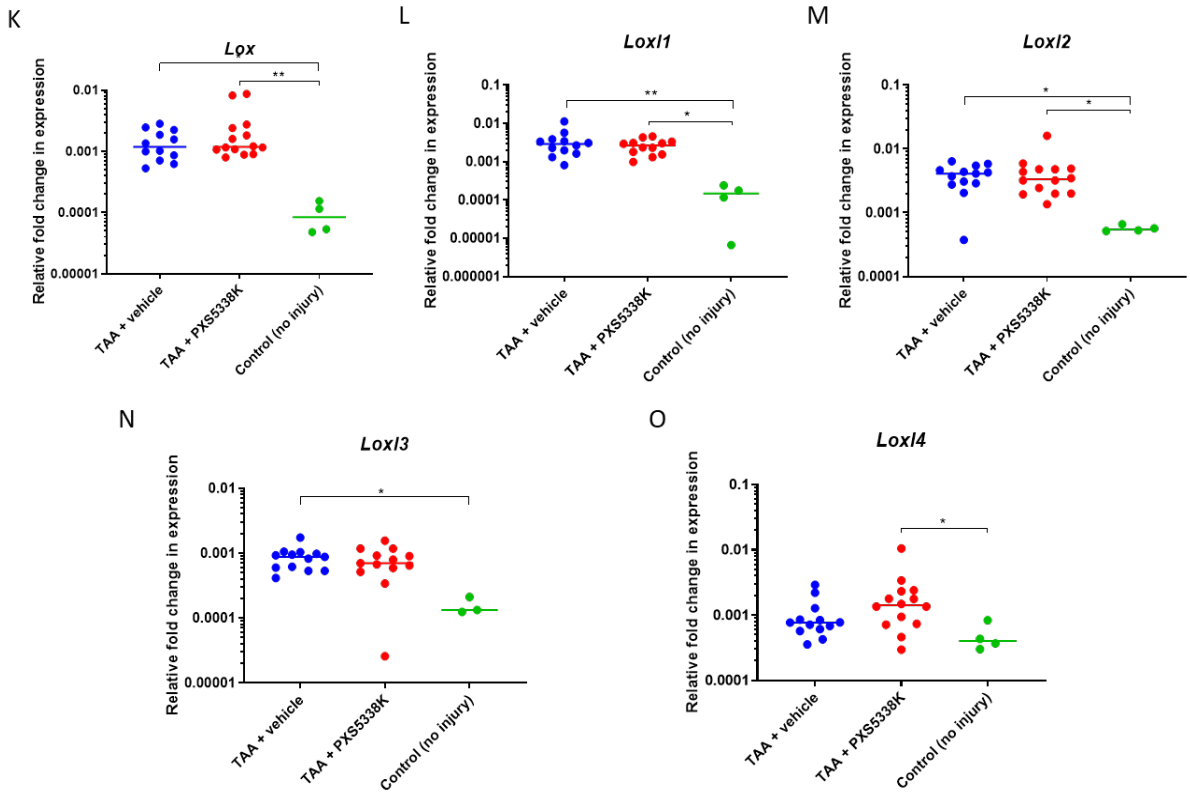


Figure 5.9 16 weeks of TAA induced liver fibrosis in mice which was not ameliorated by PXS5338K. Mice were exposed to 16 weeks of TAA *ad libitum* in drinking water with 6 weeks gavage of either vehicle or PXS5338K from week 10. A comparison group received no TAA. RNA was extracted from frozen tissue and mRNA expression measured against the house keeping gene *Gapdh*. Expression of genes upregulated during fibrogenesis was no different between the injured mice receiving vehicle or PXS5338K, but increased compared with the uninjured control group for *col1a1*, p = 0.005 (A), *col3a1*, p = 0.008 (B), *elastin*, p = 0.001 (C), *mmp9*, p = 0.002 (F), *mmp13*, p = 0.007 (G), *timp1*, p = 0.012 (H), *tgfb1*, p = 0.009 (I), *sox9*, p = 0.014 (K), *lox*, p = 0.005 (K), *loxl1*, p = 0.006 (L), *loxl2*, p = 0.013 (M), *loxl3*, p = 0.031 (M), and *loxl4*, p = 0.024 (N) There was a trend for reduced expression of *mmp2* in the uninjured control group, but this did not reach significance, p = 0.149 (D). No differences between the groups were seen for *mmp3*, p = 0.782 (E) or *acta2*, p = 0.646 (J). The KW test with post hoc analysis with Bonferroni-Dunn correction was performed to compare groups; capped lines with asterisks indicate statistically significant differences, p values *<0.05,**<0.01, ***<0.001.

5.3.3 The impact of PXS5338K on cell differentiation during TAA induced liver injury.

As discussed in chapter 4, inhibition of LOXL2 has previously been demonstrated to influence differentiation of HPCs in the ductular reaction (proliferation of periductular cells that occurs during chronic liver injury). In vitro studies by Ikenaga *et al.*

suggested preferential hepatocyte differentiation over ductular differentiation, and reduced proliferation of cells in the ductular reaction in the presence of LOXL2 antibody inhibition; the rationale being that as a key driver of fibrosis, attenuation of the ductular reaction via LOXL2 inhibition with further reduce fibrosis (276). HPCs in the ductular reaction stain positively for SOX-9; expression is lost when cells differentiate to hepatocytes but is retained on ductular cells. For this reason, IHC for SOX-9 in tissue from mice treated with TAA and PXS5338K was performed and compared with mice receiving TAA and vehicle to assess for differences in the pattern and extent of staining.

SOX-9 was upregulated in mice receiving TAA compared with the uninjured control (see Figure 5.10), but no difference was seen between the two groups receiving TAA in addition to vehicle or PXS5338K using the KW test (mean ranks 12.1, 13.8, 3.0, $p = 0.001$ for TAA + vehicle, TAA + PXS5338K, and uninjured control, respectively).

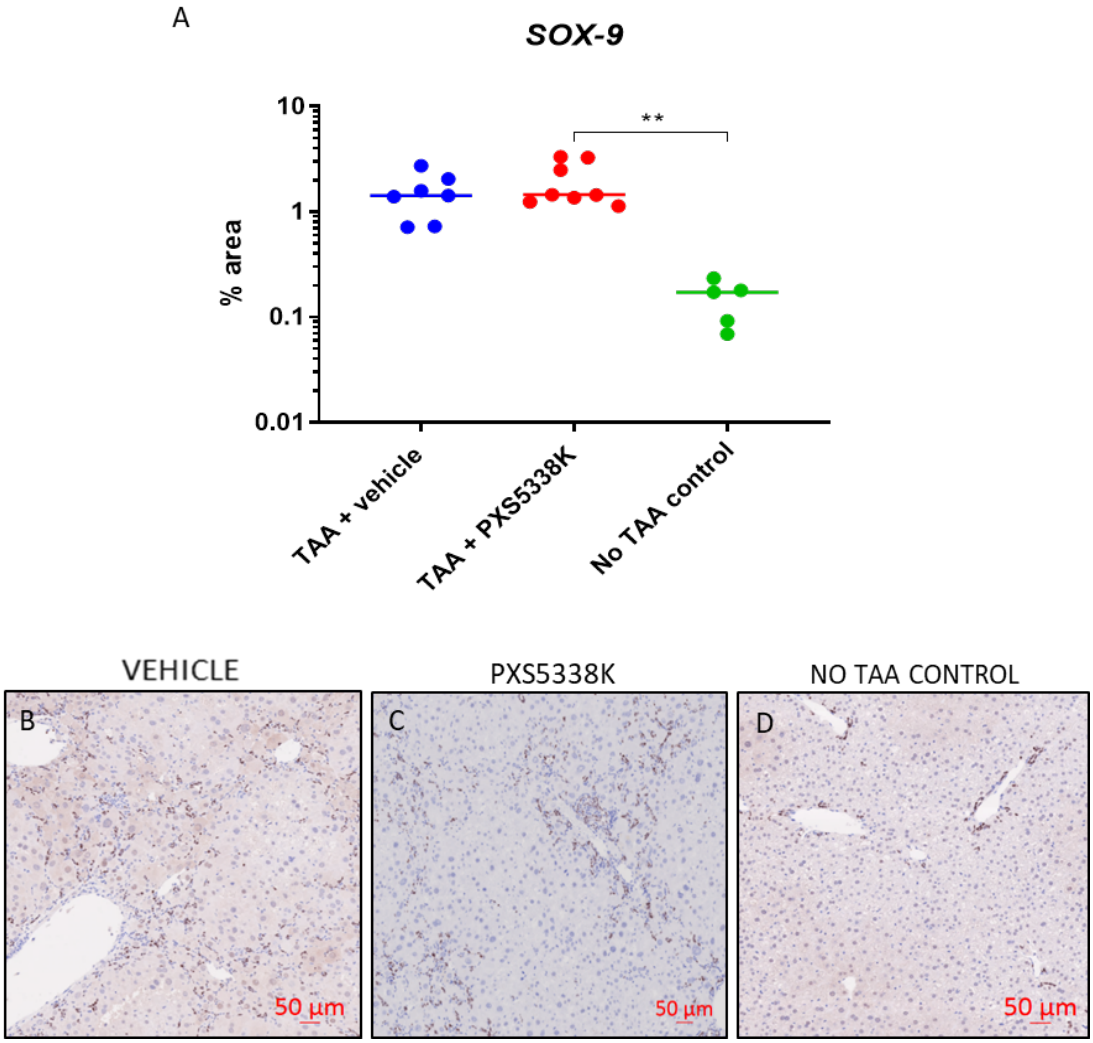


Figure 5.10 SOX-9 expression is upregulated in TAA-induced liver injury but not reduced by inhibition of LOXL2 by PXS5338K. Mice were exposed to 16 weeks of TAA *ad-libitum* in drinking water with 6 weeks gavage of either vehicle or PXS5338K from week 10. A comparison group received no TAA. IHC was performed on paraffin embedded liver sections for SOX-9 and demonstrates an increase in the ductular reaction in TAA-injured mice compared with uninjured control (A+D), but no difference in the pattern or quantity of staining in mice receiving vehicle (B) vs PXS5338K (C) (mean ranks 12.1, 13.8, 3.0, p = 0.001 for TAA + vehicle, TAA + PXS5338K, and uninjured control, respectively). Morphometric analysis was performed using Image J to calculate the % area of positive staining and statistical significance was assessed with the Kruskal-Wallace test and Bonferroni-Dunn post-hoc correction. *p<0.05.

5.3.4 The effect of PXS5338K on immune cell infiltration during TAA induced liver injury

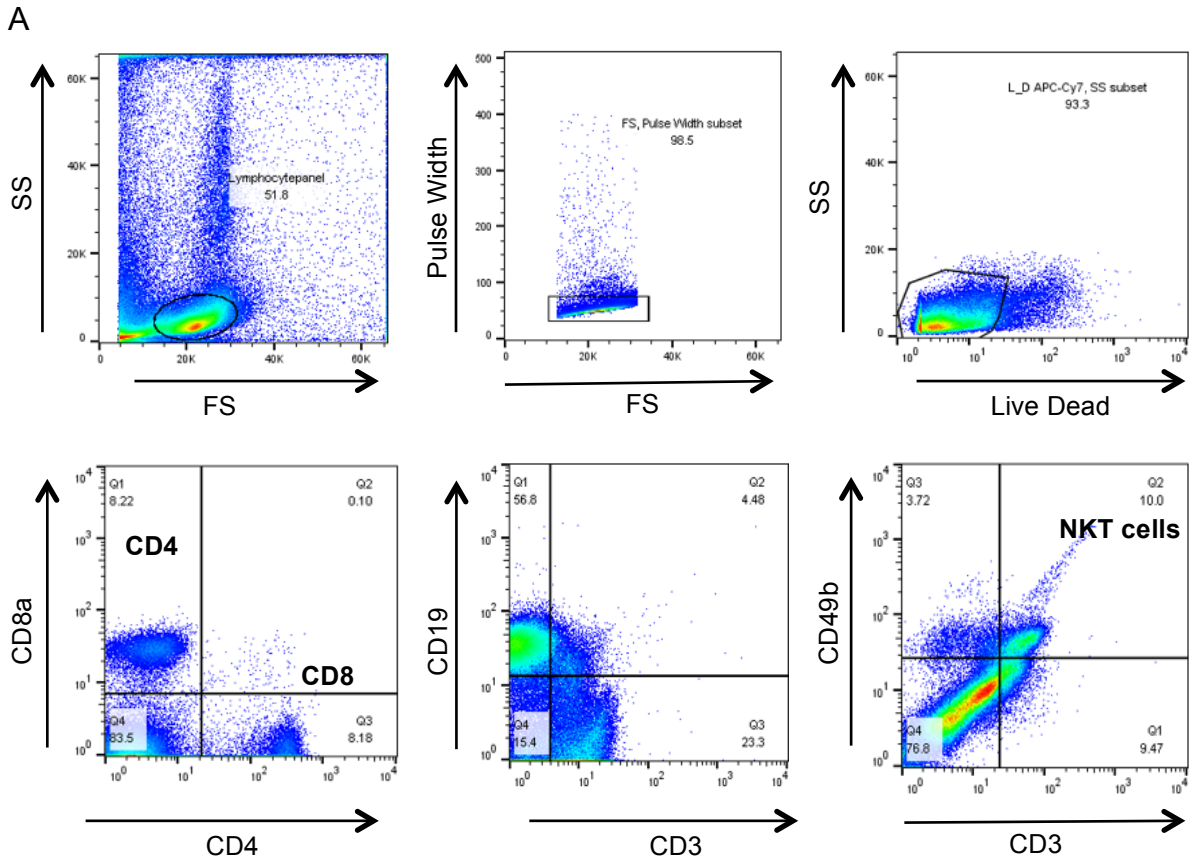
As described in 1.2.5 the immune system plays an important role during the establishment of fibrosis and subsequent fibrosis resolution. Although LOXL2 is not known to influence the immune system, to my knowledge this has not previously been investigated or published. For this reason, IHC and flow cytometry was performed on liver tissue from TAA injured mice to detect whether LOXL2 inhibition with PXS5338K influenced immune cell infiltration or altered the phenotype of inflammatory cells.

5.3.4.1 Immune cell infiltration as measured by flow cytometry

Lymphoid cells were isolated from C57Bl/6 mice receiving 16 weeks of TAA with 6 weeks of either vehicle or 3 mg/kg PXS5338K P.O. from week 10, and mice from an uninjured control group, and subsequently labelled with fluorescently conjugated antibodies as described in chapter 2.2.5.1. I considered CD4+ and CD8+ T-cells, CD19+ B-cells and CD49+ NK/NKT cells as part of a lymphoid panel and CD11b+ F4/80+ and GR1+ macrophages, and Ly6G+ neutrophils, to be the key components of a myeloid panel.

The frequency of each population of lymphocytes was examined by flow cytometry, as shown in Figure 5.11, in which the total lymphocyte population cloud was subject to gating on the live cells. CD4+(CD8-) T cells were measured as a % of live lymphocytes, with a reduced proportion of cells detected in TAA injured mice compared with uninjured control mice (mean ranks 11.6, 9.4, 22.4, $p = 0.005$, for

TAA + inhibitor, TAA + PXS5338K, and uninjured control, respectively using the KW test with post-hoc Bonferroni correction). No differences between the groups were seen for CD8+ (CD4-) T cells as a % of liver cells (mean ranks 12.7, 14.2, 11.4, p = 0.779 analysed as before. Likewise, no changes were seen in the population of CD3- CD19+ B cells or CD3- CD49b+ NKT cells calculated as a proportion of live cells (mean ranks 14.4, 13.3, 9.4, p = 0.451, and 12.7, 10.3, 19.6, p = 0.062, respectively).



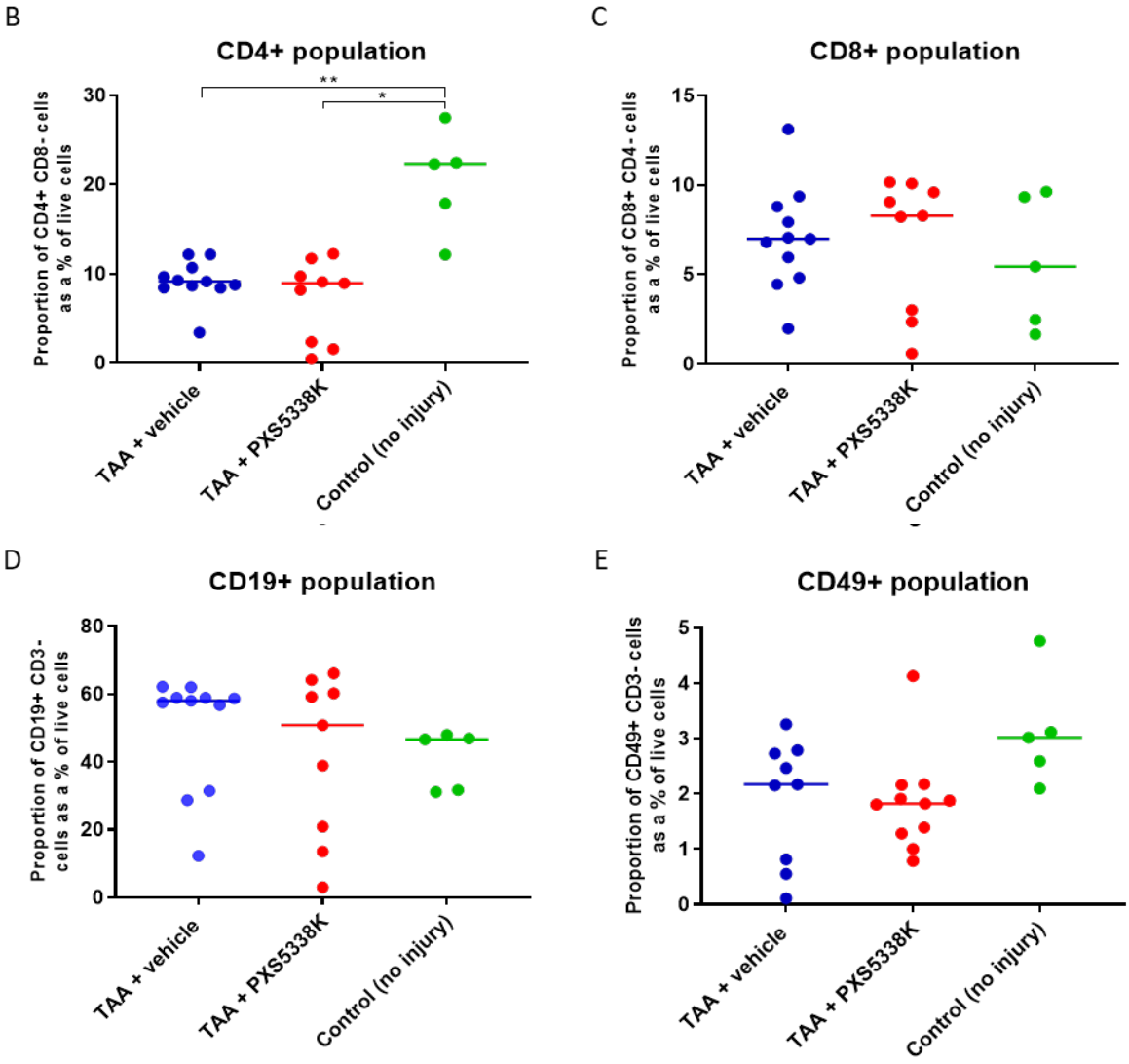


Figure 5.11 Comparison of lymphoid cell isolates from liver showed no differences in immune cell populations between mice receiving vehicle or PXS5338K by oral gavage. The gating strategy used to identify tissue-infiltrating lymphocyte populations is illustrated in (A): forward and side light scatter (FS and SS, respectively), and absence of dead cell staining defined live singlet lymphocytes. This population was further subdivided into CD4+ CD8- cells (B), CD8+ CD4- cells (C), and CD3- CD19+ (D) and CD3- CD49b+ cells (E). A reduction in CD4+ CD8- cells was seen in injured mice, but no other differences in lymphoid cell populations was observed between the groups. Statistical analysis was performed using the KW test with post-hoc Bonferroni Dunn correction. Capped lines with asterisks indicate statistically significant differences, p values *<0.05,**<0.01.

Myeloid populations

Bone marrow derived myeloid cells were isolated from the livers of C57Bl/6 mice receiving 16 weeks of TAA and 6 weeks of vehicle or PXS5338K, and mice from an

uninjured control group, and incubated with appropriate fluorochrome-labelled antibodies, as described in chapter 2.2.5.1. The frequency of monocytes was examined by flow cytometry, in which the total myeloid cloud was subject to gating on the live CD45+ population of cells, and subsequently gated on expression of CD11b and co-receptors F4/80, Ly6C and Gr1, as demonstrated in Figure 5.12. CD11b + Gr1+ granulocytes are calculated as a % of CD45+ live cells. Comparing populations of cells from mice receiving TAA + vehicle, TAA + PXS5338K and uninjured control mice using the KW test with post-hoc Bonferroni Dunn correction, mice receiving TAA + PXS5338K had a higher proportion of Gr1 + cells compared with uninjured mice; the same trend was seen in mice receiving vehicle but was not statistically significant (mean ranks 15.2, 15.7, 5.4, $p = 0.030$). A similar trend for increased inflammatory infiltrate in injured mice was seen for CD11b+ F4/80+ macrophages (calculated as a % of CD45+ live cells) and CD11b+ Ly6C+ cells (also calculated as a % of CD45+ live cells), but the trend did not meet statistical significance using the same test (mean ranks 16.7, 12.9, 7.7, $p = 0.088$, and 14.5, 15.2, 8.0, $p = 0.197$ for F4/80+ and Ly6C+ cells respectively).

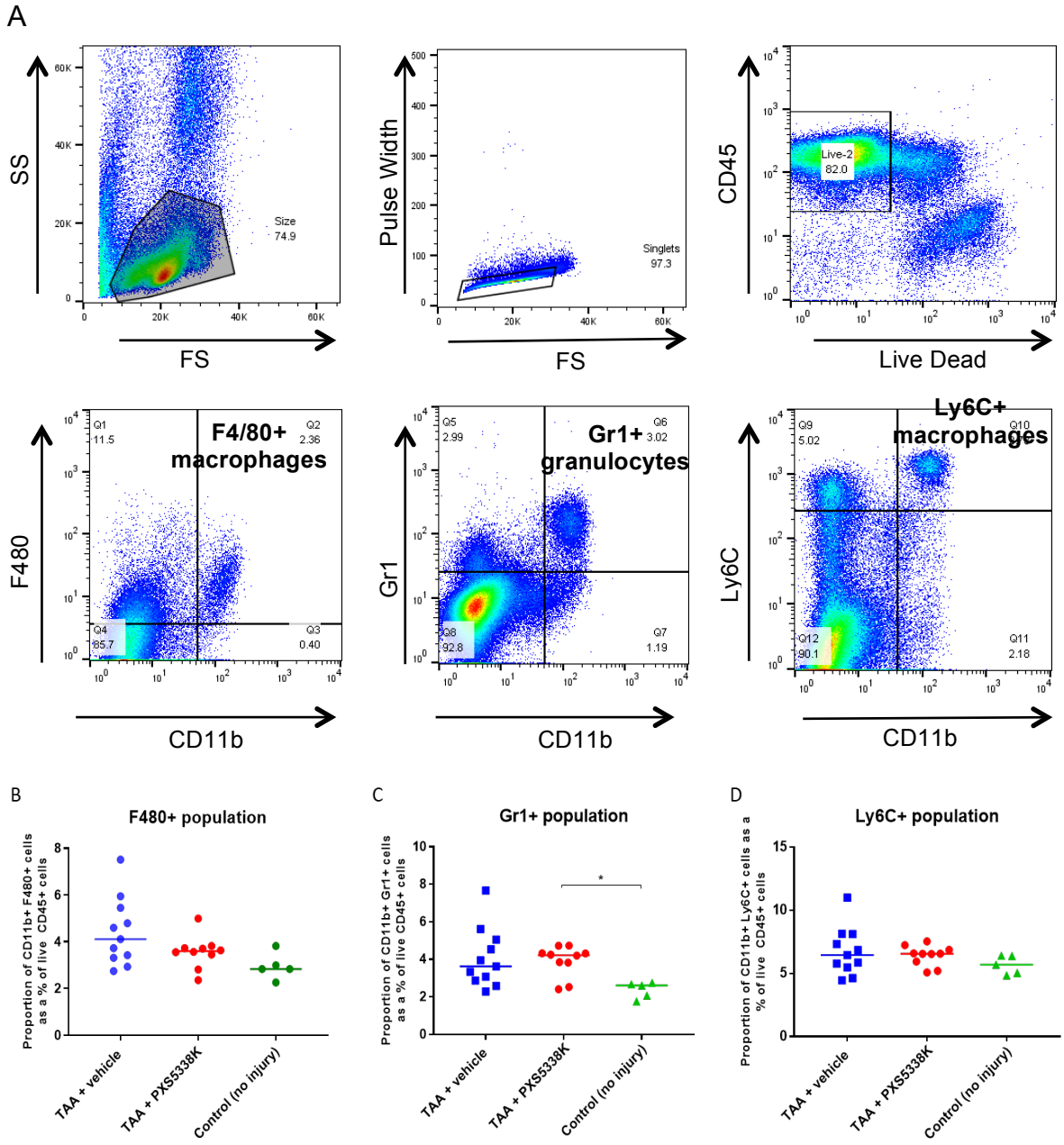
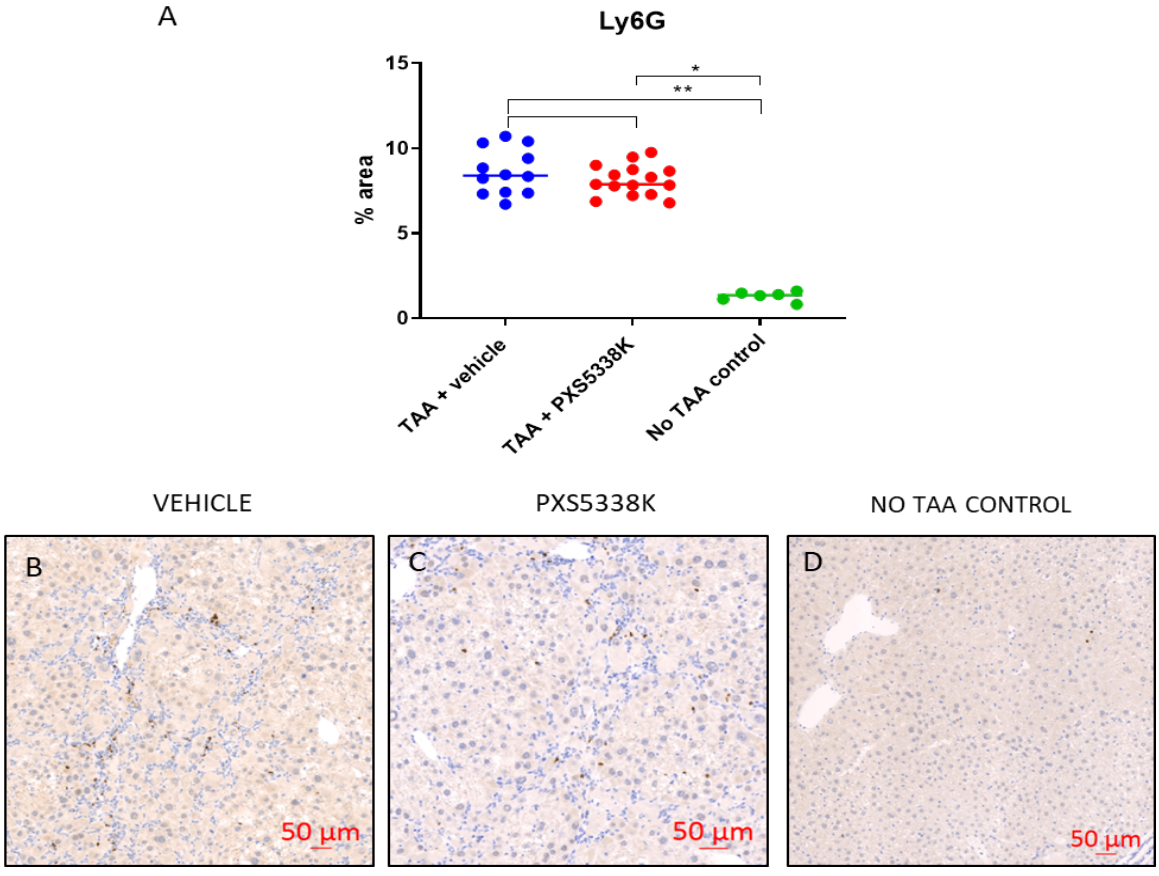


Figure 5.12 Comparison of myeloid cell isolates from liver showed no differences in immune cell populations between mice receiving vehicle or PXS5338K by oral gavage. The gating strategy used to identify tissue-infiltrating myeloid populations is illustrated in (A): forward and side light scatter (FS and SS, respectively), and absence of dead cell staining defined live singlet myeloid cells. This population was further subdivided to isolate CD11b+ F4/80+ populations, CD11b+ Ly6G+ and CD11b+ Gr1+ cells. A small increase in Gr1+ cells was observed in injured mice receiving PXS5338K but no other differences between the groups were seen for myeloid cell populations. Statistical analysis was performed using the KW test with post-hoc Bonferroni Dunn correction seen in mice receiving PXS5338K or vehicle; capped lines with asterisks indicate statistically significant differences, p values *<0.05.

5.3.4.2 Immune cell infiltration by IHC

IHC was performed for markers of immune cells to confirm the findings made by flow cytometry (Figure 5.13). As before, the B220 isoform of CD45 was used to assess the presence of B cells, F4/80 to assess macrophage infiltration, and Ly6G to assess granulocytes and neutrophil infiltration. Ly6G+ cells were upregulated in injured mice compared with uninjured controls (mean ranks for 21.6, 18.7, 3.5, p = 0.006 using the KW test and post hoc Bonferroni correction for mice receiving TAA + vehicle, TAA + PXS5338K and uninjured control, respectively. There was increased B cell infiltration in TAA injured mice, although this was only statistically significant for the mice receiving vehicle (mean ranks 14.6, 11.1, 5.8, p = 0.048, as before). The number of F4/80+ macrophages was similar for all groups (mean ranks 10.3, 12.2, 15.6, p = 0.394).



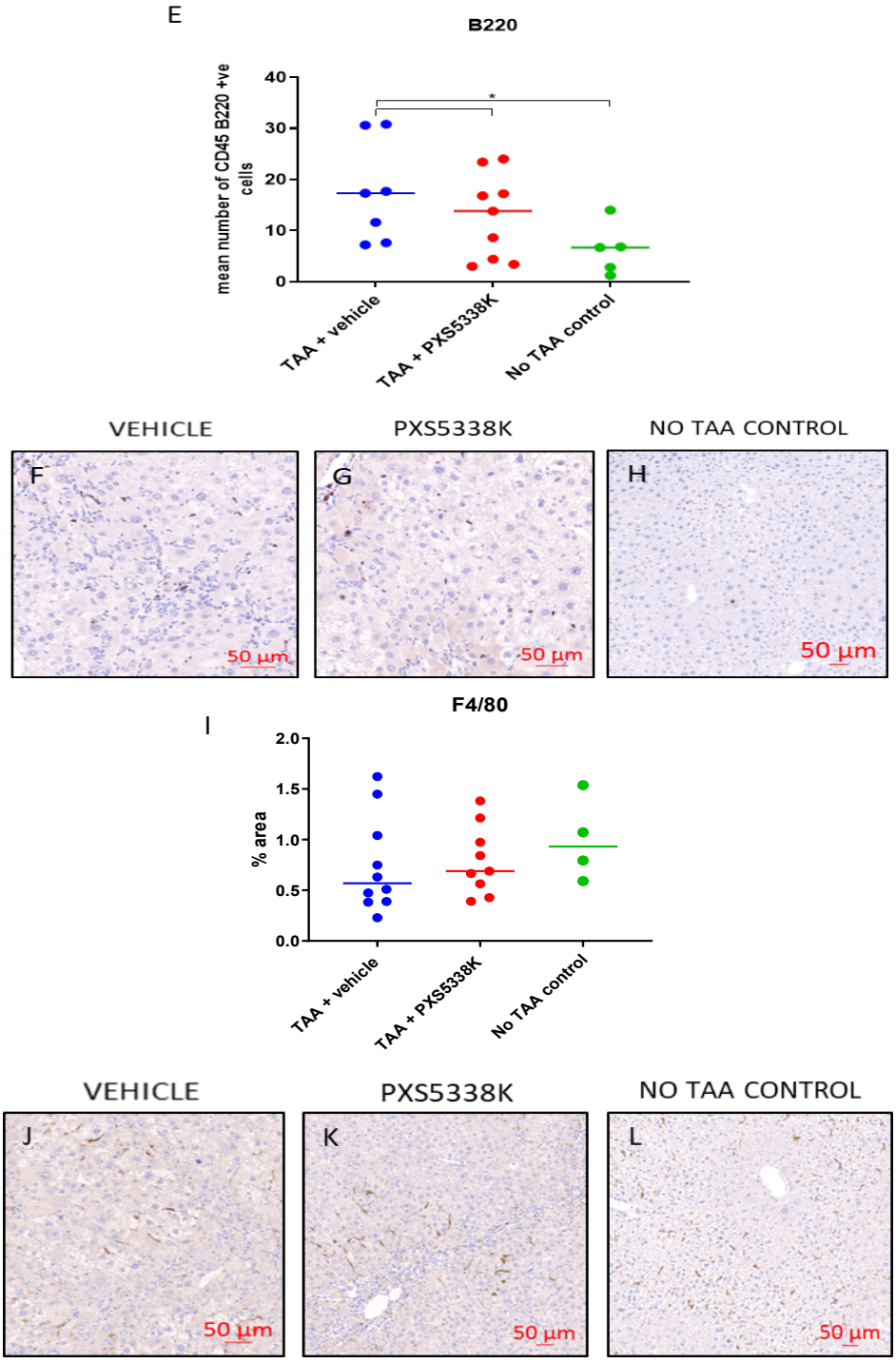


Figure 5.13 Comparison of markers of inflammatory cells in the liver showed no differences in immune cell populations between mice receiving vehicle or PXS5338K by oral gavage. IHC was performed on paraffin embedded liver sections from mice exposed to 16 weeks of TAA *ad-libitum* in drinking water with 6 weeks gavage of either vehicle or PXS5338K from week 10. A comparison group received no TAA. There was increased granulocyte and B cell infiltration in TAA injured mice (A-H), but no difference observed for F4/80+ macrophages. PXS5338K had no effect on immune cell infiltration. Statistical analysis was performed using the KW test with post-hoc Bonferroni Dunn correction; capped lines with asterisks indicate statistically significant differences, p values *<0.05.

Summary of findings

TAA induced liver injury and fibrosis in C57Bl/6 mice, exemplified by increased collagen deposition and moderate bridging fibrosis on IHC, and upregulation of profibrotic genes by qPCR. PXS5338K had no impact on liver injury or fibrosis by the same assessment, and did not alter immune cell recruitment to the liver.

5.3.5 Assessing the impact of PXS5538K on cell differentiation, inflammatory cell recruitment, and fibrosis resolution during recovery from liver injury.

Although the compound demonstrated no effect during active injury, it was not yet known whether it could impact on the resolution of fibrosis. Indeed, there is evidence that an important role of LOX/LOXLs lies in ECM remodelling (195), and this would have implications for a possible role for PXS5338K in human conditions such as treated hepatitis C or autoimmune hepatitis (AIH).

A model of fibrosis resolution was designed whereby mice were given 16 weeks of TAA drinking water taken *ad libitum*, as before, but at the end of 16 weeks, this was changed to normal undiluted drinking water. On the same day, one group of mice received 7 days of either vehicle or 3 mg/kg PXS5338K, then were culled for analysis, and a second group received 14 days of vehicle of PXS5338K prior to sacrifice.

As before, liver injury and fibrosis was assessed by serum biochemistry, IHC and expression of fibrotic markers by qPCR. The ductular reaction was assessed by IHC

for SOX-9, and immune cell infiltration was assessed by IHC and extraction of lymphocytes and monocytes for multi-colour flow cytometry.

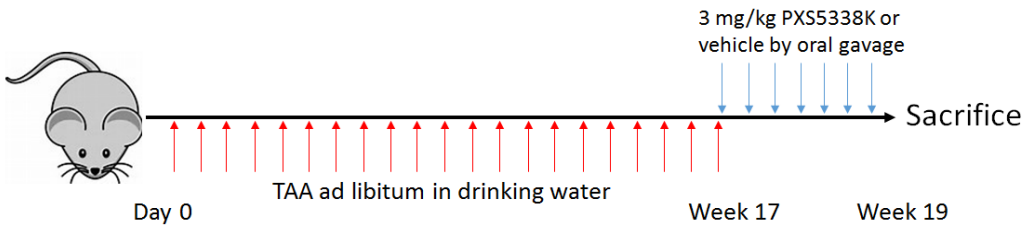


Figure 5.14 Testing PXS5338K in fibrosis resolution. TAA was given for 16 weeks then exchanged for normal drinking water; PXS5338K or vehicle was given for 2 weeks to assess efficacy in fibrosis resolution.

5.4 Assessing the impact of the TAA resolution model on the health of mice according to animal weight over time

Thirty, 6-week old male mice were exposed to 16 weeks of TAA followed by either 7 or 14 days of PXS5338K or vehicle by oral gavage. One mouse became unwell at week 10 and another became unwell following gavage and had perforated oesophagus at post-mortem, these were excluded from the analysis. 14 mice received TAA followed by 7 days of gavage with either vehicle or PXS5338K and 14 mice received TAA followed by 14 days of gavage with either vehicle or PXS5338K. All mice gained weight during 16 weeks of TAA treatment (Figure 5.15). Given that 6 weeks of PXS5338K had no impact on weight compared with vehicle, this was not assessed for the shorter period of gavage, but the median weight for each group at the end of each period of treatment were very similar.

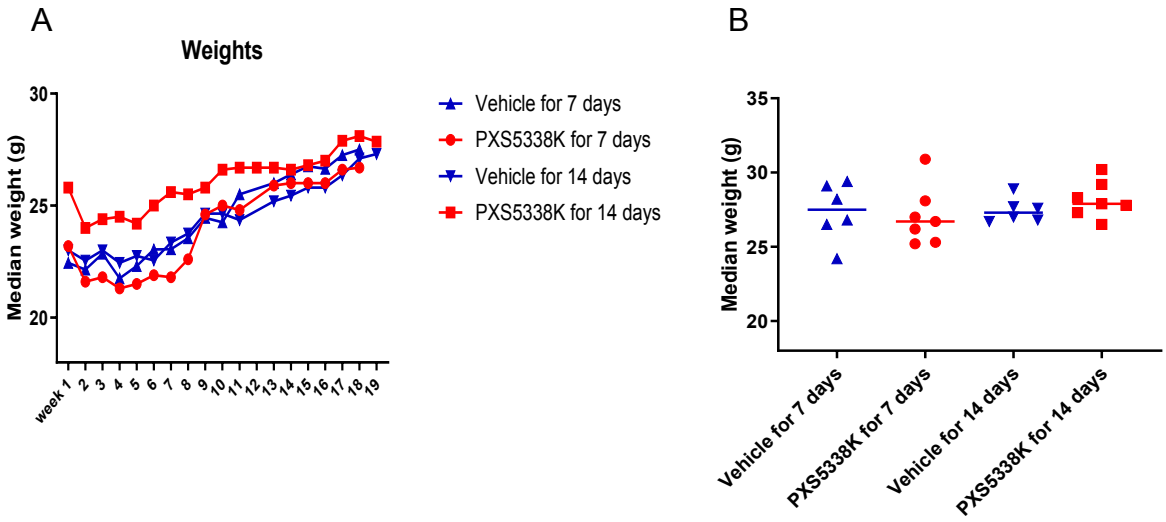


Figure 5.15 Mice exposed to 16 weeks of TAA continue to gain weight and mice treated with either 7 or 14 days of vehicle or PXS5338K have similar weights at the end of treatment. C57Bl/6 mice received 16 weeks of TAA followed by 7 or 14 days of vehicle or PXS5338K (3mg/kg) P.O. Mice continued to gain weight throughout 6 weeks of treatment and median groups weight were similar at the end of the 17- or 18-week treatment period.

5.4.1 Changes in liver serology during fibrosis resolution with and without PXS5338K following TAA induced liver injury

Serum isolated from blood retrieved during cardiac puncture was tested for markers of hepatocyte and biliary injury, as before (Figure 5.16). AST and ALT levels (as markers of liver injury) were expected to fall over 14 days (measured at day 8 and day 15 following cull) but it is worth noting that even at day 1 following liver injury ALT and AST levels were not considerably higher and so it is possible that they may have already fallen towards baseline by day 7. The MW test was used to compare the median values for mice receiving 7 days of vehicle with 7 days of PXS5338K, and then to compare the two groups of mice receiving 14 days of vehicle and PXS5338K. No differences were found between animals given 7 days of vehicle or PXS5338K, or for animals receiving 14 days of vehicle or PXS5338K for ALT (median for 7 days vehicle vs PXS5338K 40 vs 14, p = 0.145, and for 14 days 7 vs 13, p = 0.242), AST (median for 7 days vehicle vs PXS5338K, 52 vs 34, p = 0.468, and for 14 days 37 vs

37, p = 0.642), and bile acids (median for 7 days vehicle vs PXS5338K, 3 vs 20, p = 0.245, and for 14 days 4 vs 27, p = 0.719). Serum bilirubin was the same and at expected levels for all mice.

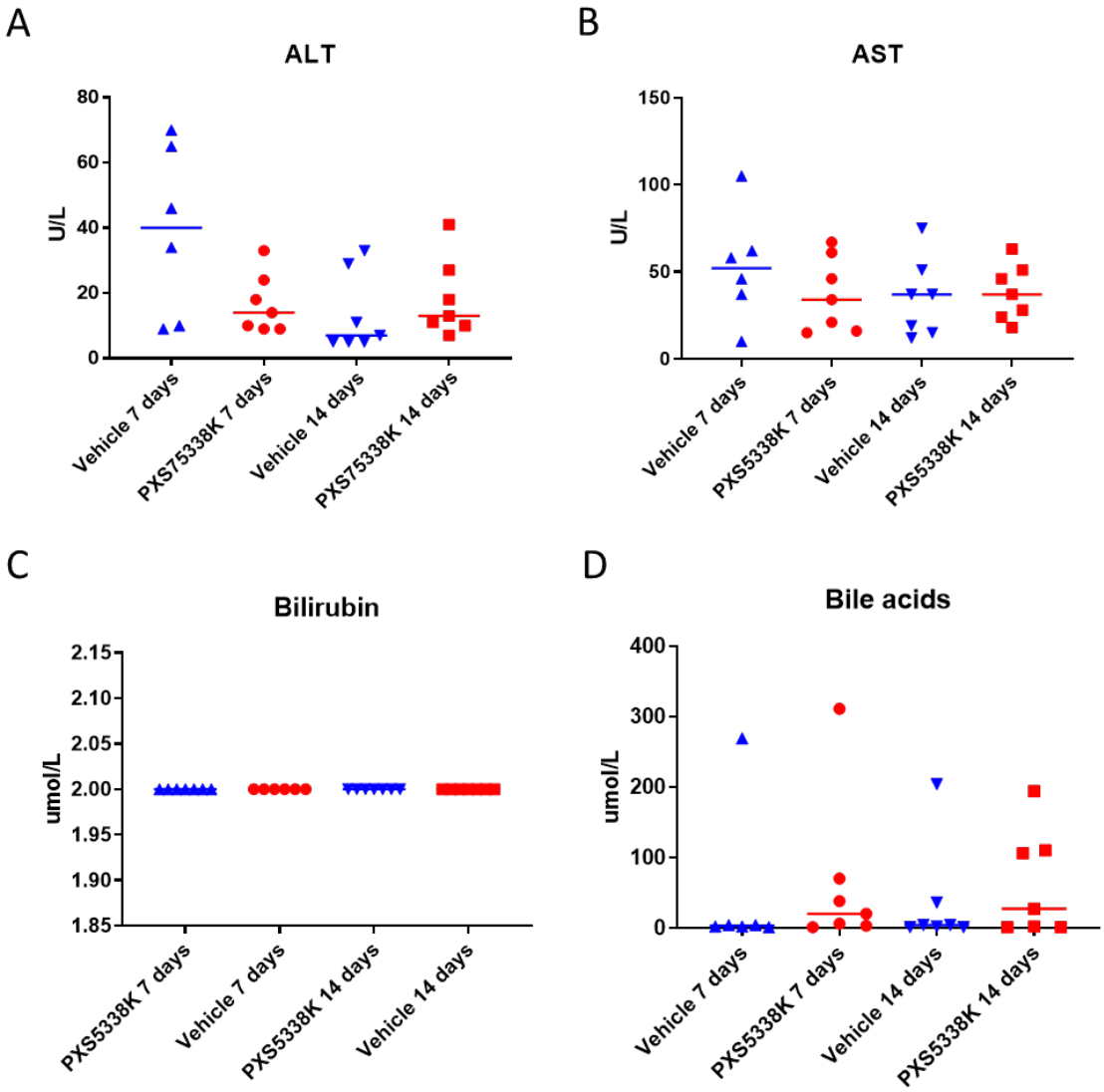


Figure 5.16 PXS5338K did not alter serum markers of hepatocyte or biliary injury in mice recovering from TAA induced liver injury. C57Bl/6 mice received 16 weeks of TAA followed by 7 or 14 days of vehicle or PXS5338K (3mg/kg) P.O. No differences were demonstrated for ALT (A), AST (B), total bilirubin (C) or bile acids (D). Comparison was made between the two groups of mice receiving vehicle or PXS5338K for 7 days, then between the two groups receiving 14 days of vehicle or compound using the MW test.

5.4.2 Assessing the impact of PXS5338K on fibrosis resolution following TAA induced liver disease

As for the TAA injury study, fibrosis was assessed by immunohistochemistry for collagen I and III, collagens with PSR stain, and α-SMA for HSC activation followed by qPCR for mRNA encoding proteins upregulated during fibrosis or remodelling of scar tissue.

As before, collagen I, collagen III, and PSR were analysed at low and high magnification (Figure 5.17-5.19). Similarly to serum markers, it was expected that % positive area for each of these markers would fall from 7 to 14 days, and that at day 7 staining may be less than that seen at peak injury in the previous TAA model. However, the key outcome was to assess differences between those mice receiving vehicle vs PXS5338K. Only analysis for collagen I showed a difference between the analyses; there was a trend for reduced collagen I with PXS5338K at both high and low resolution analysis at 7 and 14 days, and there was significant reduction when analysed at high magnification in the mice receiving PXS5338K for 14 days ($p = 0.497$, low magnification analysis and $p = 0.022$ for analysis at higher magnification). Expression of α-SMA was reduced in mice receiving PXS5338K for both 7 ($p = 0.001$) and 14 days ($p = 0.015$), compared with vehicle control.

Comparing % area for these readouts at peak injury, collagen III and PSR seem to have dropped from peak injury to day 7 (approx. 10 to 1-2% and 8-10% to 4-6%, respectively), but staining for collagen I remains at about 10% from peak injury to day 15, except for the reduction in mice receiving PXS5338K in the resolution model.

Changes between day 8 and 15 are less remarkable; certainly there is no clear reduction in staining that had been expected in any of the markers. As before, staining for α-SMA appeared to be predominantly in blood vessels. The IHC for collagen I and III was also less reliable in these samples, as only paraffin tissue was available, and so not all slides could be accurately analysed; another possible explanation for the findings described above.

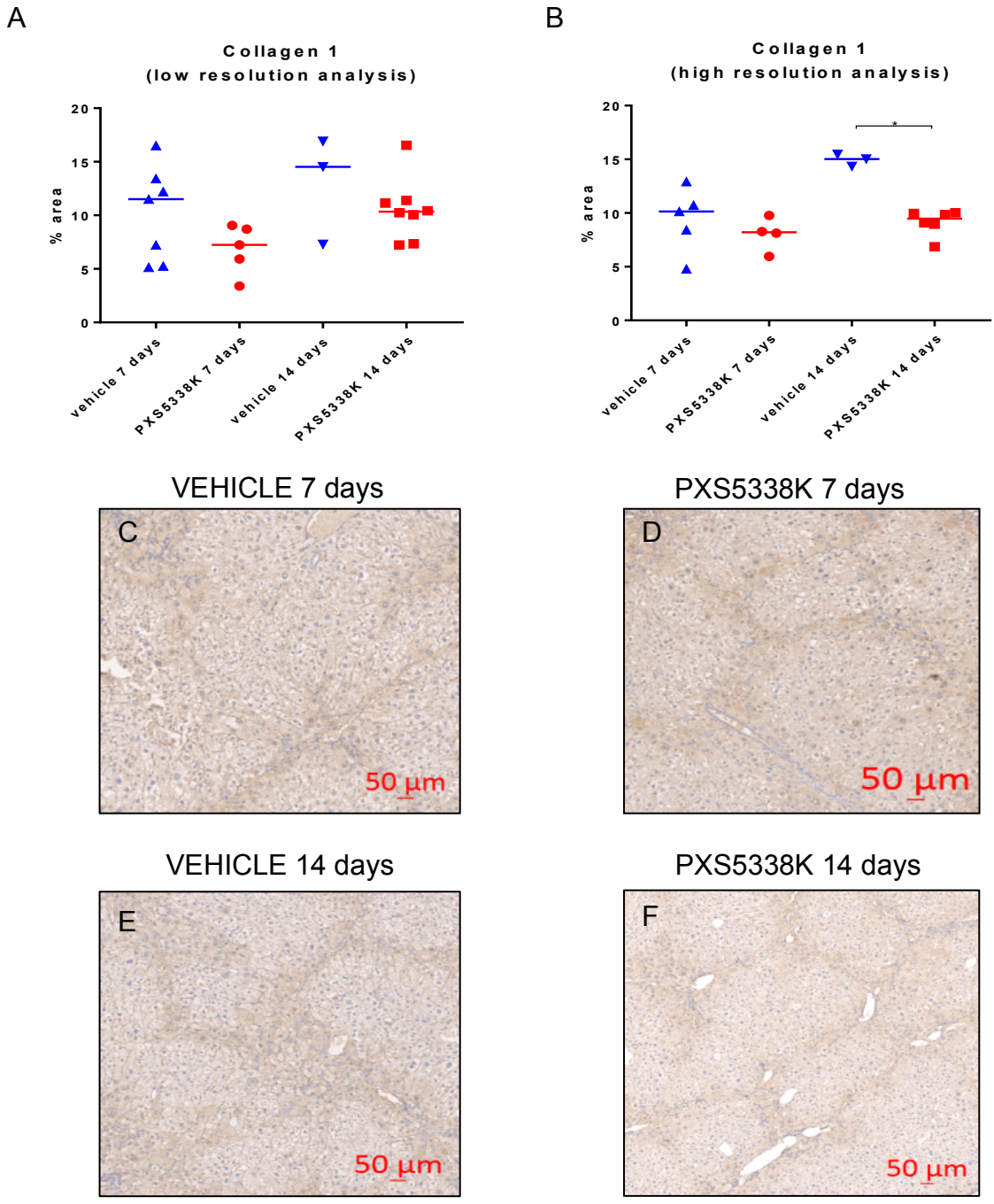


Figure 5.17 PXS5338K may reduce collagen I expression in mice recovering from TAA induced liver injury. C57Bl/6 mice received 16 weeks of TAA followed by 7 or 14 days of vehicle or PXS5338K (3mg/kg) P.O. IHC on paraffin embedded liver sections with morphometric analysis to calculate % area stained demonstrated a trend for reduced collagen I in mice receiving PXS5338K compared with vehicle (A-F). Comparison was made between the two groups of mice receiving vehicle or PXS5338K for 7 days, then between the two groups receiving 14 days of vehicle or compound using the MW test. For low resolution analysis, median % areas for vehicle vs PXS5338K at 7 days were 7.25 % vs 11.51%, p = 0.343, and for 14 days 14.53 % vs 10.33 %, p = 0.497 (A). High resolution analysis the corresponding values for 7 days were 10.20% vs 8.20 %, p = 0.286 and for 14 days 9.48 % vs 15.02 %, p = 0.024 (B). *p < 0.05.

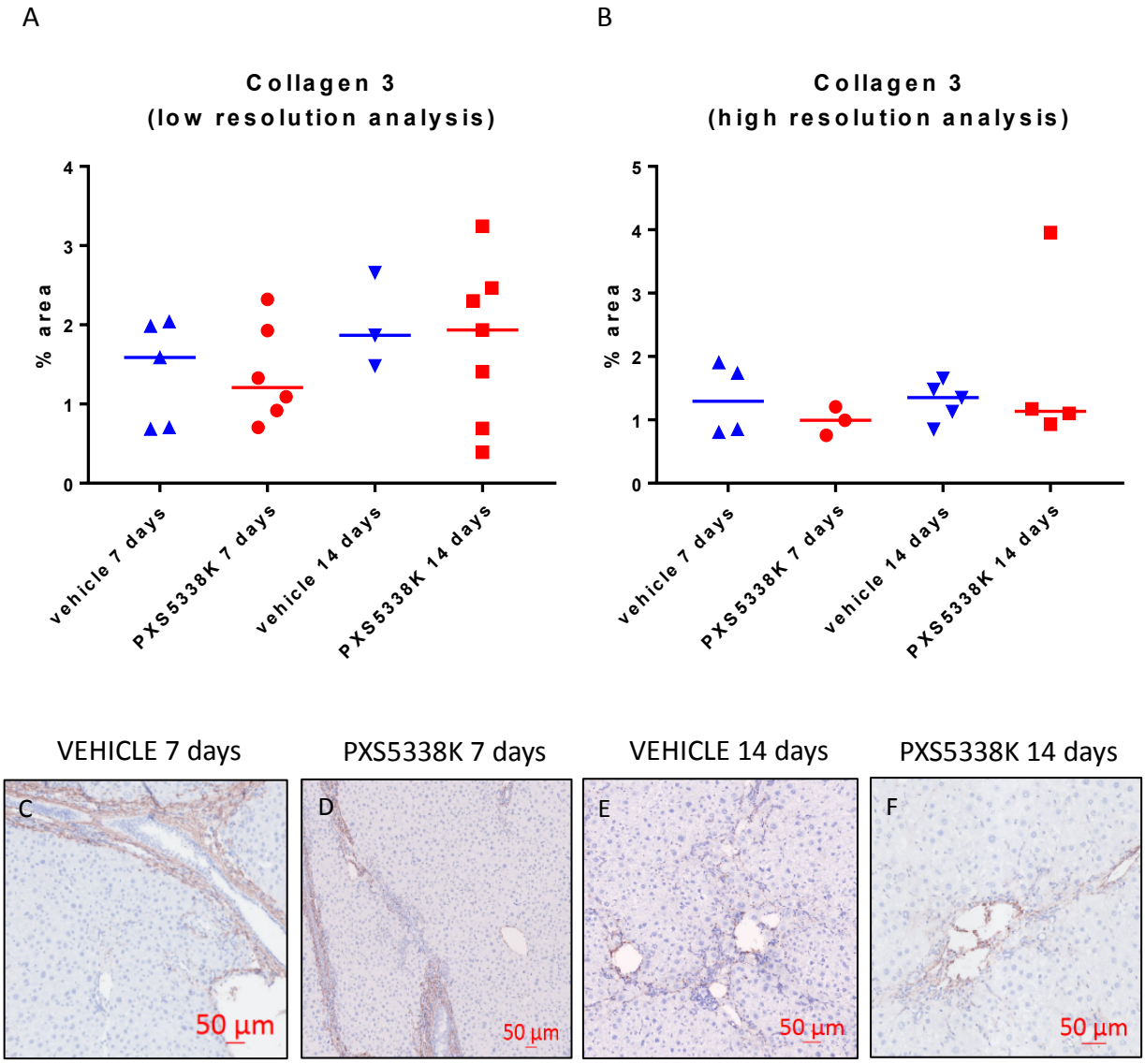


Figure 5.18 PXS5338K did not alter collagen III expression in mice recovering from TAA induced liver injury. C57Bl/6 mice received 16 weeks of TAA followed by 7 or 14 days of vehicle or PXS5338K (3mg/kg) P.O. IHC on paraffin embedded liver sections with morphometric analysis to calculate % area stained demonstrated no difference in mice receiving PXS5338K (3 mg/kg) compared with vehicle (A-F) for collagen III. Comparison was made between the two groups of mice receiving vehicle or PXS5338K for 7 days, then between the two groups receiving 14 days of vehicle or compound using the MW test. For low resolution analysis, median % areas for vehicle vs PXS5338K at 7 days were 1.59 % vs 1.21 %, p = 0.999, and for 14 days 1.90 % vs 1.93 %, p = 0.833 (A). For high resolution analysis the corresponding values for 7 days were 1.29 % vs 0.99 %, p = 0.629 and for 14 days 1.35 % vs 1.14 %, p = 0.905 (B).

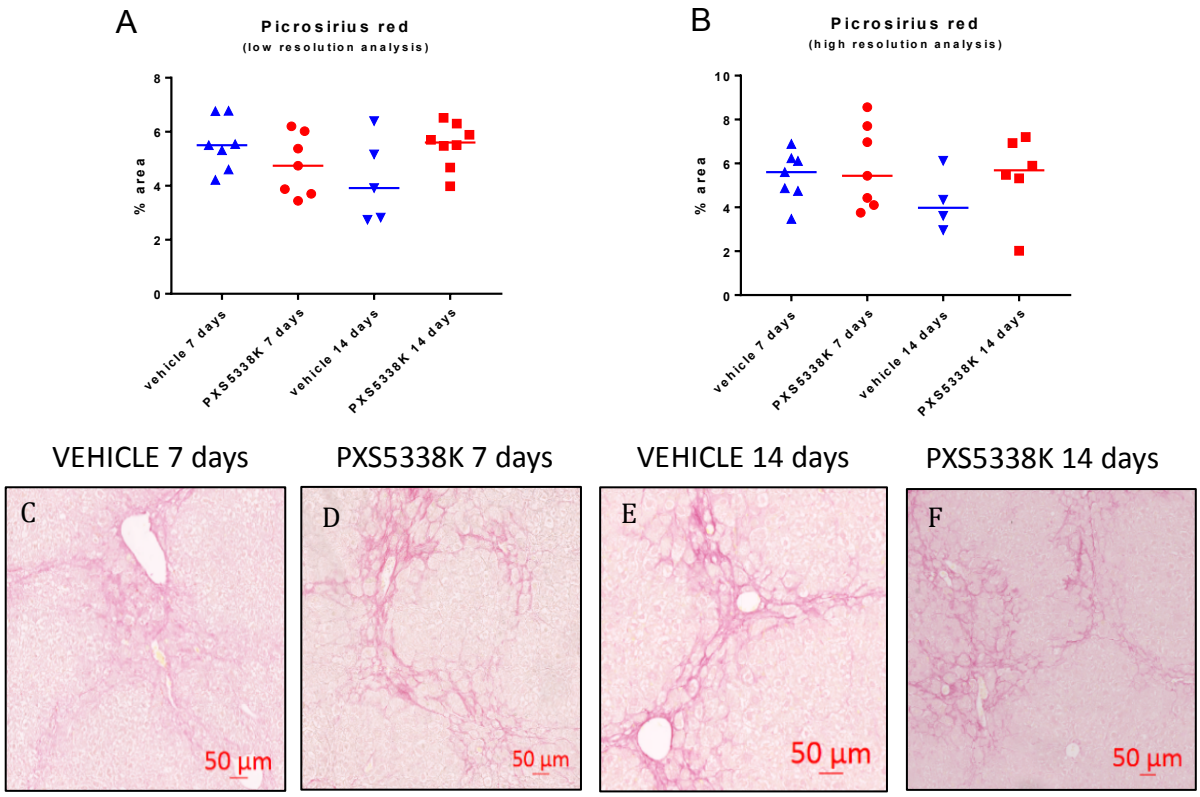


Figure 5.19 PXS5338K did not alter fibrosis by collagen PSR stain in mice recovering from TAA induced liver injury. C57Bl/6 mice received 16 weeks of TAA followed by 7 or 14 days of vehicle or PXS5338K (3 mg/kg) P.O. IHC on paraffin embedded liver sections with morphometric analysis to calculate % area stained demonstrated no difference in mice receiving PXS5338K (3 mg/kg) compared with vehicle for collagen (A-F). Comparison was made between the two groups of mice receiving vehicle or PXS5338K for 7 days, then between the two groups receiving 14 days of vehicle or compound using the W test. For low resolution analysis, median % areas for vehicle vs PXS5338K at 7 days were 5.50 % vs 4.74 %, p = 0.259, and for 14 days 3.91 % vs 5.61 %, p = 0.127 (A). High resolution analysis the corresponding values for 7 days were 5.60 % vs 5.44 %, p = 0.805 and for 14 days 3.98 % vs 5.69 %, p = 0.352 (B).

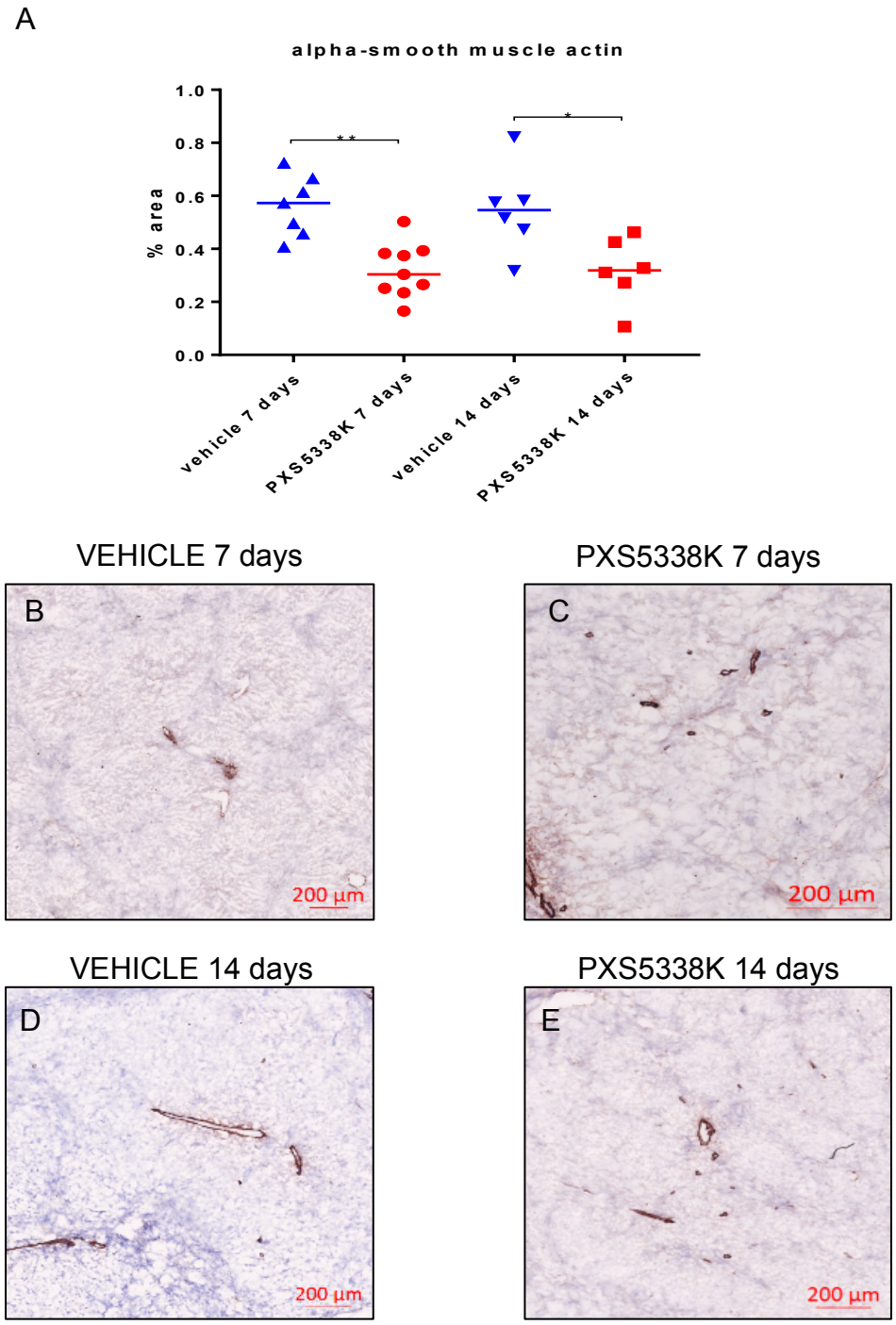
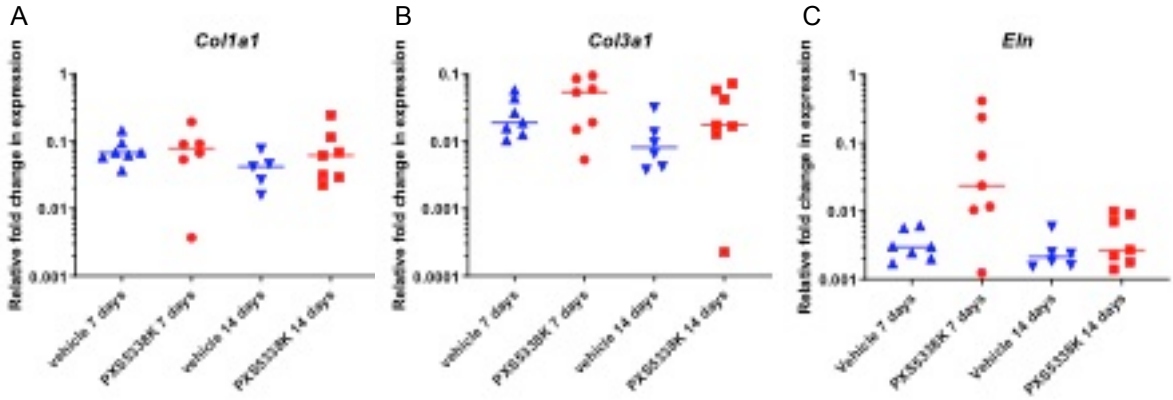
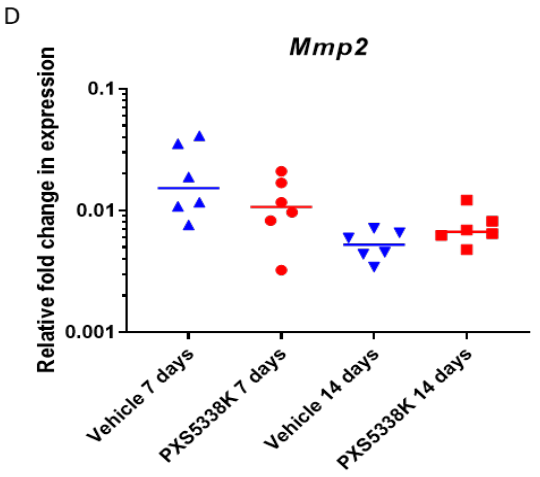
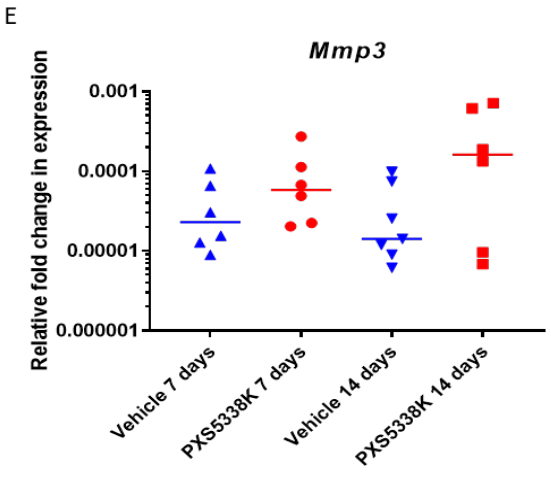


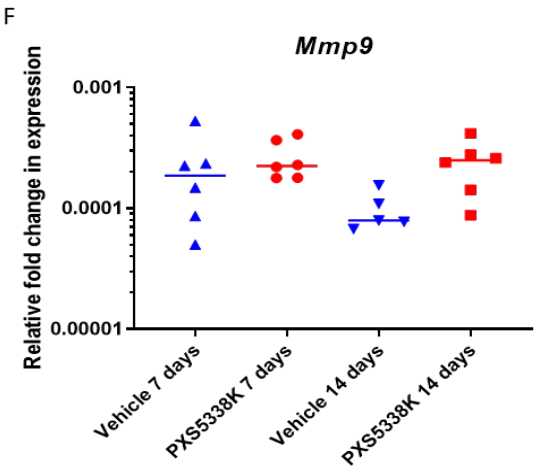
Figure 5.20 Reduced expression of α-SMA was demonstrated in mice receiving PXS5338K recovering from TAA induced liver injury. C57Bl/6 mice received 16 weeks of TAA followed by 7 or 14 days of vehicle or PXS5338K (3mg/kg) P.O. IHC on paraffin embedded liver sections with morphometric analysis to calculate % area stained demonstrated a reduction in active α-SMA expressing HSCs in mice receiving PXS5338K (3 mg/kg) compared with vehicle for collagen (A-E). Comparison was made between the two groups of mice receiving vehicle or PXS5338K for 7 days, then between the two groups receiving 14 days of vehicle or compound using the MW test. Median % areas for vehicle vs PXS5338K at 7 days were 0.57 % vs 0.30 %, p = 0.001, and for 14 days 0.55 % vs 0.33 %, p = 0.015 (A). *p <0.05, **p <0.01.

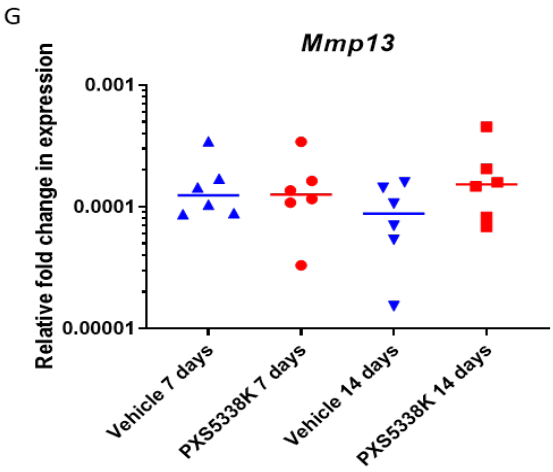
Next, expression of genes associated with fibrosis was performed by qPCR and the groups were compared, as above. No differences were seen between the groups using the MW test to compare median values for mice receiving 7 days of vehicle with 7 days of PXS5338K, and then to compare the two groups of mice receiving 14 days of vehicle and PXS5338K.











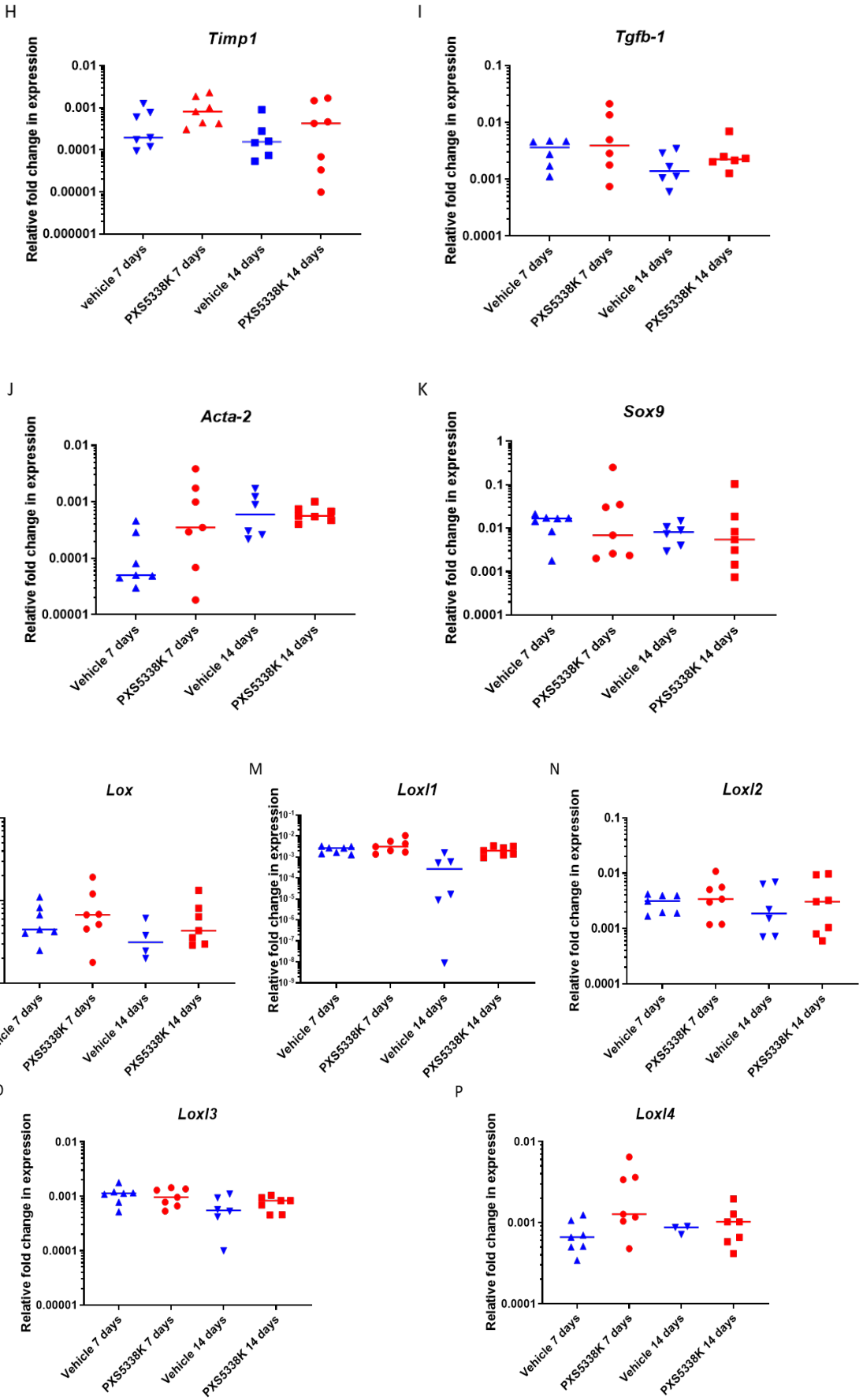

H
Timp1
Relative fold change in expression
0.01
0.001
0.0001
0.00001
0.000001
vehicle 7 days
PXS5338K 7 days
vehicle 14 days
PXS5338K 14 days
I
Tgfb-1
Relative fold change in expression
0.1
0.01
0.001
0.0001
Vehicle 7 days
PXS5338K 7 days
Vehicle 14 days
PXS5338K 14 days
J
Acta-2
Relative fold change in expression
0.01
0.001
0.0001
0.00001
Vehicle 7 days
PXS5338K 7 days
Vehicle 14 days
PXS5338K 14 days
K
Sox9
Relative fold change in expression
1
0.1
0.01
0.001
0.0001
Vehicle 7 days
PXS5338K 7 days
Vehicle 14 days
PXS5338K 14 days
L
Lox
Relative fold change in expression
0.01
0.001
0.0001
Vehicle 7 days
PXS5338K 7 days
Vehicle 14 days
PXS5338K 14 days
M
Loxl1
Relative fold change in expression
Vehicle 7 days
PXS5338K 7 days
Vehicle 14 days
PXS5338K 14 days
N
Loxl2
Relative fold change in expression
0.1
0.01
0.001
0.0001
Vehicle 7 days
PXS5338K 7 days
Vehicle 14 days
PXS5338K 14 days
O
Loxl3
Relative fold change in expression
0.01
0.001
0.0001
0.00001
Vehicle 7 days
PXS5338K 7 days
Vehicle 14 days
PXS5338K 14 days
P
Loxl4
Relative fold change in expression
0.01
0.001
0.0001
Vehicle 7 days
PXS5338K 7 days
Vehicle 14 days
PXS5338K 14 days

Figure 5.21 Administration of PXS5338K during the resolution phase did not alter mRNA expression for markers of fibrosis. C57Bl/6 mice received 16 weeks of TAA followed by 7 or 14 days of vehicle or PXS5338K (3mg/kg) P.O. RNA was extracted from frozen tissue and mRNA expression measured against the housekeeping gene *Gapdh*. Expression of genes upregulated during fibrogenesis was no different between the injured mice receiving vehicle or PXS5338K, for *col1a1*, 7 days p = 0.807 (A), 14 days p = 0.432 (B) *col3a1*, 7 days p = 0.318, 14 days p = 0.138 (B), *eln* 7 days p = 0.051, 14 days p = 0.366 (C), *mmp2*, 7 days, p = 0.329, 14 days p = 0.132 (D), *mmp3* 7 days p = 0.180, 14 days p = 0.181 (E), *mmp9*, 7 days p = 0.450, 14 days p = 0.059 (F), mmp13, 7 days p = 0.999, 14 days p = 0.143 (G), *timp1*, 7 days p = 0.098, 14 days p = 0.0485 (H), *tgfb1*, 7 days p = 0.309, 14 days 0.485 (I), *sox9*, 7 days p = 0.999, 14 days 0.731 (K), *lox*, 7 days p = 0.402. 14 days p = 0.230 (L), *loxl1*, 7 days p = 0.317, 14 days p = 0.051 (M), *loxl2*, 7 days p = 0.710, 14 days p = 0.731 (N), *loxl3*, 7 days 0.999, 14 days p = 0.509 (O), and *loxl4*, 7 days p = 0.053, 14 days 0.800 (P). Comparison was made between the two groups of mice receiving vehicle or PXS5338K for 7 days, then between the two groups receiving 14 days of vehicle or compound using the MW test.

5.4.3 Examining the effect of PXS5338K on cell differentiation during fibrosis resolution

As before, the intensity of the ductular reaction and biliary differentiation of cells was assessed by IHC for SOX-9 (Figure 5.22). Comparison was made between the two groups of mice receiving vehicle or PXS5338K for 7 days, then between the two groups receiving 14 days of vehicle or compound using the MW test. There was a trend for increased ductular reaction measured by IHC for SOX-9 which became significant for mice receiving 14 weeks of compound compared to the control group. The staining also appeared slightly different to that seen in previous experiments; while endothelial-like structures were seen in C57Bl6/ *Mdr2-/-* and TAA induced fibrosis model with SOX-9, a combination of these and individual cell staining was seen in the resolution model. This may reflect greater staining of regenerative progenitor cells following cessation of liver injury in the resolution experiment, and possibly staining of predominantly pre-existing biliary structures in previous experiments.

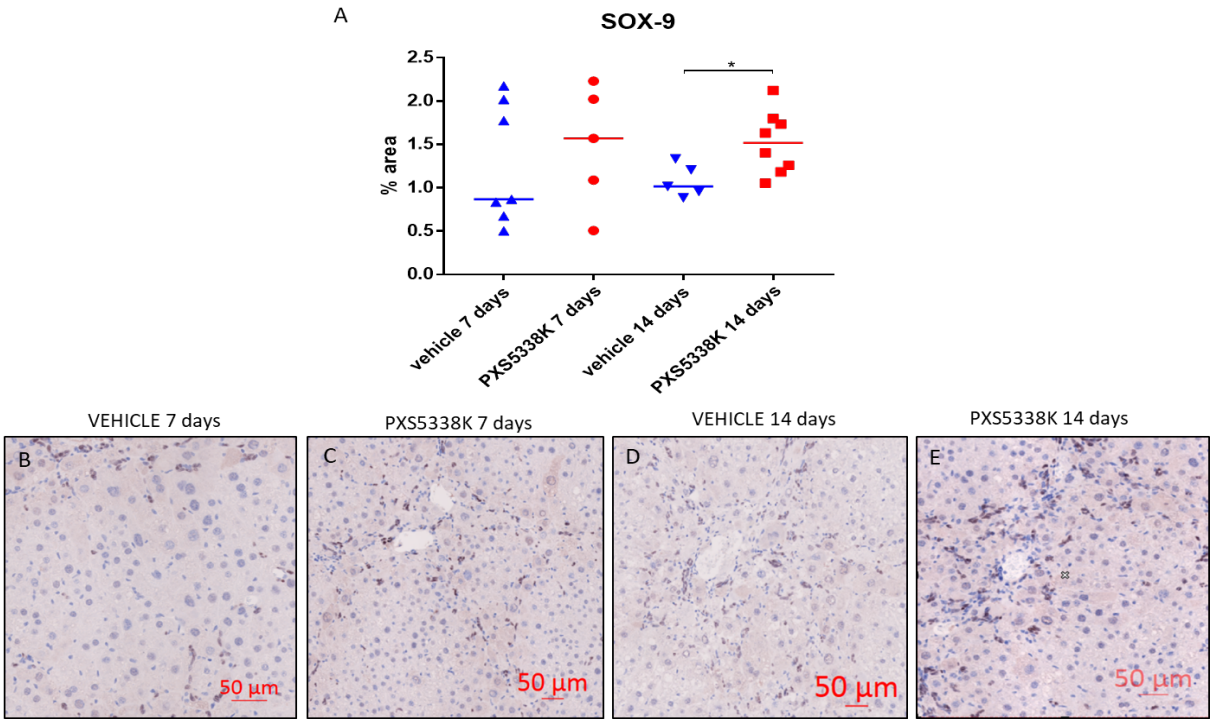


Figure 5.22 An increase in the ductular reaction was observed in mice receiving PXS5338K recovering from TAA induced liver injury. C57Bl/6 mice received 16 weeks of TAA followed by 7 or 14 days of vehicle or PXS5338K (3mg/kg) P.O. IHC on paraffin embedded liver sections with morphometric analysis to calculate % area stained demonstrated increased expression of SOX-9 the livers of in mice receiving PXS5338K (3 mg/kg) compared with vehicle for collagen (A-E). Comparison was made between the two groups of mice receiving vehicle or PXS5338K for 7 days, then between the two groups receiving 14 days of vehicle or compound using the (MW test). Median % areas for vehicle vs PXS5338K at 7 days were 0.87 % vs 1.57 %, p = 0.530, and for 14 days 1.017 % vs 1.518 %, p = 0.029 (A). *p <0.05.

5.4.4 The effects of PXS5338K on immune cell infiltration during fibrosis resolution

As before, immune cell infiltration was assessed by flow cytometry and IHC for immune cell markers.

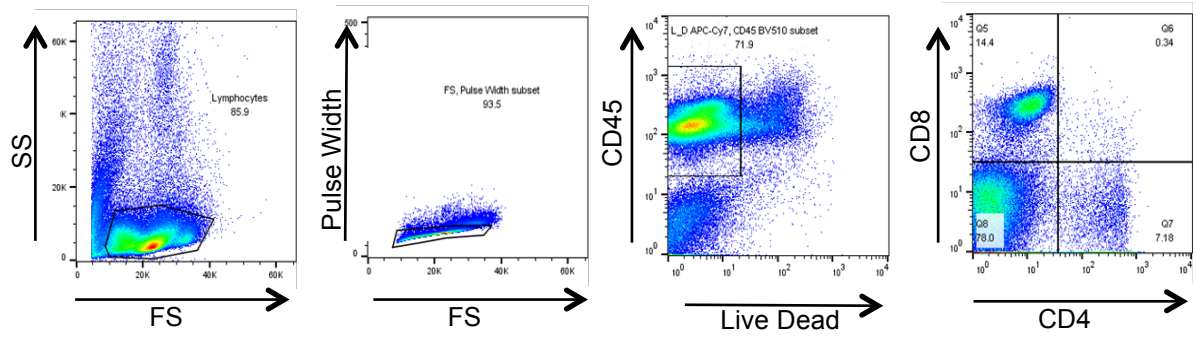
5.4.4.1 Assessment of immune cell infiltration by flow cytometry

Lymphoid populations

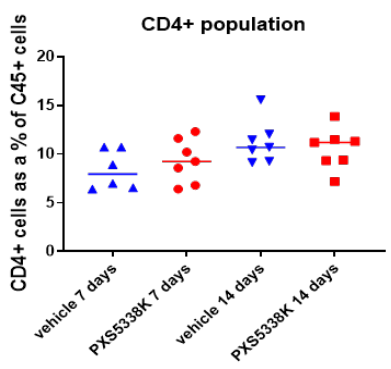
Lymphoid cells were isolated from C57Bl/6 mice receiving 16 weeks of TAA followed by 7 or 14 days of either vehicle or 3 mg/kg PXS5338K P.O., and fluorescently labelled as described in chapter 2. The frequency of each population of lymphocytes was examined by flow cytometry, in which the total lymphocyte population cloud was subject to gating on the live cells. CD4+(CD8-) T cells and CD8+ (CD4-) T cells were measured as a % of live lymphocytes, and also as a % of CD19- CD3+ live cells for the mice receiving 14 days of gavage. This was due to improved CD3 signal in these samples. No differences were seen between populations comparing the two groups of mice receiving vehicle or PXS5338K for 7 days, then between the two groups receiving 14 days of vehicle or compound using the MW test (Figure 5.23).

Similarly, CD45+ CD49b+ NK and NKT cells were calculated as a proportion of live CD45 cells (due to weak CD3 signal) for all four groups, then repeated to isolate CD3- CD49b+ NK cells and CD3+ CD49b+ NKT cells in the mice receiving 14 days gavage. CD3- CD19+ B lymphocytes were calculated as a proportion of live CD45 cells for all groups but a CD3+ was more apparent for the groups receiving 14 days of gavage.

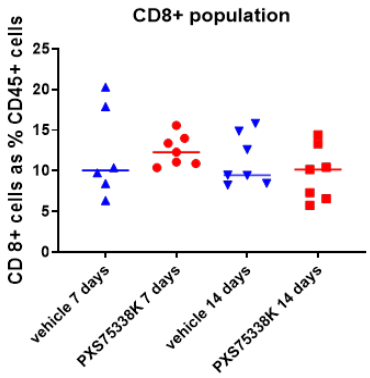
A



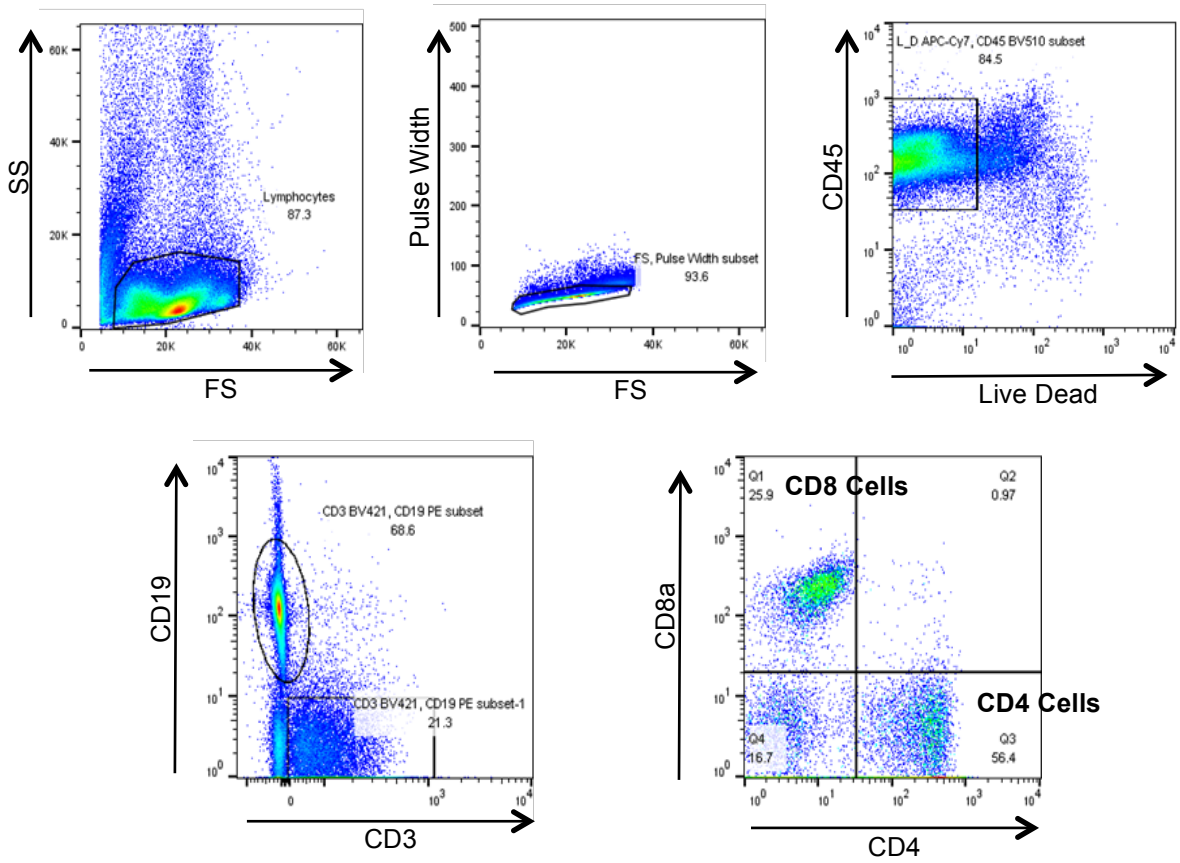
B


CD4+ population
CD4+ cells as a % of C45+ cells
20
15
10
5
0
vehicle 7 days
PXS5338K 7 days
vehicle 14 days
PXS5338K 14 days

C


CD8+ population
CD 8+ cells as % CD45+ cells
25
20
15
10
5
0
vehicle 7 days
PXS75338K 7 days
vehicle 14 days
PXS75338K 14 days

D


SS
FS
Lymphocytes
87.3
Pulse Width
FS, Pulse Width subset
93.6
CD45
L_D APC-Cy7, CD45 BV510 subset
84.5
Live Dead
CD19
CD3
CD3 BV421, CD19 PE subset
68.6
CD3 BV421, CD19 PE subset-1
21.3
CD8a
CD4
Q1
25.9
CD8 Cells
Q2
0.97
Q4
16.7
Q3
56.4
CD4 Cells

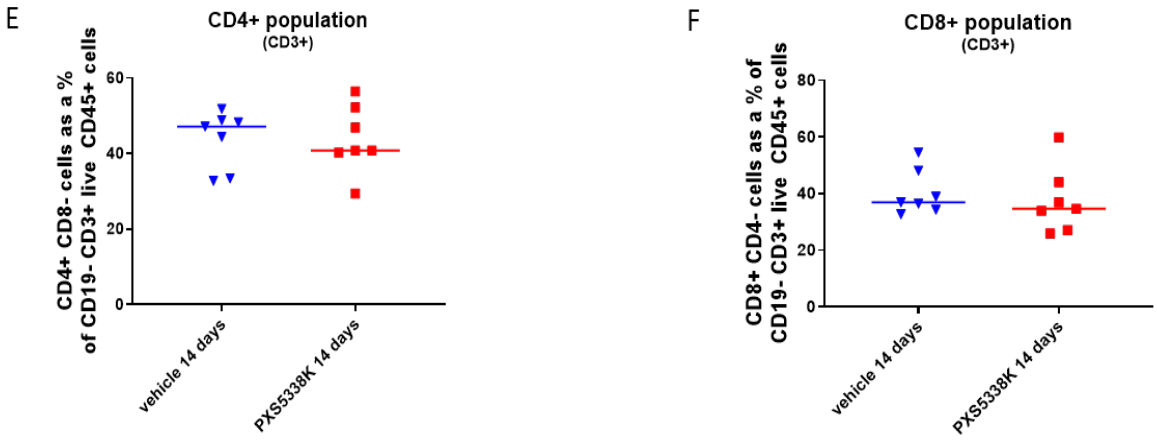


Figure 5.23 Comparison of lymphoid cell isolates from liver showed no differences in immune cell populations between mice receiving vehicle vs PXS5338K by oral gavage. The gating strategy used to identify tissue-infiltrating lymphocyte populations is illustrated in (A+D): forward and side light scatter (FS and SS, respectively), and absence of dead cell staining defined live singlet lymphocytes. This population subdivided into CD4+ CD8- cells (B+D), CD8+ CD4- cells (C+E). CD4+(CD8-) T cells and CD8+ (CD4-) T cells were measured as a % of live lymphocytes (B+C), and also as a % of CD19- CD3+ live cells for mice receiving 14 days of gavage (E+F). The MW test was used to compare the median % of two groups of mice receiving vehicle or PXS5338K for 7 days, and the two groups receiving 14 days of vehicle or PXS5338K for both gating strategies. No differences were seen between the groups at 7 or 14 days, or using either gating strategy (CD4+ T lymphocytes at 7 days, vehicle vs PXS5338K, 7.9 % vs 9.2 %, p = 0.600, and for 14 days 10.7 % vs 11.2 % (B) and for CD4+ cells as a % of CD19- CD3+ at 14 days, 47.1 % vs 40.8%, p = 0.875 (C); likewise for CD8+ T lymphocytes at 7 days, 10.1 % vs 12.3 %, p = 0.387, and 14 days, 9.5 % vs 10.2 %, p = 0.456, and for CD8+ cells as a proportion of CD19- CD3+ cells, 36.9% vs 34.6%, p = 0.477).

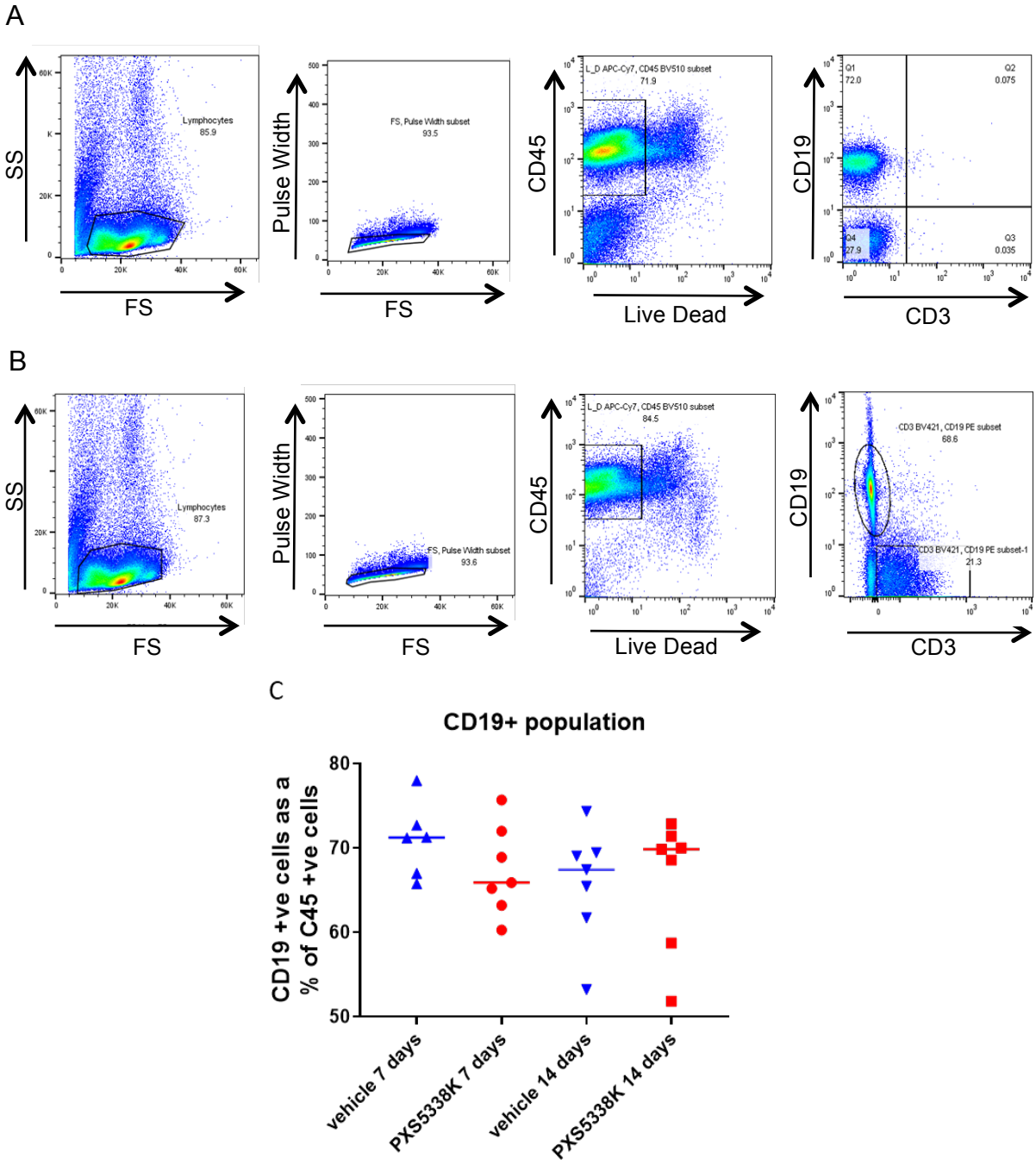
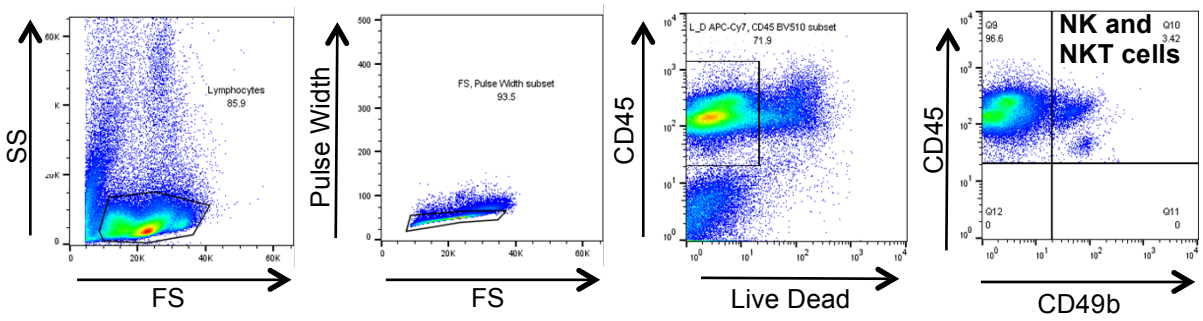
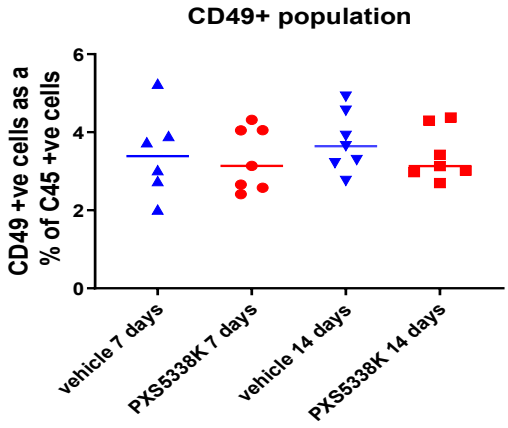


Figure 5.24 Comparison of lymphoid cell isolates from liver showed no differences in immune cell populations between mice receiving vehicle vs PXS5338K by oral gavage. The gating strategy used to identify tissue-infiltrating lymphocyte populations is illustrated in (A+B): forward and side light scatter (FS and SS, respectively), and absence of dead cell staining defined live singlet lymphocytes. This population was further subdivided into CD3-CD19+cells. A CD3+ population is better identified for the samples obtained at 14 days (B). The MW test was used to compare the median % of two groups of mice receiving vehicle or PXS5338K for 7 days, and the two groups receiving 14 days of vehicle or PXS5338K. No differences were seen between the groups at 7 days (median 71.2 % vs 65.9 %, p = 0.234) or 14 days (median 67.4 % vs 69.9 %, p = 0.620).

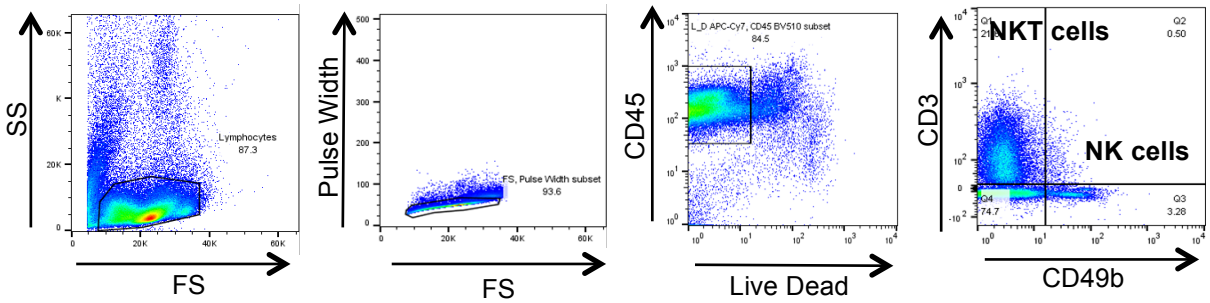
A


SS
FS
Lymphocytes
85.9
Pulse Width
FS
FS, Pulse Width subset
93.5
CD45
Live Dead
L_D APC-Cy7, CD45 BV510 subset
71.9
CD45
CD49b
NK and
NKT cells
Q9
96.6
Q10
3.42
Q12
0
Q11
0

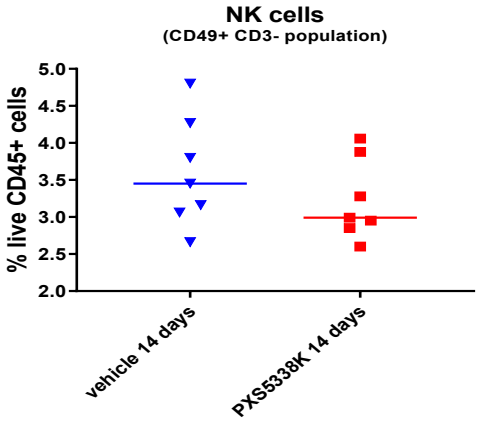
B


CD49+ population
CD49 +ve cells as a
% of C45 +ve cells
vehicle 7 days
PXS5338K 7 days
vehicle 14 days
PXS5338K 14 days

C


SS
FS
Lymphocytes
87.3
Pulse Width
FS
FS, Pulse Width subset
93.6
CD45
Live Dead
L_D APC-Cy7, CD45 BV510 subset
84.5
CD3
CD49b
NKT cells
NK cells
Q2
0.50
Q4
74.7
Q3
3.28

D


NK cells
(CD49+ CD3- population)
% live CD45+ cells
vehicle 14 days
PXS5338K 14 days

E

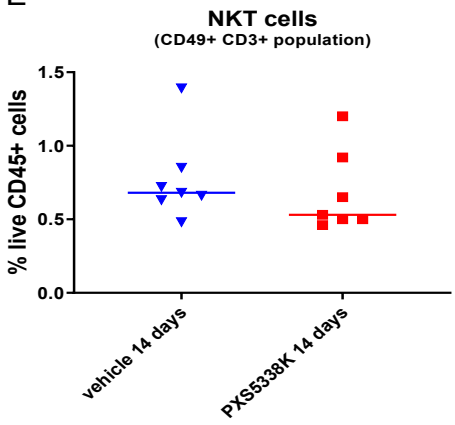

NKT cells
(CD49+ CD3+ population)
% live CD45+ cells
vehicle 14 days
PXS5338K 14 days

Figure 5.25 Comparison of lymphoid cell isoates from liver showed no differences in immune cell populations between mice receiving vehicle vs PXS5338K by oral gavage. The gating strategy used to identify tissue-infiltrating lymphocyte populations is illustrated in (A+C): forward and side light scatter (FS and SS, respectively), and absence of dead cell staining defined live singlet lymphocytes. This population was subdivided into CD45+ CD49b+ NK and NKT cells, calculated as a proportion of live CD45 cells (due to weak CD3 signal) for all groups, then repeated to isolate CD3- CD49b+ NK cells and CD3+ CD49b+ NKT populations in mice receiving 14 days of gavage. The MW test was used to compare the median % of two groups of mice receiving vehicle or PXS5338K for 7 days, and the two groups receiving 14 days of vehicle or PXS5338K for both gating strategies. No differences were seen between the groups at 7 or 14 days, or using either gating strategy (CD49b+cells at 7 days, vehicle vs PXS5338K, 3.4 % vs 3.1 %, p = 0.999, and for 14 days 3.6 % vs 3.1 %, p = 0.318 (B) and for CD3- CD49b+ NK cells at 14 days, 3.5 % vs 2.9 %, p = 0.318 (D); likewise for CD3+CD49b+ NKT cells, 0.68 % vs 0.58 %, p = 0.364 (E)).

Myeloid populations

As before, myeloid cells were isolated from the livers of C57Bl/6 mice receiving 16 weeks of TAA and either 7 or 14 days of vehicle or PXS5338K, and incubated with appropriate fluorochrome-labelled antibodies, as described in chapter 2. The frequency of monocytes was examined by flow cytometry, in which the total myeloid cloud was subject to gating on the live CD45+ population of cells, and subsequently gated on expression of CD11b and co-receptors F4/80, Ly6C and Gr1 (Figure 5.26). When isolates from mice receiving 14 days of vehicle or PXS5338K were analysed, two distinct Ly6C populations could be identified; $Ly6C^{hi}$ and $Ly6C^{int}$, and these were analysed in addition to the total Ly6C+ population. Cell populations for the two groups of mice receiving vehicle or PXS5338K for 7 days were compared, as were the two groups receiving 14 days of vehicle or compound using the MW test, and no differences were found between the groups.

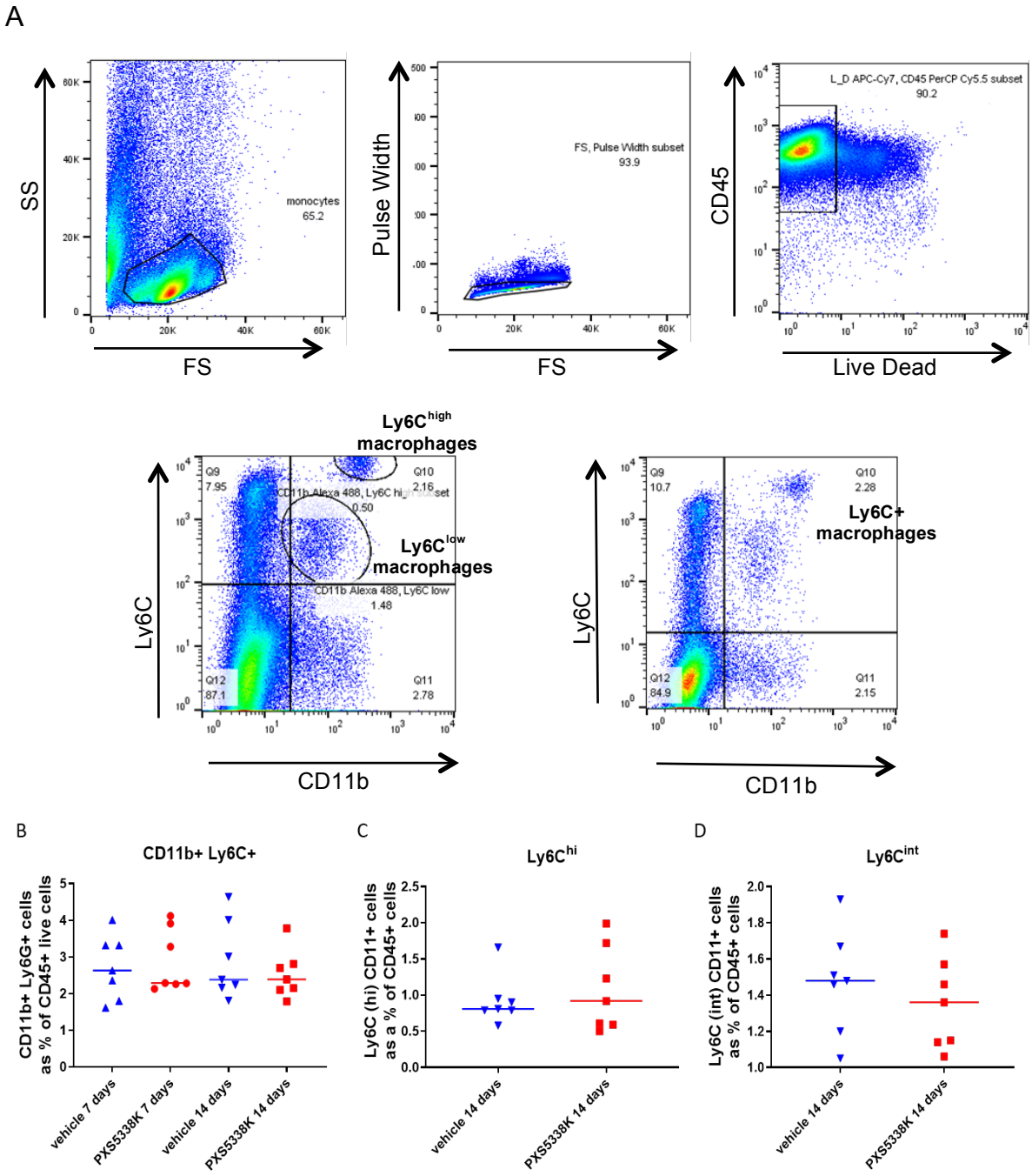


Figure 5.26 Comparison of myeloid cell isolates from liver showed no differences in immune cell populations between mice receiving vehicle or PXS5338K by oral gavage. The gating strategy used to identify tissue-infiltrating myeloid populations is illustrated in (A): forward and side light scatter (FS and SS, respectively), and absence of dead cell staining defined live singlet myeloid cells. This population was further subdivided to identify CD11b+ Ly6C+ cells, and for the mice receiving 14 days of treatment, Ly6C^{hi} and Ly6C^{int} populations. The median % of cells for the two groups of mice receiving vehicle or PXS5338K for 7 days were compared, as were the two groups receiving 14 days of vehicle or compound (MW test); no differences were found between the groups (Ly6C+ population at 7 days 2.6 % vs 2.3 %, p = 0.973 for vehicle vs PXS5338K respectively, and likewise for 14 days 2.38 % vs 2.39 %, p = 0.535, and for Ly6C^{hi} populations 0.81 % vs 0.92 %, p = 0.778, and Ly6C^{int} 1.48 % vs 1.36, p = 0.476).

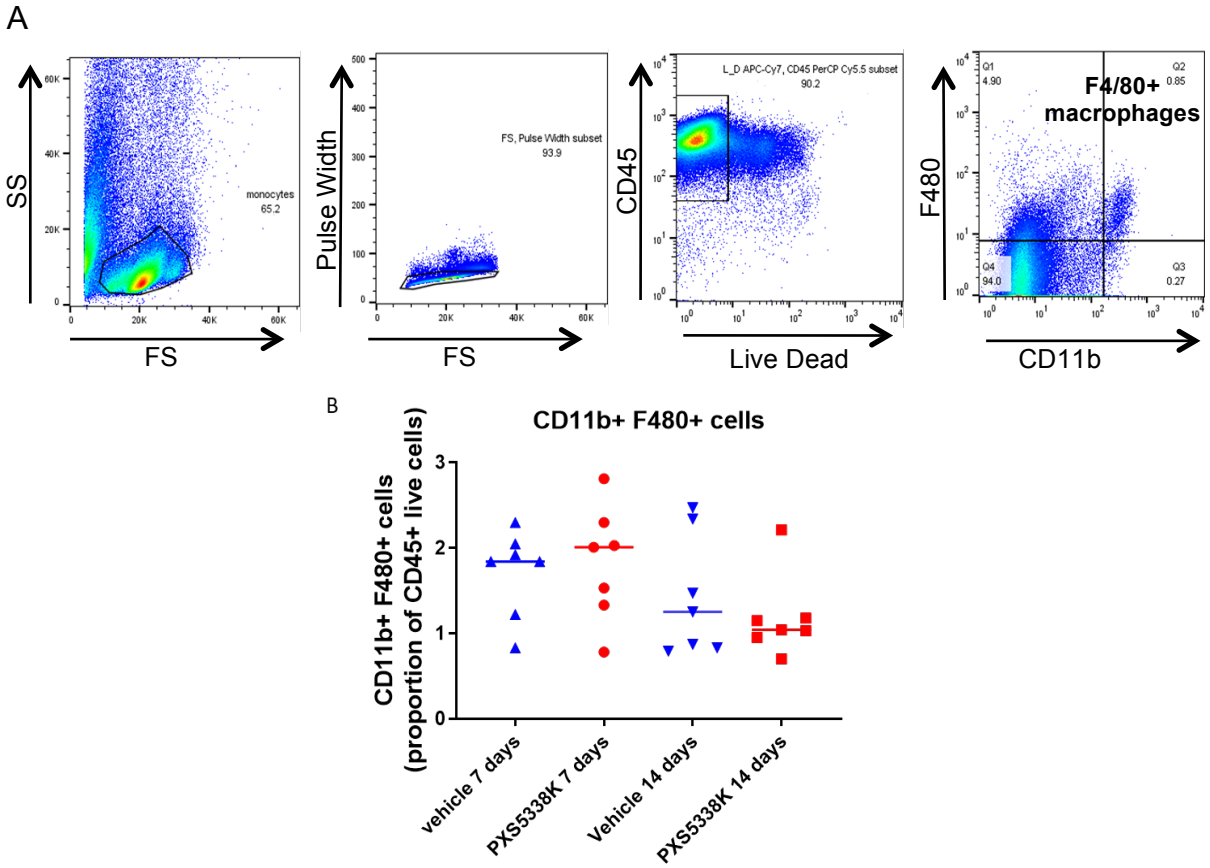


Figure 5.27 Comparison of myeloid cell isolates from liver showed no differences in immune cell populations between mice receiving vehicle vs PXS5338K by oral gavage. The gating strategy used to identify tissue-infiltrating myeloid populations is illustrated in (A): forward and side light scatter (FS and SS, respectively), and absence of dead cell staining defined live singlet myeloid cells. This population was further subdivided into CD11b+ F4/80+ cells, and the median % of cells for the two groups of mice receiving vehicle or PXS5338K for 7 days compared, as were the two groups receiving 14 days of vehicle or compound (MW test); no differences were found between the groups (F4/80+ population at 7 days, 1.8 % vs 2.0 %, p = 0.734 for vehicle vs PXS5338K respectively, and likewise for 14 days 1.3 % vs 1.0 %, p = 0.620).

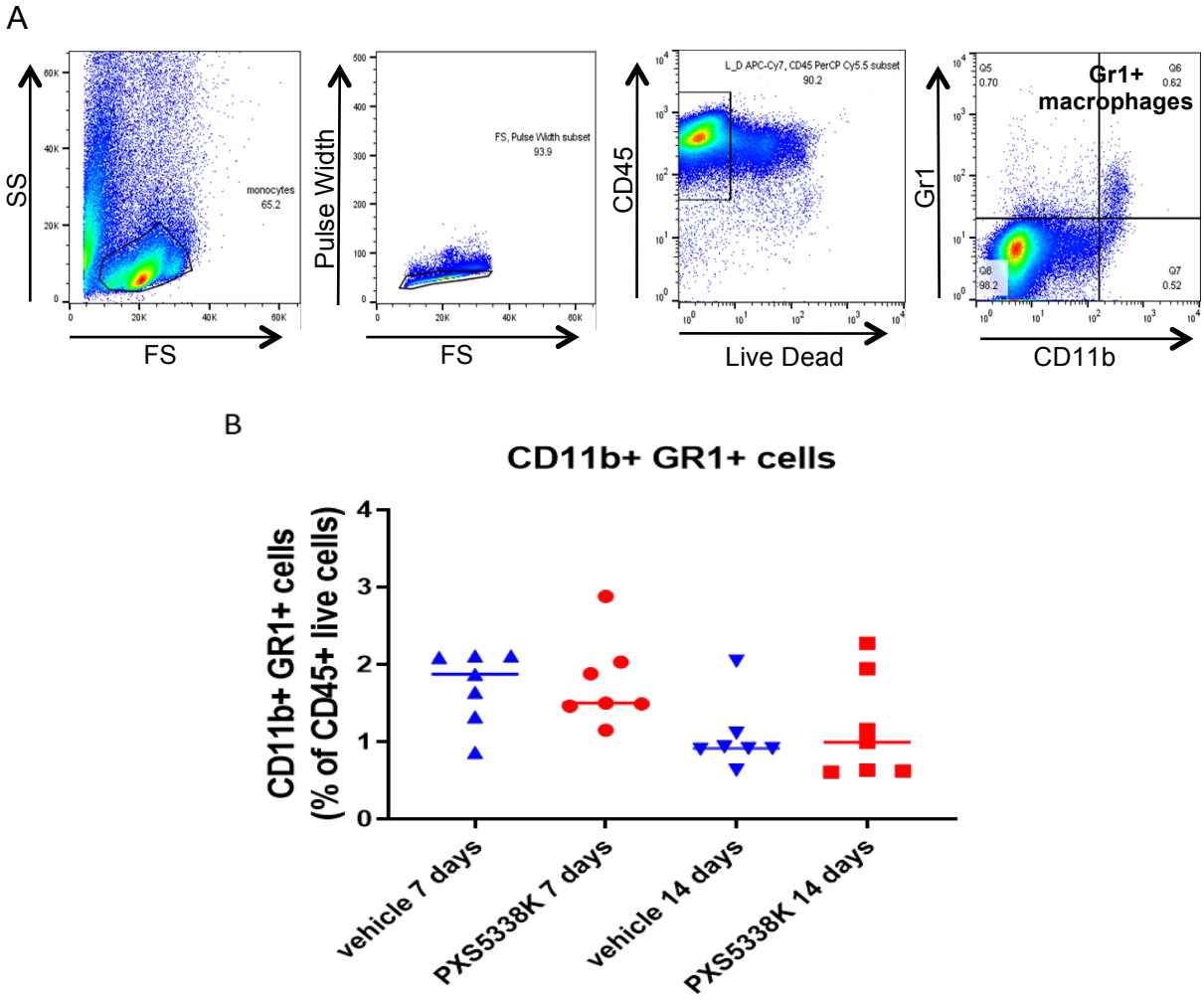


Figure 5.28 Comparison of myeloid cell isolates from liver showed no differences in immune cell populations between mice receiving vehicle or PXS5338K by oral gavage. The gating strategy used to identify tissue-infiltrating lymphocyte populations is illustrated in (A): forward and side light scatter (FS and SS, respectively), and absence of dead cell staining defined live singlet myeloid cells. This population was further subdivided to identify CD11b+ Gr1+ macrophages for the mice receiving 7 and 14 days of treatment. The median % of cells for the two groups of mice receiving vehicle or PXS5338K for 7 days were compared, as were the two groups receiving 14 days of vehicle or compound, using the MW test; no differences were found between the groups (7 days 1.8 % vs 1.5 %, p = 0.776 for vehicle vs PXS5338K respectively, and likewise for 14 days 0.9 % vs 0.9 %, p = 0.999).

5.4.4.2 Assessment of immune cell infiltration by IHC

Immune cell infiltration was also assessed by IHC. As before, the B220 isoform of CD45 was used to assess the presence of B cells, F4/80 to assess macrophage infiltration, and Ly6G to assess granulocytes and neutrophil infiltration (Figures 5.29-5.31). There was a trend for reduced Ly6G+ granulocytes in mice receiving both 7 and 14 days of PXS5338K compared to vehicle for the difference was not statistically significant (median of the mean number of cells taken from five fixed areas, for vehicle vs PXS5338K for 7 days, 5.6 vs 2.8, p = 0.168 and 5.2 vs 3.1, p = 0.168 for 14 days using the MW test). F4/80+ macrophages appeared to be increased in mice receiving PXS5338K compared with vehicle, and this was significant for 14 days treatment (median % area for 7 days of vehicle vs PXS5338K, 1.14 vs 1.92 %, p = 0.343, for 13 days 1.47 vs 2.75 %, p = 0.005). CD45 B220+ B lymphocytes were analysed by both % area positive staining, and by manual counting of cells within five fixed areas, and median numbers of cells compared. No differences were seen comparing 7 days of vehicle vs compound or 14 days of vehicle or compound (% area vehicle vs PXS5338K for 7 days 0.16 % vs 0.11 %, p = 0.509, manual counting, median mean number of cells, 5 vs 6, p = 0.113, respectively; for 14 days, vehicle vs PXS5338K, 0.21 % vs 0.20 %, p = 0.556, or counted manually, 15 .1 vs 10.6, p = 0.509).

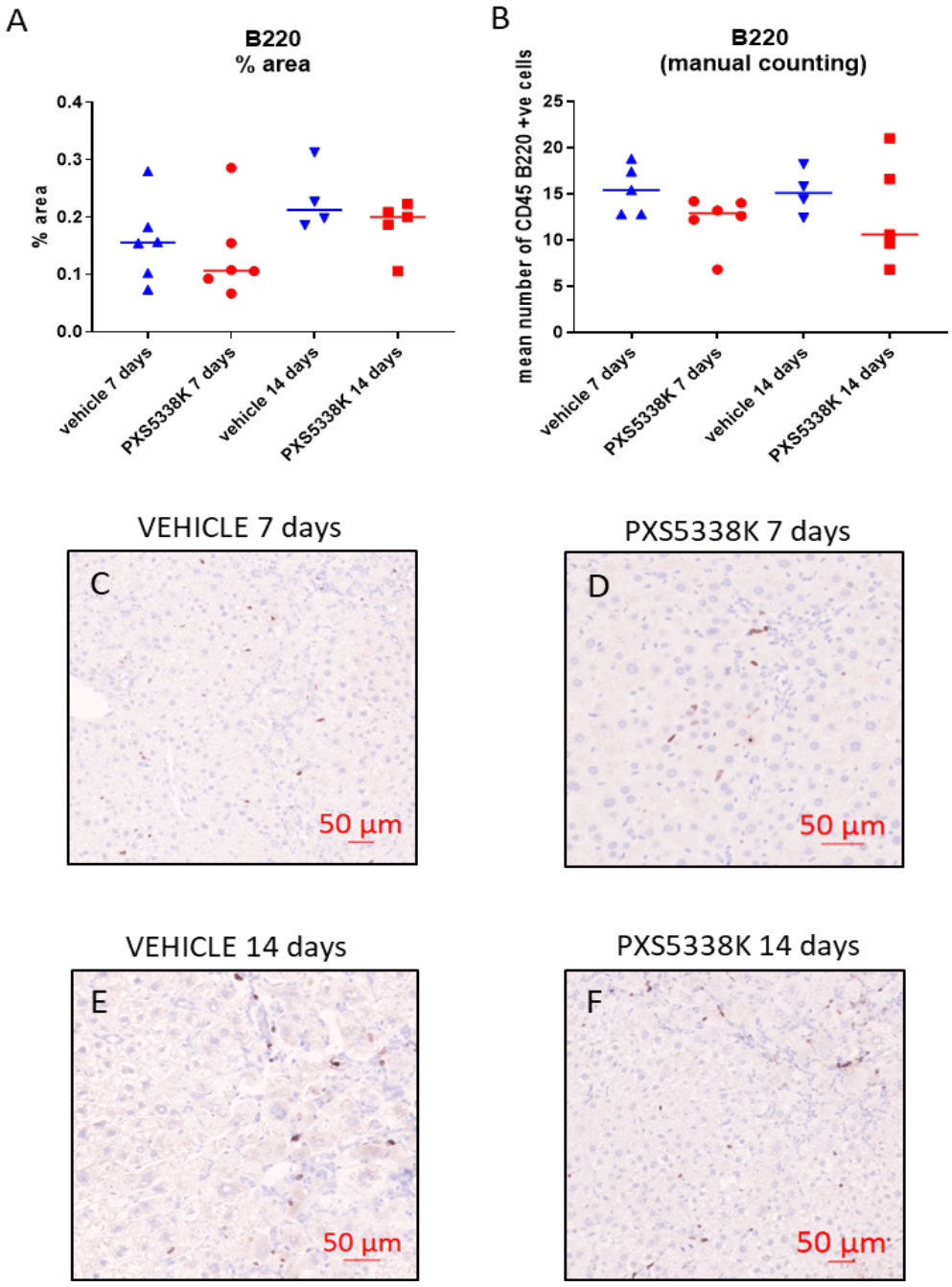


Figure 5.29 Administration of PXS5338K has no impact on B cell infiltration into the liver when delivered during fibrosis resolution. C57Bl/6 mice received 16 weeks of TAA followed by 7 or 14 days of vehicle or PXS5338K (3mg/kg) P.O. IHC on paraffin embedded liver sections with morphometric analysis to calculate % area stained as well as manual counting of cells within a fixed area showed no differences between the groups for CD45 B220+ B lymphocytes. Comparison was made between the two groups of mice receiving vehicle or PXS5338K for 7 days, then between the two groups receiving 14 days of vehicle or compound using the MW test.

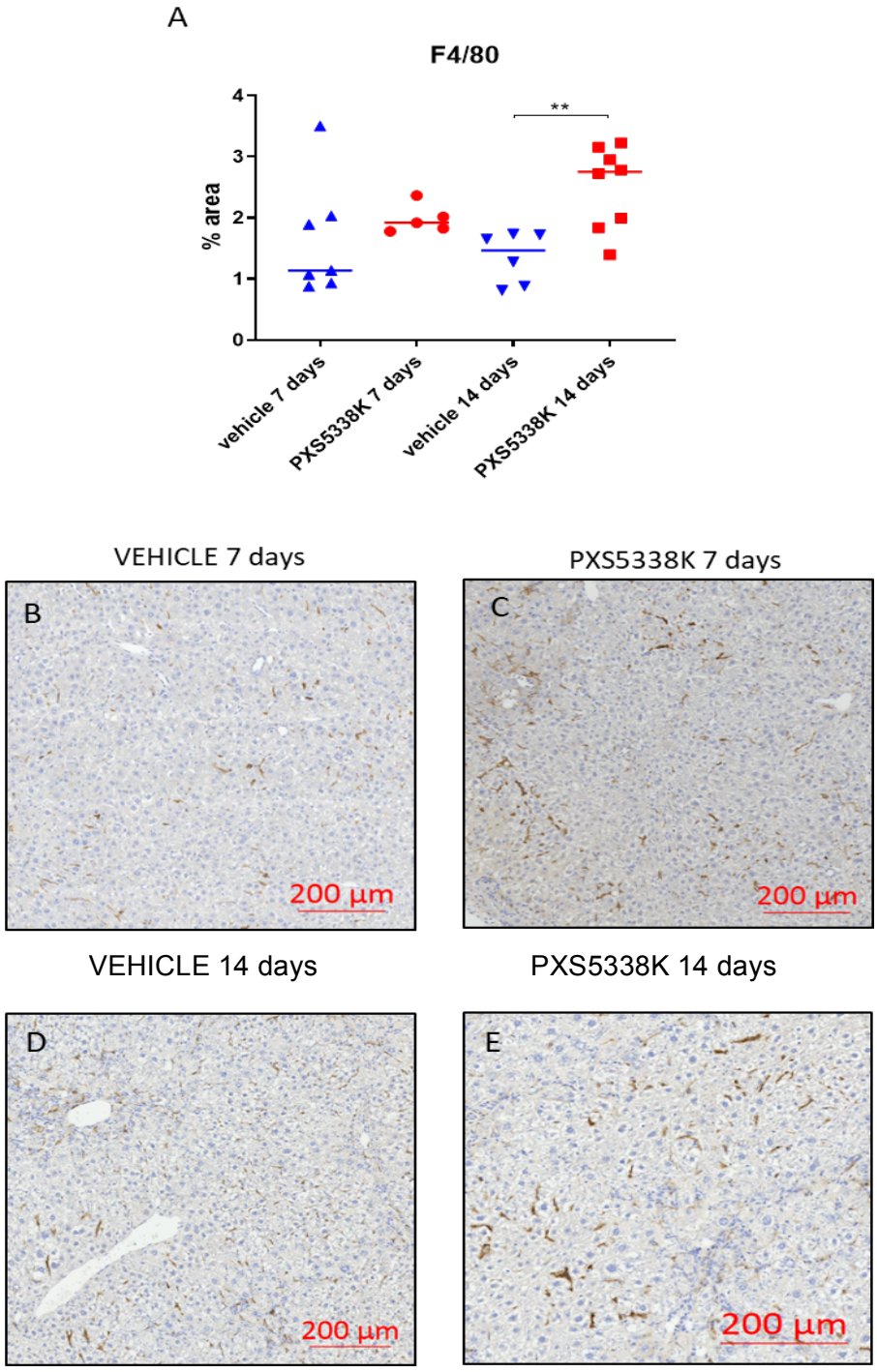


Figure 5.30 Administration of PXS5338K increases macrophage infiltration into the liver when delivered during fibrosis resolution. C57Bl/6 mice received 16 weeks of TAA followed by 7 or 14 days of vehicle or PXS5338K (3mg/kg) P.O. IHC on paraffin embedded liver sections with morphometric analysis to calculate % F4/80+ area demonstrated no differences between the groups. Comparison was made between the two groups of mice receiving vehicle or PXS5338K for 7 days, then between the two groups receiving 14 days of vehicle or compound using the MW test.

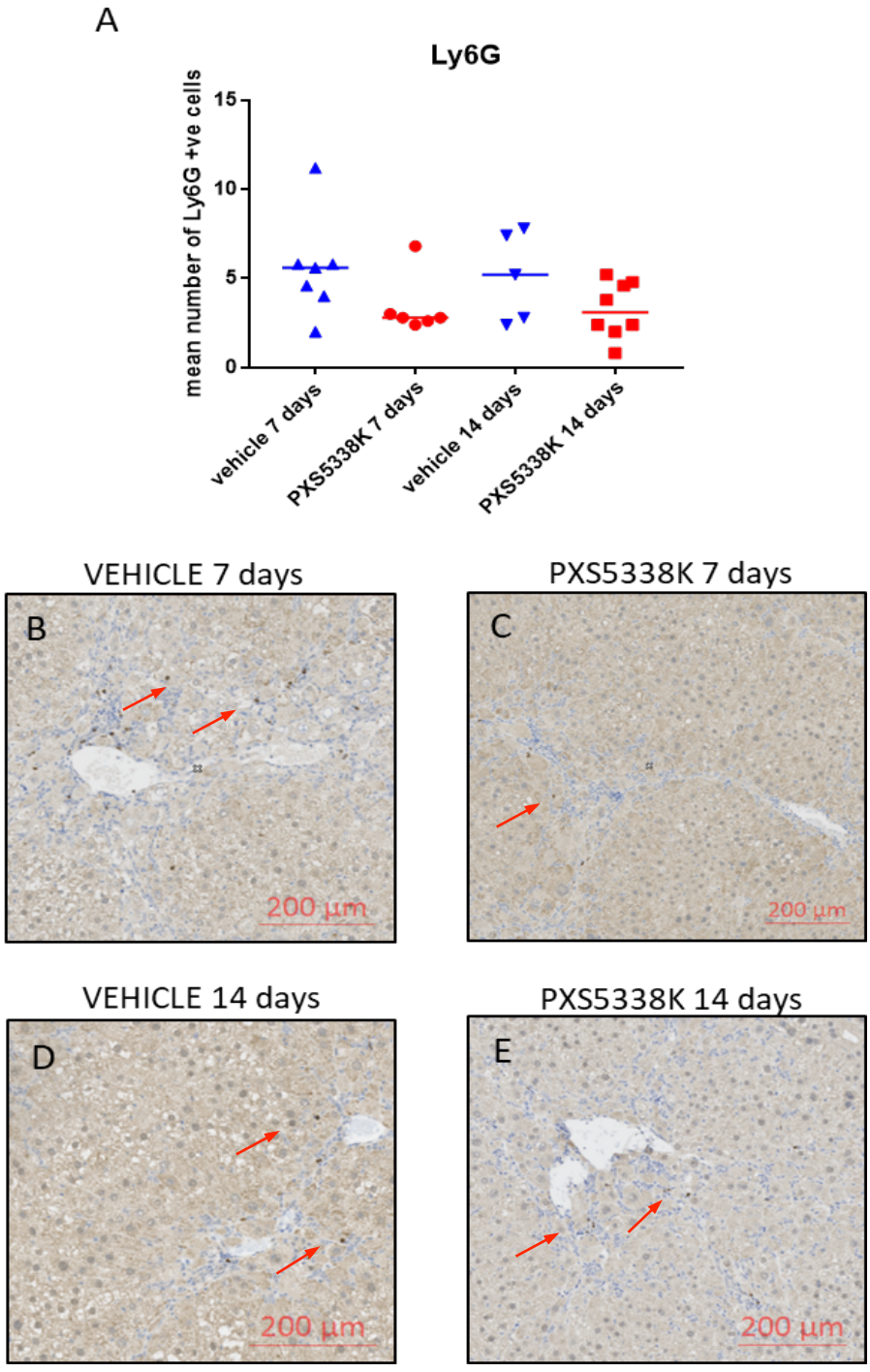


Figure 5.31 Administration of PXS5338K has no impact on granulocyte infiltration into the liver when delivered during fibrosis resolution. C57Bl/6 mice received 16 weeks of TAA followed by 7 or 14 days of vehicle or PXS5338K (3mg/kg) P.O. IHC on paraffin embedded liver sections followed by manual counting of Ly6G+ cells demonstrated no differences between the groups. Comparison was made between the two groups of mice receiving vehicle or PXS5338K for 7 days, then between the two groups receiving 14 days of vehicle or compound using the MW test.

5.5 Discussion

Sixteen weeks of TAA administered ad libitum in sweetened drinking water resulted in moderate fibrosis in C57Bl/6 mice.

There was no convincing evidence that PXS5338K was able to reduce TAA induced liver fibrosis either during liver injury or during fibrosis resolution. In the mice that received 6 weeks of compound during liver injury, a trend towards reduced AST and ALT in serum, reduced collagen I, III and PSR at IHC, and some non-significant reduction in expression of genes upregulated during fibrosis, was seen when comparing the group with mice who received vehicle. This may indicate very subtle effect on fibrosis but robust conclusions cannot be drawn. In the resolution group, there was consistent reduction in collagen I in mice receiving PXS5338K but this was not replicated in IHC for collagen III or PSR stain. Reductions in α-SMA were also seen but this appeared to be primarily in blood vessels rather than at sites where active HSCs would be seen. It is possible that within this model LOXL2 is more involved in collagen I deposition and hence lesser changes were seen for collagen III and PSR, but if this was the case, one may expect more of a reduction in collagen I in the 6 week model, and reduced collagen I mRNA expression in both.

The results for SOX-9 were conflicting. As expected, SOX-9 expression by IHC and qPCR was increased in injured livers compared with uninjured controls, suggesting increased ductular reaction in these mice in response to the injury. No change in the pattern or quantity of SOX-9 expression was observed in mice receiving PXS5338K. However, during fibrosis resolution, SOX-9 protein expression on IHC was increased

in mice receiving PXS5338K, although mRNA expression for SOX-9 did not follow the same pattern. It is possible that PXS5338K stimulates regeneration of hepatocytes via the ductular reaction, and that this process dominates during fibrosis resolution compared with liver injury; these findings do warrant further examination.

LOXL2 inhibition by PXS5338K had no effect on immune cell infiltration to the liver, either during liver injury or during fibrosis resolution. The only significant difference observed between mice receiving vehicles and PXS5338K was an increase in F4/80 positive cells on IHC in mice receiving PXS5338K for 14 days in the resolution study. A similar trend was seen in the experiment at 7 days, but not in the flow cytometry results for either experiment. These results could be interpreted in several ways; Liu et al published data to show increased F4/80+ macrophage infiltration along fibrotic septae in β-APN (pan-LOX/LOXL inhibitor) treated mice suggesting a role for LOXL2 in prevention scar degradation and ECM remodelling; this would be consistent with elevated F4/80 only in the resolution model. There was also a trend towards higher F4/80 on IHC in uninjured controls in the TAA injury experiment, however. Another explanation is that F4/80+ cells are dominant in the uninjured liver and therefore were reduced in the uninjured mice and mice 15 post TAA injury treated with PXS5338K, suggesting a role for PXS5338K in reducing liver injury. Given that these changes are inconsistent (no reduced F4/80 in PXS5338K treated mice in the first TAA injury model, and discrepancy between flow cytometry and IHC results), these results may be due to chance, or reflect fluxing macrophage populations during liver injury and resolution.

Expression of all members of the LOX family was upregulated in injured mice compared to the uninjured control animals, and this increase was more marked for LOX, LOXL1 and LOXL2. Given that the functions of these enzymes overlap, particularly those of LOX and LOXL2, it seems likely that selective inhibition of LOXL2 alone is not sufficient to reduce fibrosis. Despite some in-vitro and *in vivo* success demonstrated using a selective LOXL2 antibody (195), this was not born out in clinical studies for NAFLD, PSC or alcohol related liver cirrhosis. It was hoped that enzyme inhibition would more directly target the mechanism of action of LOXL2 in fibrosis than the antibody but these studies have not demonstrated this to be the case.

Given the success of LOXL2 in the CCl_4 model in rats, whereby PXS5153 reduced collagen content and reduced mRNA expression of profibrotic proteins (see chapter 2), a greater efficacy with PXS5338K had been expected following communication from Pharmaxis. However, later data suggested reduced oral bioavailability of PXS5338K, a smaller AUC_0-last (hr*ng/mL) and probably a shorter half-life (see 1.5.3.3.2) than PXS5153. While this may explain its' reduced efficacy, the reason for toxicity at 10 mg/kg seen at Birmingham and in another laboratory remains unclear. Higher doses of PXS5338K may more effectively inhibit the enzyme activity of LOXL2, but would not be advisable given the toxicity seen at 10 mg/kg. Increasing the frequency of dosing could be feasible, however.

More promising results were seen in the IHC for collagen I, and possibly α-SMA, in the resolution model, and so this experiment could be repeated using more frequent

dosing of PXS5338K, or indeed PXS5153, and the dosing period extended to 4 weeks, allowing more time for differences in fibrosis and extracellular remodelling to take place under the influence of enzyme inhibition.

One limitation to these studies was the inability to have measured collagen crosslinking by mass spectroscopy. This may be more pertinent with regards to fibrosis regression than % area of collagen by IHC. In fact, collagen fibrils are believed to widen, split, and become disorganised during fibrosis resolution, and therefore cover a greater % area not truly representative of the underlying physiology. Allowing a longer period in resolution (presuming LOXL2 inhibition may promote this process) may demonstrate an impact of the compound on fibrinolysis.

Another limitation was that I was unable to assess whether the enzyme inhibitor was effectively working. There were no facilities for this at Birmingam and Pharmaxis were only able to process serum samples collected within an hour of dosing (due to the short-half of the compound). Unfortunately the animal licence these experiments were carried out under did not allow for this type of experiment. It would also have been useful to check for the presence of LOXL2 and LOXL2 inhibition within the liver tissue, but again this was not feasible.

PXS5338K, and probably LOXL2, appears to have no role in immune cell recruitment during liver injury or during fibrosis resolution, but for completeness, given the changes seen with F4/80+ cells, this could be repeated comparing a greater number

of mice exposed to LOXL2 inhibition for a longer period of injury resolution, to see if a similar pattern is observed.

6. Results 4: *In vitro* effects of LOXL2 inhibition by PXS5338K in fibroblasts

6.1 Introduction

Hepatic fibrosis is a reversible wound healing response characterized by accumulation of extracellular matrix (ECM), or "scar tissue." Activation of hepatic stellate cells is the central event in hepatic fibrosis and aHSCs are considered to be the primary effector cells during fibrogenesis. Following liver injury, hepatic stellate cells receive signals secreted by damaged hepatocytes and immune cells, causing them to transdifferentiate into activated myofibroblast-like cells. As the primary ECM–producing cells in liver, activated stellate cells generate a temporary scar at the site of injury to protect the liver from further damage (277).

For this reason*, in vitro* experiments were performed to investigate whether LOXL2 inhibition with PXS5338K has any direct effect on the phenotype and function of fibroblast populations. Primary human fibroblasts from liver tissue, LX2 cells (a human hepatic stellate cell line (278), and murine 3T3 cells (control murine fibroblast cell line) were used to perform scratch wound assays, contraction assays, and to assess collagen cross-links in ECM produced by cells, with the aim to assess the potential effect of PXS5338K on fibroblast activity. LX2 and 3T3 cells were chosen as cells that were more easily accessible in the lab, particularly in the early phases of optimising experimental techniques. Given that PXS5338K had been tested in mice *in vivo*, I wanted to perform some of the *in vitro* experiments in a murine cell line, in case differences in efficacy of the compound were seen between species. For the same reason, I wanted to test the compound in a human cell line *in vitro,* given that

the compound was being developed as potential pharmacotherapy in humans, potentially highlighting any differences that may later be important. Despite several attempts, I was unable to isolate primary murine fibroblasts (which would have provided a ready supply of cells on which to optimise experiments). However, it seemed prudent to instead use primary human fibroblasts, which would again test the efficacy of the compound on human cells, but also assess the reproducibility of experimental results. These cells were less readily available, so used once experiments had been optimised.

A previously used compound PXS5153 had demonstrated reduced mature and immature collagen crosslinks in the presence of recombinant LOXL2 during *in vitro* study (231). PXS5338K has similar IC_{50} properties to PXS5153, (0.03 μM for recombinant human LOXL2 and 0.04 μM for recombinant mouse LOXL2) and so similar concentrations were used in the *in vitro* studies.

3T3 cells were originally obtained from desegregated NIH Swiss mouse embryo fibroblasts by the scientists George Todaro and Howard Green. The immortal cell line begins to thrive and stabilize in cell culture after about 20-30 generations of *in vitro* growth, following “3-day transfer, inoculum 3 x 10^5 cells” (3T3). The cell line has become a standard fibroblast cell line, are relatively easy to grow, and have an adherent, fibroblastic morphology (279, 280). The LX2 human hepatic stellate cell has been extensively characterized and retains key features of hepatic stellate cells, including cytokine signalling, neuronal gene expression, retinoid metabolism, and fibrogenesis , making them a suitable model of human hepatic fibrosis (278).

Many attempts were made to isolate murine liver fibroblasts but were largely unsuccessful (see below). For this reason, isolated primary human fibroblasts were used for *in vitro* assays where available. Some may argue that primary cells respond to stress in a more physiological manner, however, due to donor variability, their behaviour may be inconsistent between samples, a characteristic seen less frequently in cell lines (281).

6.2 Attempted isolation of murine liver fibroblasts: a mixed cell population

As described above I had limited success in isolating hepatic stellate cells from murine livers following *in situ* digestion. Cells isolated from murine livers were incubated in appropriate media to permit growth and proliferation and then stained using a variety of markers to permit identification of the populations that were isolated (Figure 6.1). I commonly found populations of cells that stained positively for Epcam and pan cytokeratin, suggesting that the population of cells may be epithelial in origin and may contain hepatocytes. A small number of CD31 positive cells were also seen, suggesting an endothelial origin, as well as F4/80 positive cells suggestive of macrophages. Sparse populations of cells positive for collagen I and α-SMA were seen day 3 following isolation, but these was not present on the cell populations stained on day 5. It seems likely that a mixed population of cells was obtained on each occasion, with more dominant populations of cells surviving and proliferating over time (see Figure 6.1). For this reason, human liver fibroblasts were used that have been previously phenotyped and are routinely used in Birmingham Liver Laboratories (282, 283). Given that the compound is being tested as a potential

therapy for fibrosis in humans, testing it on a human fibroblast cell line over murine cells was preferable.

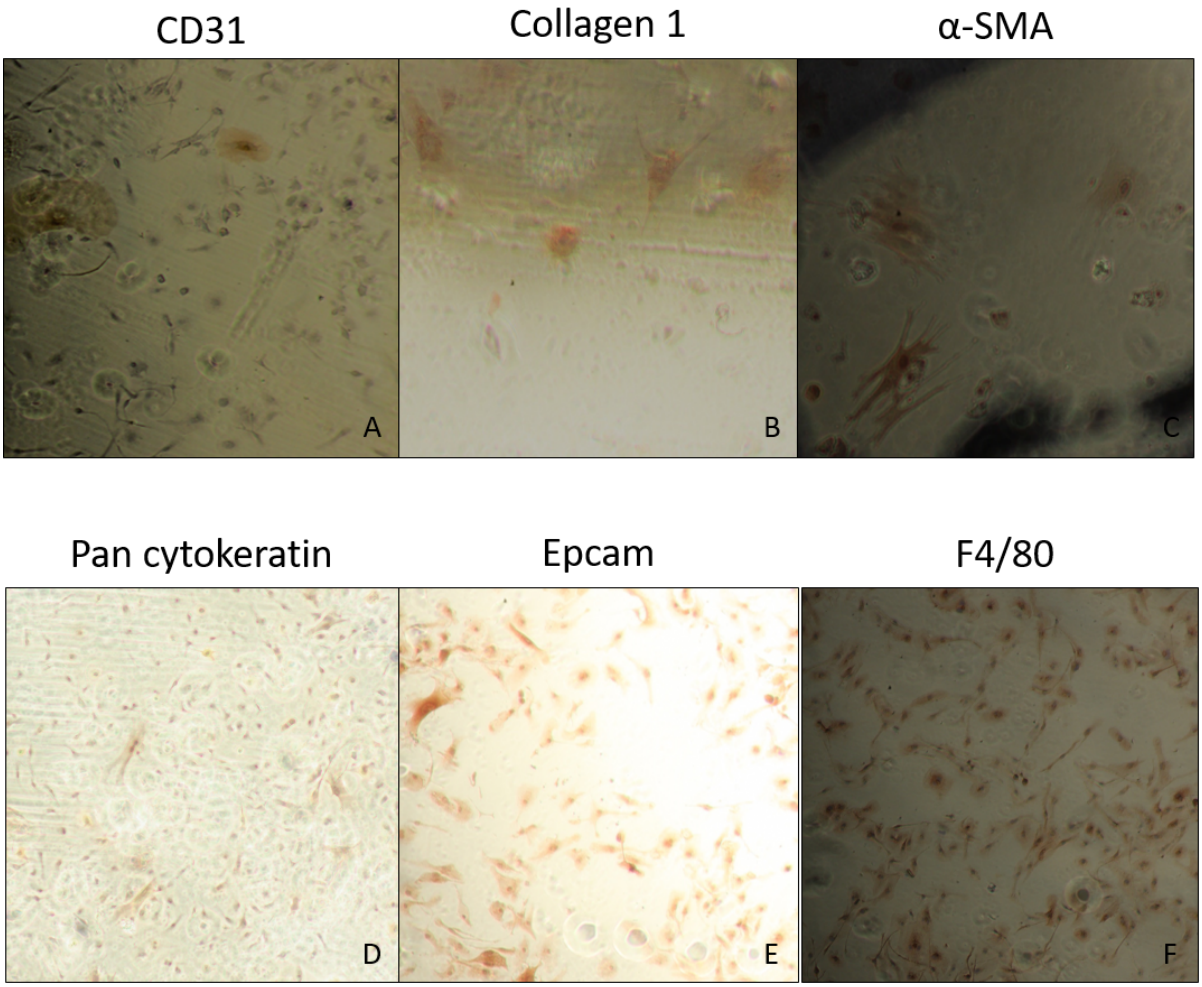


Figure 6.1 Cells isolated from murine livers using a protocol for hepatic stellate cells were a mixed population. Cells were isolated from mouse liver and incubated at 37°C in appropriate culture media. Immunocytochemistry was performed at day 3 and day 5 and images acquired. Although day on day 3 some cells stained positive for HSC markers α-SMA and collagen I (B+C), occasional cells were positive for the endothelial cell marker CD31 (A), and by day 5, markers for endothelial cells (D,E) and macrophages dominated (F).

6.3 The use of scratch wound assays to assess the impact of LOXL2 inhibition on fibroblast activity in the wound healing response.

The wound healing response is an important property of fibroblasts, and mimics the HSC response to liver injury. For this reason, the scratch wound or wound healing assay has previously been used to assess fibroblast activity across a multitude of environments. In this assay, fibroblasts become activated on the plate surface and their behaviour mimics that of a fibrotic environment. A “scratch,” created between confluent cells, permits assessment of wound closure, or wound healing, as well as cell migration and proliferation. The human hepatic stellate cell line LX2 cells were used to assess the effect of PXS5338K on the wound healing response in a scratch wound assay.

LX2 cells were seeded on 24-well plate at a concentration of 100, 000 cells per well, as outlined in detail in 2.4.3. Once the cells were confluent, scratches were applied to the well surface to generate a consistent cell-free area, and culture media added containing increasing doses of PXS5338K, or the growth factor PDGF-BB, was added to each well in triplicates.

Wound width was similar across all samples at time zero ($p = 0.862$, comparing median width at time 0 using the KW test). All wounds closed completely within 24 hours. Mean percentage (%) wound closure across triplicates was calculated at 12 and 18 hours and mean ranks for each condition were compared, then each condition compared against media alone (as a control) using the KW test with post hoc Bonferroni-Dunn correction. No differences were seen between groups, as

demonstrated in Figure 6.2. The original scratch wound area was approximately the same for all conditions except for 1000 nM PXS5338K, but this did not affect overall wound closure time.

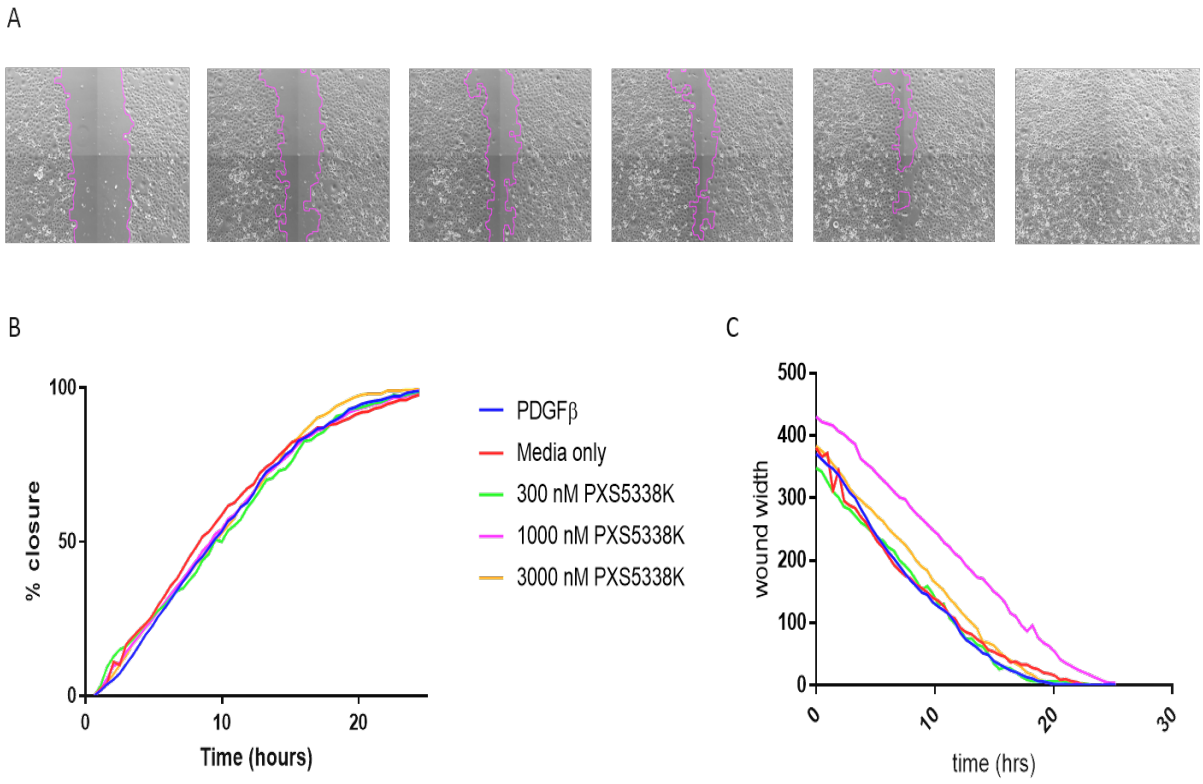


Figure 6.2 Administration of PXS5338K did not affect wound closure time in a scratch wound assay. A scratch wound was created in confluent LX2 cells and incubated at 37°C for 24 hours with media containing increasing concentrations of PXS5338K, or PDGF-BB. All wounds closed after 24 hours (A). Mean % closure across triplicates for each condition was calculated at 12 and 18 hours. No differences were seen in the rate of closure at 12 or 18 hours (mean ranks were 50.5, 66.7, 53.1, 52.7, 51.9, p = 0.976 for PDGF-BB, media alone, 300, 1000, 3000 nM, respectively at 12 hours, and likewise 50.6, 56.1, 52.9, 53.1, 52.4, p = 0.986 at 18 hours where each condition was compared against media control.).KW test was applied with post hoc correction via the Bonferroni–Dunn method.

6.4 The effect of PXS5338K on collagen cross-linking by fibroblasts *in vitro*.

To assess whether PXS5338K is able to inhibit collagen cross linking *in vitro*, LX2 cells, 3T3 cells and primary human fibroblasts were cultured in triplicates with culture media alone or containing increasing doses of PXS5338K, for one, two, or three weeks. The cells and ECM were removed and frozen at -80°C and later dry frozen as

described in 2.4.1.3. Analysis of cross-links was carried out at the Pharmaxis laboratories, but essentially mass spectrometry permitted quantitation of the immature crosslinks dihydroxylysionorleucine (DHLNL) and the trivalent mature crosslinks pyridinoline (PYD) and deoxypyridinoline (DPD) in the prepared samples. Unfortunately, quantitation of hydroxylysinonorleucine (HLNL) was not possible due low sample levels, precluding calculation of the collagen maturity ratio. The levels of Hydroxyproline were also below Limit of Quantification (<2190 pmol/mL).

The levels for all the markers were very low in the samples and hence not all concentrations could be generated for some conditions. Only those concentrations that could be more accurately generated are shown in Figure 6.3. No differences in the concentrations of immature collagen crosslinks DHLNL, or mature crosslinks PYD or DPD, were seen between samples for LX2 cells, 3T3 cells, or human fibroblasts when cultured in appropriate media for one, two or three weeks compared with any dose of PXS5338K. Mean concentrations of each type of crosslink were compared with media alone using the KW test with post-hoc Bonferroni-Dunn correction.

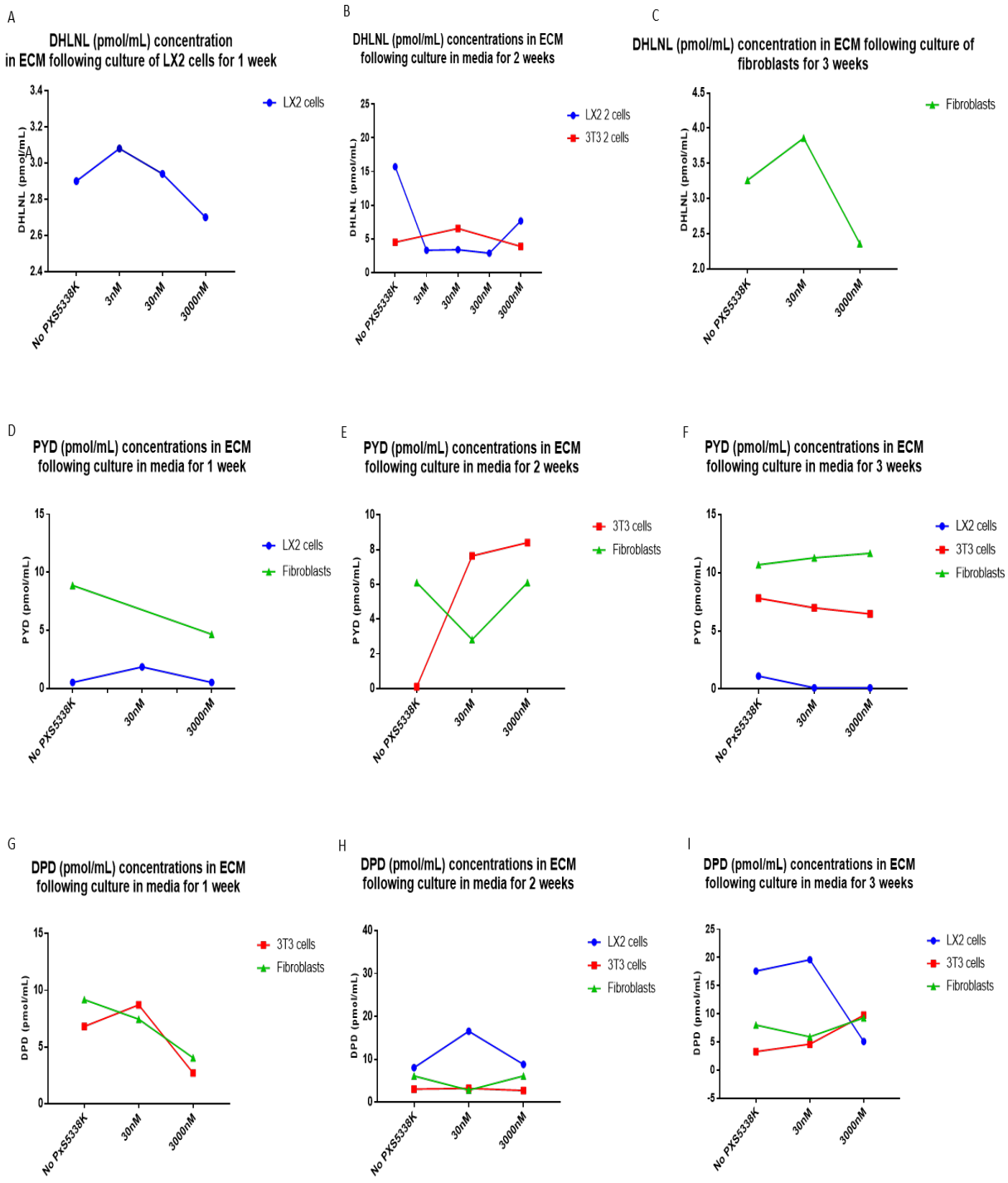


Figure 6.3 PXS5338K does not alter collagen crosslinking in vitro as measured by mass spectroscopy. LX2 cells, 3T3 cells and primary human fibroblasts were cultured in triplicates with culture media alone or containing increasing doses of PXS5338K, for one, two, or three weeks. Mass spectroscopy was used to measure collagen crosslinks in the samples. No pattern for altered concentrations of immature collagen crosslinks DHLNL or mature crosslinks PYD or DPD were observed related to PXS5338K concentration, and no differences were found comparing the concentration of each type of collagen crosslink with no PXS5338K control for 1, 2 or 3 weeks, respectively, where results were available, using the KW test and Bonferroni post-hoc correction.

6.5 The effect of PXS5338K on fibroblast activity and collagen contraction within a gel *in vitro*

The collagen contraction assay is also used to assess the fibroblast activity in the wound healing response, and so I wished to observe the effect of PXS5338K on cell-ECM interactions and the ability of fibroblasts to reorganize and contract collagen matrices *in vitro*. In addition, the LOXL2 antibody has been demonstrated to inhibit collagen gel contraction containing rat HSC-X and primary murine HSCs, and so I hoped to demonstrate PXS5338K to be as effective in this regard (195).

Isolated human fibroblasts, LX2 cells and 3T3 cells were added to collagen forming a collagen plug which was mechanically released from the well. Culture media was added, either alone, or containing increasing doses of PXS5338K, positive controls endothelin-1 or TGF-β, or the negative control 2,3, butanedione monoxime (BDM), in triplicates.

6.5.1 The effect of PXS5338K on LX2 cells within a collagen contraction assay

Several contraction assays were completed with LX2 cells but no gel contraction was visualised after 5 days, even in the presence of endothelin and TGF-β, see Figure 6.4.

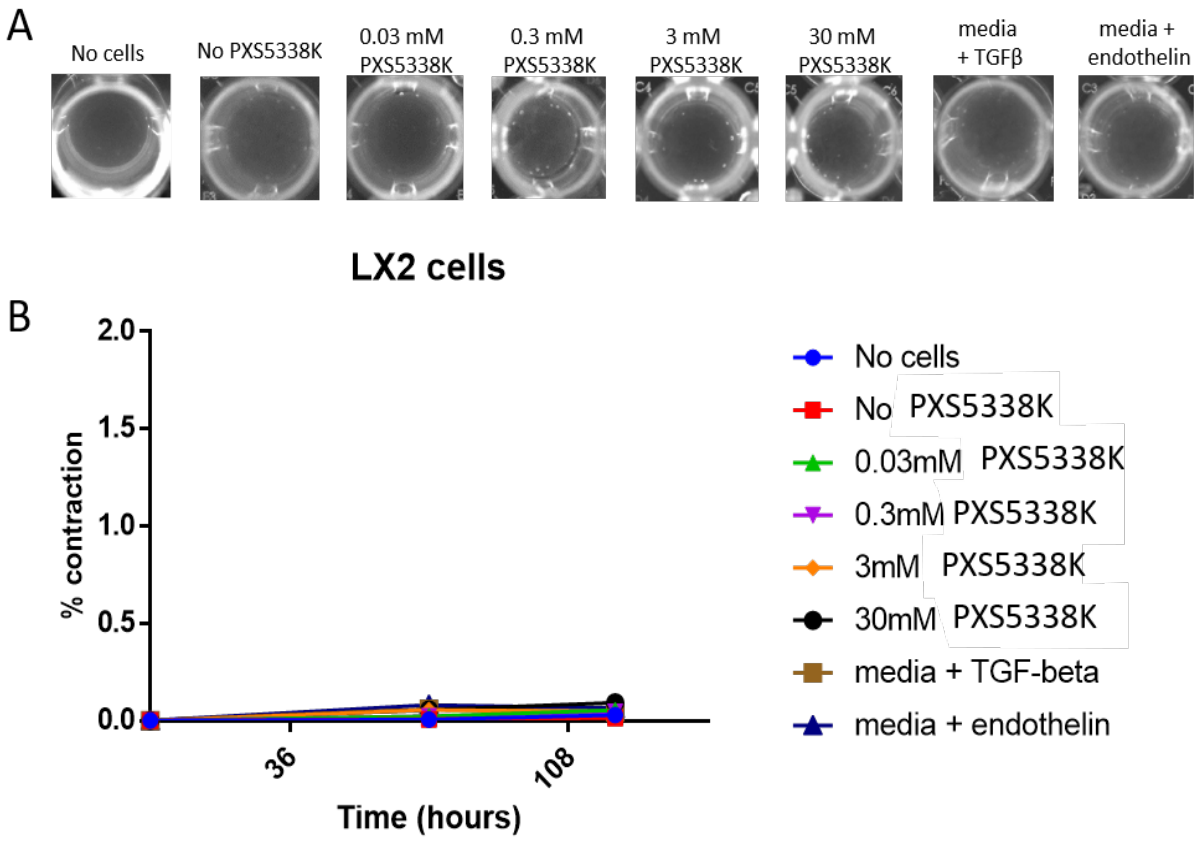


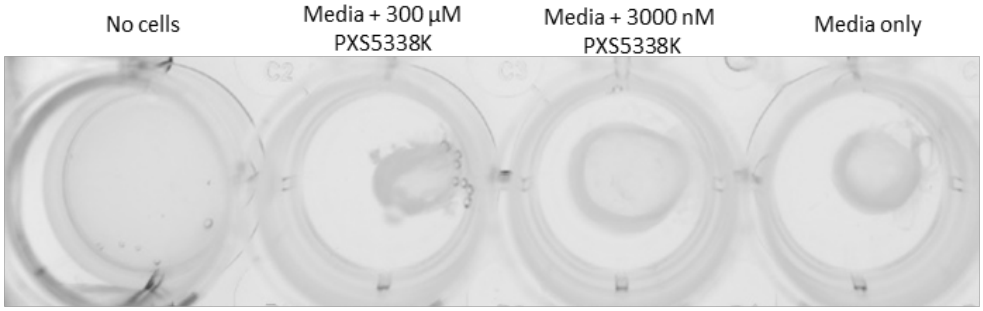
Figure 6.4 Collagen plugs containing LX2 cells, dosed with PXS5338K, TGF-β or endothelin in culture media did not contract. LX2 cells were added to collagen to form a collagen plug which was released from the well. Culture media was added, either alone or containing increasing doses of PXS5338K, positive controls endothelin-1 or TGF-β, and left to incubate at 37°C for 5 days. None of the collagen plugs contracted, and so statistical analysis was not performed.

6.5.2 The effect of PXS5338K on 3T3 cells within a collagen contraction assay

The same protocol was followed using 3T3 fibroblasts except that two different concentrations of 3T3 fibroblasts were used and the collagen gels were incubated for seven days with either media or 3000nM or 300μM PXS5338K (a dose at which one

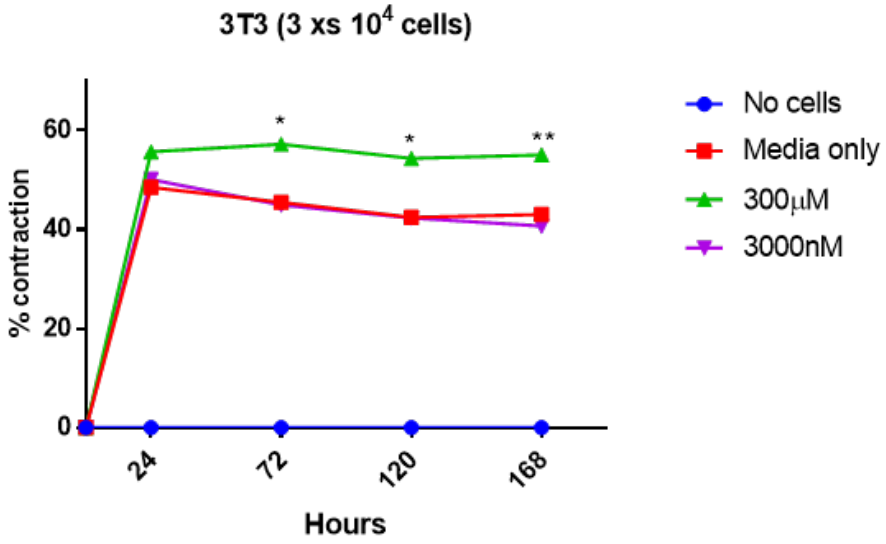
may expect to see inhibition of other members of the lysyl oxidase family of proteins). Contraction of gels was observed where cells were seeded at 3 x 10^4 or 5 x 10^4 cells per well in a 24 and 48 well plate and the extent of collagen contraction was observed. Gels containing media with 300μM PXS5338K were significantly more contracted at 72 hours ($p = 0.014$) and this became more apparent by 120 hours (day 5) ($p = 0.003$) and persisted to day 7 ($p = 0.002$). A similar pattern was seen in the gels containing 3T3 cells in a 48 well plate. Gel contraction was greater in gels containing both 300 μM and 3000 nM PXS5338K compared to media alone by 24 hours (media alone vs 3000nM, $p = 0.007$ and media vs 300 μM, $p < 0.0001$), with two way ANOVA and Bonferroni correction. A significant difference at day 7 was only observed for those cells treated with 300 μM compound. Oddly, gel contraction appeared to be promoted by the higher concentration of PXS5338K, 300 μM PXS5338K (and even 3000 nM initially), but at the end of the experiment, contraction appeared inhibited in gels containing the lower concentration of PXS5338K, 3000 nM, although difference in gel size was not statistically significant (see figure 6.5). The gels containing no cells were not analysed but are demonstrated as a negative control.

A

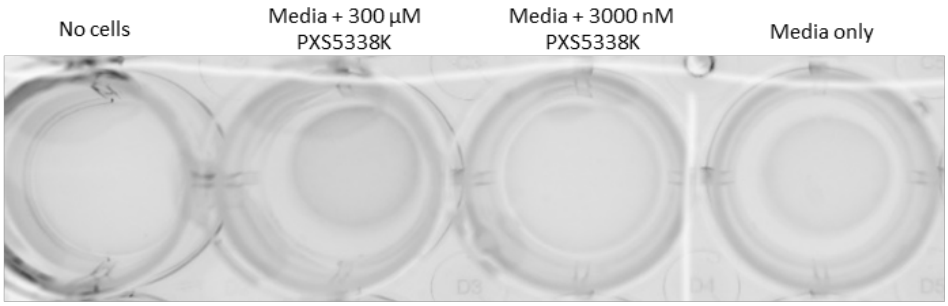


3T3 cells 24 well plate

B



C



3T3 cells 48 well plate

D

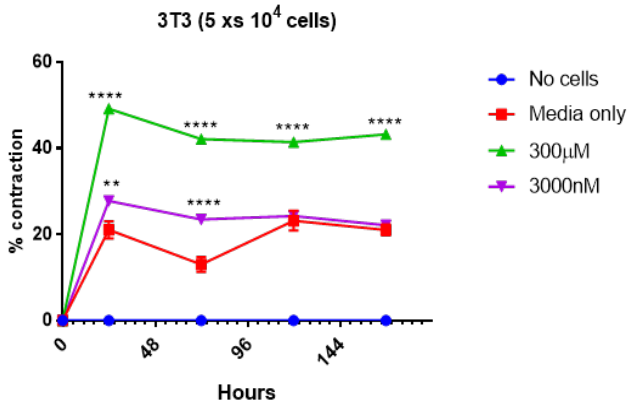


Figure 6.5 PXS5338K did not inhibit contraction in 3T3 populated collagen gels. 3T3 cells were added to collagen to form a collagen plug which was released from the well. Culture media was added, either alone, or containing increasing doses of PXS5338K, in triplicates, and left to incubate at 37°C for up to 7 days, with daily measurement of gel size using an image analyser. Collagen gels containing media with 300 µM PXS5338K were significantly more contracted at 72 hours than those containing 3000 nM PXS5338K or media alone ($p = 0.014$), and this became more apparent by 120 hours (day 5) ($p = 0.003$), persisting to day 7 ($p = 0.002$). In the 48 well plate, % collagen contraction was higher in gels containing media with 300 µM and 3000 nM PXS5338K compared to media alone by 24 hours (media alone vs 3000nM, $p = 0.007$ and media vs 300 µM, $p < 0.0001$). The difference between gel size remained significant only for gels containing the higher concentration of PXS533K (300 µM) at day 7 (C, D). *$p < 0.05$, **$p < 0.01$, ***$p < 0.001$ and ****$p < 000.1$ using 2 way ANOVA with Bonferroni correction (C,E,H) and the KW test with post-hoc correction (F).

6.5.3 The effect of PXS5338K on human fibroblasts within a collagen contraction assay

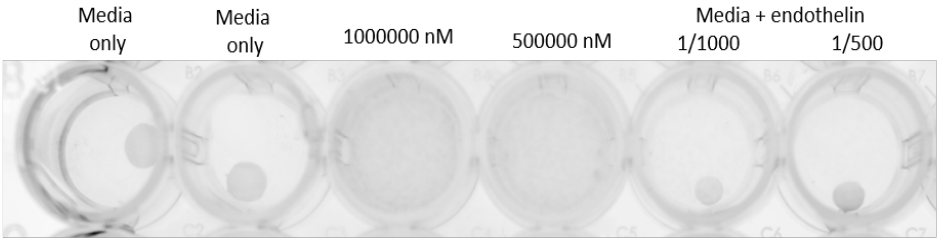
The same protocol was carried out with human liver fibroblasts. Due to scarcity of cells, a pilot study was carried out in singlets. While data regarding the concentration of PXS5338K to use in these studies was not clear, a high dose of PXS5338K was trialed. Contraction of gels was observed within 24 hours for all conditions except where high concentrations of PXS5338K where contraction of collagen gel was inhibited by PXS5338K (Figure 6.6, A).

To confirm these results, the experiment was repeated with fibroblasts in triplicates but with the concentration of PXS5338K recommended by Pharmaxis for *in vitro* experiments (30 – 3000 nM). At these concentrations, the gels in media containing compound were seen to contract equally to those in media alone, although 2,3-butanedione monoxime (BDM) demonstrated an expected inhibitory effect. This experiment was repeated several times (not all data shown) and variations included using different concentrations of cells; different sized wells, and releasing the gel at time zero (once set) and later at 24 hours (see Figure 6.6, B and C.).

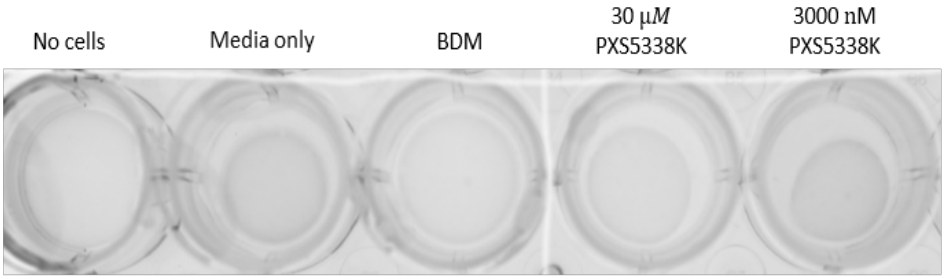
The possibility that the very high concentrations of PXS5338K previously used in the pilot experiment had resulted in death of fibroblasts, thereby preventing gel contraction, was considered. To investigate this theory, the experiment was repeated to form collagen gels and left in media using the same concentrations of PXS5338K (1000000 and 500000 nM) for 3 days. At day 3, collagenase was used to dissolve the gel and extract fibroblasts, and trypan blue used to assess cell viability. The only

observation was that the percentage of viable cells in the gels treated with 1000000 nM PXS5338K was higher than in the other samples (mean ranks 6.0, 10.5, 4.0, 13.5 for media alone, BDM, 500000 nM and 1000000 nM, respectively, $p = 0.028$ with KW test and Bonferroni post hoc correction). Data are shown in Figure 6.6, D. For this reason, the experiment was repeated in triplicates, and the concentration of PXS5338K titrated up to 1000000 nM. Contraction of the collagen gel appeared to be inhibited by PXS5338K in a dose dependant manner; the differences between the groups only became significant at higher concentrations of compound, as shown in Figure 6.6, E (mean % concentrations compared for each time point with two-way ANOVA and Tukey's multiple comparison test).

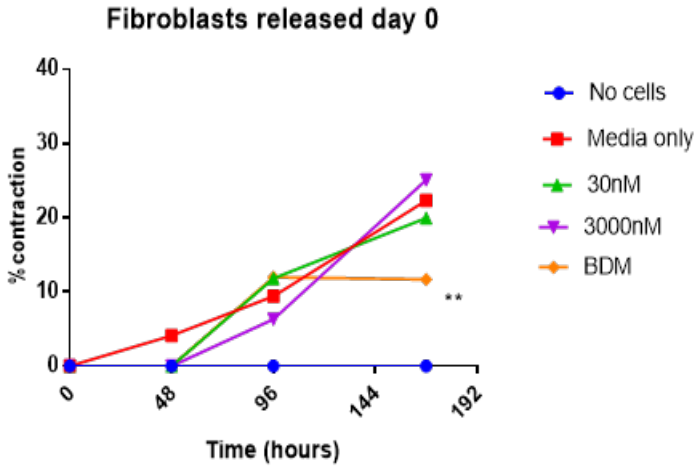
A


Media only
Media only
1000000 nM
500000 nM
Media + endothelin 1/1000
1/500

B


No cells
Media only
BDM
30 μM PXS5338K
3000 nM PXS5338K

C


Fibroblasts released day 0
% contraction
Time (hours)
0
10
20
30
40
0
48
96
144
192
**
No cells
Media only
30nM
3000nM
BDM

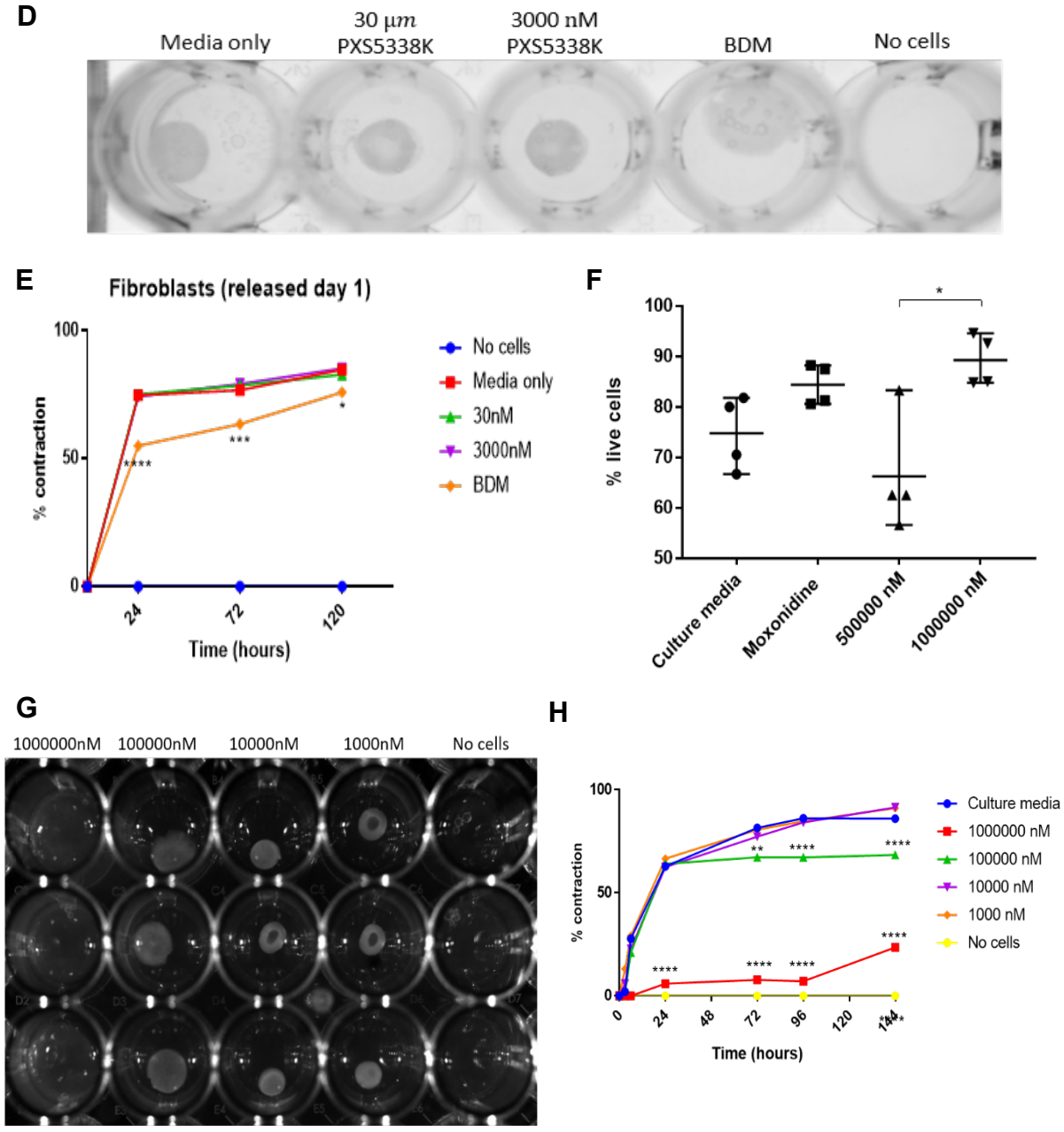


Figure 6.6 High doses of PXS5338K inhibited contraction in fibroblast populated collagen gels. Fibroblasts were added to collagen to form a collagen plug which was released from the well (A-C), except in (D, E) where it was released after 24 hours. Culture media was added, either alone, or containing increasing doses of PXS5338K, in triplicates, and left to incubate at 37°C for up to 7 days, with daily measurement of gel size using an image analyser. Inhibition of contraction was observed using high doses of PXS5338K, and enhanced collagen contraction with endothelin-1. Several repeat experiments with lower doses of PXS5338K demonstrated no change in contraction, but inhibited contraction with BDM. Fibroblasts were extracted from collagen gels and tested for viability at the end of a three day treatment period and demonstrated similar viability of cells treated with high concentrations of PXS5338K (F). The experiment was repeated and at incremental PXS5338K to high dose, and demonstrated inhibition of contraction at higher doses compared to media alone (G, H). *p < 0.05, **p < 0.01, ***p <0.001 and ****p < 000.1 using 2 way ANOVA with Bonferroni correction (C,E,H) and the KW test with post-hoc correction (F).

6.6 Discussion

PXS5338K had no impact on wound healing by scratch wound or contraction assay, or production of immature or mature collagen crosslinks DHLNL, PYD or DPD, at previously tested concentrations for *in vitro* work. Cell migration and proliferation were also unaffected as demonstrated in the scratch wound assay. Interestingly, contraction was inhibited in fibroblast containing gels in media containing high concentration PXS5338K. It is possible that at these concentrations, other members of the lysyl oxidase family are inhibited. The IC_{50} for recombinant human LOXL1 is 2.53 μM, 0.38 μM for LOXL3 and 0.11 μM for LOXL4; unfortunately only bovine data was available for LOX, at 1.6 μM (231). Inhibition of these other enzymes, particularly LOX, may have an effect on HSC activity within the collagen matrix and gel contraction. Given that a LOXL2 antibody has previously demonstrated effective inhibition of gel contraction (195), it is surprising that enzyme inhibition has been less so. It is possible that contraction of HSCs was mediated via a different mechanism than LOXL2 enzyme activity.

Alternatively, it is possible that expression of LOXL2 was too low for enzyme inhibition to be effective. Prestimulation of cells with TGF-β or PDGF may induce LOXL2 expression such that subsequent enzyme inhibition affects a measurable reduction in fibroblast contractility, migration or collagen production compared to fibroblast activity without LOXL2 inhibition.

It is also unclear why a contrary effect on gel contraction was observed with 3T3 cells (increased contraction with higher concentration of PXS5338K); in previous

contraction studies these cells have responded to stimuli as expected, but to my knowledge the effect of lysyl oxidase inhibition has not been investigated in this cell line (284, 285). Likewise, the LX2 cell line has been demonstrated to mediate collagen gel contraction in previous assays (286, 287). Importantly, the effects of endothelin-1 (to stimulate contraction) and BDM (inhibition of contraction) were observed in both human fibroblasts and 3T3 cells (results not shown), and so experimental design seems an unlikely explanation for these results. It is possible that genetic drift from early sources of LX2 and 3T3 cells had occurred, with consequential alterations in cell properties.

Ideally I would replicate the results seen using human fibroblasts using primary murine stellate cells, particularly rat fibroblasts given the results in the CCl_4 model (see 3.3). Several attempts were made to isolate murine HSCs from mice, but the results were at best a cell mixed population (predominantly epithelial cells). The reasons for cell contamination are unclear but a likely explanation would be an inaccurate or incorrect density gradient at cell separation. Further attempts to purify the cells could have been made using magnetic beads or cell sorting with flow cytometry but time constraints precluded this.

With regards to collagen cross-linking *in vitro*, the concentrations of each of the collagen crosslinks were low, and so for some measurements the analyte peak was not specific and could not be identified well; the data was therefore generated from best judgement taken on basis of confirmation transitions (different daughter ion) and peak retention times (compared to standard peak retention times). It is possible that

these inaccuracies account for the apparent lack of efficacy of PXS5338K in reducing development of mature collagen crosslinks. However the data for DHLNL are more reliable than for any other marker as the chromatography for DHLNL is much more specific and consistent across the study. Given that there is no consistent trend for a change in the concentration of DHLNL with PXS5338K, it is unlikely that the compound affects collagen crosslinking *in vitro*. Time permitting, I would have repeated the same experiments with larger numbers of cells, so that greater, more accurate data could be generated. It would also be interesting to repeat this and the scratch wound assay with higher concentrations of PXS5338K, to evaluate whether under these conditions, similar inhibitory effects are observed as were seen with the contraction assay. However, given the poor tolerability of PXS5338K at higher doses in the *Mdr2-/-* mice, higher doses of the compound is unlikely to be a safe strategy for translation of the compound into clinical use, and further investigation would not be warranted.

7. Discussion

PXS5338K, a LOXL2 enzyme inhibitor was tested across three murine models of fibrosis, the *Mdr2-/-* model of biliary fibrosis, TAA induced liver injury, and during resolution of fibrosis induced by TAA administration. The same compound was tested across several *in-vitro* studies in an attempt to understand the underlying mechanism of action, and applicability to cells derived from human sources. While there was some suggestion that the compound may accelerate fibrosis resolution (reduced collagen I and α-SMA on IHC), and reduce fibroblast contractility at high concentration during *in vitro* studies, there was little evidence to suggest PXS5338K alone will be an effective antifibrotic therapy for liver disease. Similarly PXS5303 which was tested in the fibrosis model using *I.P.* administration of TAA in mice was not effective. This is in contrast to data for a related compound, PXS5153, administered during CCl_4-induced fibrosis in rats, where the inhibitor reduced both PSR collagen stain on IHC and expression of fibrosis related mRNA. There was also some evidence for a reduced ductular reaction, often used as a marker of fibrosis severity.

PXS5153 has previously demonstrated dose-dependent reduction of LOXL2-mediated collagen oxidation and crosslinking *in vitro*, and reduced fibrosis by PSR and hydroxyproline assay in the streptozotocin/ high fat diet model of NASH in mice (231). In addition, some improvement in cardiac function was demonstrated following PXS5153 administration following induction of myocardial infarction in mice (231). The same compound was demonstrated to inhibit LOXL3 in addition to LOXL2 (IC_{50}

of 38 nM for LOXL3 and <30nM for LOXL2), and so it is possible that inhibition of both enzymes is required to significantly reduce fibrosis. PXS5338K, the compound tested extensively in my experiments, has an IC_{50} of 36 nM for LOXL2 and 138 nM for LOXL4 (see table 1.1), and a higher IC_{50} for other amine oxidases and members of the lysyl oxidase family. *Loxl4* mRNA expression was not as elevated as some of the other lysyl oxidases in injured mice relative to control (see Figure 1.5), and so it is possible that the off target effects of PXS5338K had less effect on fibrosis reduction compared to that of PXS5153 through effects on Loxl4 rather than Loxl3.

Given that other lysyl oxidases are inhibited at higher concentrations of the inhibitors, it seems likely that the reduction of collagen contraction observed during *in vitro* study using high concentration PXS5338K was due to inhibition of multiple members of the LOX family (particularly LOX), mimicking the early effects seen by Liu *et al* using β-APN which is a rather promiscuous inhibitor. While some off-target inhibition of other lysyl oxidases may be beneficial in reducing liver fibrosis, it is worth noting the negative effects associated with some of lysyl oxidase knock out models, and that these may manifest as adverse systemic effects with long-term administration.

Dr Emma Shephard has previously demonstrated significantly increased *Loxl2* mRNA expression in TAA induced liver fibrosis in mice, and LOXL2 in human liver disease (see Figure 1.5 and 1.7), suggesting that targeting LOXL2 alone may be effective. However, LOXL2 expression in different human disease types was not interrogated (for example PSC vs NAFLD); it is possible that the balance of lysyl oxidase family protein expression may vary between diseases, and so targeting

LOXL2 may have varying efficacy across diseases. mRNA data should be used with caution, however, as mRNA expression is not always reflected in the amount of protein present in tissues. In addition, proteins can undergo post translational modification; specifically LOX is initially secreted as a proenzyme that undergoes proteolytic transformation into active LOX and the lysyl oxidase propeptide LOX-PP, and so the contribution of these proteins from mRNA data is not understood.

In addition to possible variation in lysyl oxidase expression in disease types, the relative contributions of other members of the lysyl oxidase family to the fibrotic response may be organ specific; LOXL2 enzyme inhibition alone has demonstrated benefit in diabetes related glomerulosclerosis in mice, and during *in vitro* models of interstitial pulmonary fibrosis (133, 288). Isolated LOXL2 enzyme inhibition may retain therapeutic potential in these conditions.

One failing of the study was that I was unable to confirm enzyme inhibition for each compound and it would have been preferable to confirm LOXL2 enzyme inhibition in both serum and liver tissue for each of the compounds tested for each model of liver disease, and during *in vitro* studies. Unfortunately, I did not have access to a biotinylated inhibitor so could not track tissue distribution, and because the compound has a short half-life and serum samples were taken at 24 hours post dosing, sending stored samples for testing at the end of the study was not possible.

Similarly, I was unable to demonstrate LOXL2 protein expression in the livers of treated mice, and whether there was any difference between treated and untreated

groups; this was due to the lack of an effective primary LOXL2 antibody for murine tissue. For this reason *Loxl2* mRNA expression was measured by qPCR in lieu of true protein expression with the known limitation that this may not be equivalent to protein expression.

Non-alcoholic fatty liver disease (NAFLD), defined by accumulation of excess fat in the liver, is the commonest cause of liver disease in Western countries, (289, 290) and is predicted to become the leading cause of liver transplantation over the next 10 years (291). As such, NAFLD is an attractive target for emerging pharmacotherapies, and yet no drugs are currently available. Although the pathophysiology of NAFLD is yet to be fully understood, multiple pathways, including accumulation of triglycerides, insulin resistance, oxidative stress, and mitochondrial dysfunction, culminate in hepatic injury and the development of fibrosis (292, 293). For this reason, dual drug therapy targeting multiple biological pathways may be preferential to single therapy. One phase II clinical trial assessed a combination of the ASK1 inhibitor selonsertib and the LOXL2 antibody simtuzumab in NAFLD, targeting oxidative stress known to promote hepatocellular apoptosis, inflammation, and fibrosis with selonsertib, and collagen crosslinking with simtuzumab (246). Although no additional benefit with simtuzumab was demonstrated (246), the concept of targeting several pathogenic pathways to reduce liver injury in diseases such as NAFLD is the likely model for clinical trials in the future. In addition, drug combinations could be tailored to individual patients according to the predominant pathogenic pathways demonstrated on liver biopsy, or other non-invasive investigations such as MRI (127).

Despite a keen interest for drug development in NAFLD, few murine models exist which accurately reflect human pathophysiology, particularly with regards to development of fibrosis (294). This can hinder drug development, and renders human response to potential therapies yet more unpredictable. It is not surprising then, that compounds commonly fail at both preclinical and clinical stages. It is partly for this reason that Pharmaxis has taken its LOXL2 enzyme inhibitors into phase I safety and tolerability testing (295) despite mixed results in pre-clinical trials. Ideally, these studies could have been extended to test PXS5338K in disease specific murine models such as those for NAFLD, despite their inadequacies, to better predict its efficacy in different disease types.

Another consideration during drug development is the timing of drug therapy. Based on the theory that the key role of LOXL2 enzyme activity in liver fibrosis is the strengthening of collagen fibres laid down during fibrogenesis, the models I used tested administration of the compound during the latter stages of liver injury, when it was presumed collagen crosslinking was occurring. However, the more convincing evidence for efficacy was seen during fibrosis resolution, and so it is possible that inhibition of LOXL2 may have a greater role during ECM remodelling and resolution. This would have implications in human diseases such as treated viral hepatitis, haemochromatosis, and AIH, or abstinence in alcohol-related liver disease, where the injury has been removed, and reduction of fibrosis still has potential to reduce long term morbidity. Additionally, exploration of lysyl oxidases within the cancer microenvironment has suggested a more complex role than crosslinking of collagen, as discussed in 1.5.1, and this may have relevance in fibrosis resolution.

Another important consideration pertaining to timing of therapy is the presentation of liver disease. Individuals developing liver fibrosis rarely develop symptoms, and liver biochemistry, particularly in later stages of fibrosis and early cirrhosis, can be normal (296). Diagnoses are therefore often made in the latter stages of the disease, where there is advanced fibrosis and mature collagen crosslinking, and so pharmacotherapy will need to be effective at these stages of the disease, once fibrosis is established.

Upregulation of matrix metalloproteinases -1, -8, -13 and -14, which degrade fibrillary collagens, or alternatively blocking TIMP-1, which inhibits MMPs, seem like ideal targets in this regard, as discussed in 1.3.5. However, this theory oversimplifies the role of MMPs. In the initial phases of injury, MMPs -3, -9 and -10 are elevated and believed to recruit inflammatory cells to the site of injury. Conversely, MMP-2 and TIMP-1 are consistently elevated during liver injury and during resolution and may have diverse roles according to disease aetiology (127). It is likely that this dual role of MMPs explains the failure of first generation MMP inhibitors in clinical trials in which the compounds were believed to have low selectivity, and a negative impact on the role of MMPs in maintaining homeostasis. Similarly, a broad-spectrum MMP inhibitor was demonstrated to attenuate liver inflammation, but aggravated fibrosis in mice exposed to CCl_4 (297, 298). Research specifically targeting isolated MMPs or MMPs in single organs, such as vitamin A coupled liposome-based particles in the liver, is underway but has not yet reached clinical trial phase (127). Likewise, LOXL2 inhibition was expected to be most effective during matrix generation, and the mouse models I used assessed the compound during liver injury. However, I have

demonstrated potential efficacy during fibrosis resolution, suggesting that timing of therapy could be crucial. Lysyl oxidase knock out models in mice have demonstrated diverse roles across a number of organs (similar to the widespread and diverse roles of MMPs), and so organ targeted inhibition of one or more members of the LOX family may be effective, while reducing systemic effects.

The dual role of macrophage subpopulations was discussed in 1.2.7. Seki *et al*. demonstrated that inhibition of macrophage recruitment via CCR2 receptors expressed on hepatic stellate cells reduced BDL- and CCl_4-induced liver fibrosis (299). Duffield *et al*. also demonstrated that macrophages contribute to fibrogenesis via recruitment of activated myofibroblasts during the latter stages of liver injury, and that their depletion resulted in reduced scar deposition. Conversely, a role for macrophages during fibrosis resolution was also demonstrated in the same study, whereby depletion led to reduced ECM degradation, probably via a slightly different subset of CD11b positive macrophages (49). The same investigators later found that production of MMP-13 by scar-associated macrophages was likely to be their key role during fibrosis resolution (92). These macrophages are generally known as Ly-6C (Ly6C, Gr1) low expressing 'restorative' macrophages (43), whereas during liver injury, proinflammatory, profibrogenic Gr-1^{hi} (Ly-$6C^{hi}$) macrophage populations dominate. To my knowledge these subpopulations have yet to be fully characterised, but could hold therapeutic potential if targeted to the liver at the right time, possibly in combination with MMP or, indeed LOX/L inhibition. A group in Edinburgh have demonstrated reduced liver injury and fibrosis, and possibly enhanced liver regeneration, in CCl_4-induced liver injury in rats using injection of differentiated

CD11b F4/80+ bone marrow derived macrophages into the portal vein during liver injury. And yet, infusion of bone marrow derived precursors in the same experiment had a deleterious effect, emphasising the importance of using well-defined cell populations when considering cell therapy (300).

There is increasing interest in targeting fibrosis resolution, possibly attributable to successful treatment of Hepatitis C in individuals with established liver disease who may still benefit from reduction in fibrosis. For the first time, we used a TAA-induced model of fibrosis resolution to interrogate the efficacy of these compounds during liver repair. A slight reduction in fibrosis was seen in this model (reduced collagen I and α-SMA on IHC), and it is possible that this study was inadequately powered to demonstrate a true difference between groups. Unfortunately due to the length of the study (18 weeks) I was unable to carry out preliminary studies which could have enabled accurate power calculations to be performed (group sizes were estimated from similar but not identical murine models), but these results do warrant further examination of the role of LOXL2 inhibition during ECM remodelling in the liver. Other approaches could be used to investigate the effect of compounds on the organisation and alignment of collagens, in addition to use of mass spectroscopy which assesses collagen crosslinking (301). This would facilitate a better understanding of the processes underlining collagen reorganisation and remodelling during fibrosis resolution and whether therapies targeting enzymes such as the LOX family are likely to be effective.

Given the potential efficacy of PXS5153 demonstrated in CCl_4- induced injury in rats, I would have ideally tested this compound in the TAA and *Mdr2-/-* models in mice. Alternatively PXS5338K could have been tested in rats. I could have also compared LOX/lysyl oxidase expression in mice versus rats to explore whether a difference in LOXL2 expression may explain the difference in efficacy of the compounds. Combination therapy, for example targeting LOX and LOXL2, could also be tested for improved efficacy and tolerability.

In conclusion, I aimed to determine whether inhibition of LOXL2 led to an improvement in cell differentiation and liver fibrosis and regeneration, but although preliminary data with an earlier compound were promising, no benefit could be demonstrated with prolonged LOXL2 inhibition in the TAA model, or convincingly during fibrosis resolution, using the PXS5338K compound. Improving liver regeneration, potentially via manipulation of cell differentiation within the ductular reaction, remains a therapeutic target to be more fully explored.

References

1. Williams R, Alexander G, Armstrong I, Baker A, Bhala N, Camps-Walsh G, et al. Disease burden and costs from excess alcohol consumption, obesity, and viral hepatitis: fourth report of the Lancet Standing Commission on Liver Disease in the UK. Lancet. 2018;391(10125):1097-107.
2. J V. Liver disease: a preventable killer of young adults. PHE Public Health Matters. 29th September 2014.
3. http://www.liver-research.org.uk/liverresearch-assets/financialcaseforactiononliverdiseasepaper.pdf.
4. Asrani SK, Devarbhavi H, Eaton J, Kamath PS. Burden of liver diseases in the world. J Hepatol. 2019;70(1):151-71.
5. Bataller R, Brenner DA. Liver fibrosis. J Clin Invest. 2005;115(2):209-18.
6. Grose RD, Hayes PC. Review article: the pathophysiology and pharmacological treatment of portal hypertension. Aliment Pharmacol Ther. 1992;6(5):521-40.
7. Kisseleva T, Brenner DA. Hepatic stellate cells and the reversal of fibrosis. J Gastroenterol Hepatol. 2006;21 Suppl 3:S84-7.
8. Shiratori Y, Imazeki F, Moriyama M, Yano M, Arakawa Y, Yokosuka O, et al. Histologic improvement of fibrosis in patients with hepatitis C who have sustained response to interferon therapy. Ann Intern Med. 2000;132(7):517-24.
9. Liaw YF. Impact of therapy on the outcome of chronic hepatitis B. Liver Int. 2013;33 Suppl 1:111-5.
10. Filipponi F, Soubrane O, Labrousse F, Devictor D, Bernard O, Valayer J, et al. Liver transplantation for end-stage liver disease associated with alpha-1-antitrypsin deficiency in children: pretransplant natural history, timing and results of transplantation. J Hepatol. 1994;20(1):72-8.
11. Pinzani M, Luong TV. Pathogenesis of biliary fibrosis. Biochim Biophys Acta Mol Basis Dis. 2018;1864(4 Pt B):1279-83.
12. Liang S, Zhong Z, Seki E. Novel fate-tracing strategies show that hepatic stellate cells mediate fibrosis in vivo. Gastroenterology. 2014;146(7):1823-5.
13. Kisseleva T, Cong M, Paik Y, Scholten D, Jiang C, Benner C, et al. Myofibroblasts revert to an inactive phenotype during regression of liver fibrosis. Proc Natl Acad Sci U S A. 2012;109(24):9448-53.
14. Puche JE, Lee YA, Jiao J, Aloman C, Fiel MI, Munoz U, et al. A novel murine model to deplete hepatic stellate cells uncovers their role in amplifying liver damage in mice. Hepatology. 2013;57(1):339-50.
15. Gressner AM, Weiskirchen R, Breitkopf K, Dooley S. Roles of TGF-beta in hepatic fibrosis. Front Biosci. 2002;7:d793-807.
16. Mederacke I, Hsu CC, Troeger JS, Huebener P, Mu X, Dapito DH, et al. Fate tracing reveals hepatic stellate cells as dominant contributors to liver fibrosis independent of its aetiology. Nat Commun. 2013;4:2823.
17. Kinnman N, Housset C. Peribiliary myofibroblasts in biliary type liver fibrosis. Front Biosci. 2002;7:d496-503.
18. Maher JJ, Friedman SL, Roll FJ, Bissell DM. Immunolocalization of laminin in normal rat liver and biosynthesis of laminin by hepatic lipocytes in primary culture. Gastroenterology. 1988;94(4):1053-62.
19. Friedman SL. Seminars in medicine of the Beth Israel Hospital, Boston. The cellular basis of hepatic fibrosis. Mechanisms and treatment strategies. N Engl J Med. 1993;328(25):1828-35.
20. Friedman SL, Roll FJ, Boyles J, Bissell DM. Hepatic lipocytes: the principal collagen-producing cells of normal rat liver. Proc Natl Acad Sci U S A. 1985;82(24):8681-5.
21. Friedman S, Sanyal A, Goodman Z, Lefebvre E, Gottwald M, Fischer L, et al. Efficacy and safety study of cenicriviroc for the treatment of non-alcoholic steatohepatitis in adult subjects with liver fibrosis: CENTAUR Phase 2b study design. Contemp Clin Trials. 2016;47:356-65.
22. Du WD, Zhang YE, Zhai WR, Zhou XM. Dynamic changes of type I,III and IV collagen synthesis and distribution of collagen-producing cells in carbon tetrachloride-induced rat liver fibrosis. World J Gastroenterol. 1999;5(5):397-403.

23. Iredale JP, Thompson A, Henderson NC. Extracellular matrix degradation in liver fibrosis: Biochemistry and regulation. Biochim Biophys Acta. 2013;1832(7):876-83.
24. Iredale JP. Models of liver fibrosis: exploring the dynamic nature of inflammation and repair in a solid organ. J Clin Invest. 2007;117(3):539-48.
25. Henderson NC, Iredale JP. Liver fibrosis: cellular mechanisms of progression and resolution. Clin Sci (Lond). 2007;112(5):265-80.
26. Kennedy LL, Meng F, Venter JK, Zhou T, Karstens WA, Hargrove LA, et al. Knockout of microRNA-21 reduces biliary hyperplasia and liver fibrosis in cholestatic bile duct ligated mice. Lab Invest. 2016;96(12):1256-67.
27. Ramadori G, Saile B. Portal tract fibrogenesis in the liver. Lab Invest. 2004;84(2):153-9.
28. Fabris L, Spirli C, Cadamuro M, Fiorotto R, Strazzabosco M. Emerging Concepts in Biliary Repair and Fibrosis. Am J Physiol Gastrointest Liver Physiol. 2017:ajpgi 00452 2016.
29. Wang B, Zhao L, Fish M, Logan CY, Nusse R. Self-renewing diploid Axin2(+) cells fuel homeostatic renewal of the liver. Nature. 2015;524(7564):180-5.
30. Font-Burgada J, Shalapour S, Ramaswamy S, Hsueh B, Rossell D, Umemura A, et al. Hybrid Periportal Hepatocytes Regenerate the Injured Liver without Giving Rise to Cancer. Cell. 2015;162(4):766-79.
31. Gouw AS, Clouston AD, Theise ND. Ductular reactions in human liver: diversity at the interface. Hepatology. 2011;54(5):1853-63.
32. Schaub JR, Malato Y, Gormond C, Willenbring H. Evidence against a stem cell origin of new hepatocytes in a common mouse model of chronic liver injury. Cell Rep. 2014;8(4):933-9.
33. Stueck AE, Wanless IR. Hepatocyte buds derived from progenitor cells repopulate regions of parenchymal extinction in human cirrhosis. Hepatology. 2015;61(5):1696-707.
34. Gilgenkrantz H, Collin de l'Hortet A. Understanding Liver Regeneration: From Mechanisms to Regenerative Medicine. Am J Pathol. 2018;188(6):1316-27.
35. Dubuquoy L, Louvet A, Lassailly G, Truant S, Boleslawski E, Artru F, et al. Progenitor cell expansion and impaired hepatocyte regeneration in explanted livers from alcoholic hepatitis. Gut. 2015;64(12):1949-60.
36. Santodomingo-Garzon T, Swain MG. Role of NKT cells in autoimmune liver disease. Autoimmun Rev. 2011;10(12):793-800.
37. Abdel-Hakeem MS, Shoukry NH. Protective immunity against hepatitis C: many shades of gray. Front Immunol. 2014;5:274.
38. Pellicoro A, Ramachandran P, Iredale JP, Fallowfield JA. Liver fibrosis and repair: immune regulation of wound healing in a solid organ. Nat Rev Immunol. 2014;14(3):181-94.
39. Holt MP, Cheng L, Ju C. Identification and characterization of infiltrating macrophages in acetaminophen-induced liver injury. J Leukoc Biol. 2008;84(6):1410-21.
40. Ju C, Pohl LR. Tolerogenic role of Kupffer cells in immune-mediated adverse drug reactions. Toxicology. 2005;209(2):109-12.
41. Wiegard C, Frenzel C, Herkel J, Kallen KJ, Schmitt E, Lohse AW. Murine liver antigen presenting cells control suppressor activity of CD4+CD25+ regulatory T cells. Hepatology. 2005;42(1):193-9.
42. Seki S, Habu Y, Kawamura T, Takeda K, Dobashi H, Ohkawa T, et al. The liver as a crucial organ in the first line of host defense: the roles of Kupffer cells, natural killer (NK) cells and NK1.1 Ag+ T cells in T helper 1 immune responses. Immunol Rev. 2000;174:35-46.
43. Tacke F, Zimmermann HW. Macrophage heterogeneity in liver injury and fibrosis. J Hepatol. 2014;60(5):1090-6.
44. Liaskou E, Zimmermann HW, Li KK, Oo YH, Suresh S, Stamataki Z, et al. Monocyte subsets in human liver disease show distinct phenotypic and functional characteristics. Hepatology. 2013;57(1):385-98.
45. Karlmark KR, Weiskirchen R, Zimmermann HW, Gassler N, Ginhoux F, Weber C, et al. Hepatic recruitment of the inflammatory Gr1+ monocyte subset upon liver injury promotes hepatic fibrosis. Hepatology. 2009;50(1):261-74.
46. Wynn TA, Barron L. Macrophages: master regulators of inflammation and fibrosis. Semin Liver Dis. 2010;30(3):245-57.

47. Baeck C, Wei X, Bartneck M, Fech V, Heymann F, Gassler N, et al. Pharmacological inhibition of the chemokine C-C motif chemokine ligand 2 (monocyte chemoattractant protein 1) accelerates liver fibrosis regression by suppressing Ly-6C(+) macrophage infiltration in mice. Hepatology. 2014;59(3):1060-72.
48. Pradere JP, Kluwe J, De Minicis S, Jiao JJ, Gwak GY, Dapito DH, et al. Hepatic macrophages but not dendritic cells contribute to liver fibrosis by promoting the survival of activated hepatic stellate cells in mice. Hepatology. 2013;58(4):1461-73.
49. Duffield JS, Forbes SJ, Constandinou CM, Clay S, Partolina M, Vuthoori S, et al. Selective depletion of macrophages reveals distinct, opposing roles during liver injury and repair. J Clin Invest. 2005;115(1):56-65.
50. Thomas JA, Pope C, Wojtacha D, Robson AJ, Gordon-Walker TT, Hartland S, et al. Macrophage therapy for murine liver fibrosis recruits host effector cells improving fibrosis, regeneration, and function. Hepatology. 2011;53(6):2003-15.
51. Ramachandran P, Pellicoro A, Vernon MA, Boulter L, Aucott RL, Ali A, et al. Differential Ly-6C expression identifies the recruited macrophage phenotype, which orchestrates the regression of murine liver fibrosis. Proc Natl Acad Sci U S A. 2012;109(46):E3186-95.
52. Ju C, Tacke F. Hepatic macrophages in homeostasis and liver diseases: from pathogenesis to novel therapeutic strategies. Cell Mol Immunol. 2016;13(3):316-27.
53. Imamura M, Ogawa T, Sasaguri Y, Chayama K, Ueno H. Suppression of macrophage infiltration inhibits activation of hepatic stellate cells and liver fibrogenesis in rats. Gastroenterology. 2005;128(1):138-46.
54. Ide M, Kuwamura M, Kotani T, Sawamoto O, Yamate J. Effects of gadolinium chloride (GdCl(3)) on the appearance of macrophage populations and fibrogenesis in thioacetamide-induced rat hepatic lesions. J Comp Pathol. 2005;133(2-3):92-102.
55. Wynn TA. Fibrotic disease and the T(H)1/T(H)2 paradigm. Nat Rev Immunol. 2004;4(8):583-94.
56. Meng F, Wang K, Aoyama T, Grivennikov SI, Paik Y, Scholten D, et al. Interleukin-17 signaling in inflammatory, Kupffer cells, and hepatic stellate cells exacerbates liver fibrosis in mice. Gastroenterology. 2012;143(3):765-76 e3.
57. Zhang Y, Cobleigh MA, Lian JQ, Huang CX, Booth CJ, Bai XF, et al. A proinflammatory role for interleukin-22 in the immune response to hepatitis B virus. Gastroenterology. 2011;141(5):1897-906.
58. Katz SC, Ryan K, Ahmed N, Plitas G, Chaudhry UI, Kingham TP, et al. Obstructive jaundice expands intrahepatic regulatory T cells, which impair liver T lymphocyte function but modulate liver cholestasis and fibrosis. J Immunol. 2011;187(3):1150-6.
59. Jeffery HC, Braitch MK, Brown S, Oo YH. Clinical Potential of Regulatory T Cell Therapy in Liver Diseases: An Overview and Current Perspectives. Front Immunol. 2016;7:334.
60. Almeida J, Polvorosa MA, Gonzalez-Quintela A, Marcos M, Pastor I, Hernandez Cerceno ML, et al. Decreased peripheral blood CD4+/CD25+ regulatory T cells in patients with alcoholic hepatitis. Alcohol Clin Exp Res. 2013;37(8):1361-9.
61. Langhans B, Kramer B, Louis M, Nischalke HD, Huneburg R, Staratschek-Jox A, et al. Intrahepatic IL-8 producing Foxp3(+)CD4(+) regulatory T cells and fibrogenesis in chronic hepatitis C. J Hepatol. 2013;59(2):229-35.
62. Safadi R, Ohta M, Alvarez CE, Fiel MI, Bansal M, Mehal WZ, et al. Immune stimulation of hepatic fibrogenesis by CD8 cells and attenuation by transgenic interleukin-10 from hepatocytes. Gastroenterology. 2004;127(3):870-82.
63. Sung PS, Racanelli V, Shin EC. CD8(+) T-Cell Responses in Acute Hepatitis C Virus Infection. Front Immunol. 2014;5:266.
64. Shoukry NH, Grakoui A, Houghton M, Chien DY, Ghrayeb J, Reimann KA, et al. Memory CD8+ T cells are required for protection from persistent hepatitis C virus infection. J Exp Med. 2003;197(12):1645-55.
65. Novobrantseva TI, Majeau GR, Amatucci A, Kogan S, Brenner I, Casola S, et al. Attenuated liver fibrosis in the absence of B cells. J Clin Invest. 2005;115(11):3072-82.
66. Wu L, Van Kaer L. Natural killer T cells in health and disease. Front Biosci (Schol Ed). 2011;3:236-51.

67. Gao B, Radaeva S, Park O. Liver natural killer and natural killer T cells: immunobiology and emerging roles in liver diseases. J Leukoc Biol. 2009;86(3):513-28.
68. Wehr A, Baeck C, Heymann F, Niemietz PM, Hammerich L, Martin C, et al. Chemokine receptor CXCR6-dependent hepatic NK T Cell accumulation promotes inflammation and liver fibrosis. J Immunol. 2013;190(10):5226-36.
69. Waldhauer I, Steinle A. NK cells and cancer immunosurveillance. Oncogene. 2008;27(45):5932-43.
70. Radaeva S, Sun R, Jaruga B, Nguyen VT, Tian Z, Gao B. Natural killer cells ameliorate liver fibrosis by killing activated stellate cells in NKG2D-dependent and tumor necrosis factor-related apoptosis-inducing ligand-dependent manners. Gastroenterology. 2006;130(2):435-52.
71. Schuppan D, Ashfaq-Khan M, Yang AT, Kim YO. Liver fibrosis: Direct antifibrotic agents and targeted therapies. Matrix Biol. 2018;68-69:435-51.
72. Grenard P, Bresson-Hadni S, El Alaoui S, Chevallier M, Vuitton DA, Ricard-Blum S. Transglutaminase-mediated cross-linking is involved in the stabilization of extracellular matrix in human liver fibrosis. J Hepatol. 2001;35(3):367-75.
73. Aeschlimann D, Paulsson M. Transglutaminases: protein cross-linking enzymes in tissues and body fluids. Thromb Haemost. 1994;71(4):402-15.
74. Blazejewski S, Le Bail B, Boussarie L, Blanc JF, Malaval L, Okubo K, et al. Osteonectin (SPARC) expression in human liver and in cultured human liver myofibroblasts. Am J Pathol. 1997;151(3):651-7.
75. Mirza A, Liu SL, Frizell E, Zhu J, Maddukuri S, Martinez J, et al. A role for tissue transglutaminase in hepatic injury and fibrogenesis, and its regulation by NF-kappaB. Am J Physiol. 1997;272(2 Pt 1):G281-8.
76. Popov Y, Sverdlov DY, Sharma AK, Bhaskar KR, Li S, Freitag TL, et al. Tissue transglutaminase does not affect fibrotic matrix stability or regression of liver fibrosis in mice. Gastroenterology. 2011;140(5):1642-52.
77. Ricard-Blum S, Ville G. Collagen cross-linking. Int J Biochem. 1989;21(11):1185-9.
78. Herchenhan A, Uhlenbrock F, Eliasson P, Weis M, Eyre D, Kadler KE, et al. Lysyl Oxidase Activity Is Required for Ordered Collagen Fibrillogenesis by Tendon Cells. J Biol Chem. 2015;290(26):16440-50.
79. Kagan HM, Li W. Lysyl oxidase: properties, specificity, and biological roles inside and outside of the cell. J Cell Biochem. 2003;88(4):660-72.
80. Eyre DR, Weis MA, Wu JJ. Advances in collagen cross-link analysis. Methods. 2008;45(1):65-74.
81. Last JA, Armstrong LG, Reiser KM. Biosynthesis of collagen crosslinks. Int J Biochem. 1990;22(6):559-64.
82. Iredale JP, Benyon RC, Pickering J, McCullen M, Northrop M, Pawley S, et al. Mechanisms of spontaneous resolution of rat liver fibrosis. Hepatic stellate cell apoptosis and reduced hepatic expression of metalloproteinase inhibitors. J Clin Invest. 1998;102(3):538-49.
83. Iredale JP. Hepatic stellate cell behavior during resolution of liver injury. Semin Liver Dis. 2001;21(3):427-36.
84. Troeger JS, Mederacke I, Gwak GY, Dapito DH, Mu X, Hsu CC, et al. Deactivation of hepatic stellate cells during liver fibrosis resolution in mice. Gastroenterology. 2012;143(4):1073-83 e22.
85. Liu X, Xu J, Brenner DA, Kisseleva T. Reversibility of Liver Fibrosis and Inactivation of Fibrogenic Myofibroblasts. Curr Pathobiol Rep. 2013;1(3):209-14.
86. de Oliveira da Silva B, Ramos LF, Moraes KCM. Molecular interplays in hepatic stellate cells: apoptosis, senescence, and phenotype reversion as cellular connections that modulate liver fibrosis. Cell Biol Int. 2017;41(9):946-59.
87. Chen Z, Trotman LC, Shaffer D, Lin HK, Dotan ZA, Niki M, et al. Crucial role of p53-dependent cellular senescence in suppression of Pten-deficient tumorigenesis. Nature. 2005;436(7051):725-30.
88. Krizhanovsky V, Yon M, Dickins RA, Hearn S, Simon J, Miething C, et al. Senescence of activated stellate cells limits liver fibrosis. Cell. 2008;134(4):657-67.
89. Taimr P, Higuchi H, Kocova E, Rippe RA, Friedman S, Gores GJ. Activated stellate cells express the TRAIL receptor-2/death receptor-5 and undergo TRAIL-mediated apoptosis. Hepatology. 2003;37(1):87-95.

90. Guillot A, Tacke F. Liver Macrophages: Old Dogmas and New Insights. Hepatol Commun. 2019;3(6):730-43.
91. MacParland SA, Liu JC, Ma XZ, Innes BT, Bartczak AM, Gage BK, et al. Single cell RNA sequencing of human liver reveals distinct intrahepatic macrophage populations. Nat Commun. 2018;9(1):4383.
92. Fallowfield JA, Mizuno M, Kendall TJ, Constandinou CM, Benyon RC, Duffield JS, et al. Scar-associated macrophages are a major source of hepatic matrix metalloproteinase-13 and facilitate the resolution of murine hepatic fibrosis. J Immunol. 2007;178(8):5288-95.
93. Ramachandran P, Iredale JP. Liver fibrosis: a bidirectional model of fibrogenesis and resolution. QJM. 2012;105(9):813-7.
94. Issa R, Zhou X, Constandinou CM, Fallowfield J, Millward-Sadler H, Gaca MD, et al. Spontaneous recovery from micronodular cirrhosis: evidence for incomplete resolution associated with matrix cross-linking. Gastroenterology. 2004;126(7):1795-808.
95. Fernandez M, Semela D, Bruix J, Colle I, Pinzani M, Bosch J. Angiogenesis in liver disease. J Hepatol. 2009;50(3):604-20.
96. Esteban R, Pineda JA, Calleja JL, Casado M, Rodriguez M, Turnes J, et al. Efficacy of Sofosbuvir and Velpatasvir, With and Without Ribavirin, in Patients With HCV genotype 3 Infection and Cirrhosis. Gastroenterology. 2018.
97. Falize L, Guillygomarc'h A, Perrin M, Laine F, Guyader D, Brissot P, et al. Reversibility of hepatic fibrosis in treated genetic hemochromatosis: a study of 36 cases. Hepatology. 2006;44(2):472-7.
98. Lee ES, Shin MO, Yoon S, Moon JO. Resveratrol inhibits dimethylnitrosamine-induced hepatic fibrosis in rats. Arch Pharm Res. 2010;33(6):925-32.
99. Ahmad A, Ahmad R. Resveratrol mitigate structural changes and hepatic stellate cell activation in N'-nitrosodimethylamine-induced liver fibrosis via restraining oxidative damage. Chem Biol Interact. 2014;221:1-12.
100. Barreyro FJ, Holod S, Finocchietto PV, Camino AM, Aquino JB, Avagnina A, et al. The pan-caspase inhibitor Emricasan (IDN-6556) decreases liver injury and fibrosis in a murine model of non-alcoholic steatohepatitis. Liver Int. 2015;35(3):953-66.
101. Canbay A, Feldstein AE, Higuchi H, Werneburg N, Grambihler A, Bronk SF, et al. Kupffer cell engulfment of apoptotic bodies stimulates death ligand and cytokine expression. Hepatology. 2003;38(5):1188-98.
102. Canbay A, Taimr P, Torok N, Higuchi H, Friedman S, Gores GJ. Apoptotic body engulfment by a human stellate cell line is profibrogenic. Lab Invest. 2003;83(5):655-63.
103. Shiffman M FB, Vuppalanchi R, et al. A Placebo-controlled, multicenter, double-blind, randomised trial of emricasan in subjects with non-alcoholic fatty liver disease (Nafld) and raised transaminases. J Hepatology. 2015;62:S2-82S.
104. Frenette CT, Morelli G, Shiffman ML, Frederick RT, Rubin RA, Fallon MB, et al. Emricasan Improves Liver Function in Patients With Cirrhosis and High Model for End-stage Liver Disease Scores Compared With Placebo. Clin Gastroenterol Hepatol. 2018.
105. Horan GS, Wood S, Ona V, Li DJ, Lukashev ME, Weinreb PH, et al. Partial inhibition of integrin alpha(v)beta6 prevents pulmonary fibrosis without exacerbating inflammation. Am J Respir Crit Care Med. 2008;177(1):56-65.
106. Oku H, Shimizu T, Kawabata T, Nagira M, Hikita I, Ueyama A, et al. Antifibrotic action of pirfenidone and prednisolone: different effects on pulmonary cytokines and growth factors in bleomycin-induced murine pulmonary fibrosis. Eur J Pharmacol. 2008;590(1-3):400-8.
107. Noble PW, Albera C, Bradford WZ, Costabel U, Glassberg MK, Kardatzke D, et al. Pirfenidone in patients with idiopathic pulmonary fibrosis (CAPACITY): two randomised trials. Lancet. 2011;377(9779):1760-9.
108. King TE, Jr., Bradford WZ, Castro-Bernardini S, Fagan EA, Glaspole I, Glassberg MK, et al. A phase 3 trial of pirfenidone in patients with idiopathic pulmonary fibrosis. N Engl J Med. 2014;370(22):2083-92.
109. Tang LX, He RH, Yang G, Tan JJ, Zhou L, Meng XM, et al. Asiatic acid inhibits liver fibrosis by blocking TGF-beta/Smad signaling in vivo and in vitro. PLoS One. 2012;7(2):e31350.

110. Lampi MC, Reinhart-King CA. Targeting extracellular matrix stiffness to attenuate disease: From molecular mechanisms to clinical trials. Sci Transl Med. 2018;10(422).
111. Bennett RG. Relaxin and its role in the development and treatment of fibrosis. Transl Res. 2009;154(1):1-6.
112. Sherwood OD. Relaxin's physiological roles and other diverse actions. Endocr Rev. 2004;25(2):205-34.
113. Unemori EN, Amento EP. Relaxin modulates synthesis and secretion of procollagenase and collagen by human dermal fibroblasts. J Biol Chem. 1990;265(18):10681-5.
114. Unemori EN, Pickford LB, Salles AL, Piercy CE, Grove BH, Erikson ME, et al. Relaxin induces an extracellular matrix-degrading phenotype in human lung fibroblasts in vitro and inhibits lung fibrosis in a murine model in vivo. J Clin Invest. 1996;98(12):2739-45.
115. Williams EJ, Benyon RC, Trim N, Hadwin R, Grove BH, Arthur MJ, et al. Relaxin inhibits effective collagen deposition by cultured hepatic stellate cells and decreases rat liver fibrosis in vivo. Gut. 2001;49(4):577-83.
116. Bennett RG, Heimann DG, Singh S, Simpson RL, Tuma DJ. Relaxin decreases the severity of established hepatic fibrosis in mice. Liver Int. 2014;34(3):416-26.
117. Snowdon VK, Lachlan NJ, Hoy AM, Hadoke PW, Semple SI, Patel D, et al. Serelaxin as a potential treatment for renal dysfunction in cirrhosis: Preclinical evaluation and results of a randomized phase 2 trial. PLoS Med. 2017;14(2):e1002248.
118. King A, Houlihan DD, Kavanagh D, Haldar D, Luu N, Owen A, et al. Sphingosine-1-Phosphate Prevents Egress of Hematopoietic Stem Cells From Liver to Reduce Fibrosis. Gastroenterology. 2017;153(1):233-48 e16.
119. Sakaida I, Terai S, Yamamoto N, Aoyama K, Ishikawa T, Nishina H, et al. Transplantation of bone marrow cells reduces CCl4-induced liver fibrosis in mice. Hepatology. 2004;40(6):1304-11.
120. Newsome PN, Fox R, King AL, Barton D, Than NN, Moore J, et al. Granulocyte colony-stimulating factor and autologous CD133-positive stem-cell therapy in liver cirrhosis (REALISTIC): an open-label, randomised, controlled phase 2 trial. Lancet Gastroenterol Hepatol. 2018;3(1):25-36.
121. Tacke F. Targeting hepatic macrophages to treat liver diseases. J Hepatol. 2017;66(6):1300-12.
122. Boulter L, Govaere O, Bird TG, Radulescu S, Ramachandran P, Pellicoro A, et al. Macrophage-derived Wnt opposes Notch signaling to specify hepatic progenitor cell fate in chronic liver disease. Nat Med. 2012;18(4):572-9.
123. Platform ICTR. Macrophages therapy for liver cirrhosis (MATCH trial)

. http://appswhoint/trialsearch/Trial2aspx?TrialID=ISRCTN10368050 2016.
124. Fraser AR, Pass C, Burgoyne P, Atkinson A, Bailey L, Laurie A, et al. Development, functional characterization and validation of methodology for GMP-compliant manufacture of phagocytic macrophages: A novel cellular therapeutic for liver cirrhosis. Cytotherapy. 2017;19(9):1113-24.
125. Hemmann S, Graf J, Roderfeld M, Roeb E. Expression of MMPs and TIMPs in liver fibrosis - a systematic review with special emphasis on anti-fibrotic strategies. J Hepatol. 2007;46(5):955-75.
126. Roderfeld M, Weiskirchen R, Wagner S, Berres ML, Henkel C, Grotzinger J, et al. Inhibition of hepatic fibrogenesis by matrix metalloproteinase-9 mutants in mice. FASEB J. 2006;20(3):444-54.
127. Afratis NA, Klepfish M, Karamanos NK, Sagi I. The apparent competitive action of ECM proteases and cross-linking enzymes during fibrosis: Applications to drug discovery. Adv Drug Deliv Rev. 2018;129:4-15.
128. Goffin L, Fagagnini S, Vicari A, Mamie C, Melhem H, Weder B, et al. Anti-MMP-9 Antibody: A Promising Therapeutic Strategy for Treatment of Inflammatory Bowel Disease Complications with Fibrosis. Inflamm Bowel Dis. 2016;22(9):2041-57.
129. Roeb E, Behrmann I, Grotzinger J, Breuer B, Matern S. An MMP-9 mutant without gelatinolytic activity as a novel TIMP-1-antagonist. FASEB J. 2000;14(12):1671-3.
130. Atta H, El-Rehany M, Hammam O, Abdel-Ghany H, Ramzy M, Roderfeld M, et al. Mutant MMP-9 and HGF gene transfer enhance resolution of CCl4-induced liver fibrosis in rats: role of ASH1 and EZH2 methyltransferases repression. PLoS One. 2014;9(11):e112384.
131. Li Y, Liu F, Ding F, Chen P, Tang M. Inhibition of liver fibrosis using vitamin A-coupled liposomes to deliver matrix metalloproteinase-2 siRNA in vitro. Mol Med Rep. 2015;12(3):3453-61.

132. Sato Y, Murase K, Kato J, Kobune M, Sato T, Kawano Y, et al. Resolution of liver cirrhosis using vitamin A-coupled liposomes to deliver siRNA against a collagen-specific chaperone. Nat Biotechnol. 2008;26(4):431-42.
133. Barry-Hamilton V, Spangler R, Marshall D, McCauley S, Rodriguez HM, Oyasu M, et al. Allosteric inhibition of lysyl oxidase-like-2 impedes the development of a pathologic microenvironment. Nat Med. 2010;16(9):1009-17.
134. Mondovi B, Finazzi Agro A. Structure and function of amine oxidase. Adv Exp Med Biol. 1982;148:141-53.
135. Kumar V, Dooley DM, Freeman HC, Guss JM, Harvey I, McGuirl MA, et al. Crystal structure of a eukaryotic (pea seedling) copper-containing amine oxidase at 2.2 A resolution. Structure. 1996;4(8):943-55.
136. Molnar J, Fong KS, He QP, Hayashi K, Kim Y, Fong SF, et al. Structural and functional diversity of lysyl oxidase and the LOX-like proteins. Biochim Biophys Acta. 2003;1647(1-2):220-4.
137. Gacheru SN, Trackman PC, Shah MA, O'Gara CY, Spacciapoli P, Greenaway FT, et al. Structural and catalytic properties of copper in lysyl oxidase. J Biol Chem. 1990;265(31):19022-7.
138. Borel A, Eichenberger D, Farjanel J, Kessler E, Gleyzal C, Hulmes DJ, et al. Lysyl oxidase-like protein from bovine aorta. Isolation and maturation to an active form by bone morphogenetic protein-1. J Biol Chem. 2001;276(52):48944-9.
139. Uzel MI, Scott IC, Babakhanlou-Chase H, Palamakumbura AH, Pappano WN, Hong HH, et al. Multiple bone morphogenetic protein 1-related mammalian metalloproteinases process pro-lysyl oxidase at the correct physiological site and control lysyl oxidase activation in mouse embryo fibroblast cultures. J Biol Chem. 2001;276(25):22537-43.
140. Finney J, Moon HJ, Ronnebaum T, Lantz M, Mure M. Human copper-dependent amine oxidases. Arch Biochem Biophys. 2014;546:19-32.
141. Maki JM, Rasanen J, Tikkanen H, Sormunen R, Makikallio K, Kivirikko KI, et al. Inactivation of the lysyl oxidase gene Lox leads to aortic aneurysms, cardiovascular dysfunction, and perinatal death in mice. Circulation. 2002;106(19):2503-9.
142. Hornstra IK, Birge S, Starcher B, Bailey AJ, Mecham RP, Shapiro SD. Lysyl oxidase is required for vascular and diaphragmatic development in mice. J Biol Chem. 2003;278(16):14387-93.
143. Maki JM, Sormunen R, Lippo S, Kaarteenaho-Wiik R, Soininen R, Myllyharju J. Lysyl oxidase is essential for normal development and function of the respiratory system and for the integrity of elastic and collagen fibers in various tissues. Am J Pathol. 2005;167(4):927-36.
144. Almassian B, Trackman PC, Iguchi H, Boak A, Calvaresi D, Kagan HM. Induction of lung lysyl oxidase activity and lysyl oxidase protein by exposure of rats to cadmium chloride: properties of the induced enzyme. Connect Tissue Res. 1991;25(3-4):197-208.
145. Blaauboer ME, Emson CL, Verschuren L, van Erk M, Turner SM, Everts V, et al. Novel combination of collagen dynamics analysis and transcriptional profiling reveals fibrosis-relevant genes and pathways. Matrix Biol. 2013;32(7-8):424-31.
146. Liu SB, Ikenaga N, Peng ZW, Sverdlov DY, Greenstein A, Smith V, et al. Lysyl oxidase activity contributes to collagen stabilization during liver fibrosis progression and limits spontaneous fibrosis reversal in mice. FASEB J. 2016;30(4):1599-609.
147. Assaggaf MA, Kantarci A, Sume SS, Trackman PC. Prevention of phenytoin-induced gingival overgrowth by lovastatin in mice. Am J Pathol. 2015;185(6):1588-99.
148. Roy S, Ha J, Trudeau K, Beglova E. Vascular basement membrane thickening in diabetic retinopathy. Curr Eye Res. 2010;35(12):1045-56.
149. Chronopoulos A, Tang A, Beglova E, Trackman PC, Roy S. High glucose increases lysyl oxidase expression and activity in retinal endothelial cells: mechanism for compromised extracellular matrix barrier function. Diabetes. 2010;59(12):3159-66.
150. Van Bergen T, Spangler R, Marshall D, Hollanders K, Van de Veire S, Vandewalle E, et al. The Role of LOX and LOXL2 in the Pathogenesis of an Experimental Model of Choroidal Neovascularization. Invest Ophthalmol Vis Sci. 2015;56(9):5280-9.
151. Eliades A, Papadantonakis N, Bhupatiraju A, Burridge KA, Johnston-Cox HA, Migliaccio AR, et al. Control of megakaryocyte expansion and bone marrow fibrosis by lysyl oxidase. J Biol Chem. 2011;286(31):27630-8.

152. Tadmor T, Bejar J, Attias D, Mischenko E, Sabo E, Neufeld G, et al. The expression of lysyl-oxidase gene family members in myeloproliferative neoplasms. Am J Hematol. 2013;88(5):355-8.
153. Baker AM, Cox TR, Bird D, Lang G, Murray GI, Sun XF, et al. The role of lysyl oxidase in SRC-dependent proliferation and metastasis of colorectal cancer. J Natl Cancer Inst. 2011;103(5):407-24.
154. Kirschmann DA, Seftor EA, Nieva DR, Mariano EA, Hendrix MJ. Differentially expressed genes associated with the metastatic phenotype in breast cancer. Breast Cancer Res Treat. 1999;55(2):127-36.
155. Payne SL, Hendrix MJ, Kirschmann DA. Lysyl oxidase regulates actin filament formation through the p130(Cas)/Crk/DOCK180 signaling complex. J Cell Biochem. 2006;98(4):827-37.
156. Cox TR, Bird D, Baker AM, Barker HE, Ho MW, Lang G, et al. LOX-mediated collagen crosslinking is responsible for fibrosis-enhanced metastasis. Cancer Res. 2013;73(6):1721-32.
157. Trackman PC. Lysyl Oxidase Isoforms and Potential Therapeutic Opportunities for Fibrosis and Cancer. Expert Opin Ther Targets. 2016;20(8):935-45.
158. Baker AM, Bird D, Welti JC, Gourlaouen M, Lang G, Murray GI, et al. Lysyl oxidase plays a critical role in endothelial cell stimulation to drive tumor angiogenesis. Cancer Res. 2013;73(2):583-94.
159. Cox TR, Rumney RMH, Schoof EM, Perryman L, Hoye AM, Agrawal A, et al. The hypoxic cancer secretome induces pre-metastatic bone lesions through lysyl oxidase. Nature. 2015;522(7554):106-10.
160. Erler JT, Bennewith KL, Cox TR, Lang G, Bird D, Koong A, et al. Hypoxia-induced lysyl oxidase is a critical mediator of bone marrow cell recruitment to form the premetastatic niche. Cancer Cell. 2009;15(1):35-44.
161. Johnston KA, Lopez KM. Lysyl oxidase in cancer inhibition and metastasis. Cancer Lett. 2018;417:174-81.
162. Sato S, Trackman PC, Maki JM, Myllyharju J, Kirsch KH, Sonenshein GE. The Ras signaling inhibitor LOX-PP interacts with Hsp70 and c-Raf to reduce Erk activation and transformed phenotype of breast cancer cells. Mol Cell Biol. 2011;31(13):2683-95.
163. Zhao Y, Min C, Vora SR, Trackman PC, Sonenshein GE, Kirsch KH. The lysyl oxidase pro-peptide attenuates fibronectin-mediated activation of focal adhesion kinase and p130Cas in breast cancer cells. J Biol Chem. 2009;284(3):1385-93.
164. Vora SR, Palamakumbura AH, Mitsi M, Guo Y, Pischon N, Nugent MA, et al. Lysyl oxidase propeptide inhibits FGF-2-induced signaling and proliferation of osteoblasts. J Biol Chem. 2010;285(10):7384-93.
165. Palamakumbura AH, Vora SR, Nugent MA, Kirsch KH, Sonenshein GE, Trackman PC. Lysyl oxidase propeptide inhibits prostate cancer cell growth by mechanisms that target FGF-2-cell binding and signaling. Oncogene. 2009;28(38):3390-400.
166. Bais MV, Ozdener GB, Sonenshein GE, Trackman PC. Effects of tumor-suppressor lysyl oxidase propeptide on prostate cancer xenograft growth and its direct interactions with DNA repair pathways. Oncogene. 2015;34(15):1928-37.
167. Grau-Bove X, Ruiz-Trillo I, Rodriguez-Pascual F. Origin and evolution of lysyl oxidases. Sci Rep. 2015;5:10568.
168. Yanagisawa H, Davis EC, Starcher BC, Ouchi T, Yanagisawa M, Richardson JA, et al. Fibulin-5 is an elastin-binding protein essential for elastic fibre development in vivo. Nature. 2002;415(6868):168-71.
169. Lee UJ, Gustilo-Ashby AM, Daneshgari F, Kuang M, Vurbic D, Lin DL, et al. Lower urogenital tract anatomical and functional phenotype in lysyl oxidase like-1 knockout mice resembles female pelvic floor dysfunction in humans. Am J Physiol Renal Physiol. 2008;295(2):F545-55.
170. Liu X, Zhao Y, Gao J, Pawlyk B, Starcher B, Spencer JA, et al. Elastic fiber homeostasis requires lysyl oxidase-like 1 protein. Nat Genet. 2004;36(2):178-82.
171. Schlotzer-Schrehardt U. Molecular pathology of pseudoexfoliation syndrome/glaucoma--new insights from LOXL1 gene associations. Exp Eye Res. 2009;88(4):776-85.
172. Alsofi L, Daley E, Hornstra I, Morgan EF, Mason ZD, Acevedo JF, et al. Sex-Linked Skeletal Phenotype of Lysyl Oxidase Like-1 Mutant Mice. Calcif Tissue Int. 2016;98(2):172-85.

173. Lee GH, Kim DS, Chung MJ, Chae SW, Kim HR, Chae HJ. Lysyl oxidase-like-1 enhances lung metastasis when lactate accumulation and monocarboxylate transporter expression are involved. Oncol Lett. 2011;2(5):831-8.
174. Wu G, Guo Z, Chang X, Kim MS, Nagpal JK, Liu J, et al. LOXL1 and LOXL4 are epigenetically silenced and can inhibit ras/extracellular signal-regulated kinase signaling pathway in human bladder cancer. Cancer Res. 2007;67(9):4123-9.
175. Martinez VG, Moestrup SK, Holmskov U, Mollenhauer J, Lozano F. The conserved scavenger receptor cysteine-rich superfamily in therapy and diagnosis. Pharmacol Rev. 2011;63(4):967-1000.
176. Ma L, Huang C, Wang XJ, Xin DE, Wang LS, Zou QC, et al. Lysyl Oxidase 3 Is a Dual-Specificity Enzyme Involved in STAT3 Deacetylation and Deacetylimination Modulation. Mol Cell. 2017;65(2):296-309.
177. Moon HJ, Finney J, Ronnebaum T, Mure M. Human lysyl oxidase-like 2. Bioorg Chem. 2014;57:231-41.
178. Xu L, Go EP, Finney J, Moon H, Lantz M, Rebecchi K, et al. Post-translational modifications of recombinant human lysyl oxidase-like 2 (rhLOXL2) secreted from Drosophila S2 cells. J Biol Chem. 2013;288(8):5357-63.
179. Fong SF, Dietzsch E, Fong KS, Hollosi P, Asuncion L, He Q, et al. Lysyl oxidase-like 2 expression is increased in colon and esophageal tumors and associated with less differentiated colon tumors. Genes Chromosomes Cancer. 2007;46(7):644-55.
180. Hollosi P, Yakushiji JK, Fong KS, Csiszar K, Fong SF. Lysyl oxidase-like 2 promotes migration in noninvasive breast cancer cells but not in normal breast epithelial cells. Int J Cancer. 2009;125(2):318-27.
181. Lopez-Jimenez AJ, Basak T, Vanacore RM. Proteolytic processing of lysyl oxidase-like-2 in the extracellular matrix is required for crosslinking of basement membrane collagen IV. J Biol Chem. 2017;292(41):16970-82.
182. Zhang J, Yang R, Liu Z, Hou C, Zong W, Zhang A, et al. Loss of lysyl oxidase-like 3 causes cleft palate and spinal deformity in mice. Hum Mol Genet. 2015;24(21):6174-85.
183. Alzahrani F, Al Hazzaa SA, Tayeb H, Alkuraya FS. LOXL3, encoding lysyl oxidase-like 3, is mutated in a family with autosomal recessive Stickler syndrome. Hum Genet. 2015;134(4):451-3.
184. Lee JE, Kim Y. A tissue-specific variant of the human lysyl oxidase-like protein 3 (LOXL3) functions as an amine oxidase with substrate specificity. J Biol Chem. 2006;281(49):37282-90.
185. Busnadiego O, Gonzalez-Santamaria J, Lagares D, Guinea-Viniegra J, Pichol-Thievend C, Muller L, et al. LOXL4 is induced by transforming growth factor beta1 through Smad and JunB/Fra2 and contributes to vascular matrix remodeling. Mol Cell Biol. 2013;33(12):2388-401.
186. Comptour A, Rouzaire M, Belville C, Bonnin N, Daniel E, Chiambaretta F, et al. Lysyl oxidase-like 4 involvement in retinoic acid epithelial wound healing. Sci Rep. 2016;6:32688.
187. Sebban S, Golan-Gerstl R, Karni R, Vaksman O, Davidson B, Reich R. Alternatively spliced lysyl oxidase-like 4 isoforms have a pro-metastatic role in cancer. Clin Exp Metastasis. 2013;30(1):103-17.
188. Weise JB, Rudolph P, Heiser A, Kruse ML, Hedderich J, Cordes C, et al. LOXL4 is a selectively expressed candidate diagnostic antigen in head and neck cancer. Eur J Cancer. 2008;44(9):1323-31.
189. Scola N, Gorogh T. LOXL4 as a selective molecular marker in primary and metastatic head/neck carcinoma. Anticancer Res. 2010;30(11):4567-71.
190. Li RK, Zhao WY, Fang F, Zhuang C, Zhang XX, Yang XM, et al. Lysyl oxidase-like 4 (LOXL4) promotes proliferation and metastasis of gastric cancer via FAK/Src pathway. J Cancer Res Clin Oncol. 2015;141(2):269-81.
191. http://www.mousephenotype.org/data/genes/MGI:1914823 - section-associations.
192. Reiser K, McCormick RJ, Rucker RB. Enzymatic and nonenzymatic cross-linking of collagen and elastin. FASEB J. 1992;6(7):2439-49.
193. Vadasz Z, Kessler O, Akiri G, Gengrinovitch S, Kagan HM, Baruch Y, et al. Abnormal deposition of collagen around hepatocytes in Wilson's disease is associated with hepatocyte specific expression of lysyl oxidase and lysyl oxidase like protein-2. J Hepatol. 2005;43(3):499-507.
194. Aumiller V, Strobel B, Romeike M, Schuler M, Stierstorfer BE, Kreuz S. Comparative analysis of lysyl oxidase (like) family members in pulmonary fibrosis. Sci Rep. 2017;7(1):149.

195. Ikenaga N, Peng ZW, Vaid KA, Liu SB, Yoshida S, Sverdlov DY, et al. Selective targeting of lysyl oxidase-like 2 (LOXL2) suppresses hepatic fibrosis progression and accelerates its reversal. Gut. 2017.
196. Yang C, Liu J, Liu K, Du B, Shi K, Ding M, et al. Ghrelin suppresses cardiac fibrosis of post-myocardial infarction heart failure rats by adjusting the activin A-follistatin imbalance. Peptides. 2018;99:27-35.
197. Anazco C, Lopez-Jimenez AJ, Rafi M, Vega-Montoto L, Zhang MZ, Hudson BG, et al. Lysyl Oxidase-like-2 Cross-links Collagen IV of Glomerular Basement Membrane. J Biol Chem. 2016;291(50):25999-6012.
198. Bignon M, Pichol-Thievend C, Hardouin J, Malbouyres M, Brechot N, Nasciutti L, et al. Lysyl oxidase-like protein-2 regulates sprouting angiogenesis and type IV collagen assembly in the endothelial basement membrane. Blood. 2011;118(14):3979-89.
199. Moreno-Bueno G, Salvador F, Martin A, Floristan A, Cuevas EP, Santos V, et al. Lysyl oxidase-like 2 (LOXL2), a new regulator of cell polarity required for metastatic dissemination of basal-like breast carcinomas. EMBO Mol Med. 2011;3(9):528-44.
200. Peinado H, Del Carmen Iglesias-de la Cruz M, Olmeda D, Csiszar K, Fong KS, Vega S, et al. A molecular role for lysyl oxidase-like 2 enzyme in snail regulation and tumor progression. EMBO J. 2005;24(19):3446-58.
201. Payne SL, Hendrix MJ, Kirschmann DA. Paradoxical roles for lysyl oxidases in cancer--a prospect. J Cell Biochem. 2007;101(6):1338-54.
202. Barker HE, Chang J, Cox TR, Lang G, Bird D, Nicolau M, et al. LOXL2-mediated matrix remodeling in metastasis and mammary gland involution. Cancer Res. 2011;71(5):1561-72.
203. Cano A, Santamaria PG, Moreno-Bueno G. LOXL2 in epithelial cell plasticity and tumor progression. Future Oncol. 2012;8(9):1095-108.
204. Herranz N, Dave N, Millanes-Romero A, Morey L, Diaz VM, Lorenz-Fonfria V, et al. Lysyl oxidase-like 2 deaminates lysine 4 in histone H3. Mol Cell. 2012;46(3):369-76.
205. Millanes-Romero A, Herranz N, Perrera V, Iturbide A, Loubat-Casanovas J, Gil J, et al. Regulation of heterochromatin transcription by Snail1/LOXL2 during epithelial-to-mesenchymal transition. Mol Cell. 2013;52(5):746-57.
206. Martin A, Salvador F, Moreno-Bueno G, Floristan A, Ruiz-Herguido C, Cuevas EP, et al. Lysyl oxidase-like 2 represses Notch1 expression in the skin to promote squamous cell carcinoma progression. EMBO J. 2015;34(8):1090-109.
207. Bais MV, Kukuruzinska M, Trackman PC. Orthotopic non-metastatic and metastatic oral cancer mouse models. Oral Oncol. 2015;51(5):476-82.
208. Xu J, Li D, Li X, Liu Z, Li T, Jiang P, et al. 67 laminin receptor promotes the malignant potential of tumour cells up-regulating lysyl oxidase-like 2 expression in cholangiocarcinoma. Dig Liver Dis. 2014;46(8):750-7.
209. Ahn SG, Dong SM, Oshima A, Kim WH, Lee HM, Lee SA, et al. LOXL2 expression is associated with invasiveness and negatively influences survival in breast cancer patients. Breast Cancer Res Treat. 2013;141(1):89-99.
210. Wong CC, Tse AP, Huang YP, Zhu YT, Chiu DK, Lai RK, et al. Lysyl oxidase-like 2 is critical to tumor microenvironment and metastatic niche formation in hepatocellular carcinoma. Hepatology. 2014;60(5):1645-58.
211. Peng L, Ran YL, Hu H, Yu L, Liu Q, Zhou Z, et al. Secreted LOXL2 is a novel therapeutic target that promotes gastric cancer metastasis via the Src/FAK pathway. Carcinogenesis. 2009;30(10):1660-9.
212. Torres S, Garcia-Palmero I, Herrera M, Bartolome RA, Pena C, Fernandez-Acenero MJ, et al. LOXL2 Is Highly Expressed in Cancer-Associated Fibroblasts and Associates to Poor Colon Cancer Survival. Clin Cancer Res. 2015;21(21):4892-902.
213. Zhan P, Shen XK, Qian Q, Zhu JP, Zhang Y, Xie HY, et al. Down-regulation of lysyl oxidase-like 2 (LOXL2) is associated with disease progression in lung adenocarcinomas. Med Oncol. 2012;29(2):648-55.
214. Barker HE, Bird D, Lang G, Erler JT. Tumor-secreted LOXL2 activates fibroblasts through FAK signaling. Mol Cancer Res. 2013;11(11):1425-36.

215. Nishikawa R, Chiyomaru T, Enokida H, Inoguchi S, Ishihara T, Matsushita R, et al. Tumour-suppressive microRNA-29s directly regulate LOXL2 expression and inhibit cancer cell migration and invasion in renal cell carcinoma. FEBS Lett. 2015;589(16):2136-45.
216. Fukumoto I, Kikkawa N, Matsushita R, Kato M, Kurozumi A, Nishikawa R, et al. Tumor-suppressive microRNAs (miR-26a/b, miR-29a/b/c and miR-218) concertedly suppressed metastasis-promoting LOXL2 in head and neck squamous cell carcinoma. J Hum Genet. 2016;61(2):109-18.
217. Peinado H, Moreno-Bueno G, Hardisson D, Perez-Gomez E, Santos V, Mendiola M, et al. Lysyl oxidase-like 2 as a new poor prognosis marker of squamous cell carcinomas. Cancer Res. 2008;68(12):4541-50.
218. Schietke R, Warnecke C, Wacker I, Schodel J, Mole DR, Campean V, et al. The lysyl oxidases LOX and LOXL2 are necessary and sufficient to repress E-cadherin in hypoxia: insights into cellular transformation processes mediated by HIF-1. J Biol Chem. 2010;285(9):6658-69.
219. Wang M, Zhao X, Zhu D, Liu T, Liang X, Liu F, et al. HIF-1alpha promoted vasculogenic mimicry formation in hepatocellular carcinoma through LOXL2 up-regulation in hypoxic tumor microenvironment. J Exp Clin Cancer Res. 2017;36(1):60.
220. Thiery JP. Epithelial-mesenchymal transitions in tumour progression. Nat Rev Cancer. 2002;2(6):442-54.
221. Cuevas EP, Moreno-Bueno G, Canesin G, Santos V, Portillo F, Cano A. LOXL2 catalytically inactive mutants mediate epithelial-to-mesenchymal transition. Biol Open. 2014;3(2):129-37.
222. Chang J, Lucas MC, Leonte LE, Garcia-Montolio M, Singh LB, Findlay AD, et al. Pre-clinical evaluation of small molecule LOXL2 inhibitors in breast cancer. Oncotarget. 2017.
223. McCready J, Wong DS, Burlison JA, Ying W, Jay DG. An Impermeant Ganetespib Analog Inhibits Extracellular Hsp90-Mediated Cancer Cell Migration that Involves Lysyl Oxidase 2-like Protein. Cancers (Basel). 2014;6(2):1031-46.
224. Zaffryar-Eilot S, Marshall D, Voloshin T, Bar-Zion A, Spangler R, Kessler O, et al. Lysyl oxidase-like-2 promotes tumour angiogenesis and is a potential therapeutic target in angiogenic tumours. Carcinogenesis. 2013;34(10):2370-9.
225. Sharma-Bhandari A, Park SH, Kim JY, Oh J, Kim Y. Lysyl oxidase modulates the osteoblast differentiation of primary mouse calvaria cells. Int J Mol Med. 2015;36(6):1664-70.
226. Iftikhar M, Hurtado P, Bais MV, Wigner N, Stephens DN, Gerstenfeld LC, et al. Lysyl oxidase-like-2 (LOXL2) is a major isoform in chondrocytes and is critically required for differentiation. J Biol Chem. 2011;286(2):909-18.
227. Seki K, Fujimori T, Savagner P, Hata A, Aikawa T, Ogata N, et al. Mouse Snail family transcription repressors regulate chondrocyte, extracellular matrix, type II collagen, and aggrecan. J Biol Chem. 2003;278(43):41862-70.
228. Yang J, Savvatis K, Kang JS, Fan P, Zhong H, Schwartz K, et al. Targeting LOXL2 for cardiac interstitial fibrosis and heart failure treatment. Nat Commun. 2016;7:13710.
229. Burstein B, Nattel S. Atrial fibrosis: mechanisms and clinical relevance in atrial fibrillation. J Am Coll Cardiol. 2008;51(8):802-9.
230. Zhao Y, Tang K, Tianbao X, Wang J, Yang J, Li D. Increased serum lysyl oxidase-like 2 levels correlate with the degree of left atrial fibrosis in patients with atrial fibrillation. Biosci Rep. 2017;37(6).
231. Schilter H, Findlay AD, Perryman L, Yow TT, Moses J, Zahoor A, et al. The lysyl oxidase like 2/3 enzymatic inhibitor, PXS-5153A, reduces crosslinks and ameliorates fibrosis. J Cell Mol Med. 2018.
232. Tjin G, Xu P, Kable SH, Kable EP, Burgess JK. Quantification of collagen I in airway tissues using second harmonic generation. J Biomed Opt. 2014;19(3):36005.
233. Abraham T, Kayra D, McManus B, Scott A. Quantitative assessment of forward and backward second harmonic three dimensional images of collagen Type I matrix remodeling in a stimulated cellular environment. J Struct Biol. 2012;180(1):17-25.
234. Raghu G, Brown KK, Collard HR, Cottin V, Gibson KF, Kaner RJ, et al. Efficacy of simtuzumab versus placebo in patients with idiopathic pulmonary fibrosis: a randomised, double-blind, controlled, phase 2 trial. Lancet Respir Med. 2017;5(1):22-32.
235. Tjin G, White ES, Faiz A, Sicard D, Tschumperlin DJ, Mahar A, et al. Lysyl oxidases regulate fibrillar collagen remodelling in idiopathic pulmonary fibrosis. Dis Model Mech. 2017;10(11):1301-12.
236. Gitlin JD. Wilson disease. Gastroenterology. 2003;125(6):1868-77.

237. Tahashi Y, Matsuzaki K, Date M, Yoshida K, Furukawa F, Sugano Y, et al. Differential regulation of TGF-beta signal in hepatic stellate cells between acute and chronic rat liver injury. Hepatology. 2002;35(1):49-61.
238. Inagaki Y, Mamura M, Kanamaru Y, Greenwel P, Nemoto T, Takehara K, et al. Constitutive phosphorylation and nuclear localization of Smad3 are correlated with increased collagen gene transcription in activated hepatic stellate cells. J Cell Physiol. 2001;187(1):117-23.
239. Lazaridis KN, Strazzabosco M, Larusso NF. The cholangiopathies: disorders of biliary epithelia. Gastroenterology. 2004;127(5):1565-77.
240. Murawaki Y, Kusakabe Y, Hirayama C. Serum lysyl oxidase activity in chronic liver disease in comparison with serum levels of prolyl hydroxylase and laminin. Hepatology. 1991;14(6):1167-73.
241. J. A. Utility of serum lysyl oxidase-like 2 (LOXL2) measurement for the non-invasive estimation of liver fibrosis in patients with chronic Hepatitis C infection 2011.
242. GS-4997, an inhibitor of apoptosis signal-regulating kinase (ASK1), alone or in combination with simtuzumab for the treatment of nonalcoholic steatohepatitis (NASH): a randomized, phase 2 trial.
243. Harrison SA, Abdelmalek MF, Caldwell S, Shiffman ML, Diehl AM, Ghalib R, et al. Simtuzumab Is Ineffective for Patients with Bridging Fibrosis or Compensated Cirrhosis Caused by Nonalcoholic Steatohepatitis. Gastroenterology. 2018.
244. Meissner EG, McLaughlin M, Matthews L, Gharib AM, Wood BJ, Levy E, et al. Simtuzumab treatment of advanced liver fibrosis in HIV and HCV-infected adults: results of a 6-month open-label safety trial. Liver Int. 2016;36(12):1783-92.
245. Verstovsek S, Savona MR, Mesa RA, Dong H, Maltzman JD, Sharma S, et al. A phase 2 study of simtuzumab in patients with primary, post-polycythaemia vera or post-essential thrombocythaemia myelofibrosis. Br J Haematol. 2017;176(6):939-49.
246. Benson AB, 3rd, Wainberg ZA, Hecht JR, Vyushkov D, Dong H, Bendell J, et al. A Phase II Randomized, Double-Blind, Placebo-Controlled Study of Simtuzumab or Placebo in Combination with Gemcitabine for the First-Line Treatment of Pancreatic Adenocarcinoma. Oncologist. 2017;22(3):241-e15.
247. Hecht JR, Benson AB, 3rd, Vyushkov D, Yang Y, Bendell J, Verma U. A Phase II, Randomized, Double-Blind, Placebo-Controlled Study of Simtuzumab in Combination with FOLFIRI for the Second-Line Treatment of Metastatic KRAS Mutant Colorectal Adenocarcinoma. Oncologist. 2017;22(3):243-e23.
248. Rodriguez HM, Vaysberg M, Mikels A, McCauley S, Velayo AC, Garcia C, et al. Modulation of lysyl oxidase-like 2 enzymatic activity by an allosteric antibody inhibitor. J Biol Chem. 2010;285(27):20964-74.
249. Lee HW, Ryu HW, Kang MG, Park D, Oh SR, Kim H. Selective inhibition of monoamine oxidase A by purpurin, an anthraquinone. Bioorg Med Chem Lett. 2017;27(5):1136-40.
250. Mostert S, Petzer A, Petzer JP. Indanones as high-potency reversible inhibitors of monoamine oxidase. ChemMedChem. 2015;10(5):862-73.
251. Jarolimek W BA, Cao L, Deodhar M, Findlay A, et al. Inhibition of lysyl oxidase like 2 reduces collagen accumulation and collagen cross-links in CCl_4-induced liver fibrosis. Accessed September 2016.
252. Stangenberg S, Saad S, Schilter HC, Zaky A, Gill A, Pollock CA, et al. Lysyl oxidase-like 2 inhibition ameliorates glomerulosclerosis and albuminuria in diabetic nephropathy. Sci Rep. 2018;8(1):9423.
253. Perez Tamayo R. Is cirrhosis of the liver experimentally produced by CCl4 and adequate model of human cirrhosis? Hepatology. 1983;3(1):112-20.
254. Reif S, Aeed H, Shilo Y, Reich R, Kloog Y, Kweon YO, et al. Treatment of thioacetamide-induced liver cirrhosis by the Ras antagonist, farnesylthiosalicylic acid. J Hepatol. 2004;41(2):235-41.
255. Li X, Benjamin IS, Alexander B. Reproducible production of thioacetamide-induced macronodular cirrhosis in the rat with no mortality. J Hepatol. 2002;36(4):488-93.
256. Kang JS, Wanibuchi H, Morimura K, Wongpoomchai R, Chusiri Y, Gonzalez FJ, et al. Role of CYP2E1 in thioacetamide-induced mouse hepatotoxicity. Toxicol Appl Pharmacol. 2008;228(3):295-300.
257. Lee J, Homma T, Fujii J. Mice in the early stage of liver steatosis caused by a high fat diet are resistant to thioacetamide-induced hepatotoxicity and oxidative stress. Toxicol Lett. 2017;277:92-103.

258. Kitamura K, Nakamoto Y, Akiyama M, Fujii C, Kondo T, Kobayashi K, et al. Pathogenic roles of tumor necrosis factor receptor p55-mediated signals in dimethylnitrosamine-induced murine liver fibrosis. Lab Invest. 2002;82(5):571-83.
259. Liedtke C, Luedde T, Sauerbruch T, Scholten D, Streetz K, Tacke F, et al. Experimental liver fibrosis research: update on animal models, legal issues and translational aspects. Fibrogenesis Tissue Repair. 2013;6(1):19.
260. Georgiev P, Jochum W, Heinrich S, Jang JH, Nocito A, Dahm F, et al. Characterization of time-related changes after experimental bile duct ligation. Br J Surg. 2008;95(5):646-56.
261. Starkel P, Leclercq IA. Animal models for the study of hepatic fibrosis. Best Pract Res Clin Gastroenterol. 2011;25(2):319-33.
262. Chang ML, Yeh CT, Chang PY, Chen JC. Comparison of murine cirrhosis models induced by hepatotoxin administration and common bile duct ligation. World J Gastroenterol. 2005;11(27):4167-72.
263. Popov Y, Patsenker E, Fickert P, Trauner M, Schuppan D. Mdr2 (Abcb4)-/- mice spontaneously develop severe biliary fibrosis via massive dysregulation of pro- and antifibrogenic genes. J Hepatol. 2005;43(6):1045-54.
264. Fickert P, Stoger U, Fuchsbichler A, Moustafa T, Marschall HU, Weiglein AH, et al. A new xenobiotic-induced mouse model of sclerosing cholangitis and biliary fibrosis. Am J Pathol. 2007;171(2):525-36.
265. Ikenaga N, Liu SB, Sverdlov DY, Yoshida S, Nasser I, Ke Q, et al. A new Mdr2(-/-) mouse model of sclerosing cholangitis with rapid fibrosis progression, early-onset portal hypertension, and liver cancer. Am J Pathol. 2015;185(2):325-34.
266. Dolle L, Theise ND, Schmelzer E, Boulter L, Gires O, van Grunsven LA. EpCAM and the biology of hepatic stem/progenitor cells. Am J Physiol Gastrointest Liver Physiol. 2015;308(4):G233-50.
267. Tarlow BD, Finegold MJ, Grompe M. Clonal tracing of Sox9+ liver progenitors in mouse oval cell injury. Hepatology. 2014;60(1):278-89.
268. Rokusz A, Veres D, Szucs A, Bugyik E, Mozes M, Paku S, et al. Ductular reaction correlates with fibrogenesis but does not contribute to liver regeneration in experimental fibrosis models. PLoS One. 2017;12(4):e0176518.
269. Desmet V, Roskams T, Van Eyken P. Ductular reaction in the liver. Pathol Res Pract. 1995;191(6):513-24.
270. Potikha T, Stoyanov E, Pappo O, Frolov A, Mizrahi L, Olam D, et al. Interstrain differences in chronic hepatitis and tumor development in a murine model of inflammation-mediated hepatocarcinogenesis. Hepatology. 2013;58(1):192-204.
271. Baghdasaryan A, Fuchs CD, Osterreicher CH, Lemberger UJ, Halilbasic E, Pahlman I, et al. Inhibition of intestinal bile acid absorption improves cholestatic liver and bile duct injury in a mouse model of sclerosing cholangitis. J Hepatol. 2016;64(3):674-81.
272. Lammert F, Wang DQ, Hillebrandt S, Geier A, Fickert P, Trauner M, et al. Spontaneous cholecysto- and hepatolithiasis in Mdr2-/- mice: a model for low phospholipid-associated cholelithiasis. Hepatology. 2004;39(1):117-28.
273. Saijou E, Enomoto Y, Matsuda M, Yuet-Yin Kok C, Akira S, Tanaka M, et al. Neutrophils alleviate fibrosis in the CCl4-induced mouse chronic liver injury model. Hepatol Commun. 2018;2(6):703-17.
274. Clouston AD, Powell EE, Walsh MJ, Richardson MM, Demetris AJ, Jonsson JR. Fibrosis correlates with a ductular reaction in hepatitis C: roles of impaired replication, progenitor cells and steatosis. Hepatology. 2005;41(4):809-18.
275. Richardson MM, Jonsson JR, Powell EE, Brunt EM, Neuschwander-Tetri BA, Bhathal PS, et al. Progressive fibrosis in nonalcoholic steatohepatitis: association with altered regeneration and a ductular reaction. Gastroenterology. 2007;133(1):80-90.
276. Ikenaga N, Peng ZW, Vaid KA, Liu SB, Yoshida S, Sverdlov DY, et al. Selective targeting of lysyl oxidase-like 2 (LOXL2) suppresses hepatic fibrosis progression and accelerates its reversal. Gut. 2017;66(9):1697-708.
277. Friedman SL. Hepatic stellate cells: protean, multifunctional, and enigmatic cells of the liver. Physiol Rev. 2008;88(1):125-72.

278. Xu L, Hui AY, Albanis E, Arthur MJ, O'Byrne SM, Blaner WS, et al. Human hepatic stellate cell lines, LX-1 and LX-2: new tools for analysis of hepatic fibrosis. Gut. 2005;54(1):142-51.
279. Todaro GJ, Green H. Quantitative studies of the growth of mouse embryo cells in culture and their development into established lines. J Cell Biol. 1963;17:299-313.
280. http://www.nih3t3.com/.
281. Kaur G, Dufour JM. Cell lines: Valuable tools or useless artifacts. Spermatogenesis. 2012;2(1):1-5.
282. Wilhelm A, Aldridge V, Haldar D, Naylor AJ, Weston CJ, Hedegaard D, et al. CD248/endosialin critically regulates hepatic stellate cell proliferation during chronic liver injury via a PDGF-regulated mechanism. Gut. 2016;65(7):1175-85.
283. Bhogal RH, Hodson J, Bartlett DC, Weston CJ, Curbishley SM, Haughton E, et al. Isolation of primary human hepatocytes from normal and diseased liver tissue: a one hundred liver experience. PLoS One. 2011;6(3):e18222.
284. Hinz B, Celetta G, Tomasek JJ, Gabbiani G, Chaponnier C. Alpha-smooth muscle actin expression upregulates fibroblast contractile activity. Mol Biol Cell. 2001;12(9):2730-41.
285. Ngo P, Ramalingam P, Phillips JA, Furuta GT. Collagen gel contraction assay. Methods Mol Biol. 2006;341:103-9.
286. Li Z, Ding Q, Ling LP, Wu Y, Meng DX, Li X, et al. Metformin attenuates motility, contraction, and fibrogenic response of hepatic stellate cells in vivo and in vitro by activating AMP-activated protein kinase. World J Gastroenterol. 2018;24(7):819-32.
287. Li X, Zhang XT, Zhang MY, Wang GC, Feng H, Zhang CQ. [Effects of desmopressin acetate and pituitrin on proliferation, contraction, and secretion of hepatic stellate cells]. Zhonghua Gan Zang Bing Za Zhi. 2016;24(8):569-74.
288. Stangenberg S, Saad S, Schilter HC, Zaky A, Gill A, Pollock CA, et al. Lysyl oxidase-like 2 inhibition ameliorates glomerulosclerosis and albuminuria in diabetic nephropathy. Scientific Reports. 2018;8(1):9423.
289. Williams CD, Stengel J, Asike MI, Torres DM, Shaw J, Contreras M, et al. Prevalence of nonalcoholic fatty liver disease and nonalcoholic steatohepatitis among a largely middle-aged population utilizing ultrasound and liver biopsy: a prospective study. Gastroenterology. 2011;140(1):124-31.
290. Browning JD, Szczepaniak LS, Dobbins R, Nuremberg P, Horton JD, Cohen JC, et al. Prevalence of hepatic steatosis in an urban population in the United States: impact of ethnicity. Hepatology. 2004;40(6):1387-95.
291. Wong RJ, Aguilar M, Cheung R, Perumpail RB, Harrison SA, Younossi ZM, et al. Nonalcoholic steatohepatitis is the second leading etiology of liver disease among adults awaiting liver transplantation in the United States. Gastroenterology. 2015;148(3):547-55.
292. Haas JT, Francque S, Staels B. Pathophysiology and Mechanisms of Nonalcoholic Fatty Liver Disease. Annu Rev Physiol. 2016;78:181-205.
293. Dowman JK, Tomlinson JW, Newsome PN. Pathogenesis of non-alcoholic fatty liver disease. QJM. 2010;103(2):71-83.
294. Anstee QM, Goldin RD. Mouse models in non-alcoholic fatty liver disease and steatohepatitis research. Int J Exp Pathol. 2006;87(1):1-16.
295. http://www.pharmaxis.com.au/product-pipeline/amine-oxidase-platform/loxloxl2/.
296. Mofrad P, Contos MJ, Haque M, Sargeant C, Fisher RA, Luketic VA, et al. Clinical and histologic spectrum of nonalcoholic fatty liver disease associated with normal ALT values. Hepatology. 2003;37(6):1286-92.
297. Overall CM, Kleifeld O. Tumour microenvironment - opinion: validating matrix metalloproteinases as drug targets and anti-targets for cancer therapy. Nat Rev Cancer. 2006;6(3):227-39.
298. de Meijer VE, Sverdlov DY, Popov Y, Le HD, Meisel JA, Nose V, et al. Broad-spectrum matrix metalloproteinase inhibition curbs inflammation and liver injury but aggravates experimental liver fibrosis in mice. PLoS One. 2010;5(6):e11256.
299. Seki E, de Minicis S, Inokuchi S, Taura K, Miyai K, van Rooijen N, et al. CCR2 promotes hepatic fibrosis in mice. Hepatology. 2009;50(1):185-97.

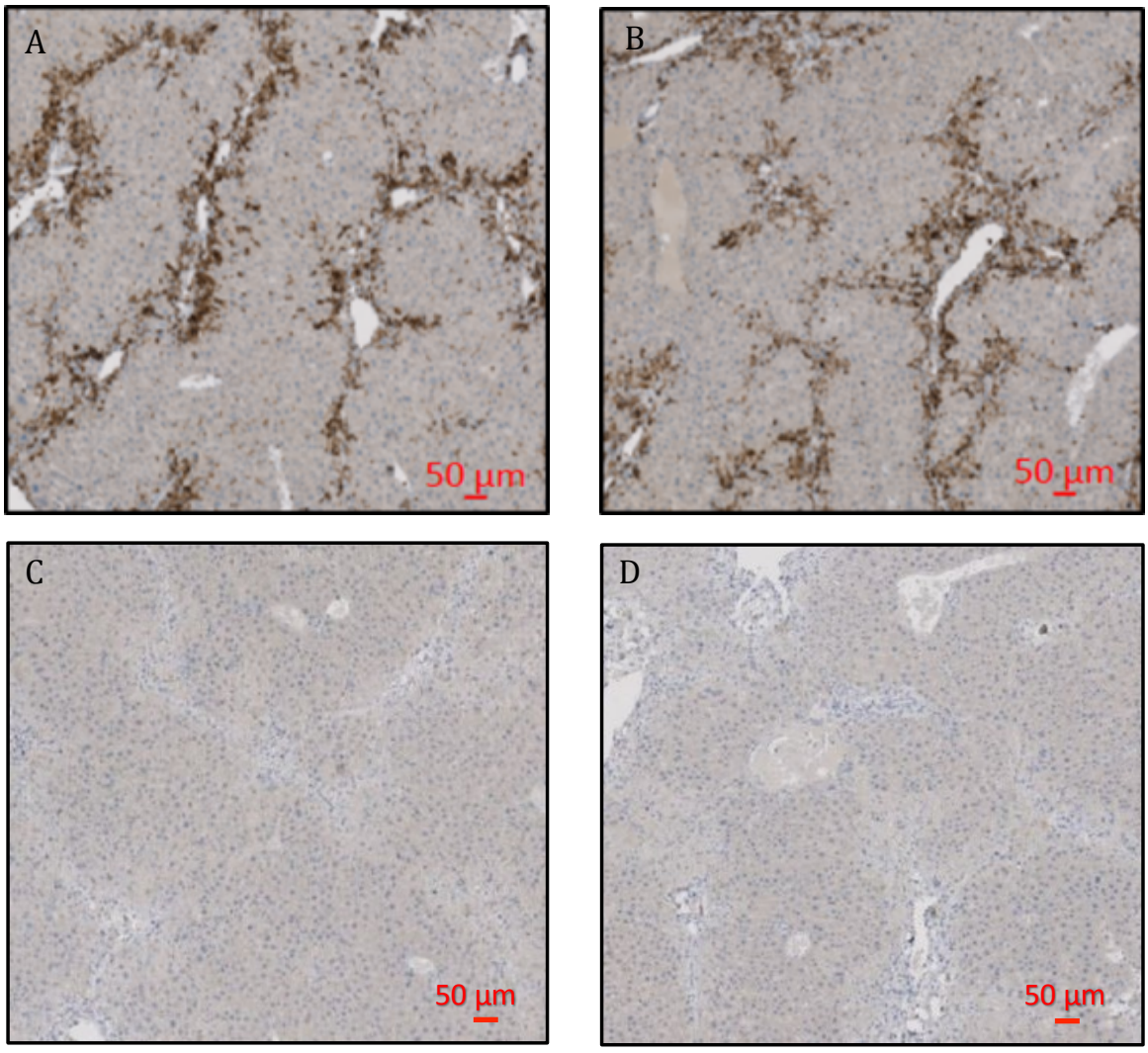
300. Haideri SS, McKinnon AC, Taylor AH, Kirkwood P, Starkey Lewis PJ, O'Duibhir E, et al. Injection of embryonic stem cell derived macrophages ameliorates fibrosis in a murine model of liver injury. npj Regenerative Medicine. 2017;2(1):14.
301. Wolman M, Kasten FH. Polarized light microscopy in the study of the molecular structure of collagen and reticulin. Histochemistry. 1986;85(1):41-9.

Appendix

Pharmaxis TAA model: CD45

Vehicle

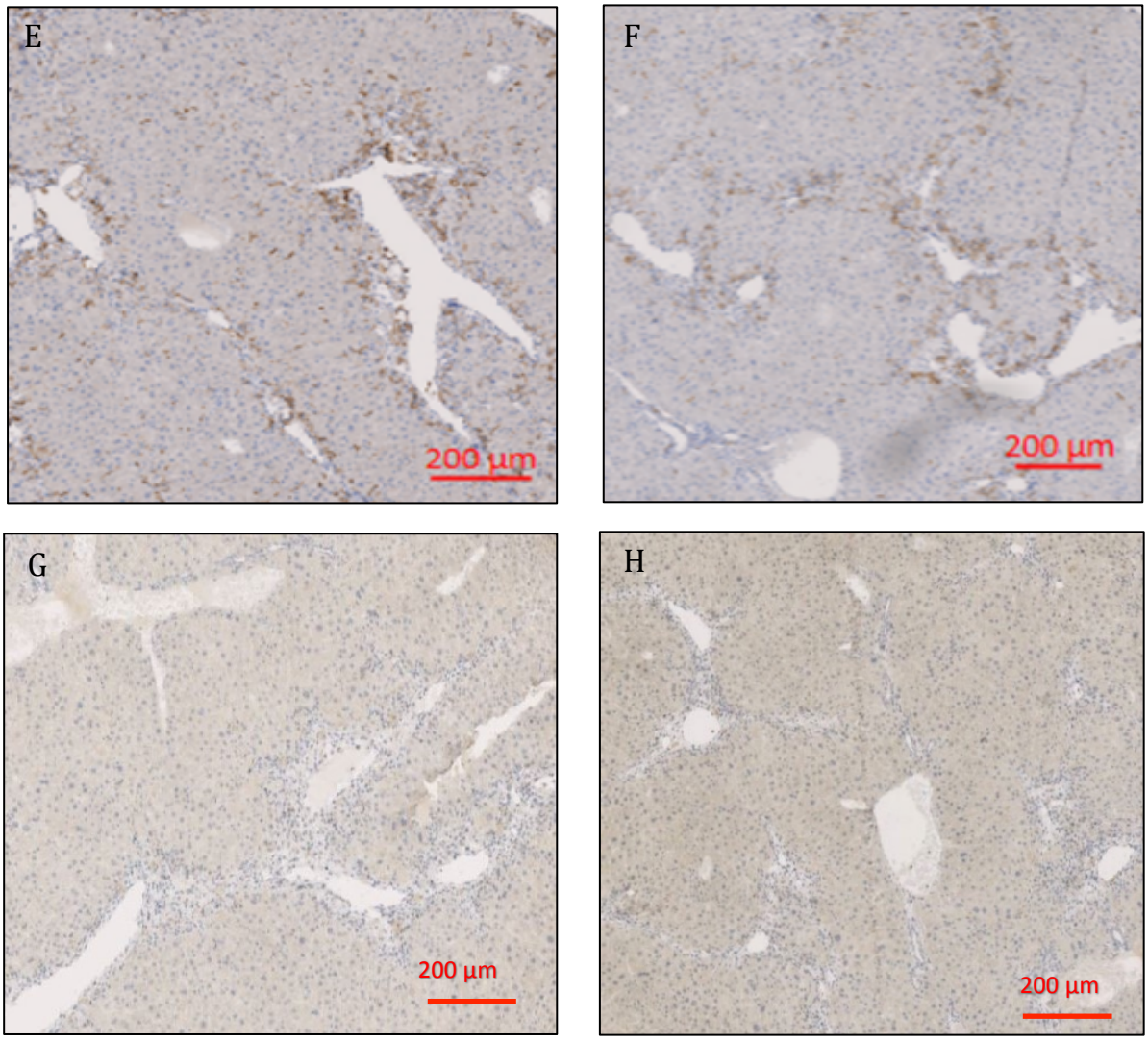
PXS5303



Pharmaxis TAA model: F4/80

Vehicle

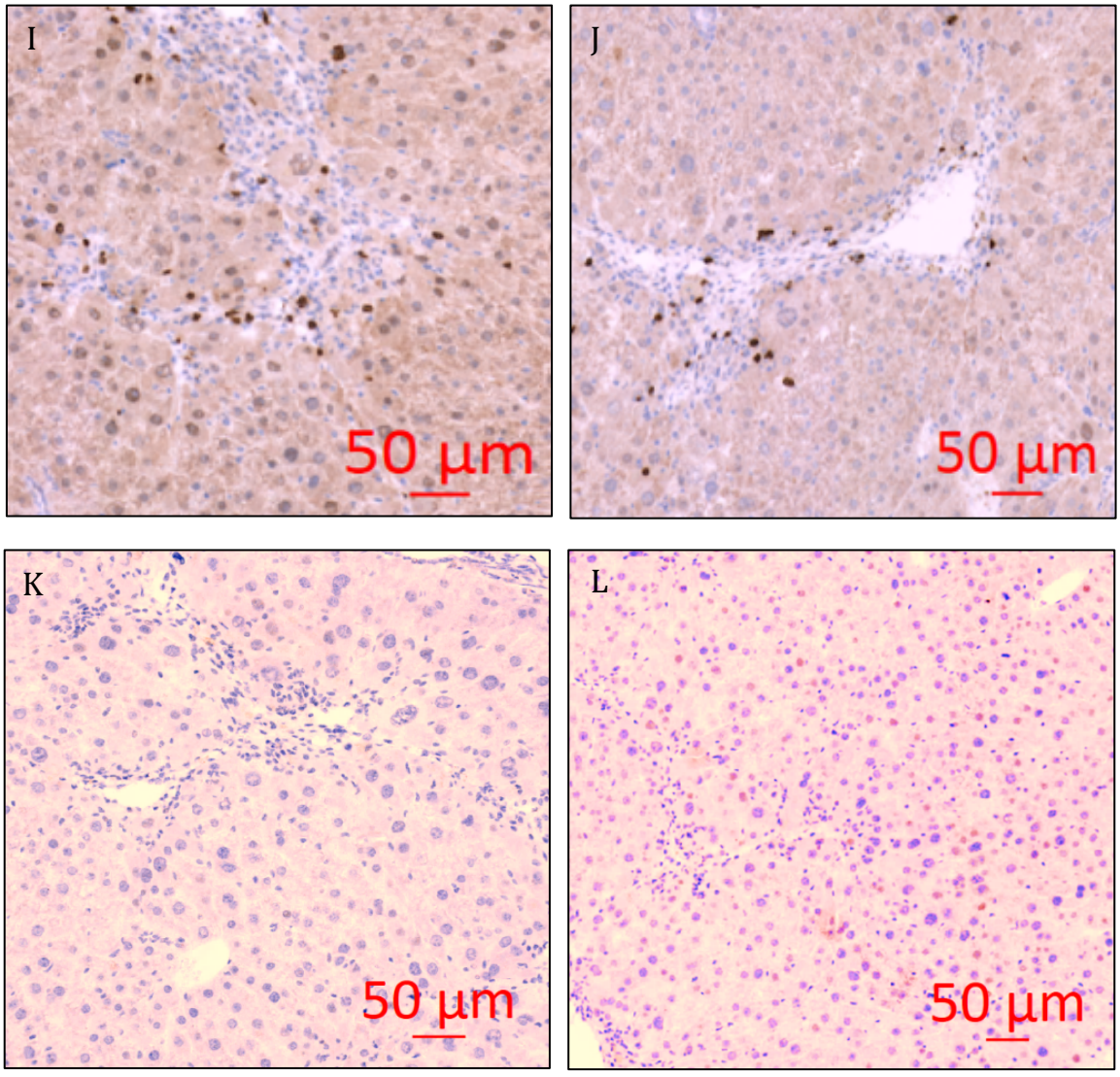
PXS5303



Pharmaxis TAA model: Ly6C

Vehicle

PXS5303



Pharmaxis TAA model: Myeloperoxidase

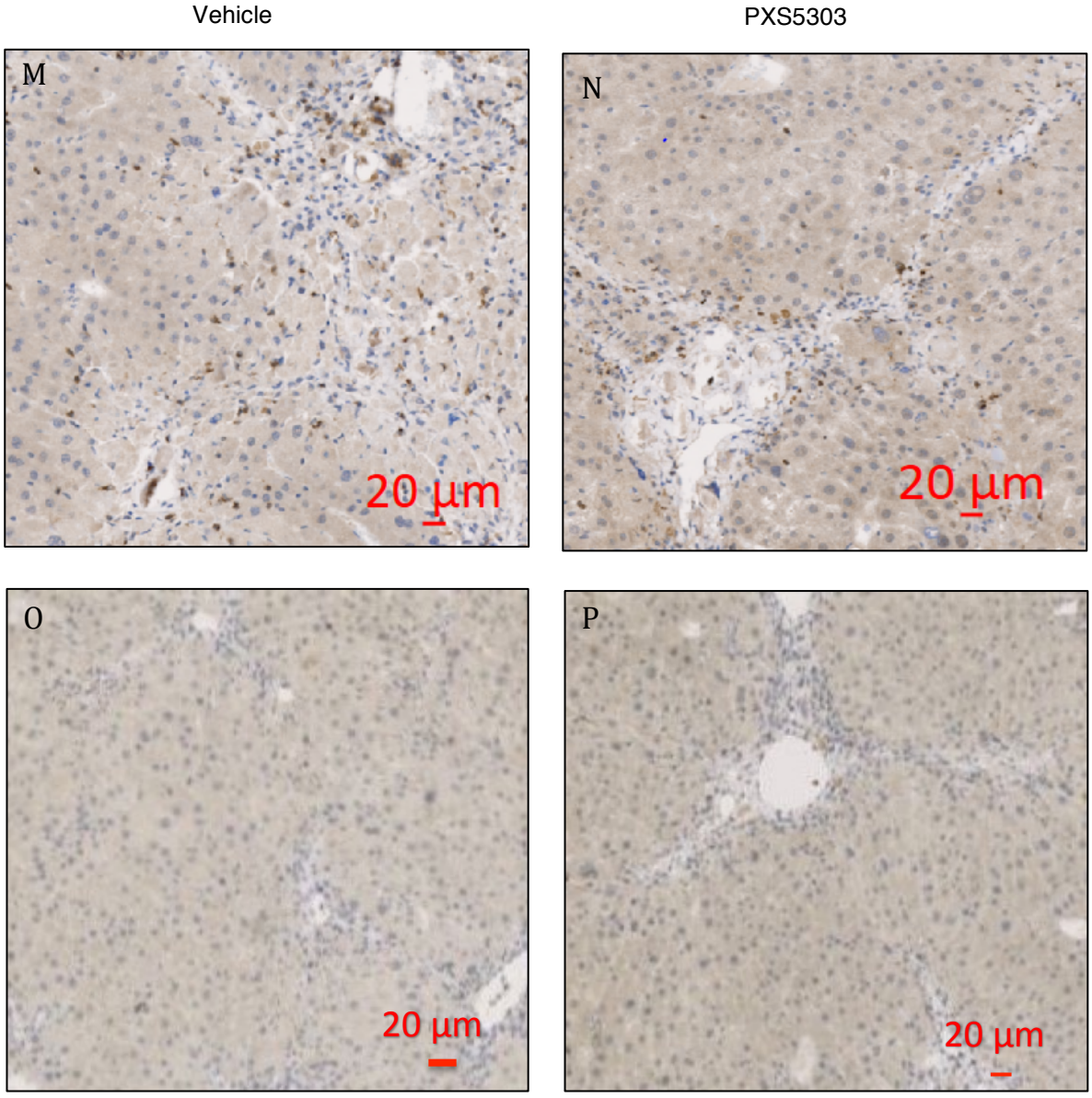
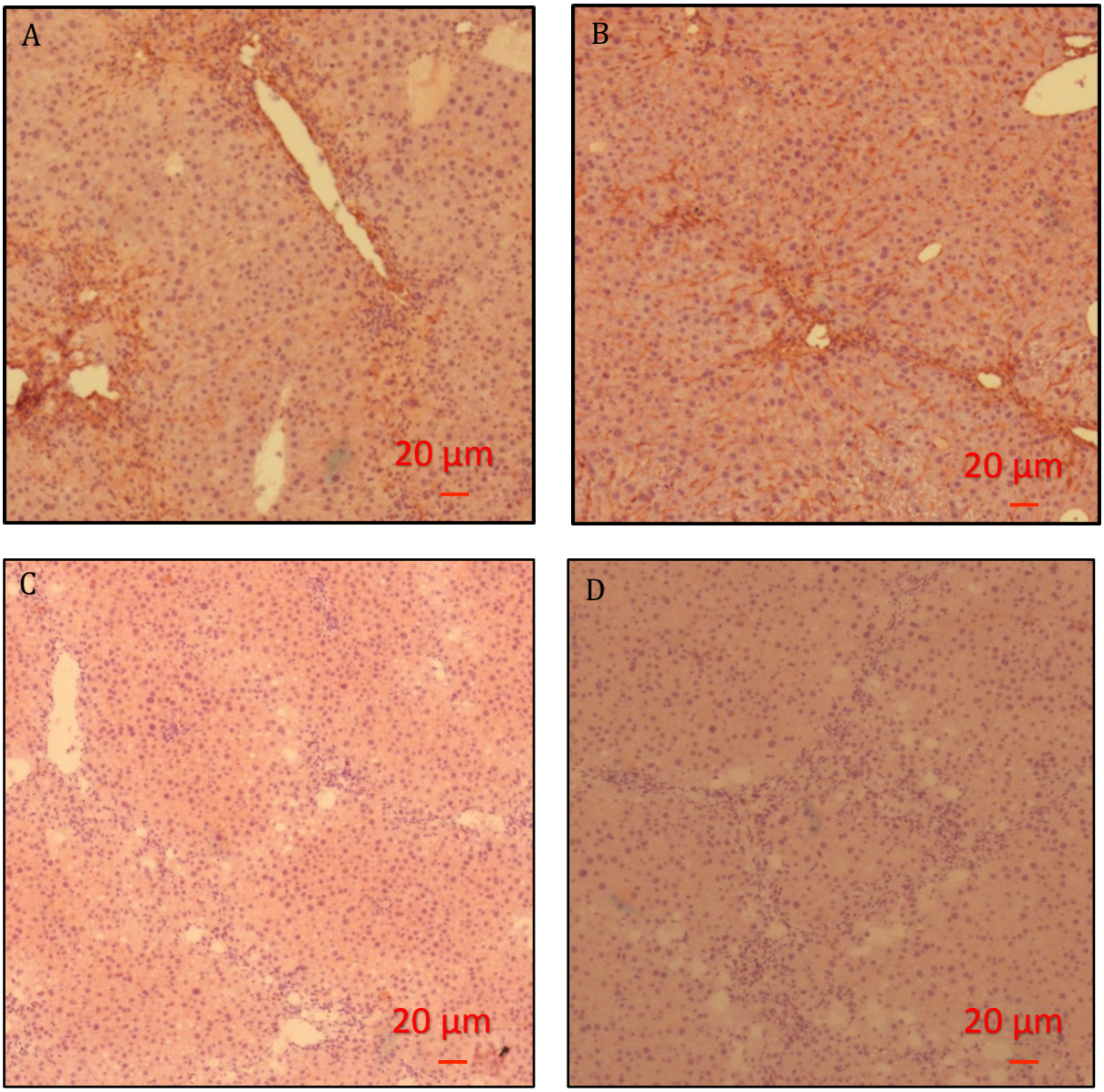


Figure 3.2 (S) LOXL2 inhibition has little effect on inflammatory markers in the TAA model. BALB/c mice received a regimen of 12 weeks of TAA at a dose of 200 mg/kg via I.P. injection, with vehicle, or PXS5303 administered orally from week 9. IHC was performed on paraffin embedded slides cut at 3µm is shown for the group receiving vehicle (images on the left), and the group receiving PXS5303 (images on the right), with the test antibodies shown in the top panels and corresponding isotype controls shown in the panels below for CD45 (A-D), F4/80 (E-H), Ly6C (I-L), and MPO (M-P).

Pharmaxis TAA model: Collagen I

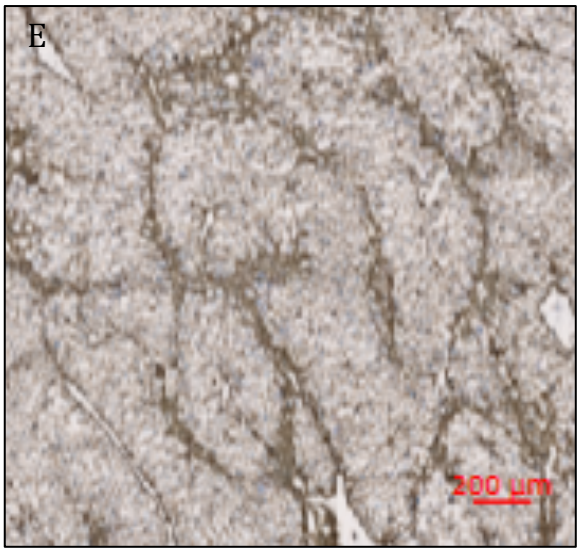
Vehicle

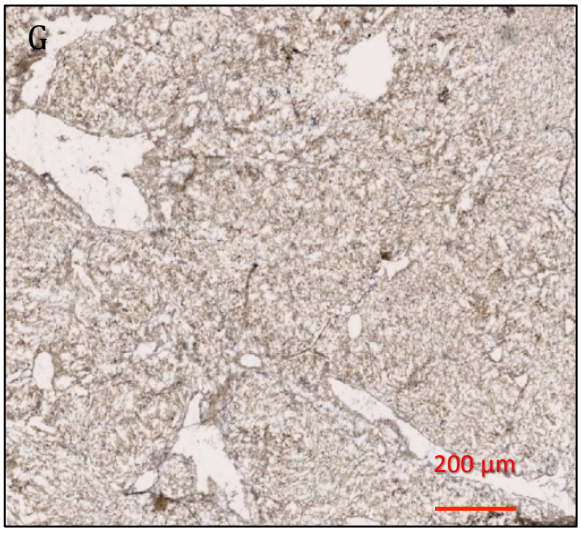
PXS5303



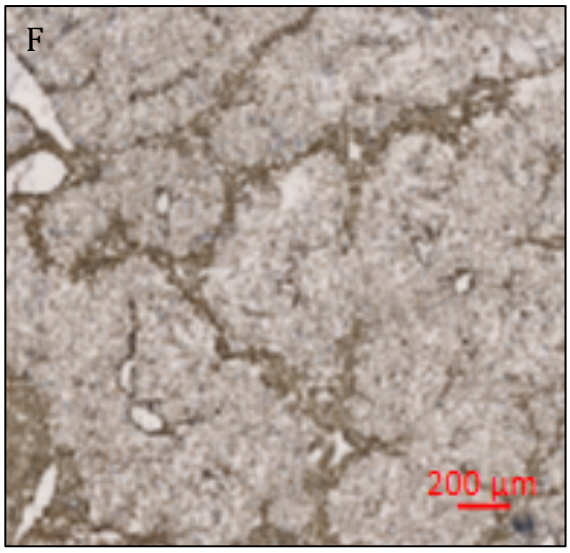
Pharmaxis TAA model: Collagen III

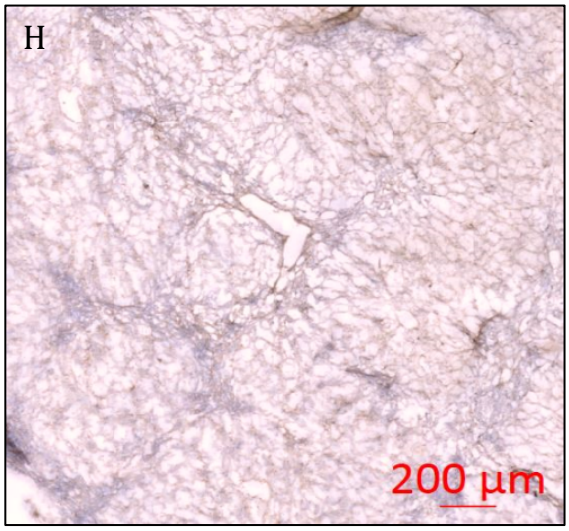
Vehicle





PXS5303





Pharmaxis TAA model: α-SMA

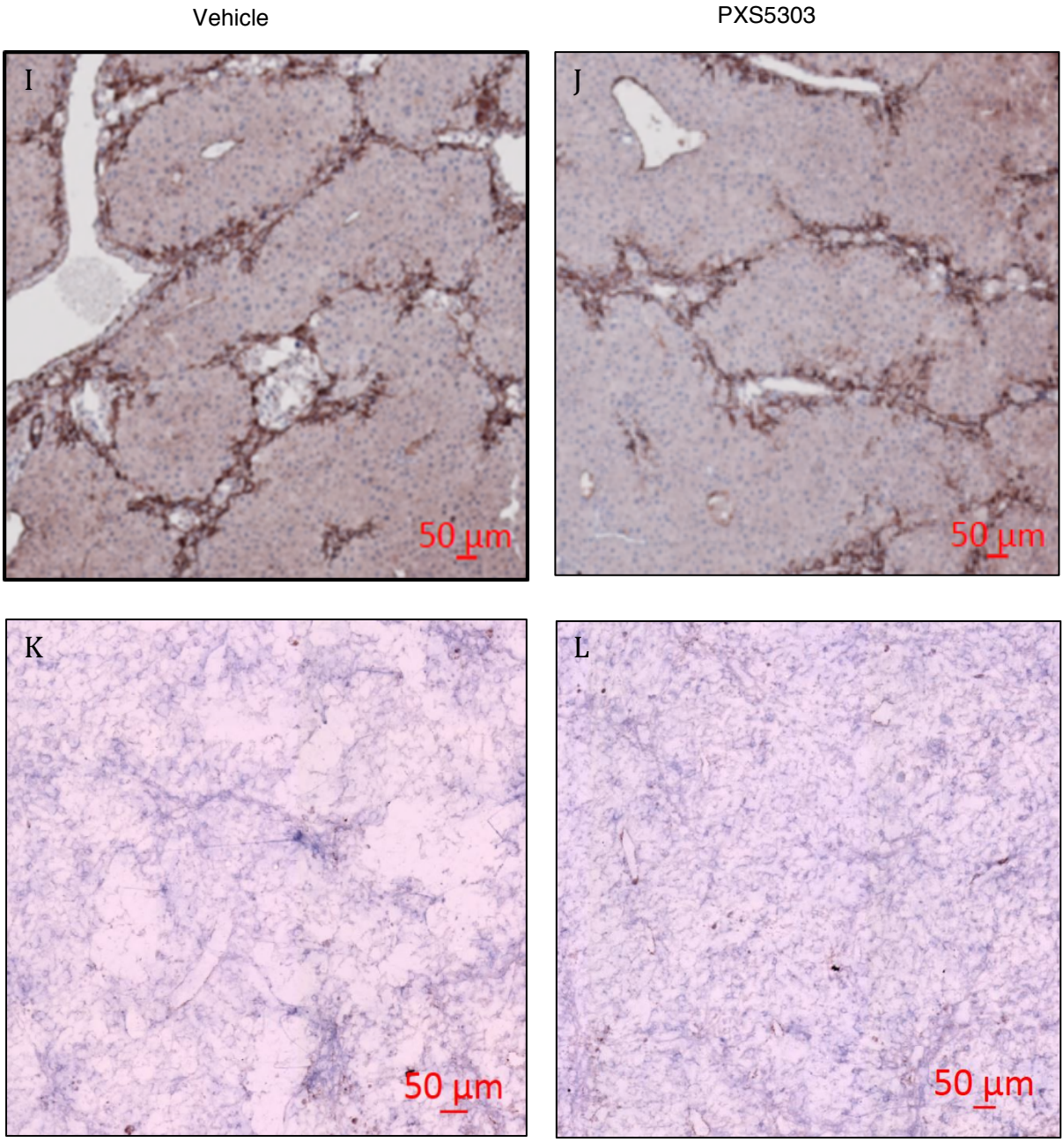
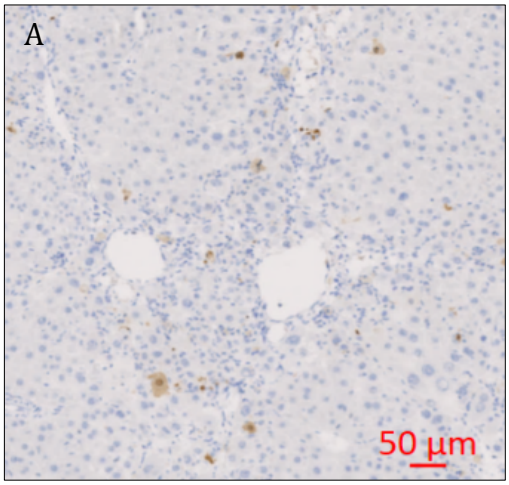


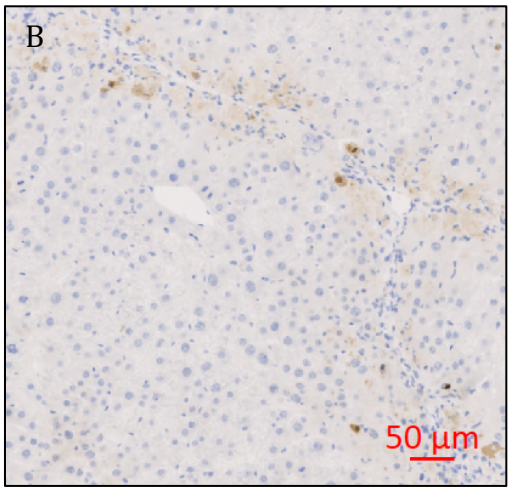
Figure 3.3 (S) LOXL2 inhibition has minimal impact on fibrosis by IHC in the TAA model. BALB/c mice received 12 weeks of TAA at a dose of 200 mg/kg via I.P. injection in addition to vehicle or PXS5303 orally from week 9, and were culled at week 12. IHC was performed on paraffin embedded sections for the untreated (left), and treated groups (right) to assess for Collagen I (A-D) Collagen III (E-H) and α-SMA (I-L), with test antibody shown in the top panel and corresponding isotype controls shown below for each group.

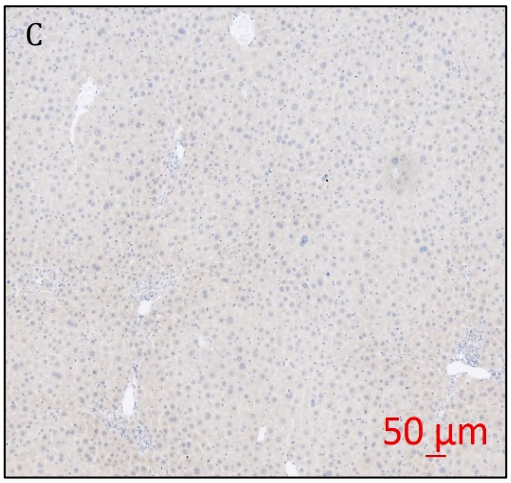
Pharmaxis TAA model: Cleaved caspase 3

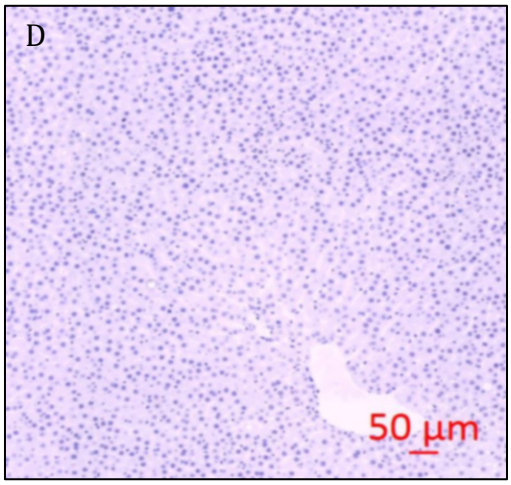
VEHICLE

PXS5303





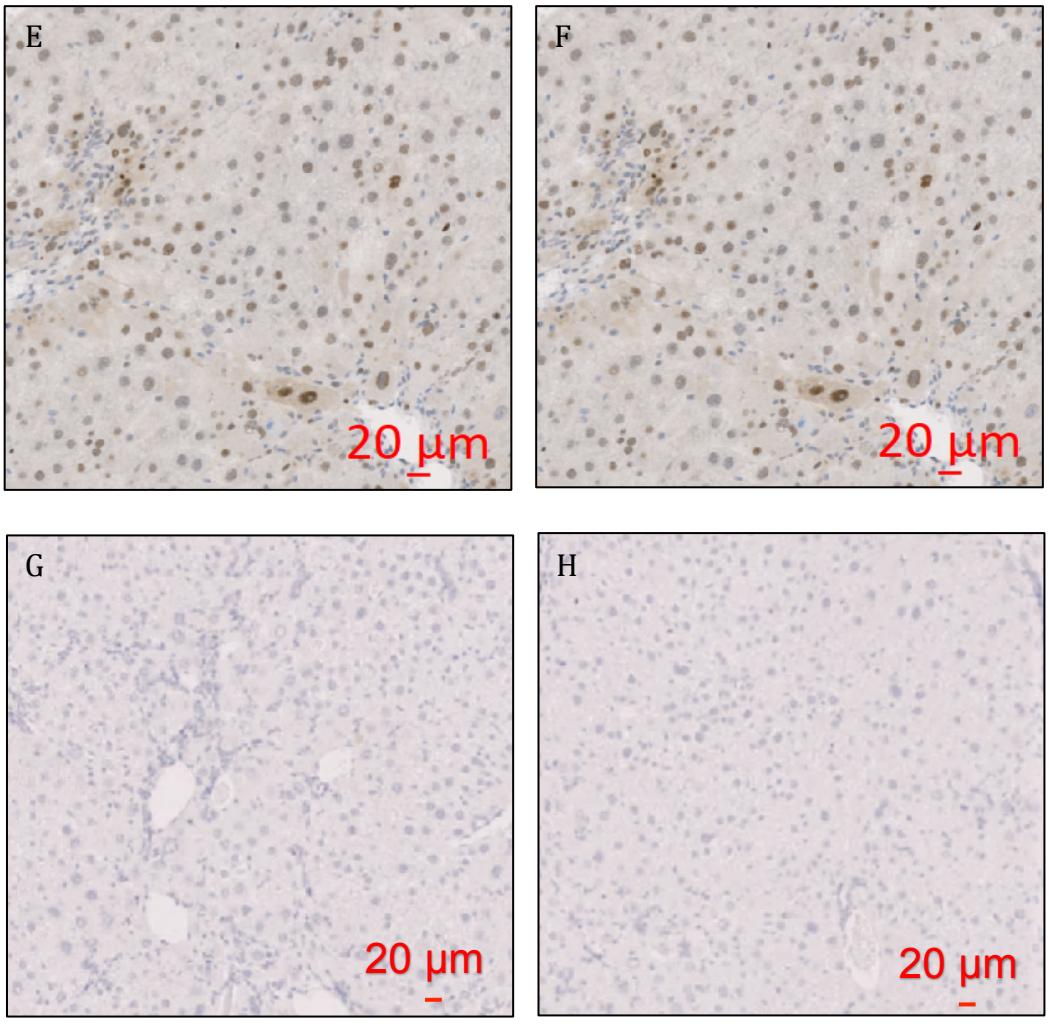




Pharmaxis TAA model: Ki67

VEHICLE

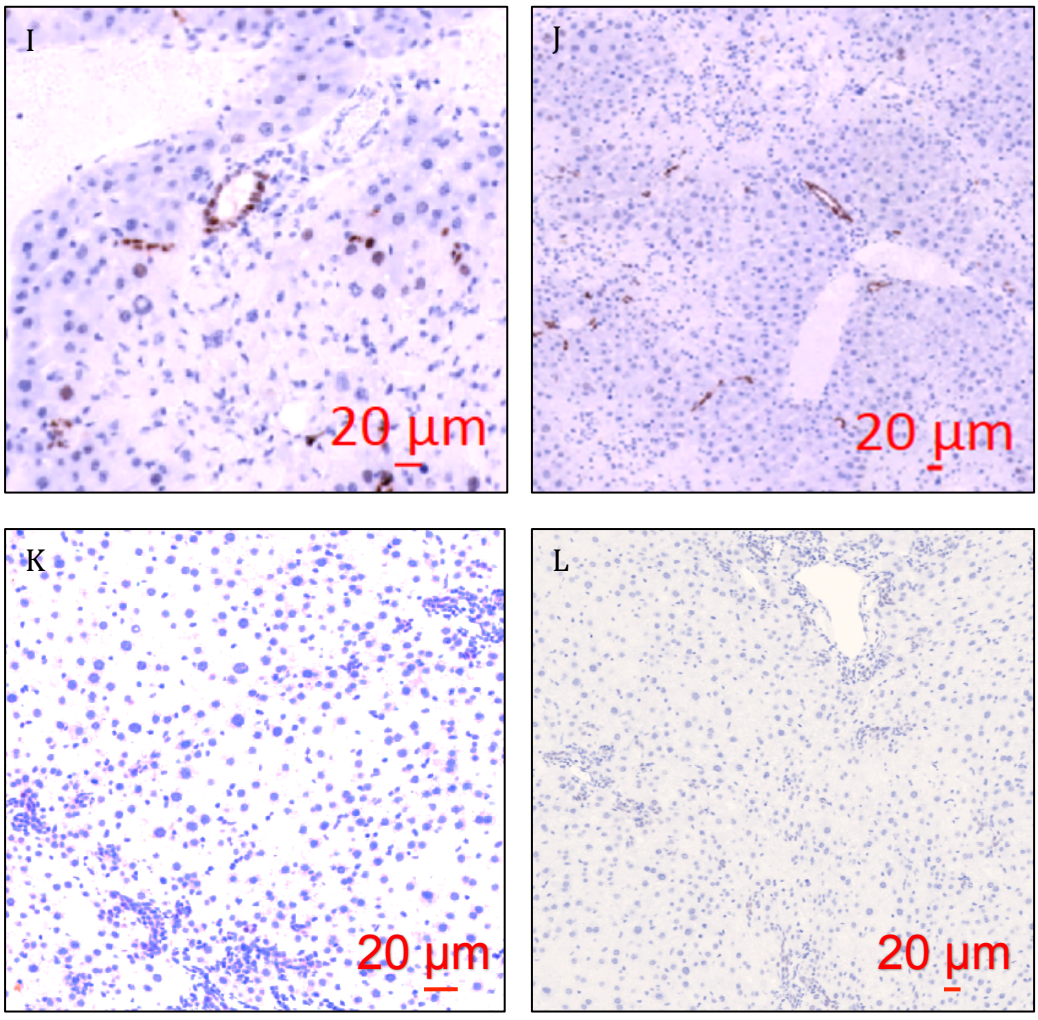
PXS5303



Pharmaxis TAA model: SOX-9

VEHICLE

PXS5303



Pharmaxis TAA model: EpCAM

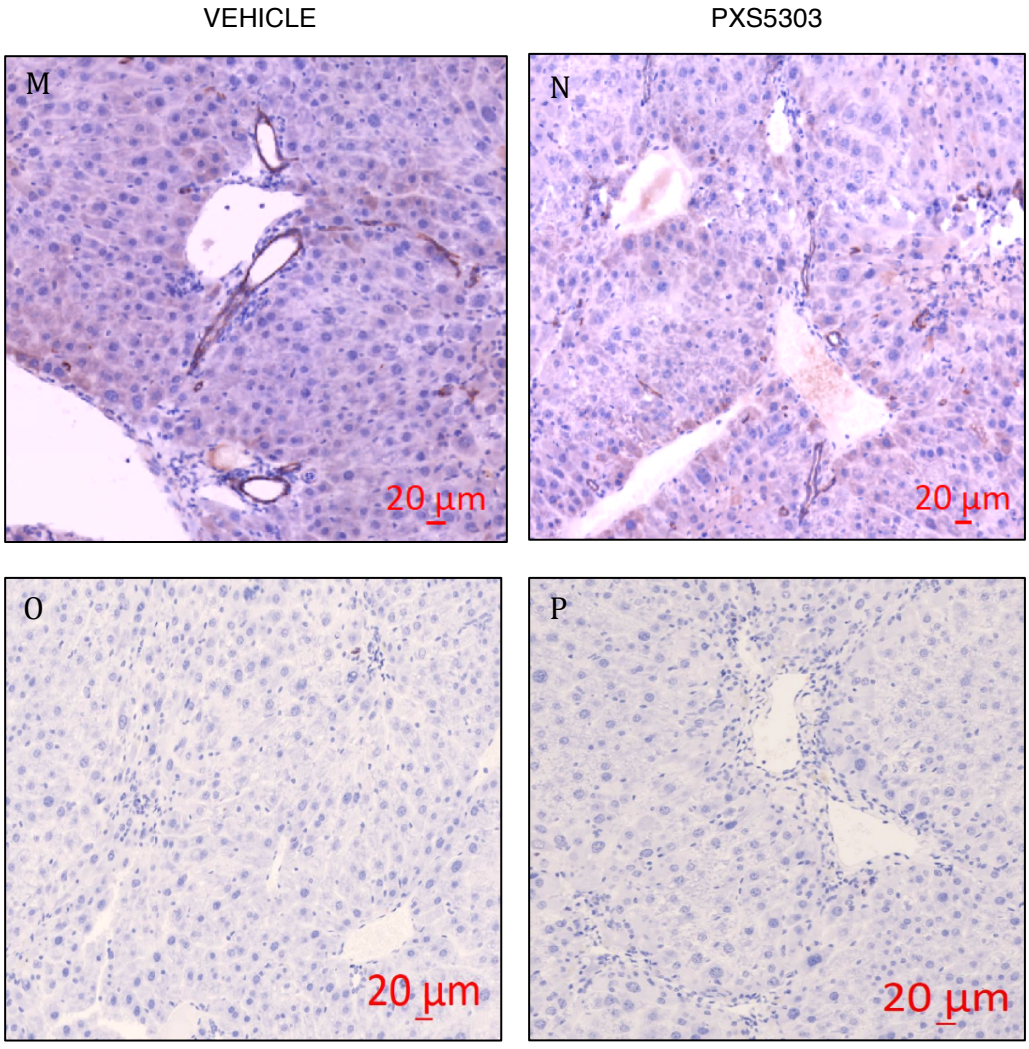


Figure 3.5 (A) LOXL2 inhibition had little effect on apoptosis, and no effect on proliferation or differentiation in the TAA model. BALB/c mice received 12 weeks of TAA at a dose of 200 mg/kg via I.P. injection in addition to vehicle or PXS5303 orally from week 9, and were culled at week 12. Apoptosis, proliferation and differentiation was assessed using IHC for cleaved caspase 3 (A-D), Ki67 (E-H), and both SOX-9 (I-L) and EpCAM (M-P), respectively. The untreated is shown on the left and the PXS5303 treated group is on the right, with test antibodies on the top panel and corresponding isotype controls demonstrated below.

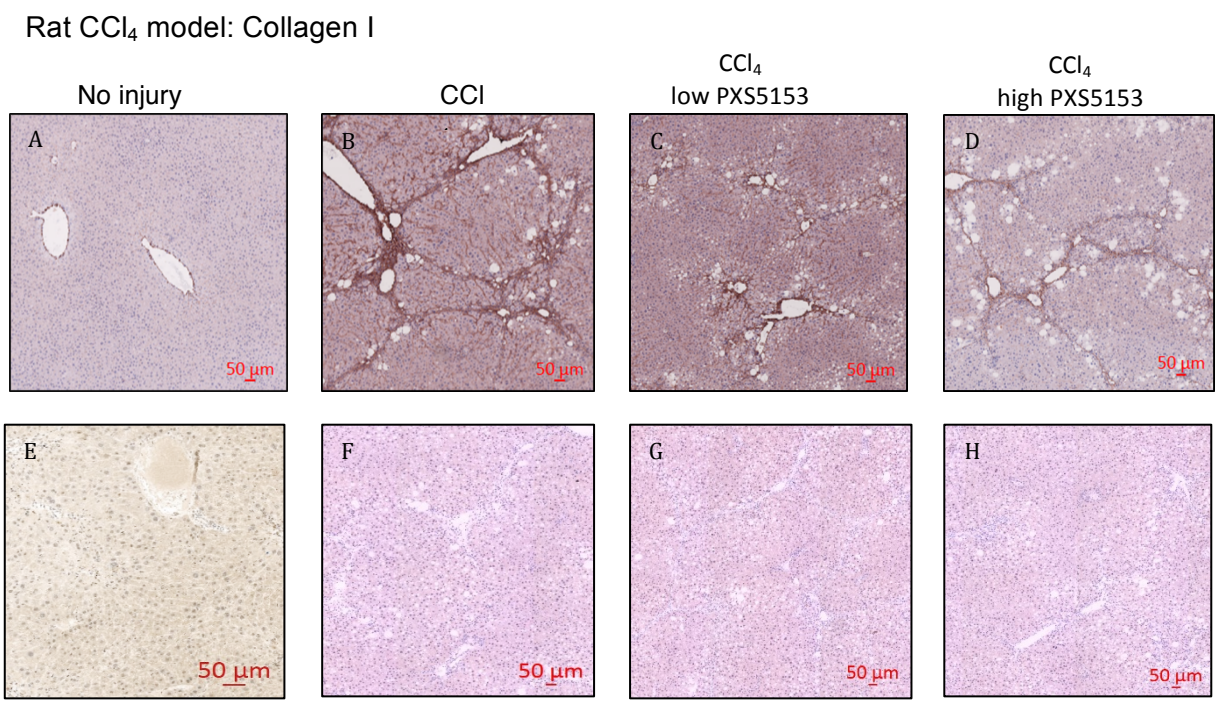


Figure 3.8 (A) Rats receiving oral CCl_4 develop fibrosis which is attenuated by LOXL2 inhibition. Sprague Dawley rats were administered with vehicle (vehicle), or 0.25 µL/g CCl_4 orally 3 times per week for 6 weeks (CCl_4). In addition to CCl_4, 15 mice received low dose (low) PXS5153 from day 0, or high dose (high) PXS5153 from week 4. At week 6 the rats were sacrificed and dissected liver tissue was sectioned, frozen, and later cut for paraffin embedded slides. These were stained using immunohistochemistry for Collagen-1-alpha (A-D) on the top panel, and corresponding isotype controls demonstrated below (E-H).

Rat CCl_4 model: Myeloperoxidase

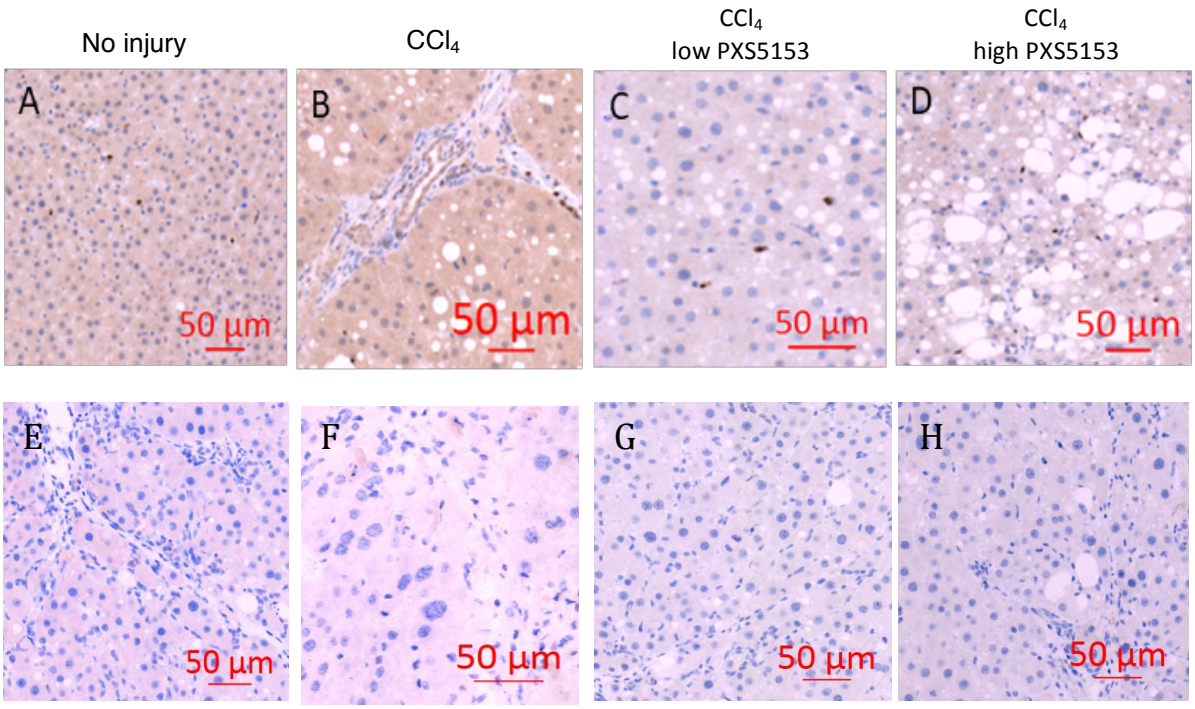


Figure 3.10 (A) Minimal changes in apoptosis and the ductular reaction were seen in rats receiving LOXL2 inhibitor following injury with CCl_4. Sprague Dawley rats were administered with vehicle, or 0.25 µL/g CCl_4 P.O. 3 times per week for 6 weeks. In addition, 15 mice received low dose PXS5153 from day 0 or high dose PXS5153 from week 4. At week 6 the rats were sacrificed and dissected liver tissue was sectioned, frozen, and later cut for paraffin embedded slides. These were stained using immunohistochemistry for MPO (A-H). Comparison was made between rats subjected to CCl_4 liver injury and rats receiving low and high dose PXS5153 in addition to CCl_4 induced liver injury, and uninjured rats as a control, in addition to corresponding isotype controls demonstrated on the panel below.

Rat CCl_4 model: Cleaved caspase 3

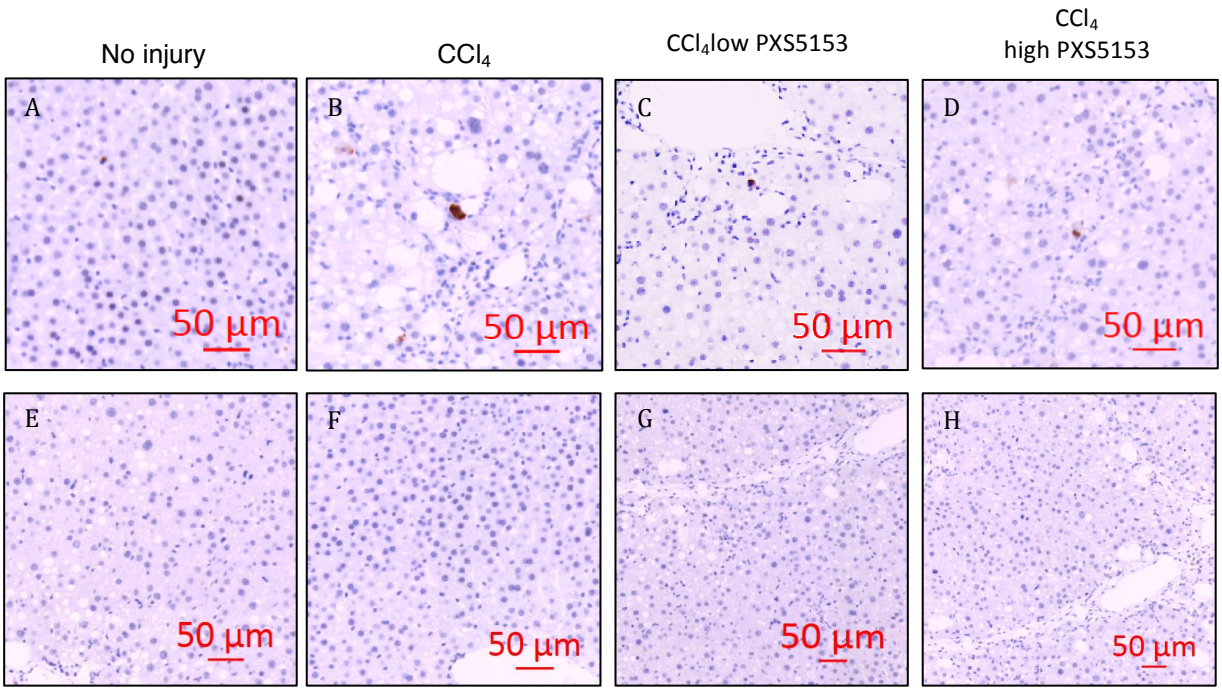


Figure 3.10 (A) Minimal changes in apoptosis and the ductular reaction were seen in rats receiving LOXL2 inhibitor following injury with CCl_4. Sprague Dawley rats were administered with vehicle, or 0.25 µL/g CCl_4 P.O. 3 times per week for 6 weeks. In addition, 15 mice received low dose PXS5153 from day 0 or high dose PXS5153 from week 4. At week 6 the rats were sacrificed and dissected liver tissue was sectioned, frozen, and later cut for paraffin embedded slides. These were stained using immunohistochemistry for cleaved caspase 3 (A-H). Comparison was made between rats subjected to CCl_4 liver injury and rats receiving low and high dose PXS5153 in addition to CCl_4 induced liver injury, and uninjured rats as a control. IHC for cleaved caspase 3 is demonstrated in the top panel with corresponding isotype controls demonstrated below.

Rat CCl_4 model: EpCAM

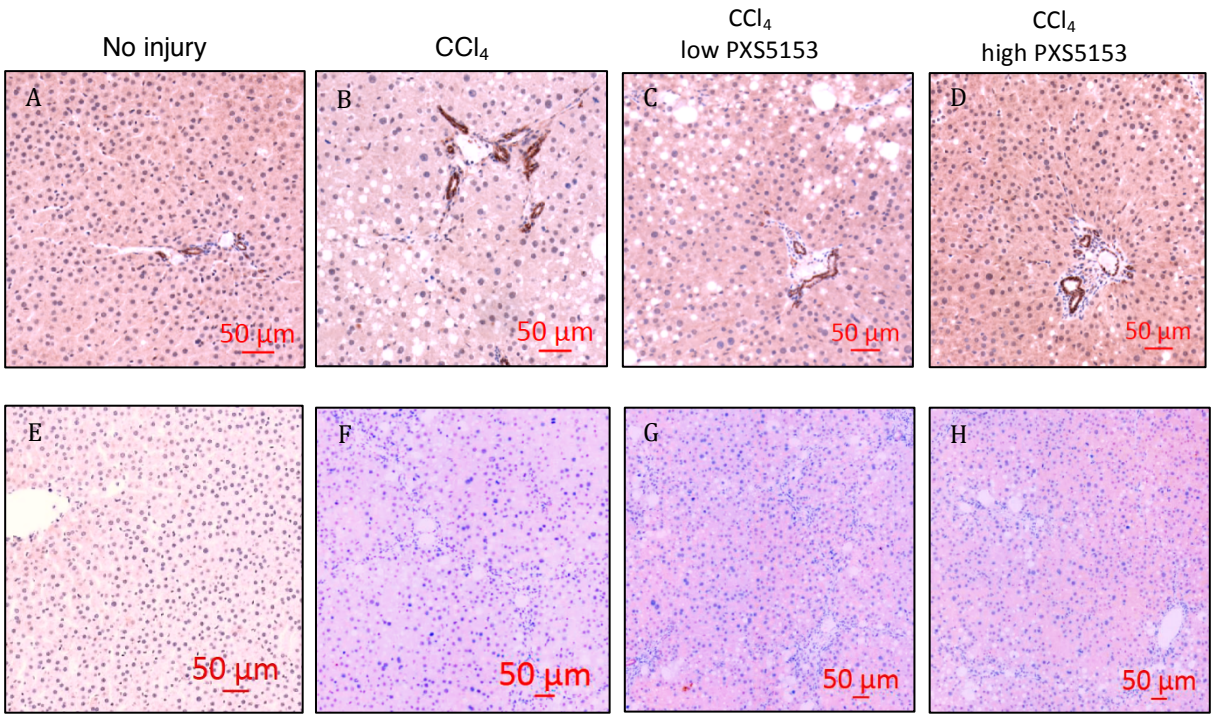


Figure 3.10 (A) Minimal changes in apoptosis and the ductular reaction were seen in rats receiving LOXL2 inhibitor following injury with CCl_4. Sprague Dawley rats were administered with vehicle, or 0.25 µL/g CCl_4 P.O. 3 times per week for 6 weeks. In addition, 15 mice received low dose PXS5153 from day 0 or high dose PXS5153 from week 4. At week 6 the rats were sacrificed and dissected liver tissue was sectioned, frozen, and later cut for paraffin embedded slides. These were stained using immunohistochemistry for EpCAM, on the panel above, with the isotype controls in the panel below (A-H).

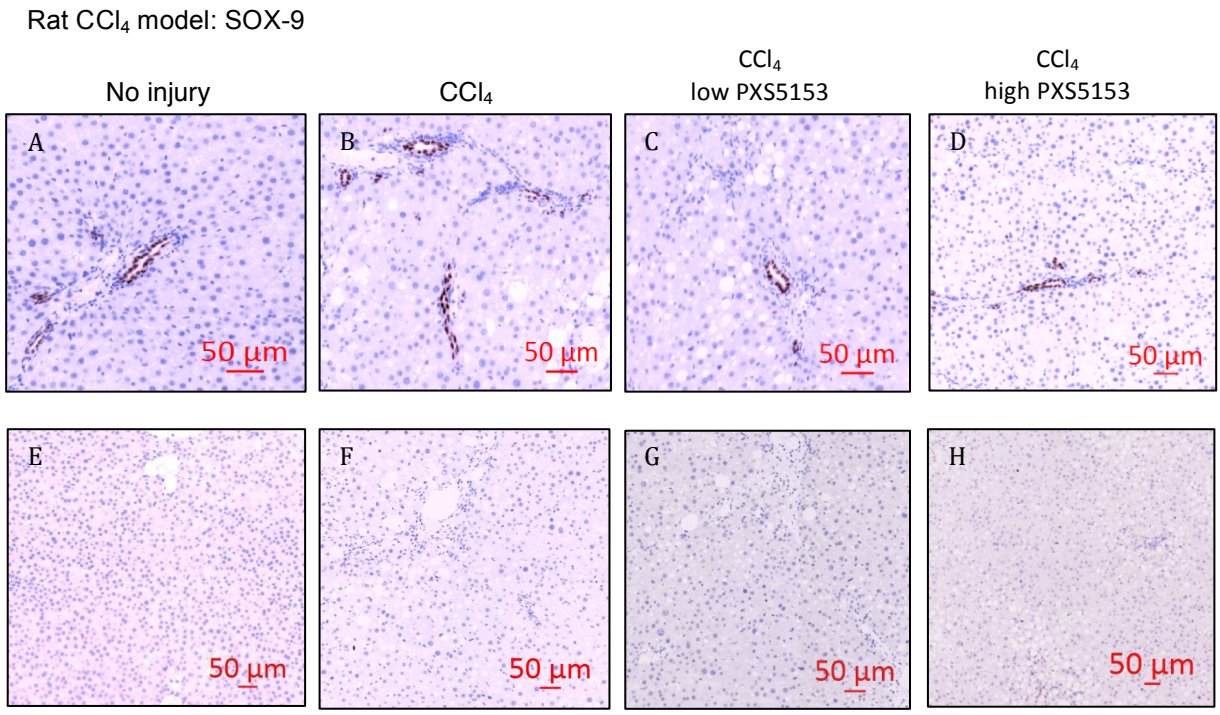


Figure 3.10 (A) Minimal changes in apoptosis and the ductular reaction were seen in rats receiving LOXL2 inhibitor following injury with CCl_4. Sprague Dawley rats were administered with vehicle, or 0.25 µL/g CCl_4 P.O. 3 times per week for 6 weeks. In addition, 15 mice received low dose PXS5153 from day 0 or high dose PXS5153 from week 4. At week 6 the rats were sacrificed and dissected liver tissue was sectioned, frozen, and later cut for paraffin embedded slides. These were stained using immunohistochemistry for cleaved SOX-9 (A-H). Comparison was made between rats subjected to CCl_4 liver injury and rats receiving low and high dose PXS5153 in addition to CCl_4 induced liver injury, and uninjured rats as a control, demonstrated in the top panel, in addition to isotype controls demonstrated below.

FVB *Mdr2*-/- model: α-SMA

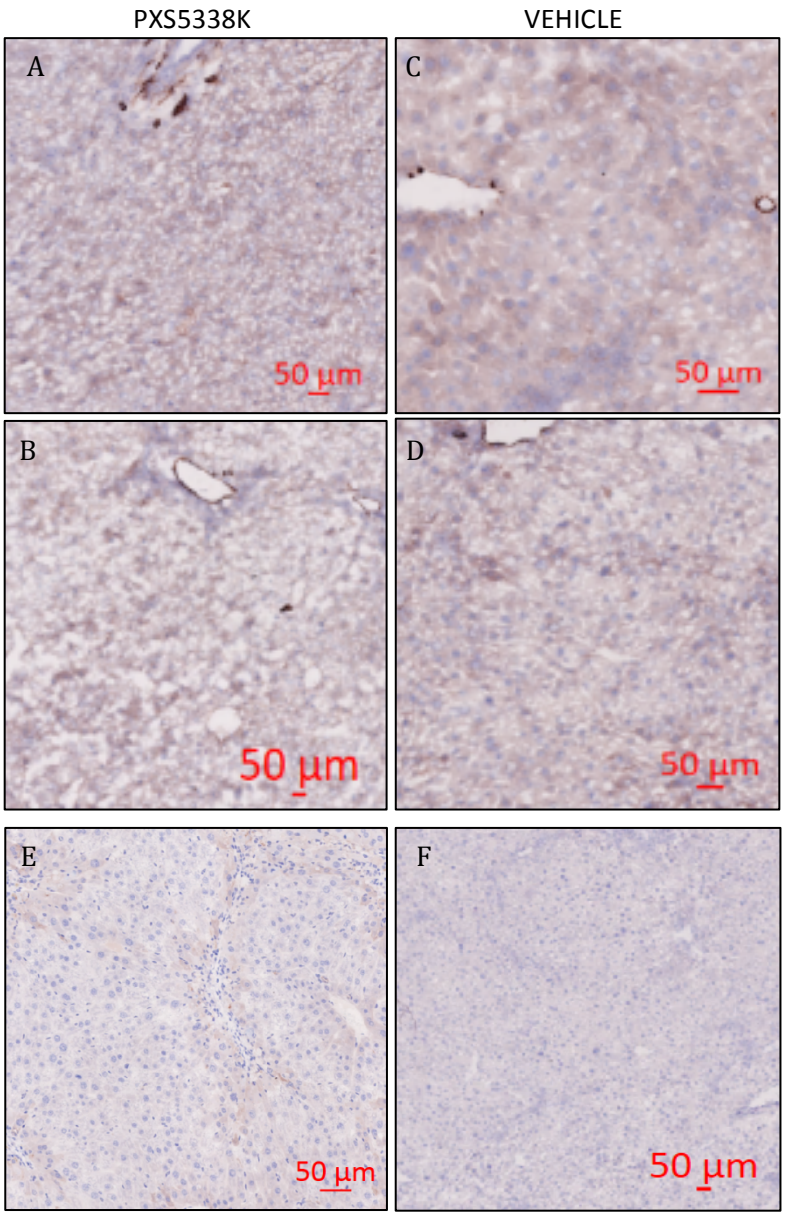


Figure 4.5 (S) PXS5338K had no effect on hepatic stellate cell activation. Immunohistochemistry was performed on liver tissue cut on frozen slides from FVB *Mdr2*-/- mice receiving eight or nine gavages of either PXS5338K (A and B respectively) at 10 mg/kg, or 9 gavages of vehicle (C, D), for α-SMA. Isotype controls are shown for each group respectively (E, F).

FVB *Mdr2-/-* model: cleaved caspase 3

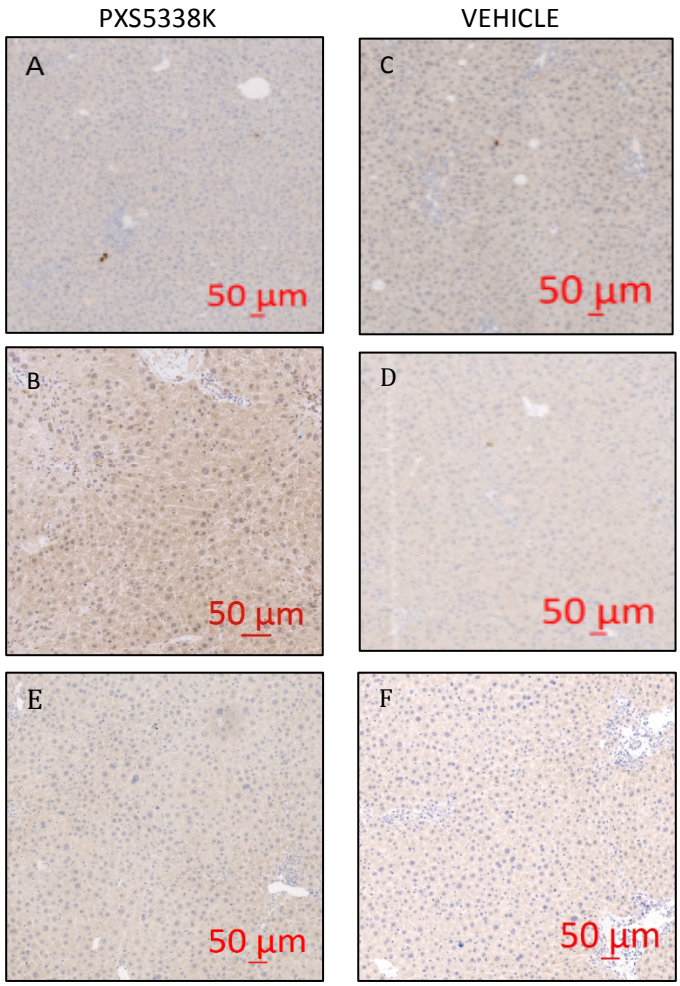


Figure 4.6 (A) PXS5338K has no effect on apoptosis in the liver. Immunohistochemistry was performed on liver tissue cut on paraffin slides from FVB *Mdr2-/-* mice receiving eight or nine gavages of either PXS5338K (A and B respectively, and isotype control E) at 10 mg/kg, or 9 gavages of vehicle (D,E and isotype control F), for cleaved caspase 3.

FVB *Mdr2*-/- model: CD45

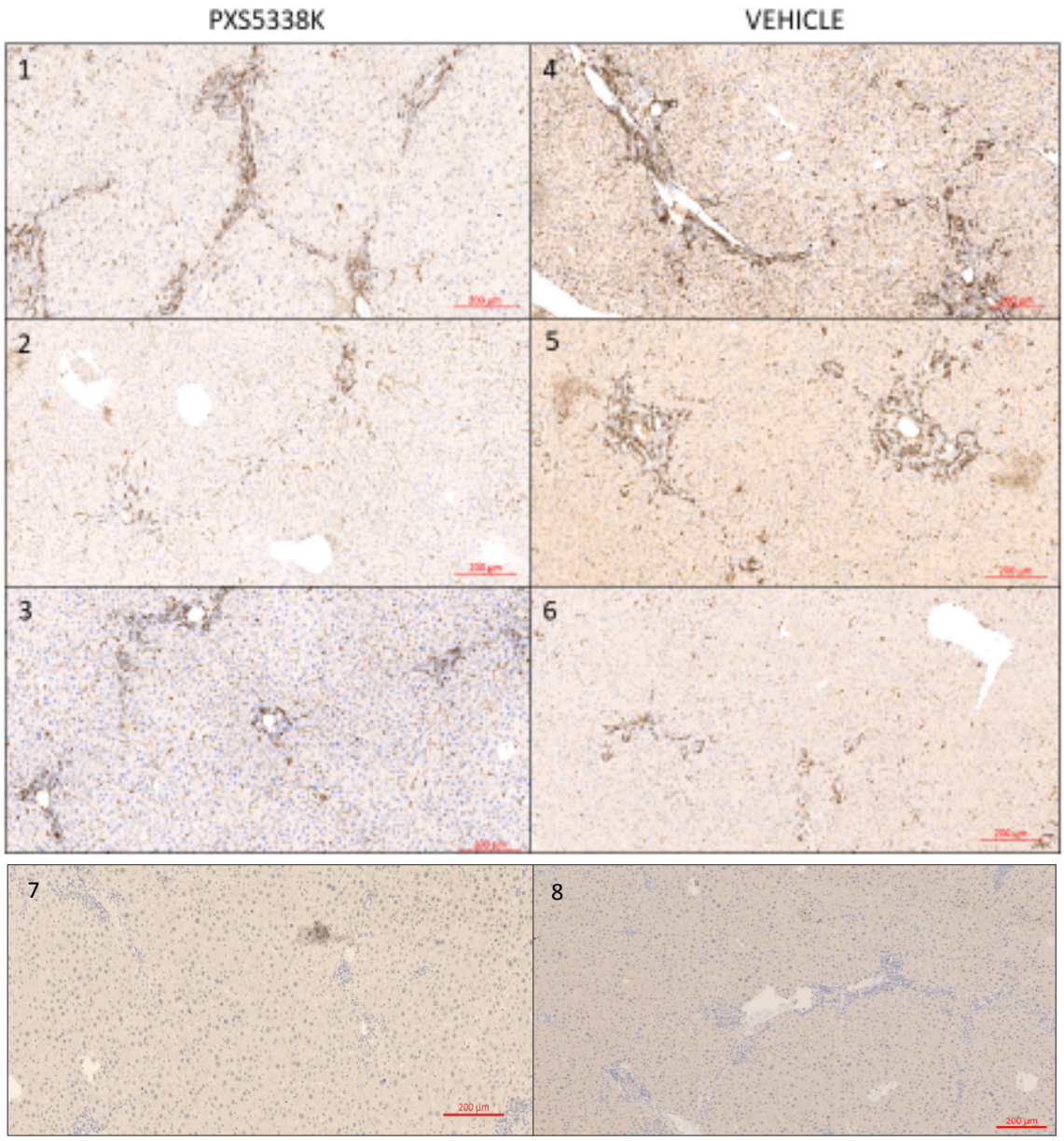


Figure 4.7 (A) Immune cell infiltration as measured by CD45 was similar in mice receiving PXS5338K and vehicle. Immunohistochemistry was performed on liver tissue cut on paraffin slides from FVB *Mdr2*-/- mice receiving five, eight or nine gavages of either PXS5338K (mice 1, 2 and 3 respectively) at 10 mg/kg P.O., or 9 gavages of vehicle P.O. (mice 4-6), for CD45. Isotype controls for mice receiving PXS5338K and vehicle are demonstrated in (7) and (8) respectively.

FVB *Mdr2-/-* model: SOX-9

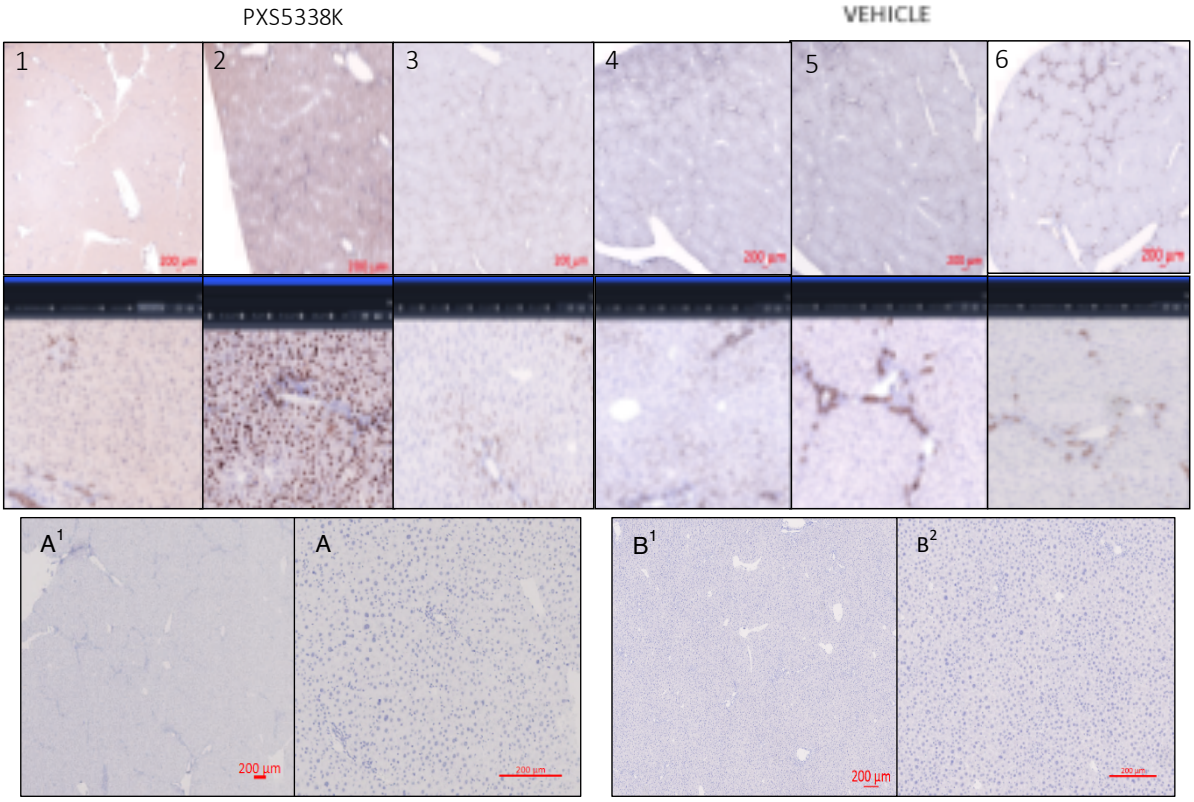
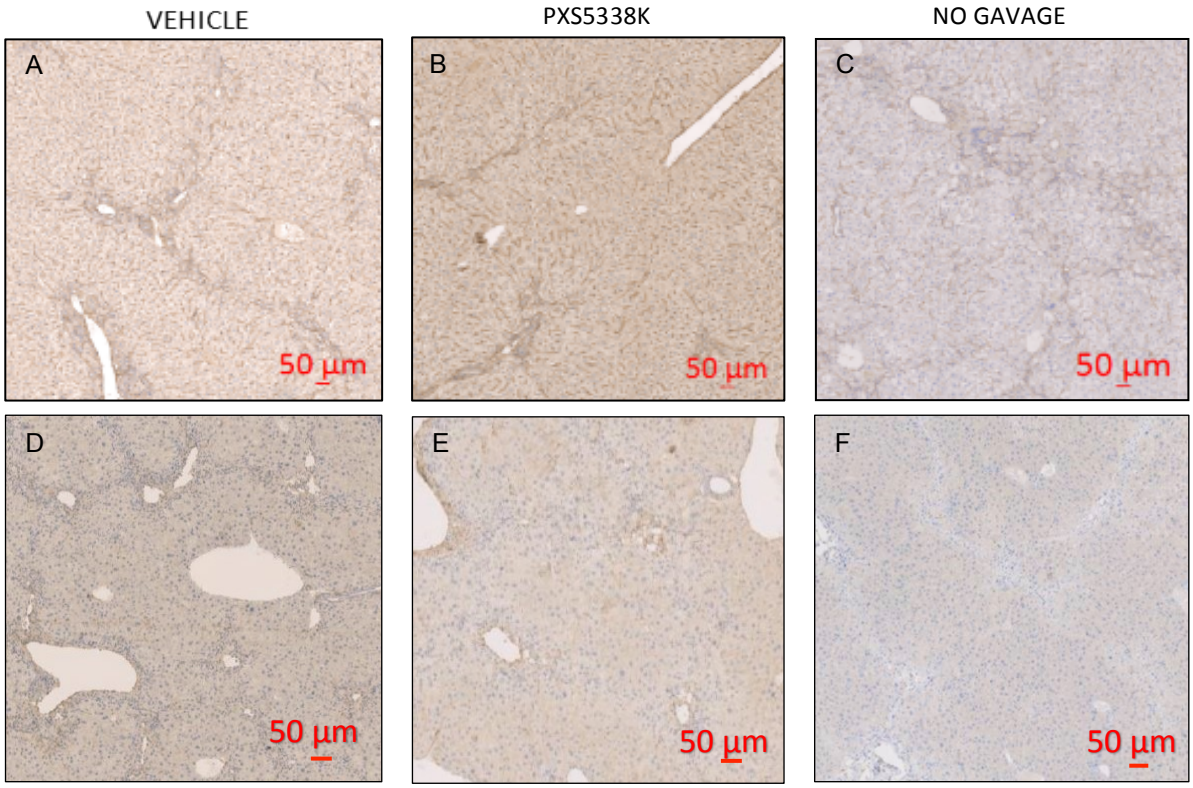
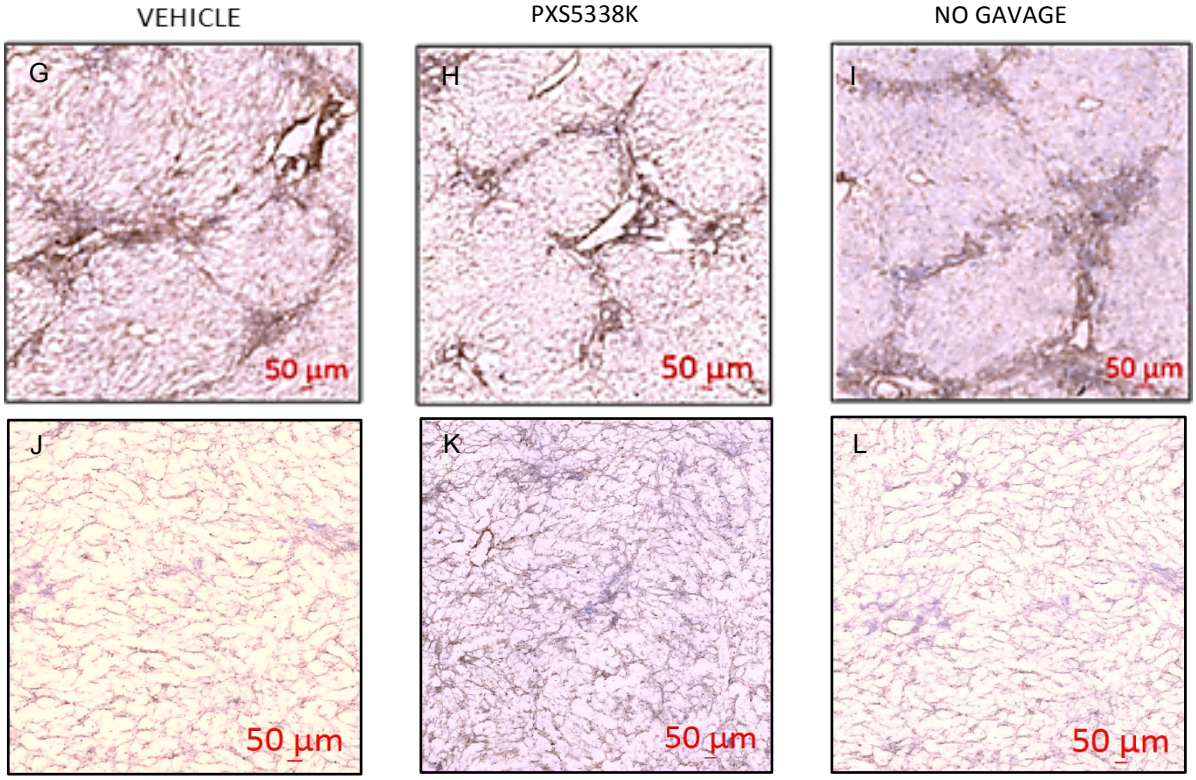


Figure 4.8 (A) Some FVB *Mdr2-/-* mice receiving PXS5338K displayed a different pattern of SOX-9 positive cells compared with those receiving vehicle, in whom biliary structures were predominantly stained positive. Immunohistochemistry was performed on liver tissue cut on paraffin slides from FVB *Mdr2-/-* mice receiving gavage of either PXS5338K (1-3) at 10 mg/kg, or 9 gavages of vehicle (4-6), for SOX-9. Liver tissue from all 6 animals are shown at low and high magnification; those mice receiving PXS5338K (5, 8 and 9 doses for animals in 1, 2 and 3 respectively), and 9 doses of vehicle in animals 4, 5 and 6. Isotype controls are demonstrated for animals receiving PXS5338K or vehicle (A^1 and A^2) and (B^1 and B^2), respectively.

C57Bl6/ *Mdr2-/-* model: Collagen I



Collagen III



Alpha-SMA

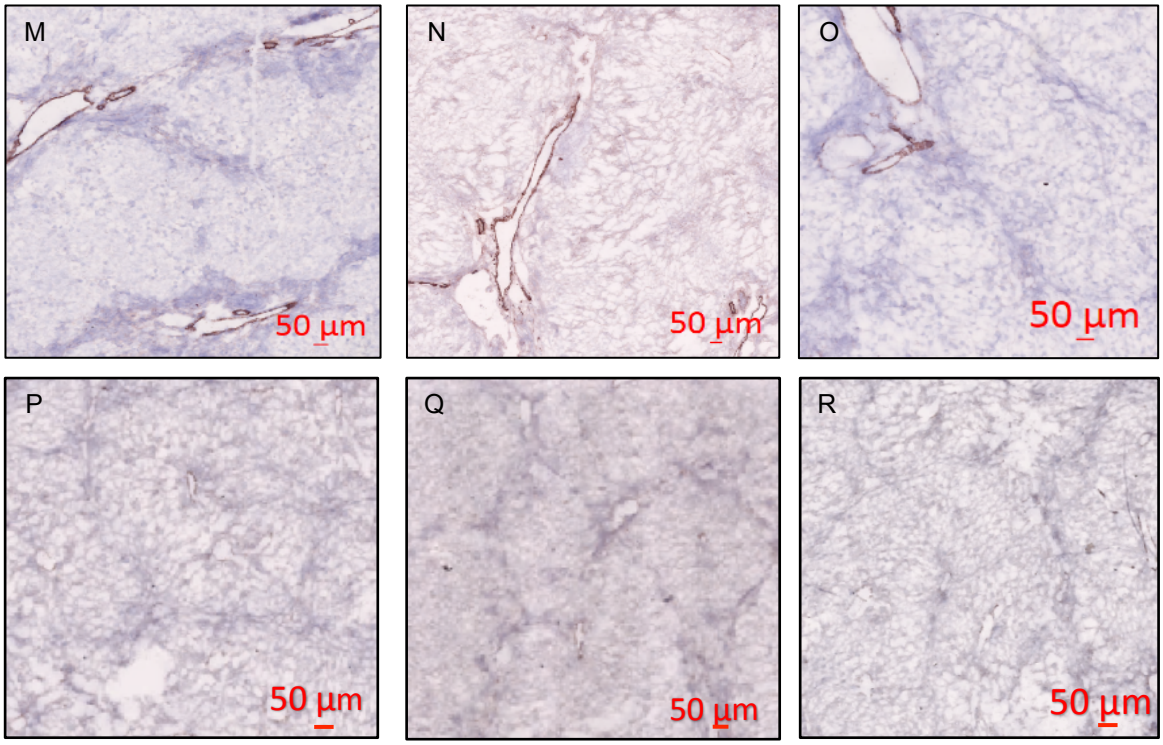


Figure 4.13 (A) PXS5338K did not improve fibrosis in C57Bl6/ *Mdr2-/-* mice for liver injury were no different between animals administered with PXS5338K vs vehicle, or no gavage. 41 nine week old C57Bl/6 *Mdr2-/-*mice received 9 doses of vehicle, 3 mg/kg PXS5338K, or nil by oral gavage. Paraffin embedded, or frozen, slides were cut at 3 µm and IHC with morphometric analysis was performed for PSR (A-E) and collagen I (F-J) (analysis at low and high resolution), collagen III (K-N) and α-SMA (O-R). Test antibodies are in the top panels, with corresponding isotype controls demonstrated below each group.

C57Bl6/ *Mdr2-/-* model: Sox-9

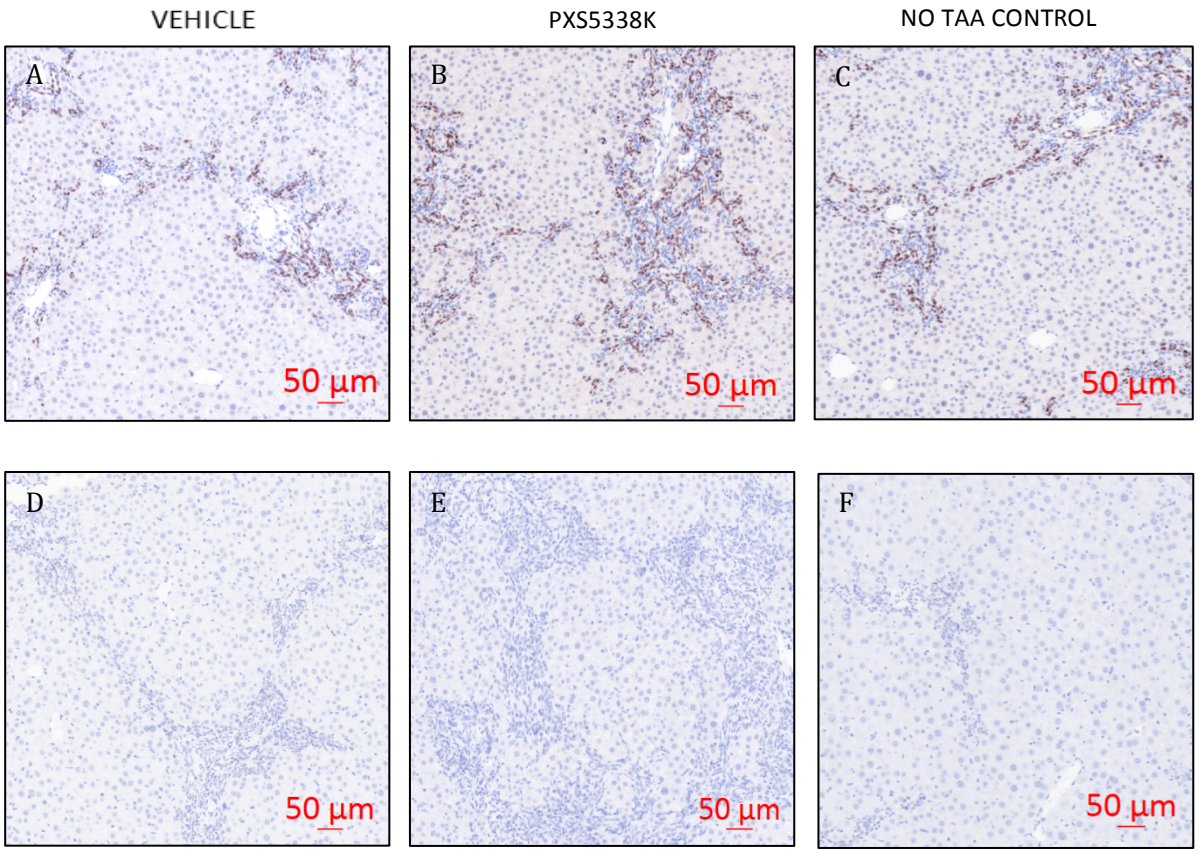
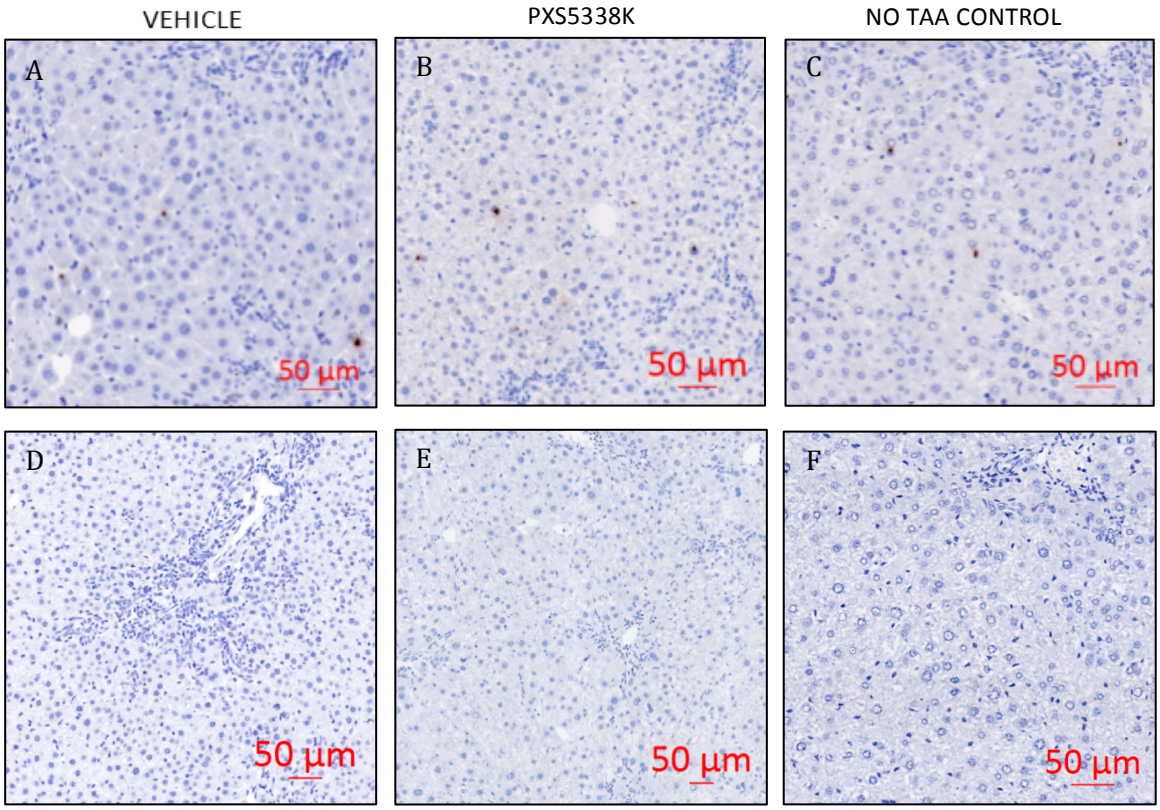
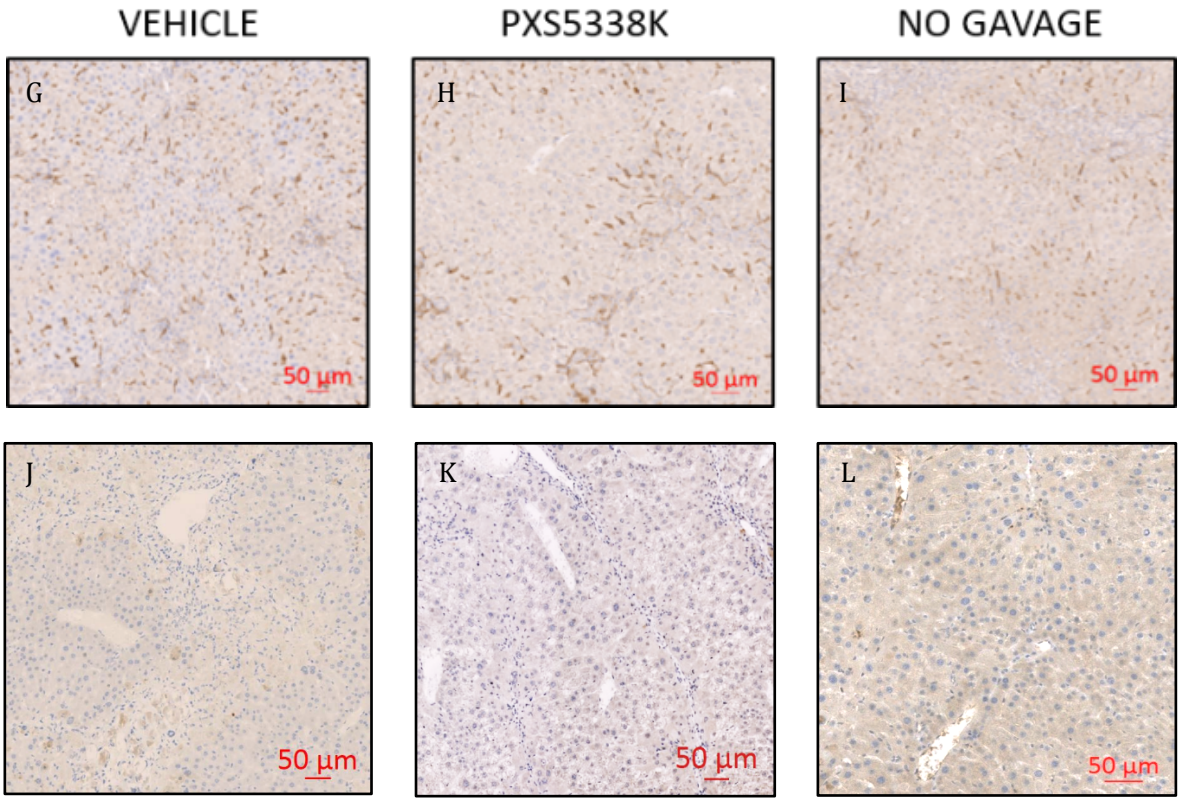


Figure 4.16 (A) Administration of PXS5338K at 3 mg/kg does not alter cell proliferation or differentiation according to SOX-9 IHC in C57Bl6/ *Mdr2-/-* mice. 36 nine week old C57Bl/6 *Mdr2-/-* mice received 9 doses of vehicle, or 3 mg/kg PXS5338K, by oral gavage, with 5 C57Bl/6 receiving no gavage. Paraffin-embedded liver tissue was used to assess presence of SOX-9 with IHC and representative images are demonstrated with isotype controls for each group below (A-F).

C57Bl6/ *Mdr2-/-* B220



C57Bl/6 *Mdr2-/-* model: F4/80



C57Bl/6 *Mdr2-/-* model: Ly6G

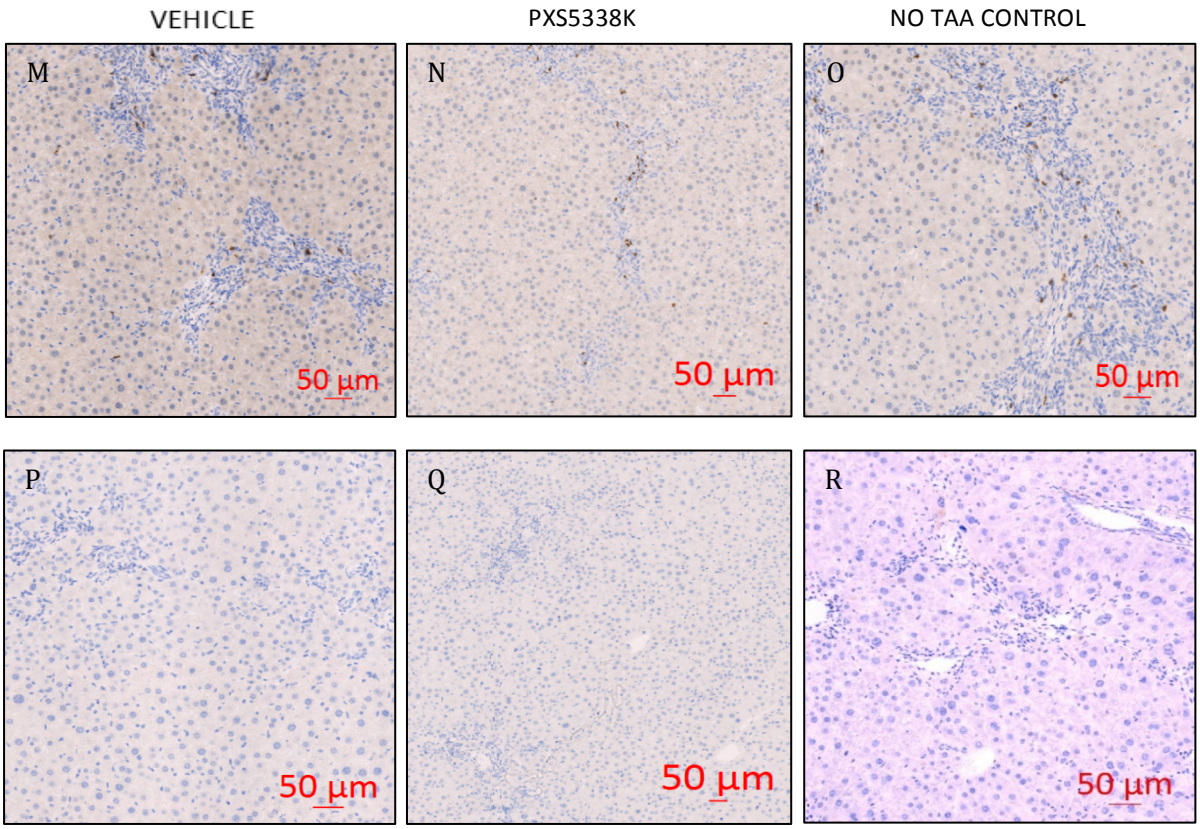
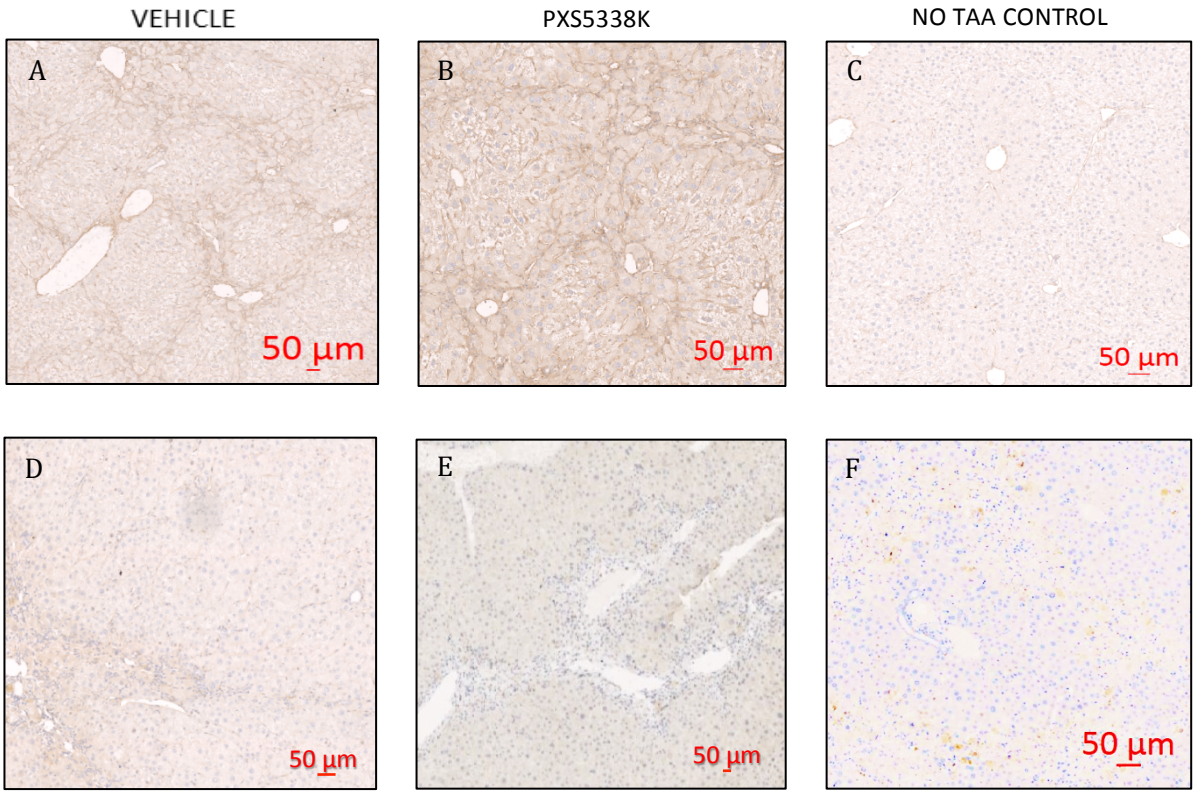
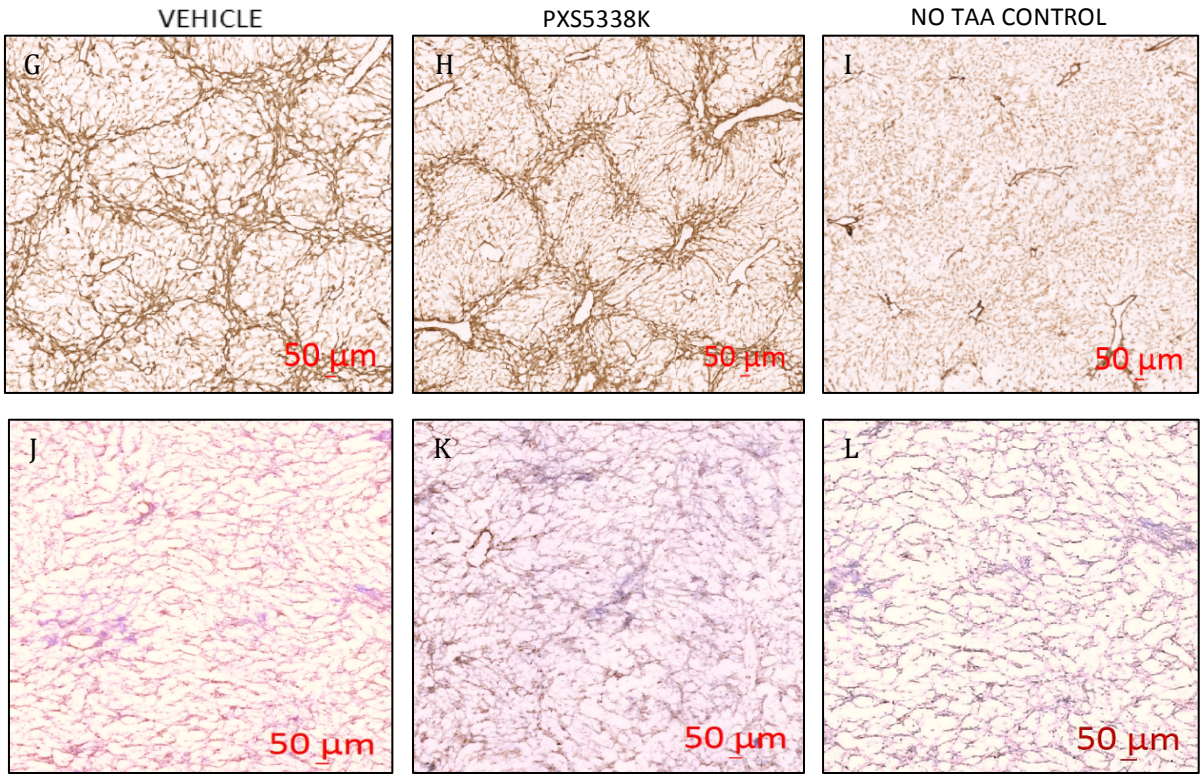


Figure 4.20 (A) PXS5338K does not alter liver infiltration of B220 CD45 positive, F4/80 positive or LY6G positive cells during liver injury. 36 nine week old C57Bl/6 *Mdr2-/-*mice received 9 doses of vehicle, or 3 mg/kg PXS5338K, by oral gavage, with 5 C57Bl/6 receiving no gavage. Paraffin-embedded liver tissue was used to assess presence of B220 CD45+ (A-F), F4/80+ (G-L) and Ly6G+ cells (M-R), and are demonstrated in the top panels, with corresponding isotype controls below.

TAA model: Collagen I



TAA model: Collagen III



TAA model: α-SMA

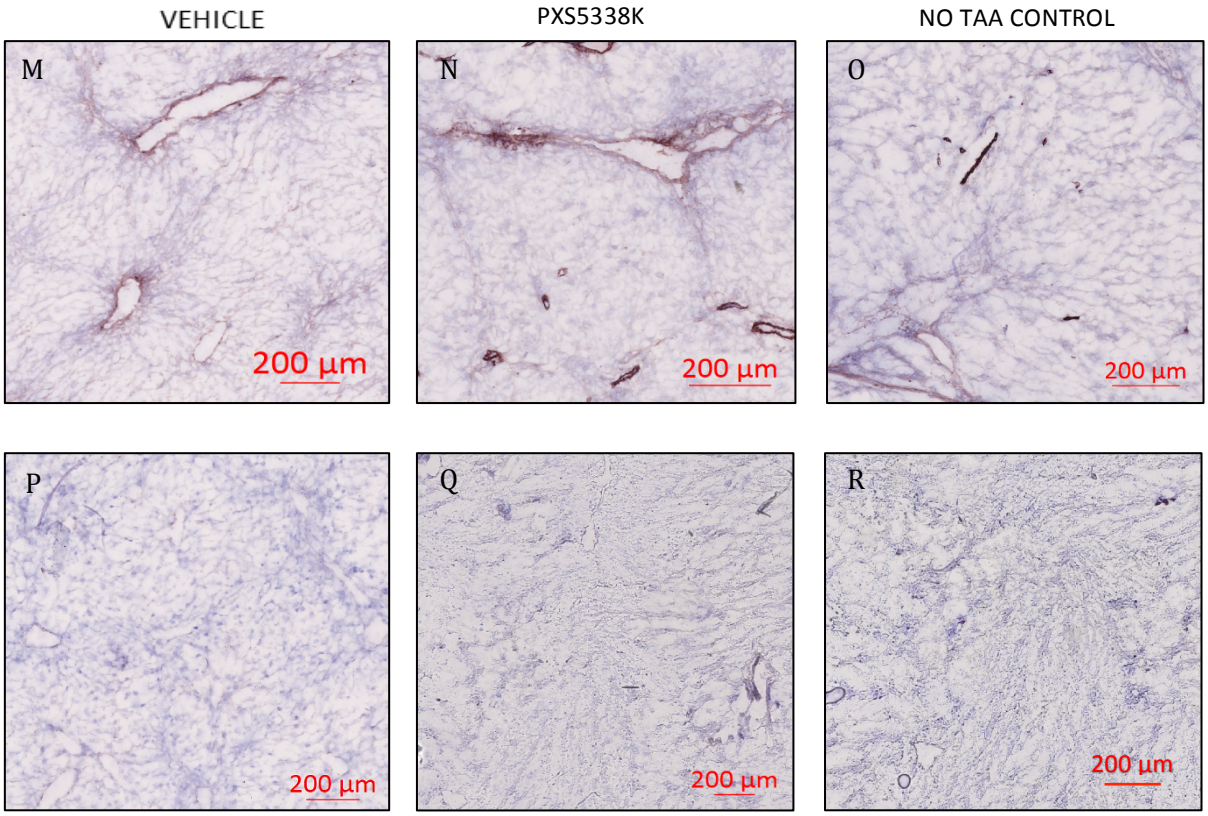


Figure 5.8 (A) 16 weeks of TAA induced liver fibrosis in mice which was not ameliorated by PXS5338K. Mice were exposed to 16 weeks of TAA ad libitum in drinking water with 6 weeks gavage of either vehicle or PXS5338K from week 10. A comparison group received no TAA. IHC was performed on paraffin embedded liver sections for Collagen I, collagen III and α-SMA (A-R), with test antibodies in the top panel and associated isotype controls for each group demonstrated below.

TAA model SOX-9

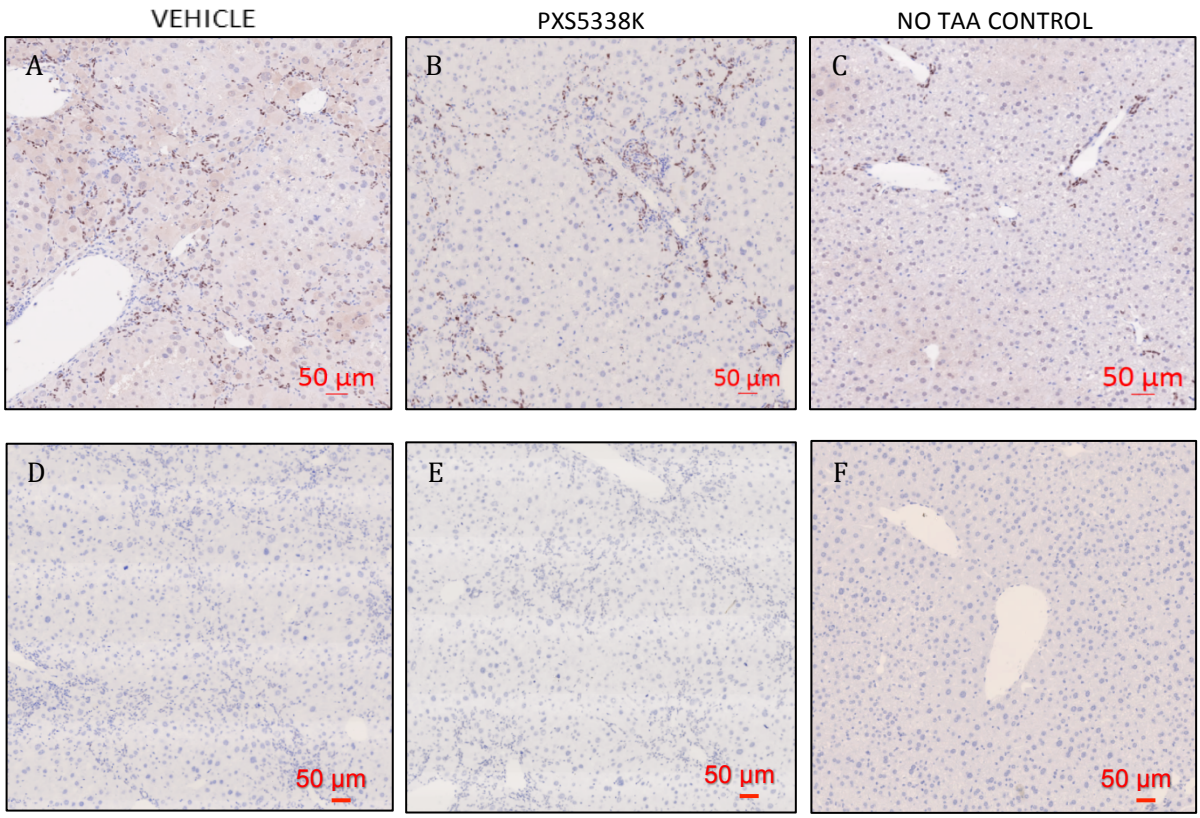
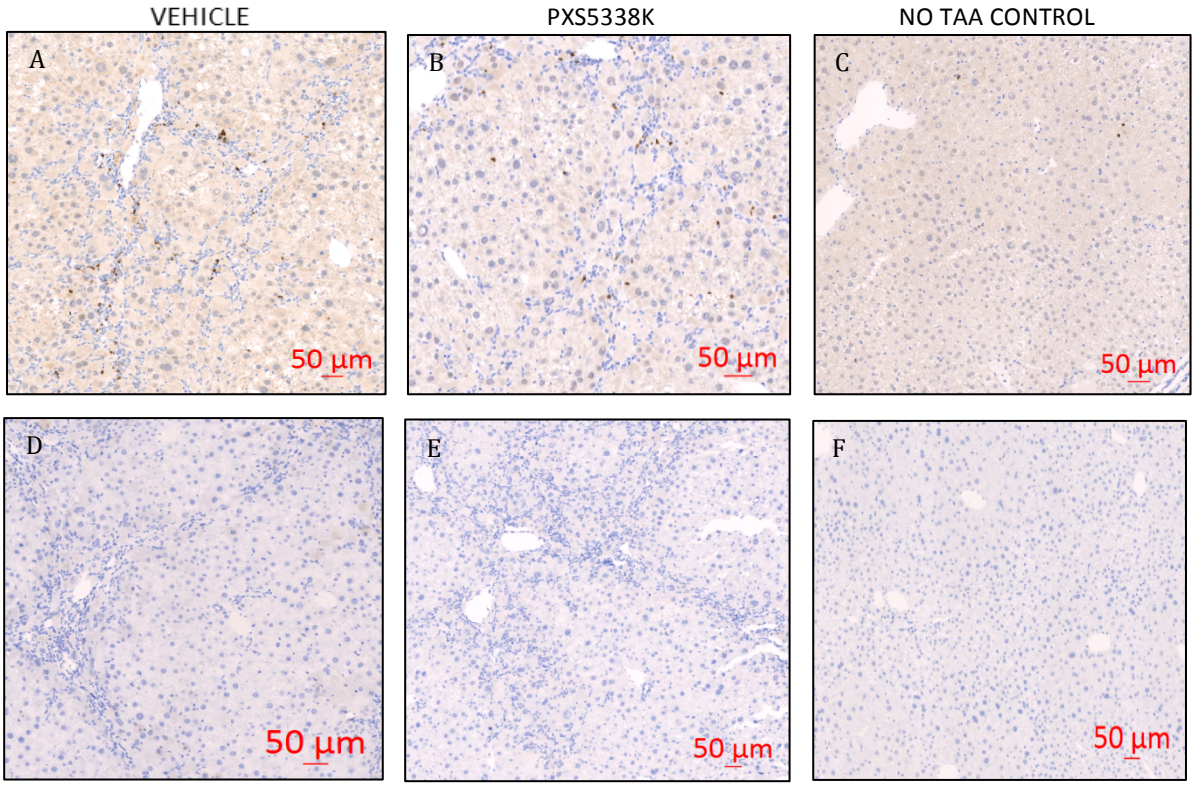
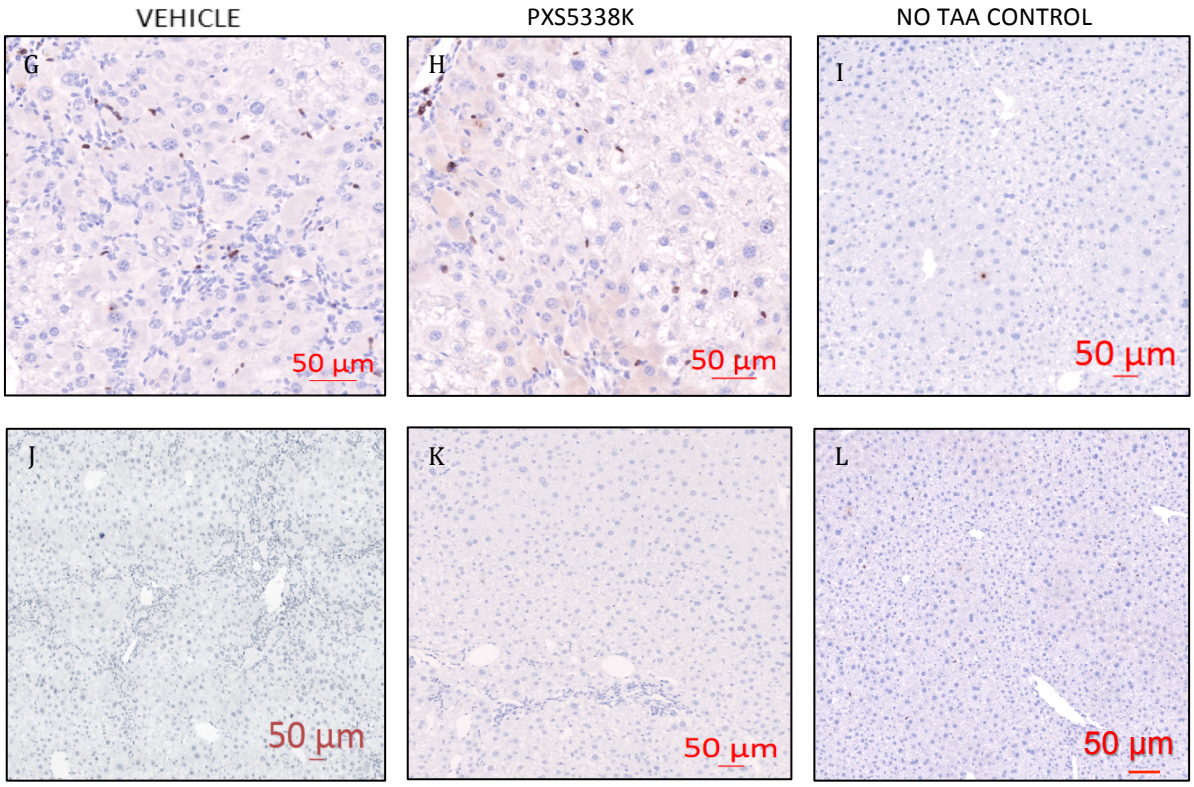


Figure 5.10 (A) SOX-9 expression is upregulated in TAA-induced liver injury but not reduced by inhibition of LOXL2 by PXS5338K. Mice were exposed to 16 weeks of TAA *ad-libitum* in drinking water with 6 weeks gavage of either vehicle or PXS5338K from week 10. A comparison group received no TAA. IHC was performed on paraffin embedded liver sections for SOX-9 and associated isotype controls are demonstrated for each group (A-F).

TAA model: Ly6g



TAA model: B220



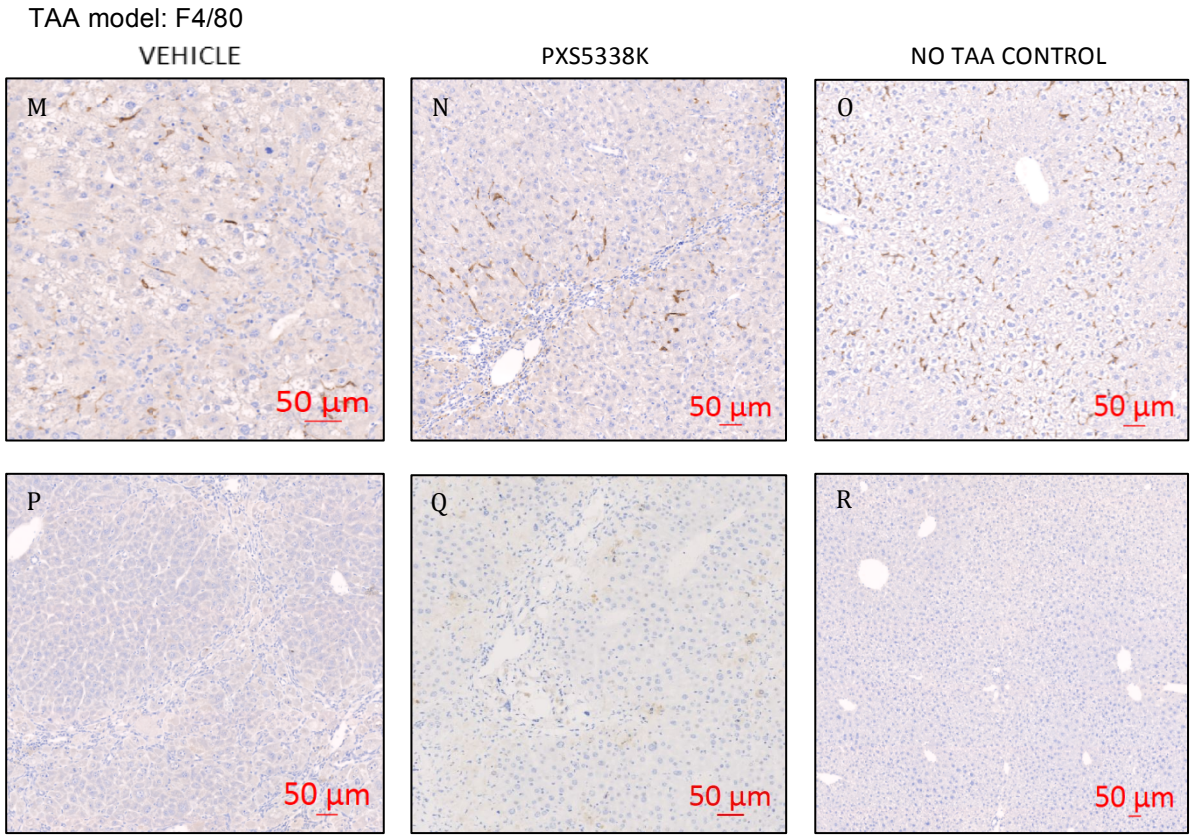


Figure 5.13 (A) Comparison of markers of inflammatory cells in the liver showed no differences in immune cell populations between mice receiving vehicle or PXS5338K by oral gavage. IHC for Ly6G, B220 and F4/80 was performed on paraffin embedded liver sections from mice exposed to 16 weeks of TAA *ad-libitum* in drinking water with 6 weeks gavage of either vehicle or PXS5338K from week 10. A comparison group received no TAA. Test antibodies are demonstrated in each top panel, with corresponding isotype controls shown below (A-R).

Resolution model: Collagen I

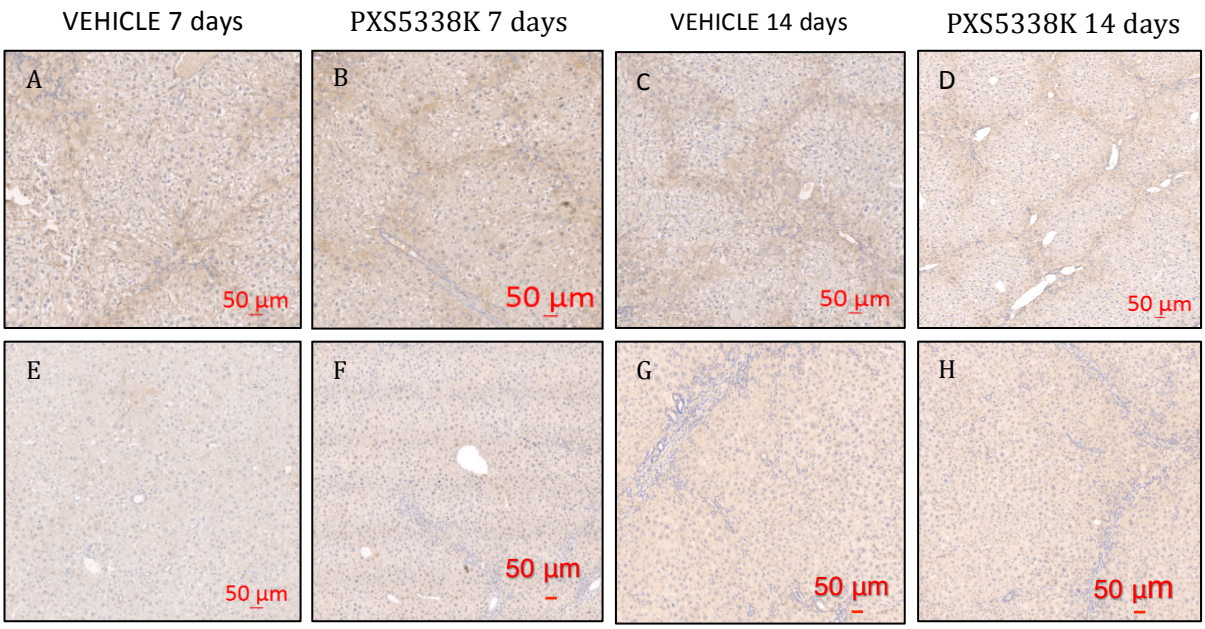


Figure 5.17 (A) PXS5338K may reduce collagen I expression in mice recovering from TAA induced liver injury. C57Bl/6 mice received 16 weeks of TAA followed by 7 or 14 days of vehicle or PXS5338K (3mg/kg) P.O. IHC was performed on paraffin embedded liver sections for collagen I (A-D) and are demonstrated with corresponding isotype controls for each group (E to H).

Resolution model: Collagen III

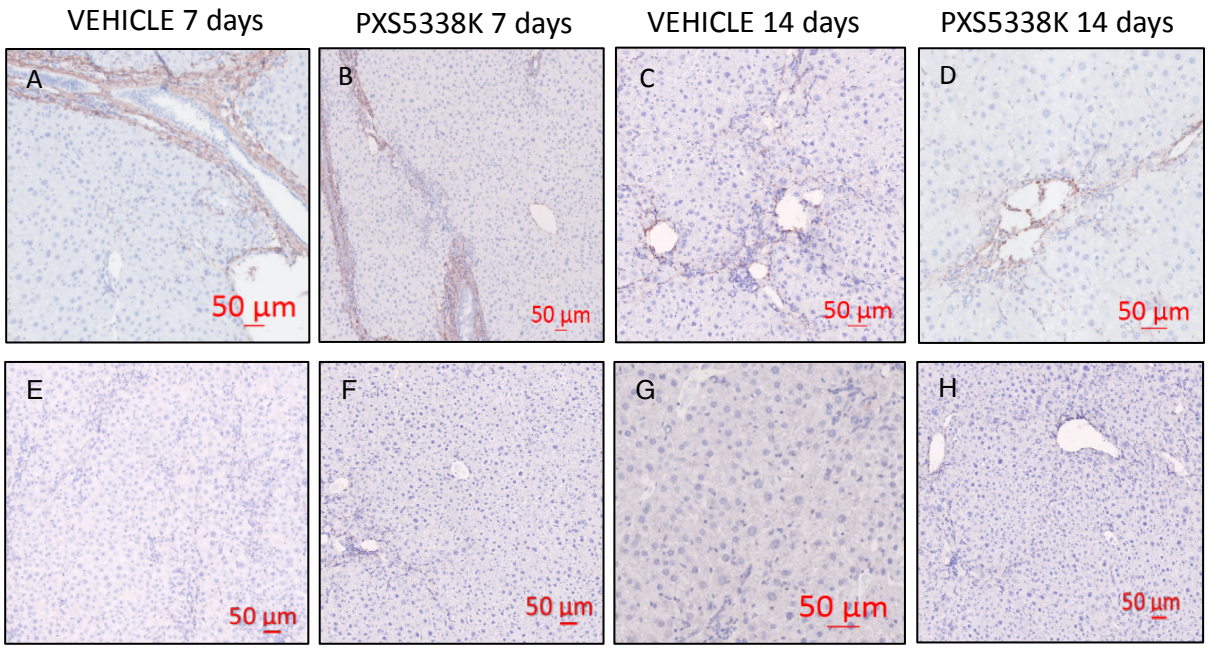


Figure 5.18 (A) PXS5338K did not alter collagen III expression in mice recovering from TAA induced liver injury. C57Bl/6 mice received 16 weeks of TAA followed by 7 or 14 days of vehicle or PXS5338K (3mg/kg) P.O. IHC on paraffin embedded liver sections was performed for collagen III (A-D) and are demonstrated with associated isotype controls each group below (E-H).

Resolution model: α-SMA

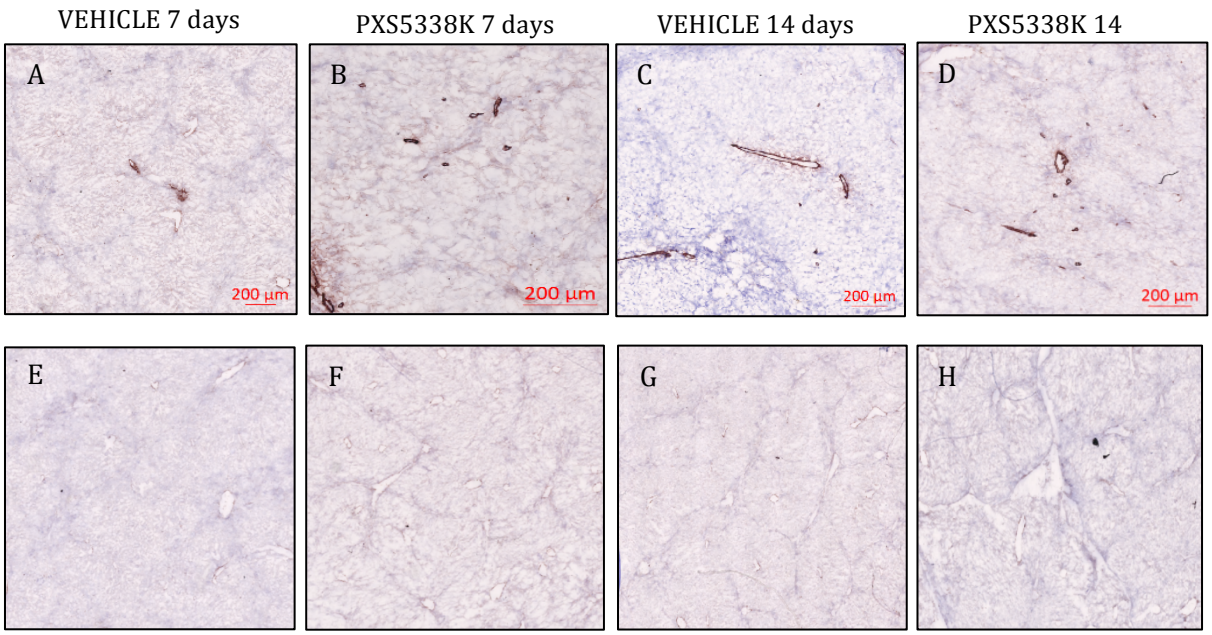


Figure 5.20 (A) Reduced expression of α-SMA was demonstrated in mice receiving PXS5338K recovering from TAA induced liver injury. C57Bl/6 mice received 16 weeks of TAA followed by 7 or 14 days of vehicle or PXS5338K (3mg/kg) P.O. IHC on paraffin embedded liver sections (A-D) are demonstrated alongside isotype controls.

Resolution model: SOX-9

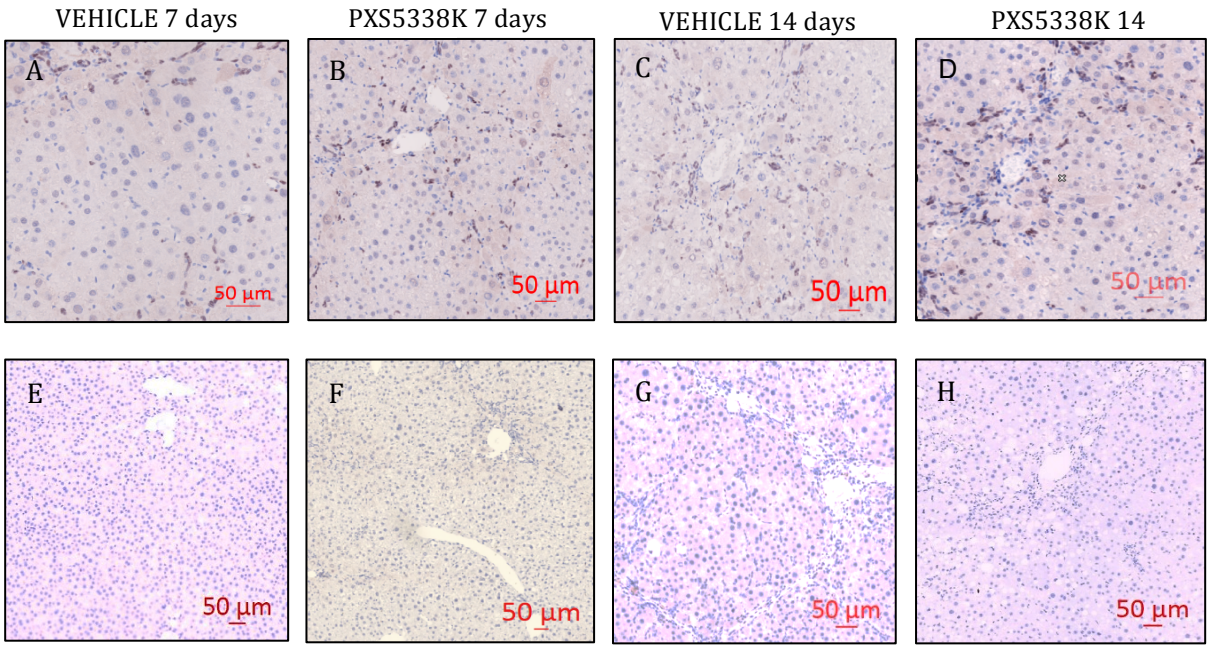


Figure 5.22 (A). An increase in the ductular reaction was observed in mice receiving PXS5338K recovering from TAA induced liver injury. C57Bl/6 mice received 16 weeks of TAA followed by 7 or 14 days of vehicle or PXS5338K (3mg/kg) P.O. IHC for SOX-9 on paraffin embedded liver sections (A-D) are demonstrated with associated isotype controls (E-H).

Resolution model: B220

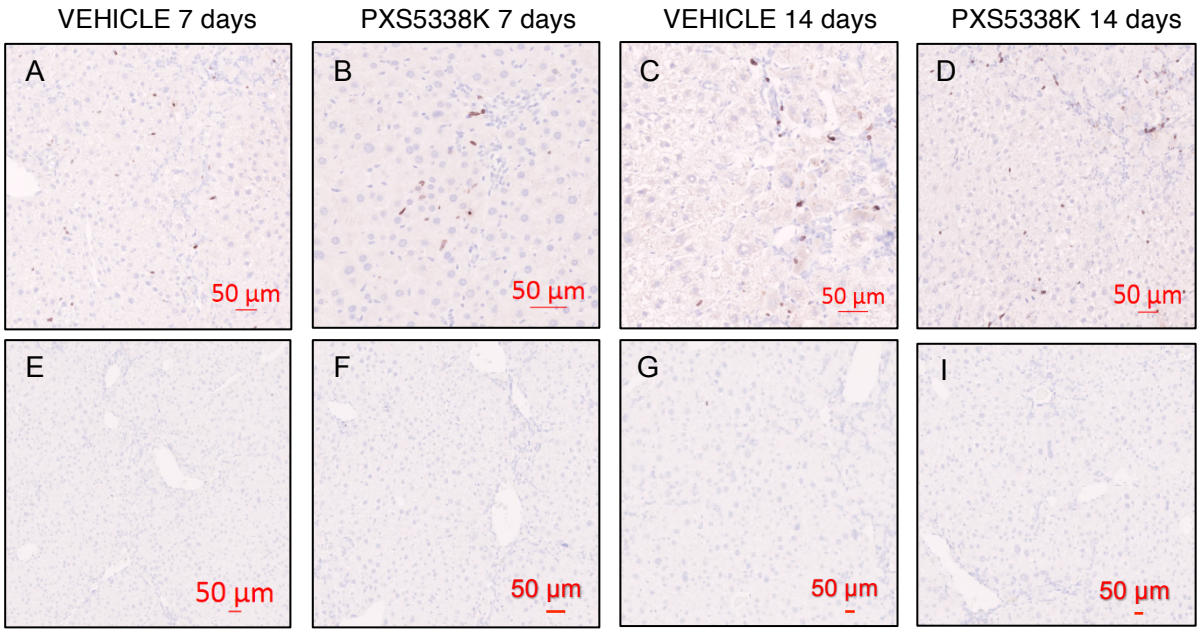


Figure 5.29 (A) Administration of PXS5338K has no impact on B cell infiltration into the liver when delivered during fibrosis resolution. C57Bl/6 mice received 16 weeks of TAA followed by 7 or 14 days of vehicle or PXS5338K (3mg/kg) P.O. IHC on paraffin embedded liver sections for CD45 B220+ B lymphocytes are demonstrated (A-D) with appropriate isotype controls for each groups below (E-H).

F4/80

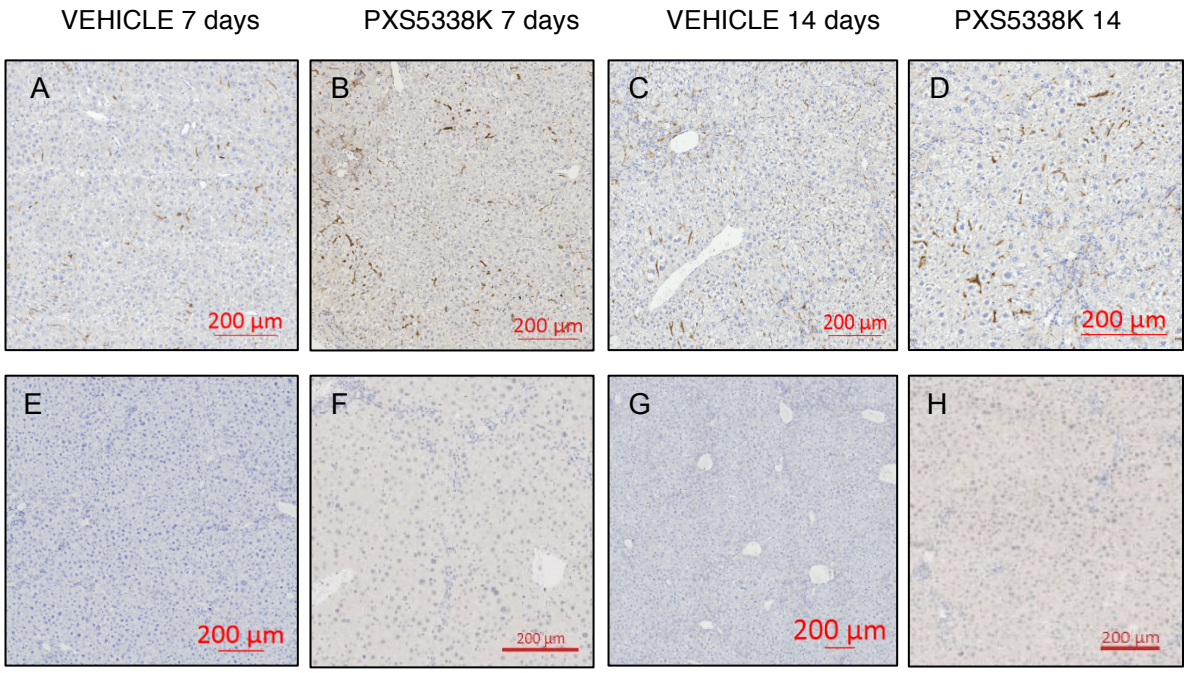


Figure 5.30 (A) Administration of PXS5338K increases macrophage infiltration into the liver when delivered during fibrosis resolution. C57Bl/6 mice received 16 weeks of TAA followed by 7 or 14 days of vehicle or PXS5338K (3mg/kg) P.O. IHC on paraffin embedded liver sections for F4/80 with are demonstrated (A-D) with corresponding isotype controls for each group below (E-H)

Ly6G

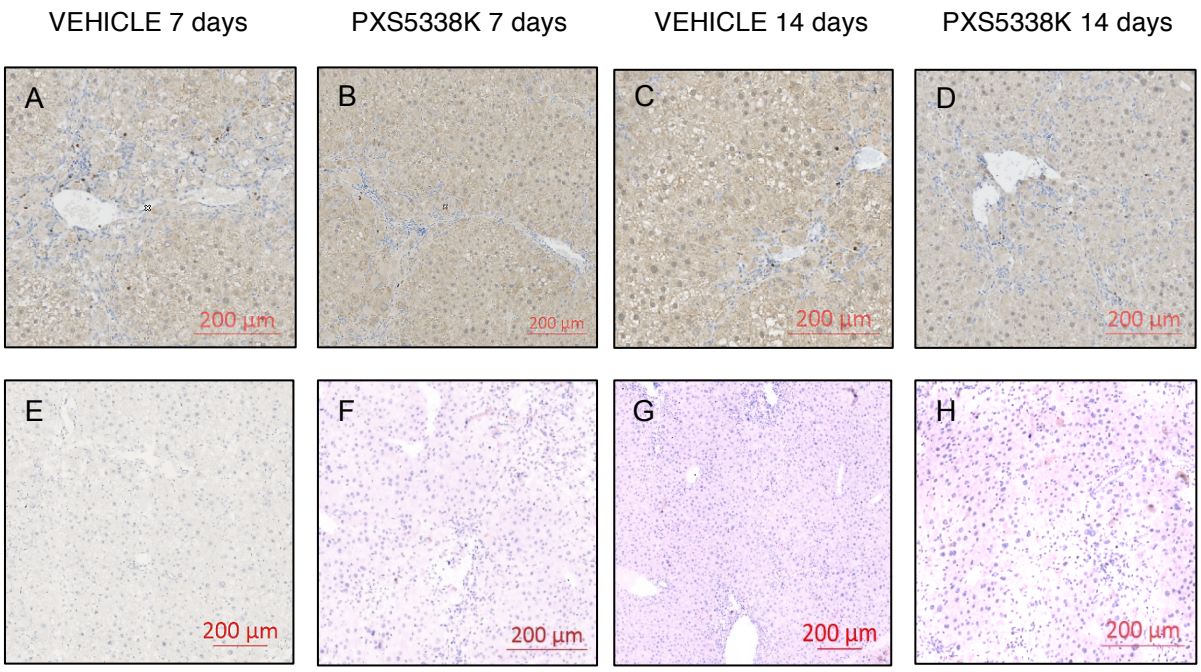


Figure 5.31 (A) Administration of PXS5338K has no impact on granulocyte infiltration into the liver when delivered during fibrosis resolution. C57Bl/6 mice received 16 weeks of TAA followed by 7 or 14 days of vehicle or PXS5338K (3mg/kg) P.O. IHC for Ly6G on paraffin embedded liver sections was performed (A-D) and is demonstrated with appropriate isotype controls below (E-H).